ISSN 0021-3438 (Print)
ISSN 2412-8783 (Online)

IZVESTIYA
NON-FERROUS METALLURGY

Vol. 30, No. 3, 2024

Scientific and Technical Journal
Founded in 1958
4 Issues per year

ИЗВЕСТИЯ ВУЗОВ
ЦВЕТНАЯ МЕТАЛЛУРГИЯ

Том 30, № 3, 2024

Научно-технический журнал
Основан в 1958 г.
Выходит 4 раза в год

ISSN 0021-3438 (Print)
ISSN 2412-8783 (Online)

IZVESTIYA NON-FERROUS METALLURGY

Vol. 30, No. 3 2024

Scientific and Technical Journal Founded in 1958 4 Issues per year http://cvmet.misis.ru

Journal is included into the List of the peer-reviewed scientific publications recommended by the Highest Attestation Commission of the Ministry of Education and Science of the Russian Federation for publishing the results of doctoral and candidate dissertations

Abstracting/Indexing: Russian Science Citation Index (RSCI), Chemical Abstracts (Online), INIS, OCLC ArticleFirst, Ulrich's Periodicals Directory, VINITI Database (Abstract Journal)

Founder

National University of Science and Technology "MISIS"
Address: 4 build. 1 Leninskiy Prosp., Moscow 119049, Russia
http://www.misis.ru

Address: NUST MISIS, 4 build. 1 Leninskiy Prosp., Moscow 119049, Russia

Phone: +7 (495) 638-45-35

E-mail: izv.vuz@misis.ru

Certificate of registration No. 015842 (13.03.1997)
Re-registration PI No. ФС77-79229 (25.09.2020)

Subscription: Ural-Press Agency

Signed print 26.09.2024. Format 60×90 1/8.
Offset paper No. 1. Digital printing. Quires 12
Order 20566. Free price

Printed in the printing house of the MISIS Publish House
4 build. 1 Leninskiy Prosp., Moscow 119049, Russia. Phone/fax: +7 (499) 236-76-17

ИЗВЕСТИЯ ВУЗОВ
ЦВЕТНАЯ МЕТАЛЛУРГИЯ

ISSN 0021-3438 (Print)
ISSN 2412-8783 (Online)

Том 30, № 3
2024

Научно-технический журнал Основан в 1958 г. Выходит 4 раза в год http://cvmet.misis.ru

Журнал включен в Перечень рецензируемых научных изданий, рекомендованных ВАК Минобрнауки РФ для публикации результатов диссертаций на соискание ученых степеней

Журнал включен в базы данных: Russian Science Citation Index (RSCI), Chemical Abstracts (Online), INIS, OCLC ArticleFirst, Ulrich's Periodicals Directory, РИНЦ, БД/РЖ ВИНИТИ

Учредитель

ФГАОУ ВО Национальный исследовательский технологический университет «МИСИС»
Адрес: 119049, г. Москва, Ленинский пр-т, 4, стр. 1
http://www.misis.ru

Редакция журнала

Адрес: 119049, г. Москва, Ленинский пр-т, 4, стр. 1, НИТУ МИСИС
Тел.: +7 (495) 638-45-35
E-mail: izv.vuz@misis.ru

Свидетельство о регистрации № 015842 от 13.03.1997 г.
Перерегистрация ПИ № ФС77-79229 от 25.09.2020 г.

Подписка: Агентство «Урал-пресс»

Ведущий редактор – О.В. Соснина
Выпускающий редактор – А.А. Кудинова
Дизайн и верстка – Е.А. Легкая

Подписано в печать 26.09.2024. Формат 60×90 1/8.
Бум. офсетная № 1. Печать цифровая. Усл. печ. л. 12
Заказ 20566. Цена свободная

Отпечатано в типографии Издательского Дома МИСИС
119049, г. Москва, Ленинский пр-т, 4, стр. 1. Тел./факс: +7 (499) 236-76-17

CONTENTS

СОДЕРЖАНИЕ

METALLURGY OF NON-FERROUS METALS / МЕТАЛЛУРГИЯ ЦВЕТНЫХ МЕТАЛЛОВ

UDC 669.334: 669.014
https://doi.org/10.17073/0021-3438-2024-3-5-24

Research article
Научная статья

Effectiveness of secondary copper electrolytic refining slime decopperization

S.O. Vydysh, E.V. Bogatyreva

National University of Science and Technology "MISIS"
4 Bld. 1 Leninsky Prosp., Moscow 119049, Russia

✉ Elena V. Bogatyreva (Helen_Bogatureva@mail.ru)

Abstract: The relevance of replacing the slime–H_2SO_4–H_2O system used for processing slimes from secondary copper electrolytic refining (SCER) with a slime–$NH_3 \cdot H_2O$–$(NH_4)_2SO_4$–H_2O system has been substantiated. Comprehensive studies of the characteristics of SCER slime samples were conducted. It was found that about 90 % of the copper is distributed between the Cu_2O phase and other phases, with a total copper content of 55.12 %. A new phase, $Cu_4(OH)_6SO_4$, corresponding to the mineral brochantite, was discovered, with a content in the slime of 6.40 %. Silver, with a concentration of 2.43 % in the slime, is present in metallic form at 69.1 %, with the remainder in the form of AgCl. The contents of associated components $PbSO_4$, $BaSO_4$, and SnO_2 are 13.52 %, 9.33 %, and 4.73 %, respectively. To substantiate the feasibility of low-temperature hydrometallurgical opening of the slime components and the conditions necessary for its implementation, determined by the specific qualitative and quantitative compositions of the slime, a thermodynamic analysis of the slime–$NH_3 \cdot H_2O$–$(NH_4)_2SO_4$–H_2O system was performed. This analysis allowed for the discovery and mathematical description of the dependencies of copper leaching indicators on the composition of the ammonia-ammonium mixture (ammonia buffer). A nomogram for the theoretical calculation of the minimum excess $NH_3 \cdot H_2O/NH_4^+$ over the stoichiometrically necessary amount required for the complete formation of the copper ammine complex was constructed according to the equilibrium ammonia-ammonium solution's pH and copper concentration. Thermodynamic calculations determined the optimal composition and consumption of ammonia-ammonium solutions, as well as the characteristics of the leach pulp, such as the concentration of $[Cu(NH_3)_4]^{2+}$ and the redox potential. Technological studies demonstrated the possibility of effective and selective extraction of copper from SCER slimes at a rate of no less than 99 % in the slime–$NH_3 \cdot H_2O$–$(NH_4)_2SO_4$–H_2O system, which was confirmed experimentally. Studies of the kinetics of copper leaching from slime in the slime–$NH_3 \cdot H_2O$–$(NH_4)_2SO_4$–H_2O system were conducted. The activation energy of the ammonia-ammonium copper leaching process from SCER slime (E_a = 5±0.25 kJ/mol) was determined within the temperature range from 15 to 45 °C at a total buffer system concentration $[NH_3 \cdot H_2O] + [NH_4^+]$ of 1 and 2 mol/L, as well as the order of reaction at a temperature of 24±1 °C, which is 0.24±0.02 and 0.91±0.05 for $[NH_3 \cdot H_2O] + [NH_4^+]$ concentrations above 1.5 mol/L and below 1.5 mol/L, respectively. A change in the kinetic mode of leaching with the limitation of the reaction rate by adsorption of reagents on the surface of solid particles to diffusion was detected when the total buffer system concentration $[NH_3 \cdot H_2O] + [NH_4^+]$ was reduced below 1.5 mol/L. The equation for the formal kinetics of the investigated process in the slime–$NH_3 \cdot H_2O$–$(NH_4)_2SO_4$–H_2O system was determined.

Keywords: copper, silver, secondary copper, slime, phase composition, thermodynamic analysis, leaching, kinetics, kinetic models, leaching rate, buffer systems, resource conservation.

For citation: Vydysh S.O., Bogatyreva E.V. Effectiveness of secondary copper electrolytic refining slime decopperization. *Izvestiya. Non-Ferrous Metallurgy*. 2024;30(3):5–24. https://doi.org/10.17073/0021-3438-2024-3-5-24

Эффективность обезмеживания шламов электролитического рафинирования вторичной меди

С.О. Выдыш, Е.В. Богатырева

Национальный исследовательский технологический университет «МИСИС»
Россия, 119049, г. Москва, Ленинский пр-т, 4, стр. 1

✉ Елена Владимировна Богатырева (Helen_Bogatureva@mail.ru)

Аннотация: Обоснована актуальность замены системы шлам–H_2SO_4–H_2O для переработки шламов электролитического рафинирования вторичной меди (ЭРВМ) системой шлам–$NH_3 \cdot H_2O$–$(NH_4)_2SO_4$–H_2O. Выполнены комплексные исследования характеристик образца шлама ЭРВМ. Установлено, что около 90 % меди распределено между фазами Cu_2O и прочими при общем содержании Cu 55,12 %. Обнаружена новая фаза $Cu_4(OH)_6SO_4$, соответствующая минералу брошантит, содержание которой в шламе составляет 6,40 %. Серебро при его концентрации в шламе 2,43 % на 69,1 % присутствует в металлическом состоянии, остальное в соединении AgCl. Содержание попутных компонентов $PbSO_4$, $BaSO_4$ и SnO_2 составляет 13,52, 9,33 и 4,73 % соответственно. Для обоснования возможности низкотемпературного гидрометаллургического вскрытия компонентов шлама и необходимых для его реализации режимов, обусловленных особенностями качественного и количественного составов шлама, выполнен термодинамический анализ системы шлам–$NH_3 \cdot H_2O$–$(NH_4)_2SO_4$–H_2O, позволивший обнаружить и математически описать зависимости показателей процесса выщелачивания меди от состава аммиачно-аммонийной смеси (аммиачного буфера). Построена номограмма теоретического расчета минимального избытка $NH_3 \cdot H_2O/NH_4^+$ от стехиометрически необходимого количества, требуемого для полного протекания реакции комплексообразования аммиаката меди в соответствии с величинами pH равновесного аммиачно-аммонийного раствора и концентрации в нем меди. Термодинамическими расчетами определены оптимальный состав аммиачно-аммонийных растворов и их расход, а также характеристики пульпы выщелачивания: концентрация $[Cu(NH_3)_4]^{2+}$ и окислительно-восстановительный потенциал. Технологические расчеты показали возможность эффективного и селективного извлечения меди из шламов ЭРВМ не менее чем 99 % в системе шлам–$NH_3 \cdot H_2O$–$(NH_4)_2SO_4$–H_2O, что подтверждено экспериментально. Проведены исследования кинетики выщелачивания меди из шлама в системе шлам–$NH_3 \cdot H_2O$–$(NH_4)_2SO_4$–H_2O. Определена энергия активации процесса аммиачно-аммонийного выщелачивания меди из шлама ЭРВМ (E_a = 5±0,25 кДж/моль) в интервале температур от 15 до 45 °C при суммарной концентрации буферной системы $[NH_3 \cdot H_2O] + [NH_4^+]$ 1 и 2 моль/л, а также порядок по реагенту при температуре 24±1 °C, равный 0,24±0,02 и 0,91±0,05 для $[NH_3 \cdot H_2O] + [NH_4^+]$ более 1,5 моль/л и менее 1,5 моль/л соответственно. Обнаружена смена кинетического режима выщелачивания с лимитированием скорости процесса адсорбцией реагентов на поверхности твердых частиц на диффузионный при снижении суммарной концентрации буферной системы $[NH_3 \cdot H_2O] + [NH_4^+]$ ниже 1,5 моль/л. Определено уравнение формальной кинетики исследованного процесса в системе шлам–$NH_3 \cdot H_2O$–$(NH_4)_2SO_4$–H_2O.

Ключевые слова: медь, серебро, вторичная медь, шлам, фазовый состав, термодинамический анализ, выщелачивание, кинетика, кинетические модели, скорость выщелачивания, буферные системы, ресурсосбережение.

Для цитирования: Выдыш С.О., Богатырева Е.В. Эффективность обезмеживания шламов электролитического рафинирования вторичной меди. *Известия вузов. Цветная металлургия*. 2024;30(3):5–24. https://doi.org/10.17073/0021-3438-2024-3-5-24

Introduction

The global economic recovery in the post-COVID period led to a sharp increase in demand for refined copper in 2023, amounting to 4.6 % compared to 2022, while the growth in primary copper production was only 0.5 % [1]. The deficit in refined copper was compensated by the inclusion of secondary copper resources in processing, which, for the first time, increased the share of secondary copper above 20% in the production of refined copper [2; 3]. The depletion of global copper ore reserves at the current level of production is estimated to occur within the next 50—100 years, but a deficit in refined copper production may already reach more than 8 million tons in the next decade [4; 5]. According to forecasts, by 2030, the production of refined copper is expected to decrease by 10 % compared to 2025, while consumption is projected to increase by 22 % [5].

By 2030, the development of new copper deposits is planned, which could increase global copper production by 1.7 to 3.3 million tons per year [5]. The increased processing of secondary copper resources could contribute not only to offsetting the global deficit of refined copper but also to stabilizing copper prices on the stock market.

The copper refining technology, both for primary and secondary raw materials, according to GOST 859-2014, consists of two stages—fire refining and electrolytic refining [6]. During the process of electrolytic copper refining, anode slimes are formed, which act as concentrators for rare and precious metals. The composition of these slimes is determined by the electrolysis parameters and the composition of the anode copper, and it varies widely [7; 8], with mass percentages as follows:

Cu	1.00—53.40	Te	0.01—9.00
Ag	0.10—24.00	Pb	0.60—51.40
Au	0.02—5.40	Sn	0.10—12.10
Se	0.10—21.00	Ni	0.01—10.90

A distinctive feature of secondary copper electrolytic refining slimes (SCER) is the increased content of tin and nickel and the decreased content of selenium and tellurium. The processing of SCER and primary copper electrolysis slimes is similar, but lead and tin remain unextracted and end up in the production waste—slag from the Dore alloy smelting [7—13]. In addition to the low utilization of raw materials, Dore alloy smelting has the following disadvantages [7; 14; 15]:

— high capital costs for pyrometallurgical processing;

— high energy consumption;

— elevated concentrations of lead in the workplace air, ranging from 0.5 to 3.0 mg/m^3, which is 50 to 300 times higher than the maximum allowable concentrations (MAC) in the workplace air;

— significant generation of solid waste (slag output ranges from 0.9 to 1.2 tons per ton of slime).

In accordance with modern requirements for diversified raw material utilization and the potential increase in SCER slime volumes, the development of technology for deeper processing of these slimes with the simultaneous extraction of lead and tin is a timely and relevant task. Hydrometallurgical methods appear to be the most promising solution for this challenge.

Hydrometallurgical technologies for processing anode slimes have not yet found widespread application due to the following drawbacks [7; 9; 11; 13; 14]:

— multi-stage processes;

— production of solutions with low precious metals concentration and contaminated with impurities of base metals;

— generation of significant volumes of waste solutions that require disposal.

However, improvements in hydrometallurgical slime processing, aimed at reducing or eliminating these drawbacks, will simplify the management and control of technological processes, which is particularly relevant in the context of implementing the “Industry 4.0” program. This program focuses on the digitalization of technological processes to improve production efficiency [16; 17].

Most technological schemes of modern enterprises for processing copper-electrolyte slimes begin with decopperization—copper removal, which is carried out under autoclave conditions in a sulfuric acid solution with a concentration of 100 to 250 g/L at temperatures ranging from 80 to 140 °C, pressure up to 0.7 MPa, a liquid-to-solid ratio (L/S) of (5÷10) : 1, and the supply of oxygen as an oxidant for 8—16 hours [7—9; 11—15]. The use of sulfuric acid is justified by the feasibility of returning Cu-containing solutions to the main copper production process. During autoclave oxidative leaching of copper-electrolyte slime, the destruction of copper selenides and tellurides occurs effectively, contributing to the increased extraction of copper into the leach solution, reaching 99 %, as well as the dissolution of nickel oxide, compared to atmospheric decopperization of anode slime through aeration in a sulfuric acid solution. However, given the low content of selenium and tellurium in SCER slime, the use of capital-intensive autoclave leaching is irrational, while atmospheric decopperization of anode slime through aeration in a sulfuric acid solution has low specific productivity in terms of decopperized slime (up to 67.5 kg/m^3 per operation) [7].

Intensification of the sulfuric acid leaching process of copper from slime can be facilitated by using hydrogen peroxide as an oxidizer instead of oxygen [18]. The rate of copper dissolution during atmospheric leaching in a solution of 200 g/L H_2SO_4 and 12.5 g/L H_2O_2 is $7{,}4\cdot10^{-8}$ g-ion/(cm^2·s), which is 76.6 % lower than during autoclave treatment — $2{,}8\cdot10^{-7}$ g-ion/(cm^2·s). However, the use of hydrogen peroxide as an oxidizer may lead to silver losses in the leach solution due to its oxidation. Additionally, sulfuric acid methods for SCER slime decopperization have the following drawbacks:

— the necessity of using corrosion-resistant equipment;

— difficulty in filtering sulfuric acid pulps containing tin and barium, due to the possible formation of metastannic acid H_2SnO_3 or recrystallization of $BaSO_4$.

These drawbacks can be mitigated by transitioning from the slime—H_2SO_4—H_2O_2—H_2O system to the less aggressive and neutral to tin dioxide system of slime—$NH_3\cdot H_2O$—$(NH_4)_2SO_4$—H_2O—O_2, where oxygen from the air can be used as the oxidizer [19]. The application of ammonia-ammonium (AA) leaching for copper-bearing mono- and polymetallic raw materials has been studied in works [19—29]. It is known that the oxidative dissolution of copper proceeds stepwise through the following reactions [28; 30]

$$Cu + 2NH_3 + 0.25O_2 + 0.5H_2O = [Cu(NH_3)_2]^+ + OH^-, \quad (1)$$

$$[Cu(NH_3)_2]^+ + 2NH_3 + 0.25O_2 + 0.5H_2O = [Cu(NH_3)_4]^{2+} + OH^-, \quad (2)$$

$$[Cu(NH_3)_4]^{2+} + Cu = 2[Cu(NH_3)_2]^+. \quad (3)$$

In the initial stage, the process follows the electrochemical mechanism according to reactions (1) and (2), but as the concentration of $[Cu(NH_3)_4]^{2+}$ ions increases, an autocatalytic mechanism of copper dissolution according to reaction (3) is initiated, which enhances the dissolution rate [20—25; 30]. In raw materials with high contents of oxidized Cu-bearing components, copper leaching may initially proceed via the autocatalytic mechanism. In the absence of copper sulfides and chalcogenides, the use of autoclave leaching with oxygen supply is irrational, as it may lead to silver losses with the ammonia-ammonium solution [27]. Nickel also tends to form ammoniacal complex compounds, allowing its co-extraction with copper into the solution [29; 31]. However, depending on the concentration ratios of ammonia and copper, the forms of the resulting complexes and their proportion in the solution may vary (Fig. 1) [30], which can influence the AA-leaching process of copper from SCER slime.

The evaluation of the thermodynamic and kinetic characteristics of metallurgical and chemical-metallurgical processes not only supports the justification of their operating modes but also provides the opportunity for mathematical modeling to develop an automatic control scheme [30]. The study of leaching kinetics is necessary to determine the mechanism of the process, the rate-limiting stage, to justify the technological modes of the process, to identify directions for its intensification, and for management and automation [32].

The aim of this work is to improve the efficiency, resource, and energy conservation of SCER slime decopperization in the process of low-temperature ammonia-ammonium leaching.

Objectives of the work:

— To determine the characteristics of the research object—SCER slime;

— To conduct a thermodynamic analysis of the SCER slime decopperization process in the slime—$NH_3 \cdot H_2O$—$(NH_4)_2SO_4$—H_2O—O_2 system to assess the composition and consumption of the AA-leach solution, ensuring copper extraction into the solution of no less than 99 %;

— To test the developed decopperization modes on the research object;

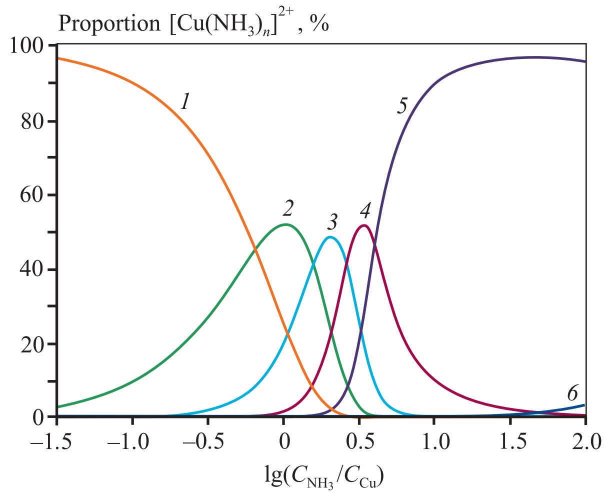

Fig. 1. Dependence of the proportion of various copper cations in an ammonia-ammonium solution on the molar ratio of ammonia to copper in the solution at C_{Cu} = 0.01 mol/L [30]
1 – Cu^{2+}; *2* – $[Cu(NH_3)]^{2+}$; *3* – $[Cu(NH_3)_2]^{2+}$; *4* – $[Cu(NH_3)_3]^{2+}$; *5* – $[Cu(NH_3)_4]^{2+}$; *6* – $[Cu(NH_3)_5]^{2+}$

Рис. 1. Зависимость доли различных катионов меди в аммиачно-аммонийном растворе от мольного соотношения аммиака и меди в растворе при C_{Cu} = 0,01 моль/л [30]
1 – Cu^{2+}; *2* – $[Cu(NH_3)]^{2+}$; *3* – $[Cu(NH_3)_2]^{2+}$; *4* – $[Cu(NH_3)_3]^{2+}$; *5* – $[Cu(NH_3)_4]^{2+}$; *6* – $[Cu(NH_3)_5]^{2+}$

— To determine the activation energy and order of reaction for the ammonia buffer $[NH_3 \cdot H_2O] + [NH_4^+]$ in the AA-leaching process of SCER slime, leading to the derivation of the formal kinetics equation.

1. Characteristics and methods of research on slime from secondary copper electrolytic refining

Analyses of the composition of SCER slime and the processing products were conducted using modern research methods and equipment, such as:

transmission electron microscopy using the S-3400N scanning electron microscope (SEM) by Hitachi High-Technologies Corporation (Japan), equipped with a NORAN *X*-ray energy-dispersive spectrometer;

— *X*-ray fluorescence analysis on the ARL9900 WorkStation ("Thermo Fisher Scientific", Switzerland);

— granulometric analysis on the MicroSizer-201 laser particle size analyzer;

— density assessment of the research object using the AccuPyc 1340 helium pycnometer (Micromeritics, USA);

— determination of copper content in the leach solution and residue by iodometric titration with sodium thiosulfate;

— determination of silver content by gravimetric analysis (precipitation of silver iodide from solution) [33; 34].

The results of the chemical and phase analyses of the secondary copper electrolytic refining slime are presented below, wt.%:

Cu	55.12
Ag	2.43
Pb	9.24
Sn	3.72
Ba	5.45
SiO_2	1.21
Others	22.83

Cu_2O	26.3
$PbSO_4$	13.5
$BaSO_4$	9.3
$Cu_4(OH)_6SO_4$*	6.4
SnO_2	4.8
Cu	2.0
Total crystalline phases	62.3

* Corresponding to brochantite.

It is evident that the "others" category in the research object amounts to 22.83 %, of which more than 72 % consists of oxygen and sulfur. The total amount of crystalline phases in the slime corresponds to 62.3 %, with the remaining 37.7 % represented by *X*-ray amorphous phases. This underscores the importance of calculating the rational composition of the slime (Table 1).

Information about the presence of the $Cu_4(OH)_6SO_4$ phase, corresponding to the mineral brochantite, in copper-electrolyte slimes is absent in the available literature [7—15]. Copper, which constitutes 55.12 % of the slime, is distributed among the Cu_2O, $Cu_4(OH)_6SO_4$, metallic copper, and other phases at 42.4 %, 6.5 %, 3.6 %, and 47.5 %, respectively. The high copper content in the "others" category is associated with unidentified reflections in the *X*-ray phase analysis. Silver is concentrated in two phases: metallic silver, which contains 69.1 % of the total silver content, and silver chloride.

It can be seen from Table 2 that SCER slime is a fine-grained material, with over 80 % of the particles being smaller than 48.2 μm. The specific surface area of the particles in the research object was 115.14 dm^2/g, and the density of the slime was 5260 kg/m^3.

Fig. 2 presents a micrograph of SCER slime obtained by SEM and analyzed at points using energy-dispersive *X*-ray spectroscopy. Copper (I) oxide is represented by spheroidal particles, lead sulfate by dendritic particles, and tin oxide by acicular particles.

The following reagents were used in the study: aqueous ammonia, ammonium sulfate, ammonium bicarbonate, sodium thiosulfate pentahydrate, and potassium iodide (all of analytical grade).

Leaching of the slime (**Method I**) was carried out at a molar ratio of $\Theta = [NH_3 \cdot H_2O] : [(NH_4)_2SO_4] = 4$ mol/mol and with a minimal excess of $NH_3 \cdot H_2O/NH_4^+$ over the stoichiometrically necessary quantity (SNQ) for reaction (31) (see below) of $\chi = 20$ %, which, based on the results of thermodynamic analysis, in the AA-solution in the slime—$NH_3 \cdot H_2O$—$(NH_4)_2SO_4$—H_2O—O_2 system, are preferable for achieving the goal of resource and energy conservation. Air was used as the oxidizer, with a flow rate of 190 ± 2 L/h. The solution, at a liquid-to-solid ratio (L/S) of 12 : 1, without heating ($t = 24$ °C), was mixed with a sample of the research material with a total mass of 80 g. The process continued until the redox potential (ORP) of the pulp reached +260 ± 10 mV relative to the standard hydrogen electrode (52 ± 10 mV relative

Table 1. **Rational composition of secondary copper electrolytic refining slime**

Таблица 1. Рациональный состав шлама электролитического рафинирования вторичной меди

Phase	Content, wt.%									Total
	Cu	Pb	Ba	Sn	Ag	SiO_2	S	O	Others	
Cu_2O	23.36	–	–	–	–	–	–	2.94	–	26.30
$PbSO_4$	–	9.24	–	–	–	–	1.43	2.85	–	13.52
$BaSO_4$	–	–	5.45	–	–	–	1.27	2.54	–	9.26
$Cu_4(OH)_6SO_4$	3.60	–	–	–	–	–	0.45	2.35	–	6.40
SnO_2	–	–	–	3.72	–	–	–	1.01	–	4.73
Cu	2.00	–	–	–	–	–	–	–	–	2.00
Ag	–	–	–	–	1.68	–	–	–	–	1.68
SiO_2	–	–	–	–	–	1.21	–	–	–	1.21
AgCl	–	–	–	–	0.75	–	–	–	0.25	1.00
Others	26.16	–	–	–	–	–	1.66	–	6.08	33.90
Total	55.12	9.24	5.45	3.72	2.43	1.21	4.81	11.69	6.33	100.00

Table 2. **Integral granulometric composition of secondary copper electrolytic refining slime**

Таблица 2. Интегральный гранулометрический состав шлама электролитического рафинирования вторичной меди

Maximum particle diameter of the fraction, μm	1.88	4.09	9.49	16.7	22.8	29.3	37.0	48.2	69.7	600
Percentage of particles with diameter from 0 to maximum within the fraction, %	10	20	30	40	50	60	70	80	90	100

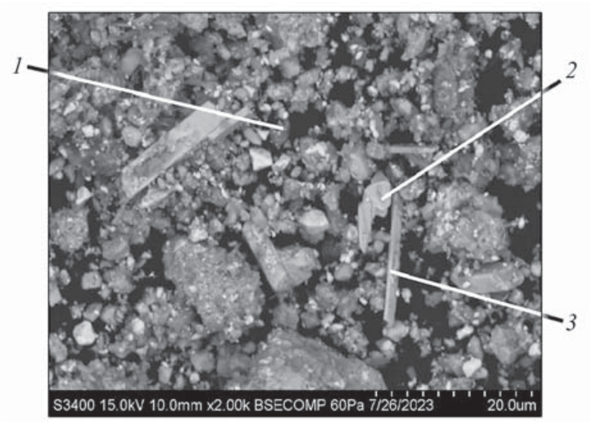

Fig. 2. Micrograph of the research object – SCER slime
1 – Cu_2O, *2* – $PbSO_4$, *3* – SnO_2

Рис. 2. Микрофотография объекта исследования – шлама ЭРВМ
1 – Cu_2O, *2* – $PbSO_4$, *3* – SnO_2

to the silver chloride electrode). The resulting pulp was filtered using a Buchner funnel through a "blue ribbon" filter; the residue on the filter was washed with ammoniacal water with a concentration of 0.1 mol/L (L/S ~ 1 : 1) and then with distilled water (L/S ~ 1 : 5). The leach solution and the wash water were combined and analyzed for copper content (iodometric titration with sodium thiosulfate) and silver content (gravimetrically—by precipitating silver iodide, drying, and weighing it on XS 204 analytical scales (Mettler-Toledo, Switzerland)). The leaching residue was dried in a 2B 151 laboratory oven (SNOL, Russia) and weighed on SPS 202 laboratory technical scales (OHAUS, USA) to determine its yield.

Kinetic studies of AA-leaching of slime (**Method II**) were conducted at a molar ratio of $[NH_3 \cdot H_2O]$: : $[(NH_4)_2SO_4]$ = 4 mol/mol and a concentration of $C_{\Sigma[NH_3 \cdot H_2O]+[NH_4^+]}$ = 0.5÷3.5 mol/L. Oxygen from the air was used as the oxidizer, with a flow rate ranging from 18 ± 1 to 155 ± 2 L/h. A sample of the research material weighing 5 g was added to the solution at a liquid-to-solid ratio (L/S) of 100 : 1 and a temperature of 15—45 °C. The total duration of the process ranged from 5 to 30 minutes. During the experiment, samples of the leach solution were taken and analyzed for copper content using iodometric titration with sodium thiosulfate. The total volume of the samples taken did not exceed 5 % of the solution volume. Based on the results obtained, the dependencies of the degree of leaching on the duration of the process were plotted for t = 15÷45 °C and buffer mixture concentrations $C_{\Sigma[NH_3 \cdot H_2O]+[NH_4^+]}$ = 1 and 2 mol/L to determine the activation energy, as well as for $C_{\Sigma[NH_3 \cdot H_2O]+[NH_4^+]}$ = = 0.5÷3.5 mol/L and t = 25 °C to evaluate the reaction order. The dependencies of $\ln(d\alpha/d\tau)$ — $1/T$ and $\ln(d\alpha/d\tau)$ — $\ln C$ (where $d\alpha/d\tau$ are the slope coefficients of the tangents at the values of the leaching degree α = 0) were plotted, and from the tangents of their slopes, the activation energy and reaction orders were determined, respectively.

2. Results and discussion

2.1. Thermodynamic analysis

The thermodynamic analysis of the slime—$NH_3 \cdot H_2O$—$(NH_4)_2SO_4$—H_2O—O_2 system was carried out due to the need to justify effective conditions for the extraction of SCER slime components. This is related to selecting the composition of the leaching solution that ensures high copper recovery in the AA-leaching process.

Thermodynamic calculations of the probable reactions in the studied slime— $NH_3 \cdot H_2O$—$(NH_4)_2SO_4$—H_2O—O_2 system were performed using reference data on the thermodynamic parameters of the slime components and the potential products of their interaction with the leaching system [31; 35; 36].

In work [29], it was recommended that copper dissolution in ammonia solutions $[NH_3 \cdot H_2O]$ and $[NH_4^+]$ be conducted in the pH range of 9—11, which ensures the maximum activity of $[Cu(NH_3)_4]^{2+}$ ions participating in the autocatalytic oxidation reaction of copper. To oxidize $[Cu(NH_3)_2]$ + ions to $[Cu(NH_3)_4]^{2+}$, according to the mechanism described by reactions (1)—(3), oxygen from the air is supplied to the system. The oxidation potential of oxygen depends on the pH and, under normal conditions, can be calculated using the equation [37]:

$$E^0 = 1.228 - 0.059\text{pH}, \tag{4}$$

where pH is the hydrogen ion concentration.

According to equation (4), for pH values of 9, 10, and 11, the oxidation potential of the oxygen half-reaction:

$$O_2 + 2H_2O + 4e^- = 4OH^- \tag{5}$$

is E^0 = +0.697, +0.638 and +0.579 V, respectively.

The results of the Gibbs energy calculation, equilibrium constants, and redox potentials of probable reactions in the slime—$NH_3 \cdot H_2O$—$(NH_4)_2SO_4$—H_2O—O_2 system for the phases Cu, Ag, and Pb are presented in Table 3. The analysis of these data showed that most chemical reactions (6)—(8), (10), (12), (14), (16), (18)—(20), (22)—(28) are thermodynamically probable. However, for processes (11)—(16), (21), and (22), which are not redox reactions, the dissolution reactions of metal compounds and the formation of their ammine complexes

Table 3. **Results of Gibbs energy (ΔG^0_{298}), equilibrium constants, and redox potential calculations of probable reactions in the slime–$NH_3 \cdot H_2O$–$(NH_4)_2SO_4$–H_2O–O_2 system**

Таблица 3. Результаты расчета энергии Гиббса (ΔG^0_{298}), констант равновесий и окислительно-восстановительного потенциала вероятных реакций в системе шлам–$NH_3 \cdot H_2O$–$(NH_4)_2SO_4$–H_2O–O_2

№	Reaction	E^0, V	ΔG^0_{298}, kJ/mol Me	$\lg K_a$
(6)	$Cu + 2NH_3 \cdot H_2O + 0.25O_2 = [Cu(NH_3)_2]^+ + OH^- + 1.5H_2O$	+0.817 (pH = 9)	–78.8	+13.8
		+0.758 (pH = 10)	–73.1	+12.8
		+0.699 (pH = 11)	–67.5	+11.8
(7)	$[Cu(NH_3)_2]^+ + 2NH_3 \cdot H_2O + 0.25O_2 = [Cu(NH_3)_4]^{2+} + OH^- + 1.5H_2O$	+0.707 (pH = 9)	–68.2	+12.0
		+0.648 (pH = 10)	–62.5	+11.0
		+0.589 (pH = 11)	–56.8	+10.0
(8)	$0.5[Cu(NH_3)_4]^{2+} + 0.5Cu = [Cu(NH_3)_2]^+$	+0.110	–5.3	+0.9
(9)	$Cu + 2NH_4^+ + 0.25O_2 + OH^- = [Cu(NH_3)_2]^+ + 1.5H_2O$	–	–106.0	+18.6
(10)	$[Cu(NH_3)_2]^+ + 2NH_4^+ + 0.25O_2 + OH^- = [Cu(NH_3)_4]^{2+} + 1.5H_2O$	–	–87.2	+15.3
(11)	$0.5Cu_2O + 2NH_3 \cdot H_2O = [Cu(NH_3)_2]^{2+} + OH^- + 1.5H_2O$	–	+21.2	–3.7
(12)	$0.5Cu_2O + 2NH_4^+ + OH^- = [Cu(NH_3)_2]^{2+} + 1.5H_2O$	–	–31.9	+5.6
(13)	$CuO + 4NH_3 \cdot H_2O = [Cu(NH_3)_4]^{2+} + 2OH^- + 3H_2O$	–	+41.5	–7.3
(14)	$CuO + 4NH_4^+ + 2OH^- = [Cu(NH_3)_4]^{2+} + 3H_2O$	–	–64.8	+11.4
(15)	$Cu(OH)_2 + 4NH_3 \cdot H_2O = [Cu(NH_3)_4]^{2+} + 2OH^- + 4H_2O$	–	+34.8	–6.1
(16)	$Cu(OH)_2 + 4NH_4^+ + 2OH^- = [Cu(NH_3)_4]^{2+} + 4H_2O$	–	–71.4	+12.5
(17)	$0.25Cu_4(OH)_6SO_4 + 4NH_3 \cdot H_2O = [Cu(NH_3)_4]^{2+} + 0.25SO_4^{2-} + 1.5OH^- + 4H_2O$	–	+24.7	–4.3
(18)	$0.25Cu_4(OH)_6SO_4 + 4NH_4^+ + 2.5OH^- = [Cu(NH_3)_4]^{2+} + 0.25SO_4^{2-} + 4H_2O$	–	–81.5	+14.3
(19)	$Ag + 2NH_3 \cdot H_2O + 0.25O_2 = [Ag(NH_3)_2]^+ + OH^- + 1.5H_2O$	+0.330 (pH = 9)	–31.9	+5.6
		+0.271 (pH = 10)	–26.2	+4.6
		+0.212 (pH = 11)	–20.5	+3.6
(20)	$Ag + 2NH_4^+ + 0.25O_2 + OH^- = [Ag(NH_3)_2]^+ + 1.5H_2O$	–	–57.6	+10.1
(21)	$AgCl + 2NH_3 \cdot H_2O = [Ag(NH_3)_2]^+ + Cl^- + 2H_2O$	–	+12.6	–2.2
(22)	$AgCl + 2NH_4^+ + 2OH^- = [Ag(NH_3)_2]^+ + Cl^- + 2H_2O$	–	–40.5	+7.1
(23)	$AgCl + 2NH_3 \cdot H_2O + Cu = [Cu(NH_3)_2]^+ + Ag + Cl^- + 2H_2O$	+0.342	–33.0	+5.8
(24)	$AgCl + 2NH_4^+ + Cu + 2OH^- = [Cu(NH_3)_2]^+ + Ag + Cl^- + 2H_2O$	–	–88.9	+15.6
(25)	$AgCl + [Cu(NH_3)_2]^+ + 2NH_3 \cdot H_2O = [Cu(NH_3)_4]^{2+} + Ag + Cl^- + 2H_2O$	+0.232	–22.4	+3.9
(26)	$AgCl + [Cu(NH_3)_2]^+ + 2NH_4^+ + 2OH^- = [Cu(NH_3)_4]^{2+} + Ag + Cl^- + 2H_2O$	–	–70.1	+12.3
(27)	$[Ag(NH_3)_2]^+ + Cu = [Cu(NH_3)_2]^+ + Ag$	+0.487	–47.0	+8.2
(28)	$[Ag(NH_3)_2]^+ + [Cu(NH_3)_2]^+ = [Cu(NH_3)_4]^{2+} + Ag$	+0.377	–36.4	+6.4

with the ammonium ion are thermodynamically more probable than with the ammonia hydrate. Therefore, it is necessary to establish the dependence of the equilibrium concentration of copper and silver ammines on the concentration of free ammonia hydrate ($[NH_3 \cdot H_2O]$) and ammonium ion ($[NH_4^+]$), as well as on the pH value, which depends on the molar ratio of ammonia hydrate and ammonium ion in the solution, i.e., on Θ [38]. The $[NH_3 \cdot H_2O] + [NH_4^+]$ mixture, in the form of an ammonium salt of a strong acid, creates a buffer system [39]:

$$NH_3 \cdot H_2O \rightleftarrows NH_4^+ + OH, \qquad (29)$$

and therefore, it is assumed that the equilibrium pH of the system equals the initial value.

To determine the effect of the equilibrium pH and the total concentration of free $NH_3 \cdot H_2O$ and NH_4^+ ions (i.e., not bound in complexes $[NH_3 \cdot H_2O + NH_4^+]_{free}$), considering the buffer system equilibrium from reaction (29), on the concentrations of copper and silver ammines, the reactions (11) and (12), (13) and (14), (15) and (16), (21) and (22) from Table 3 were combined, yielding the following equations:

$$0.5Cu_2O + 2x[NH_3 \cdot H_2O] + \\ + 2(1-x)NH_4^+ + 2(1-x)OH^- = \\ = [Cu(NH_3)_2]^+ + OH^- + 1.5H_2O, \quad (30)$$

$$CuO + 4x[NH_3 \cdot H_2O] + \\ + 4(1-x)NH_4^+ + 4(1-x)OH^- = \\ = [Cu(NH_3)_4]^{2+} + 2OH^- + 3H_2O, \quad (31)$$

$$Cu(OH)_2 + 4x[NH_3 \cdot H_2O] + \\ + 4(1-x)NH_4^+ + 4(1-x)OH^- = \\ = [Cu(NH_3)_4]^{2+} + 2OH^- + 4H_2O, \quad (32)$$

$$AgCl + 2x[NH_3 \cdot H_2O] + \\ + 2(1-x)NH_4^+ + 2(1-x)OH^- = \\ = [Ag(NH_3)_2]^+ + Cl^- + 2H_2O, \quad (33)$$

where x and $(1-x)$ are the molar fractions of $NH_3 \cdot H_2O$ and NH_4^+ in the ammonia-ammonium solution, respectively.

It is known that the solubility of $[Cu(NH_3)_4]SO_4$ in water is 16.9 g/100 g H_2O, corresponding to a concentration of $[Cu(NH_3)_4]^{2+}$ 0.74 mol/L [31]. The solubility of copper ammines is primarily influenced by the concentration of free ammonia, and at $C_{NH_3 \cdot H_2O} = 7.2$ mol/L and $C_{(NH_4)_2SO_4} = 2.3$ mol/L a concentration of $[Cu(NH_3)_4]^{2+}$ 1.7 mol/L was achieved [40]. However, in the study [41], it was found that increasing the concentrations of ammonia and ammonium chloride to 10.84 and 5.44 mol/L, respectively, promoted the solubility of copper tetraammine to 2.8 mol/L. It is probable that the ratio of ammonia molecules to ammonium ions in the solution, as well as the type of ammonium salt, affects the solubility of copper ammines. Therefore, in this study, it is assumed that the maximum concentration of $[Cu(NH_3)_4]^{2+}$ is 2.8 mol/L, by analogy with $NH_3 \cdot H_2O$—NH_4Cl—H_2O solutions.

The dependencies of the equilibrium concentrations of $[Cu(NH_3)_2]^+$, $[Cu(NH_3)_4]^{2+}$, and $[Ag(NH_3)_2]^+$ ions on the solution pH and $[NH_3 \cdot H_2O + NH_4^+]_{free}$ for reactions (30)—(33), without considering the influence of additional factors on the system, are shown in Fig. 3.

From Fig. 3, it can be seen that the maximum solubility of $[Cu(NH_3)_2]^+$ and $[Cu(NH_3)_4]^{2+}$ in AA-solutions is achieved at pH = 9.37, which corresponds to a molar fraction of $NH_3 \cdot H_2O$ in the solution of 0.57 (see Fig. 4). As this increases, the pH of the AA-solution and the solubility of AgCl rise, which may lead to undesirable silver losses in the leach solution and reduce the selectivity of decopperization.

However, in the study [41], it was found that increasing the molar fraction of ammonia hydrate in the AA-solution positively affects the transition of oxidized copper into the leach solution. The solubility of oxygen in the solution, which is influenced by the salt content, significantly affects the course of oxidative leaching. The increase in $NH_3 \cdot H_2O$ concentration in the solution has little effect on this parameter, but at a concentration of 1 mol/L $(NH_4)_2SO_4$, the solubility of oxygen in the solution decreases by 35 % compared to its solubility in water [42—44].

Given the above, for effective copper extraction with AA-solutions, a pH range of 9.25—10.00 is recommended, corresponding to a molar fraction of ammonia hydrate $[NH_3 \cdot H_2O] = 50 \div 85$ % (see. Fig. 4) [38].

From Fig. 3, it can be seen that the lowest equilibrium concentration of $[Cu(NH_3)_4]^{2+}$ in the ammonia-ammonium system, under otherwise equal conditions, is observed for reaction (31). The Gibbs free energy values of reactions (13) and (14), which make up the overall reaction (31), are more positive than those for (15) and (16), which make up reaction (32). This indicates that the thermodynamics of $[Cu(NH_3)_4]^{2+}$ complex formation will be least favorable when the AA-solution interacts with copper oxide (CuO). Therefore, the thermodynamically necessary quantity (TNQ) of $NH_3 \cdot H_2O$ and NH_4^+, as well as the minimum excess of $NH_3 \cdot H_2O$ and NH_4^+ over the stoichiometrically necessary quantity (SNQ) for the AA system, must be established for reaction (31). The equilibrium constant, TNQ of $NH_3 \cdot H_2O$ and NH_4^+, and the minimum excess of $NH_3 \cdot H_2O$ and NH_4^+ over SNQ for reaction (31), ensuring 100 % dissolution of Cu, are determined by the following equations [32]:

$$K_a = \frac{\left[[Cu(NH_3)_4]^{2+}\right] \cdot \left[OH^-\right]^2}{[NH_3 \cdot H_2O]^{4x} \cdot [NH_4^+]^{4\cdot(1-x)} \cdot [OH^-]^{4\cdot(1-x)}}, \quad (34)$$

$$TNQ_{NH_3 \cdot H_2O} = SNQ_{NH_3 \cdot H_2O} + \\ + \sqrt[4]{\frac{\left[[Cu(NH_3)_4]^{2+}\right]}{K_a K_d^{4\cdot(1-x)} \cdot 10^{2\cdot(14-pH)}}} \cdot \frac{1}{\left[[Cu(NH_3)_4]^{2+}\right]}, \quad (35)$$

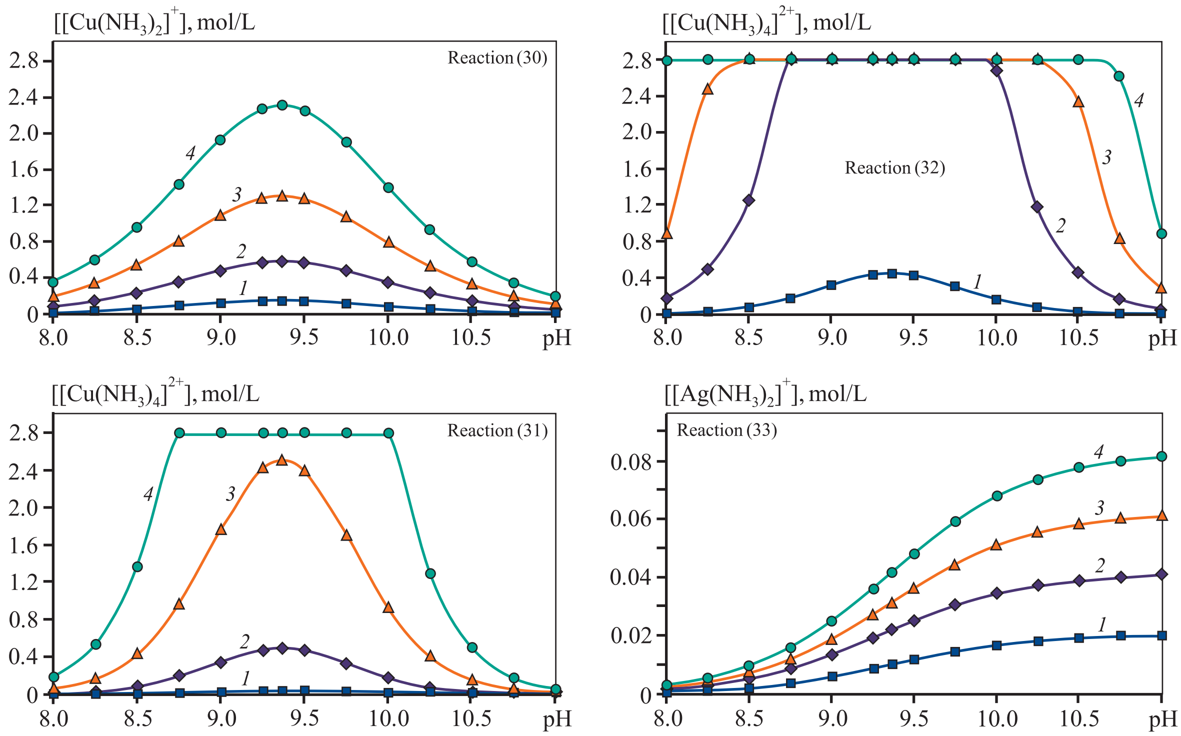

Fig. 3. Dependences of changes in the equilibrium concentrations of $[Cu(NH_3)_2]^+$, $[Cu(NH_3)_4]^{2+}$ and $[Ag(NH_3)_2]^+$ ions on the pH of the solution and $[NH_3{\cdot}H_2O + NH_4^+]_{free}$ for reactions (30)–(33)

$[NH_3{\cdot}H_2O + NH_4^+]_{free}$, mol/L: 0.25 (*1*), 0.50 (*2*), 0.75 (*3*) and 1.0 (*4*)

Рис. 3. Зависимости равновесных концентраций ионов $[Cu(NH_3)_2]^+$, $[Cu(NH_3)_4]^{2+}$ и $[Ag(NH_3)_2]^+$ от pH раствора и $[NH_3{\cdot}H_2O + NH_4^+]_{своб}$ для реакций (30)–(33)

$[NH_3{\cdot}H_2O + NH_4^+]_{своб}$, моль/л: 0,25 (*1*), 0,50 (*2*), 0,75 (*3*) и 1,0 (*4*)

$$\mathrm{TNQ}_{NH_4^+} = \mathrm{SNQ}_{NH_4^+} + \sqrt[4]{\frac{[[Cu(NH_3)_4]^{2+}]K_d^{4x}\cdot 10^{2\cdot(14-\mathrm{pH})}}{K_a}}\cdot\frac{1}{[[Cu(NH_3)_4]^{2+}]}, \quad (36)$$

$$\chi_{NH_3\cdot H_2O} = \chi_{NH_4^+} = \left(\frac{\mathrm{TNQ}}{\mathrm{SNQ}} - 1\right)\cdot 100\ \%, \quad (37)$$

where K_a is the equilibrium constant of reaction (31); $K_d = [NH_4^+][OH^-]/[NH_3{\cdot}H_2O] = 10^{-4.75}$ is the dissociation constant of $NH_3{\cdot}H_2O$ in water [31]); $\mathrm{TNQ}_{NH_3\cdot H_2O}$, $\mathrm{TNQ}_{NH_4^+}$ are the thermodynamically necessary quantities of $NH_3{\cdot}H_2O$ and NH_4^+, mol/mol CuO; $\mathrm{SNQ}_{NH_3\cdot H_2O}$, $\mathrm{SNQ}_{NH_4^+}$ are the stoichiometrically necessary quantities of $NH_3{\cdot}H_2O$ and NH_4^+, mol/mol CuO; χ is the minimum excess of $NH_3{\cdot}H_2O/NH_4^+$ over SNQ for reaction (31).

According to equations (35) and (36), the TNQ of $NH_3{\cdot}H_2O$ and NH_4^+ for reaction (31) depends on the molar concentration of the complex ion $[Cu(NH_3)_4]^{2+}$ in the AA-solution and the equilibrium pH, which, like the equilibrium constant K_a, depends on the molar fraction of $[NH_3{\cdot}H_2O]$ in the solution.

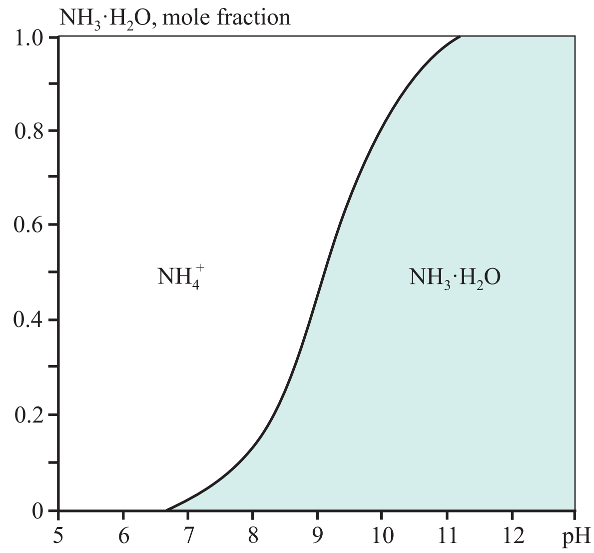

Fig. 4. Dependence of the mole fraction of $NH_3{\cdot}H_2O$ in an ammonia-ammonium solution on pH at an activity coefficient $\gamma_{NH_4^+} = 1$, $t = 25$ °C and $P = 1$ atm [38]

Рис. 4. Зависимость мольной доли $NH_3{\cdot}H_2O$ в аммиачно-аммонийном растворе от pH при коэффициенте активности $\gamma_{NH_4^+} = 1$, $t = 25$ °C и $P = 1$ атм [38]

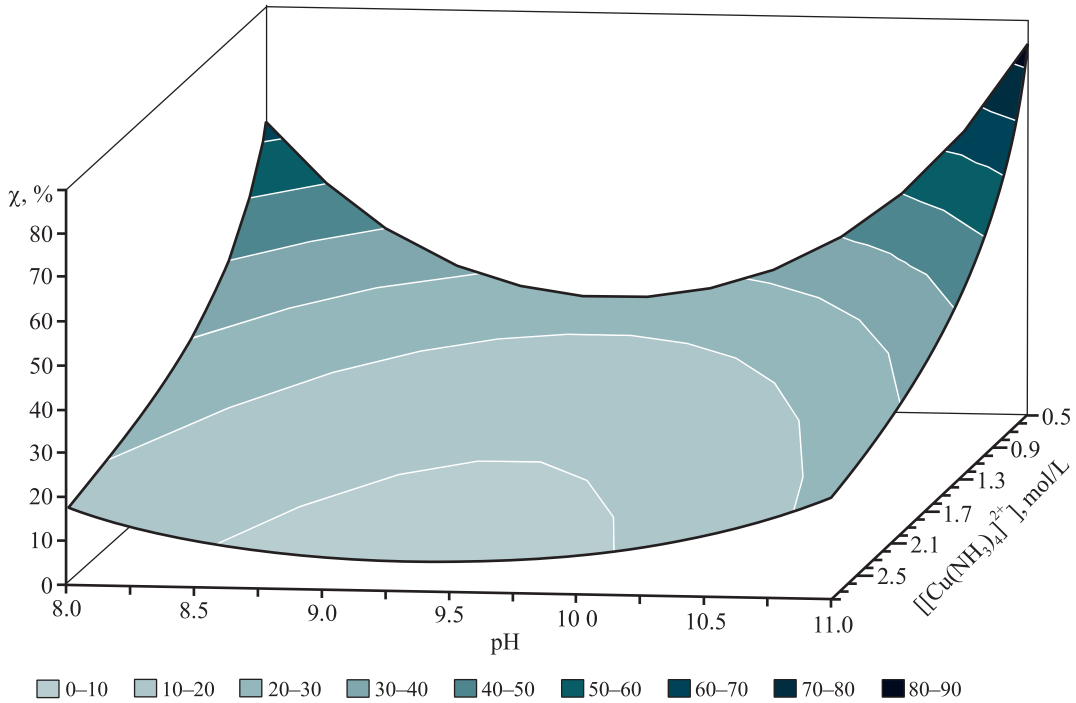

Fig. 5. Surface plot of the dependence of the minimum excess of $NH_3{\cdot}H_2O/NH_4^+$ over SNQ, necessary for the complete progress of reaction (31), on the equilibrium pH of the ammonia-ammonium solution and the concentration of $[Cu(NH_3)_4]^{2+}$

Рис. 5. Поверхность зависимости величины минимального избытка $NH_3{\cdot}H_2O/NH_4^+$ от СНК, необходимого для полного протекания реакции (31), от равновесного pH аммиачно-аммонийного раствора и концентрации в нем $[Cu(NH_3)_4]^{2+}$

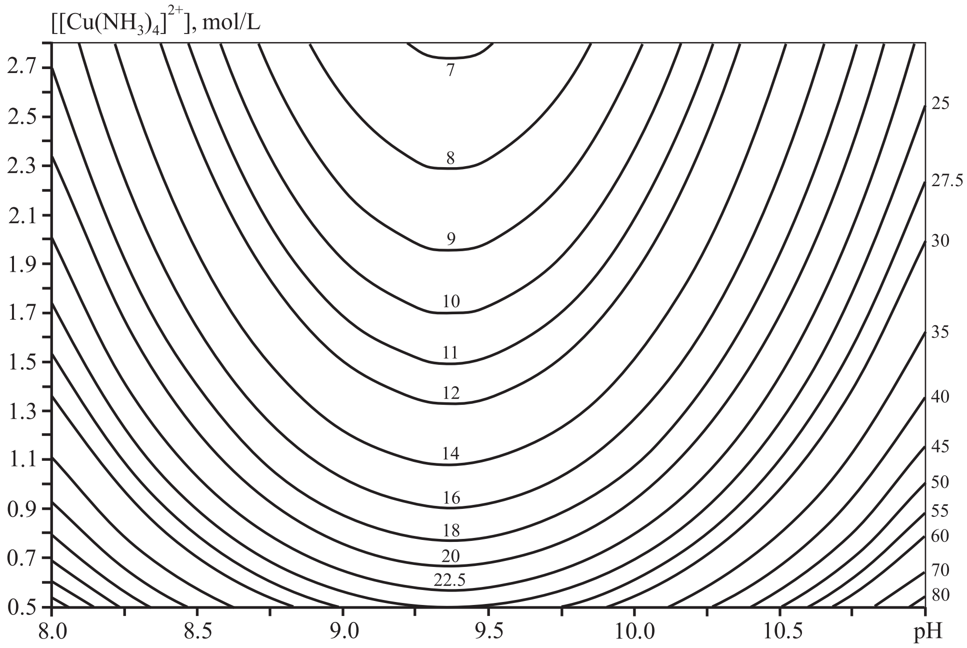

Fig. 6. Nomogram for the theoretical calculation of the minimum excess of $NH_3{\cdot}H_2O/NH_4^+$ over SNQ, necessary for the complete progress of reaction (31), in accordance with the equilibrium pH values of the ammonia-ammonium solution and the concentration of $[Cu(NH_3)_4]^{2+}$

Рис. 6. Номограмма теоретического расчета минимального избытка $NH_3{\cdot}H_2O/NH_4^+$ от СНК, необходимого для полного протекания реакции (31), в соответствии с величинами pH равновесного аммиачно-аммонийного раствора и концентрации в нем $[Cu(NH_3)_4]^{2+}$

Fig. 5 and 6 present, respectively, the surface plot and the nomogram for the theoretical calculation of the minimum excess of $NH_3 \cdot H_2O/NH_4^+$ over SNQ, necessary for the complete progress of reaction (31), depending on the equilibrium pH of the AA-solution and the concentration of $[Cu(NH_3)_4]^{2+}$ in it. It is evident that an increase in the concentration of $[Cu(NH_3)_4]^{2+}$ reduces the required excess of $NH_3 \cdot H_2O$ over SNQ needed for the complete progress of reaction (31). However, the authors of [45] found that as the copper concentration in the ammonia etching solution increases from 0.6 to 1.0 mol/L, the dissolution rate decreases by almost half due to the probable saturation of the diffusion layer with the products of reaction (3) [46]. Therefore, it is advisable to limit the maximum allowable copper concentration in the AA-leaching solution of secondary copper electrorefining slime to no more than 0.8 mol/L for more intensive process progress.

The onset of silver transition during ammonia-ammonium leaching of copper can be monitored by the redox potential (ORP) of the pulp. The standard ORP value for the oxidation of silver in ammonia $[NH_3 \cdot H_2O]$ is +0.367 V, which is significantly higher than that of copper (I) and (II): $E_{[Cu(NH_3)_2]^+/Cu} = -0.120$ V, $E_{[Cu(NH_2)_4]^{2+}/Cu} = -0.065$ V [31]. However, considering the mechanism of copper oxidation in ammonia solutions (reactions (1)—(3)), the ORP of the system may be determined by the half-reaction of oxidation $[Cu(NH_3)_2]^+$ to $[Cu(NH_3)_4]^{2+}$, with a standard value of –0.01 V [35]. According to the Pourbaix diagram for the Cu—NH$_3$—H$_2$O system (Fig. 7), the potential of the half-reaction for the oxidation $[Cu(NH_3)_2]^+$ to $[Cu(NH_3)_4]^{2+}$ remains constant at pH > 9.25, when the molar fraction of $[NH_3 \cdot H_2O]$ in the AA-solution is more than 50 %. Figure 8 presents the calculated dependence of the Cu(II) fraction and the concentration of silver in the AA leaching solution for copper on the ORP of the pulp at equilibrium concentrations of $[NH_3 \cdot H_2O + NH_4^+]_{free}$ ranging from 0.5 to 1.0 mol/L and a molar fraction of $[NH_3 \cdot H_2O]$ in the AA-solution greater than 50 %, without considering the influence of additional factors on the system [30; 31; 35].

According to the data in Fig. 8, the concentration of silver ammine in the solution begins to increase when the ORP of the AA-leaching pulp for copper exceeds 130, 145, and 165 mV for equilibrium concentrations of $[NH_3 \cdot H_2O]$ = 1.00, 0.75 and 0.50 mol/L, respectively. However, based on reactions (27) and (28) (Table 3), there is a high thermodynamic probability of $[Ag(NH_3)_2]^+$ reduction by copper and the complex ion $[Cu(NH_3)_2]^+$. Therefore, to avoid incomplete copper transition from SCER slime into the AA-leach-

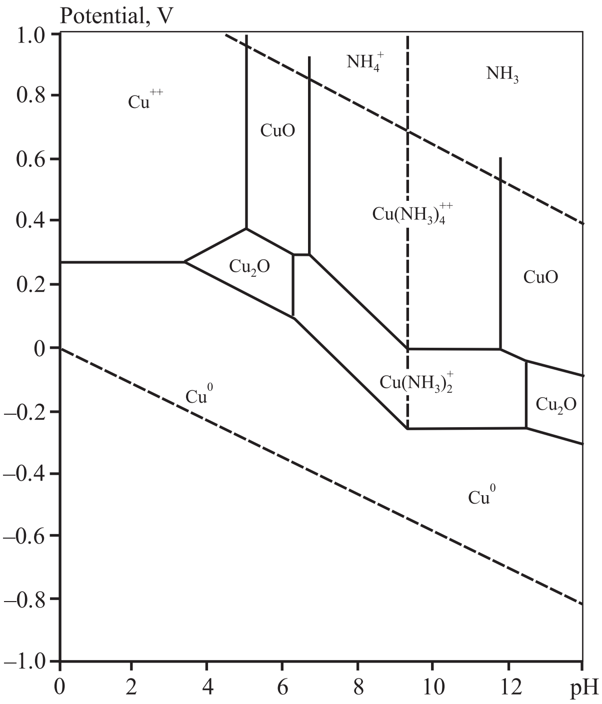

Fig. 7. Pourbaix diagram for the Cu–NH$_3$–H$_2$O system [29]
t = 25 °C, P = 1 atm, activity: $a_{Cu^{2+}} = 1$, $a_{NH_3} = 1$

Рис. 7. Диаграмма Пурбе Cu–NH$_3$–H$_2$O [29]
t = 25 °C, P = 1 атм, активность: $a_{Cu^{2+}} = 1$, $a_{NH_3} = 1$

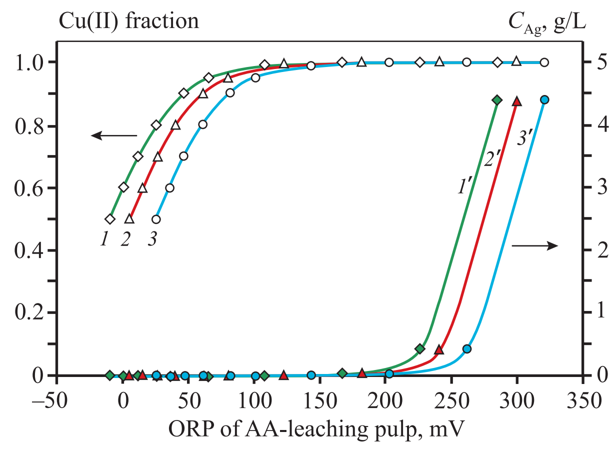

Fig. 8. Calculated dependence of the Cu(II) fraction and silver concentration in the ammonia-ammonium leaching solution for copper on the ORP of the pulp, at equilibrium concentrations of $[NH_3 \cdot H_2O + NH_4^+]_{free}$ = 1.0 mol/L (*1*, *1′*), 0.75 mol/L (*2*, *2′*), and 0.5 mol/L (*3*, *3′*), with a molar fraction of $[NH_3 \cdot H_2O]$ greater than 50 % in the AA solution

Рис. 8. Расчетная зависимость доли Cu(II) и концентрации серебра в растворе аммиачно-аммонийного выщелачивания меди от показателя ОВП пульпы при равновесных концентрациях $[NH_3 \cdot H_2O + NH_4^+]_{своб}$ = 1,0 моль/л (*1*, *1′*), 0,75 моль/л (*2*, *2′*) и 0,5 моль/л (*3*, *3′*) и мольной доли в АА-растворе $[NH_3 \cdot H_2O]$ более 50 %

ing solution, it is advisable to monitor the ORP, which should be maintained at +225 ± 10, +240 ± 10, and +260 ± 10 mV relative to the standard hydrogen electrode (SHE) at $[NH_3 \cdot H_2O+NH_4^+]_{free}$ = 1.00, 0.75, and 0.50 mol/L, respectively.

To assess the objectivity of the conclusions and recommendations made above based on the thermodynamic analysis, technological studies of the AA-leaching process for copper from SCER slime were conducted.

2.2. Technological studies on ammonia-ammonium leaching of copper from secondary copper electrorefining slime in the $-NH_3 \cdot H_2O-(NH_4)_2SO_4-H_2O-O_2$ system

According to the results of the thermodynamic analysis, the following regime is recommended for leaching copper from SCER slime (**Method I**): Θ = 4 mol/mol (corresponding to an initial pH = 9.55); L/S = 12 : 1 (to obtain a leach solution with a copper concentration of 0.72 ± 0.01 mol/L); χ = 20 % of the stoichiometrically necessary quantity (SNQ) for reaction (31), and an air flow rate of 190 ± 2 L/h until the ORP reaches +260 ± 10 mV relative to the SHE (52 ± 10 mV relative to the silver chloride electrode (SCE)) at an equilibrium concentration of $[NH_3 \cdot H_2O+NH_4^+]_{free}$ = = 0.58 mol/L.

Experimental results show that the recommended conditions for the decopperization of SCER slime using an ammonia-ammonium solution ensure the absence of silver in the leach solution at a pulp ORP of +269 mV relative to the SHE and +61 mV relative to the SCE, with a copper recovery rate of 99.4 %.

To manage the decopperization process of SCER slime in the slime—$NH_3 \cdot H_2O$—$(NH_4)_2SO_4$—H_2O—O_2 system, it is necessary to clarify the mechanism and kinetic patterns of the process.

2.3. Comprehensive studies of the kinetics of the ammonia-ammonium leaching process for secondary copper electrorefining slime in the slime$-NH_3 \cdot H_2O-(NH_4)_2SO_4-H_2O-O_2$ system

To study the kinetics of leaching, model equations are applied that describe processes occurring in both diffusion and kinetic domains [47—53], using equations such as the "shrinking sphere" model, Ginstling—Brounshtein, Erofeev—Kolmogorov, and others. However, the first two are only suitable for describing the leaching rate of monodisperse material with particles of the same shape [30], and the Erofeev—Kolmogorov equation is not applicable for determining the process regime [54]. Therefore, the identification of the leaching regime was based on the values of activation energy and reaction order, determined using Method II, presented above in Section 1.

The complexation reaction of copper ammine (31) is reversible, but its equilibrium constant at pH = 9.55 in the system and Θ = 4 mol/mol is K_a = 92.44 (see Table 4), allowing the copper leaching process from SCER slime to be considered practically irreversible. Then the formal kinetics equation for the investigated copper leaching process from slime into the solution is:

$$\frac{d\alpha}{d\tau} = ke^{-E_a/(RT)} C^{n_1}_{\sum[NH_3 \cdot H_2O]+[NH_4^+]} P^{n_2}_{O_2} S, \qquad (38)$$

where k is a constant factor; E_a is the apparent activation energy of the chemical process, J/mol; R = = 8.31 J/(mol·K) is the universal gas constant; T is the process temperature, K; $C_{\Sigma[NH_3 \cdot H_2O]+[NH_4^+]}$ is the total concentration of $[NH_3 \cdot H_2O]$ + $[NH_4^+]$ in the solution; P_{O_2} is the oxygen pressure; n_1 is the reaction order for the $NH_3 \cdot H_2O$—$(NH_4)_2SO_4$; n_2 is the reaction order for oxygen from the air; S is the surface area of the slime particles, dm^2/g.

The apparent activation energy and reaction orders are parameters dependent on the nature of the interaction between components in the system. Investigating the influence of temperature and concentrations on the leaching rate while stabilizing other characteristics will allow their values to be determined and conclusions drawn about the regime of the process.

Fig. 9 shows the dependence of $\ln(d\alpha/d\tau)$ on $\ln C_{\Sigma[NH_3 \cdot H_2O]+[NH_4^+]}$ for the AA-leaching of copper from SCER slime at a total concentration of $[NH_3 \cdot H_2O]$ + $[NH_4^+]$ ranging from 0.5 to 3.5 mol/L, with an L/S ratio of 100 : 1, temperature of 24 °C, $[NH_3 \cdot H_2O]$: $[(NH_4)_2SO_4]$ = 4 mol/mol (corresponding to pH = 9.55), and an air flow rate of v_{air} = 95±2 L/h. The nature of this dependence indicates a change in the leaching regime around $C_{\Sigma[NH_3 \cdot H_2O]+[NH_4^+]}$ = 1.5 mol/L. It is suggested that below this concentration, the leaching process occurs in the external diffusion region with a reaction order $n_1 \approx 0.91 \approx 1$, while at $C_{\Sigma[NH_3 \cdot H_2O]+[NH_4^+]}$ 1.5 mol/L, the process shifts to a kinetic regime, where the rate is limited by the adsorption of reagents on the surface of solid particles, with an apparent reaction order $n_1 = 0.24$.

Accordingly, the determination of the activation energy was carried out on both sides of the transition region: at a total concentration $C_{\Sigma[NH_3 \cdot H_2O]+[NH_4^+]}$ = 1 and 2 mol/L. The study results are presented in Fig. 10 as the dependence of $\ln(d\alpha/d\tau)$ on $1/T$, with temperature

Table 4. **Equilibrium constants values for reaction (31) at different pH levels**

Таблица 4. Значения констант равновесия реакции (31) с учетом pH

pH	8.75	9.00	9.25	9.50	9.55	9.75	10.00	10.25
K_a	27.82	75.91	122.08	103.00	92.44	48.98	16.02	4.4

ranging from 15 to 45 °C, where the upper limit is justified by increased ammonia losses with further temperature increase [24]. It can be seen that in both cases, the apparent activation energy of the process was 5 ± ± 0.25 kJ/mol, which is consistent with the assumptions about the AA-leaching process of copper proceeding in the external diffusion regime at $C_{\Sigma[NH_3 \cdot H_2O]+[NH_4^+]}$ = = 1 mol/L and in the kinetic regime with the rate limited by reagent adsorption on the surface of solid particles at $C_{\Sigma[NH_3 \cdot H_2O]+[NH_4^+]} = 2$ mol/L.

In addition to the ammonia and ammonium salts involved in forming complexes, oxygen from the air is used as a reagent in the slime—$NH_3 \cdot H_2O$—$(NH_4)_2SO_4$—H_2O—O_2 system. However, due to the difficulty of maintaining a certain concentration of oxygen in the solution, this influence was assessed by increasing the air flow rate in the leaching system from 18 to 156 L/h. It was found that changing the air flow rate in the studied range hardly affects the process rate. It is evident that across the entire range, the rate of oxygen supply to the leaching system was significantly higher than its consumption rate, resulting in a constant dissolved oxygen concentration.

For a more unambiguous interpretation of the kinetic study results, a literature review was conducted. It was found in [55] that the diffusion coefficient of copper ammine in solution decreases from $6 \cdot 10^{-6}$ to $2.5 \cdot 10^{-6}$ cm^2/s as the copper concentration in the AA-solution increases from 0.5 to 10 g/L, and further increases in copper concentration to 80 g/L reduce it to $1{,}67 \cdot 10^{-6}$ cm^2/s. These factors, along with the decrease in oxygen solubility in solutions as their salt content increases, can significantly reduce the overall copper transition rate into the ammonia-ammonium solution, as indicated by the results in [45]. Only the application of autoclave ammonia leaching of copper at an oxygen pressure of 7.8 atm promotes the transition from the diffusion regime to the kinetic regime, where the rate-limiting step becomes the formation and dissolution of copper ammines [20; 23]. This confirms the advisability of limiting the final copper concentration to 0.8 mol/L, as recommended based on the thermodynamic analysis.

In [56], it was established that reaction (1) proceeds in the external diffusion region of reaction if the concentration of dissolved oxygen is more than 280 times

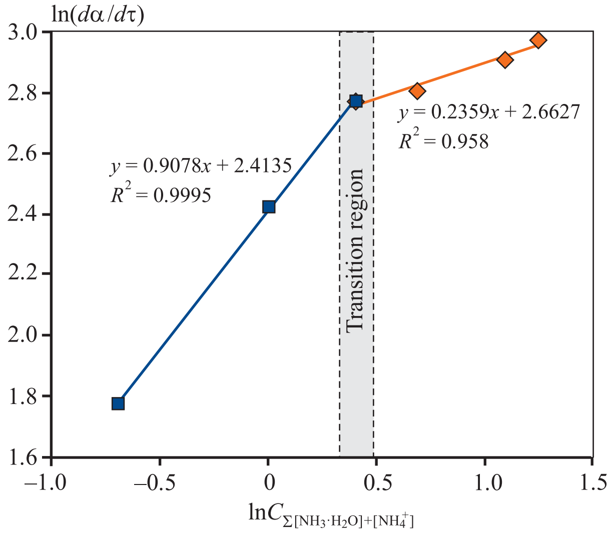

Fig. 9. Dependence of $\ln(d\alpha/d\tau)$ on $\ln C_{\Sigma[NH_3 \cdot H_3O] + [NH_4^+]}$ for ammonia-ammonium leaching of copper from secondary copper electrolytic refining slime

L : S = 100 : 1; t = 24 °C; $[NH_3 \cdot H_2O] : [(NH_4)_2SO_4]$ = 4 mol/mol (corresponds to pH = 9.55); v_{air} = 95±2 L/h)

Рис. 9. Зависимость $\ln(d\alpha/d\tau)$ от $\ln C_{\Sigma[NH_3 \cdot H_3O] + [NH_4^+]}$ для аммиачно-аммонийного выщелачивания меди из шлама ЭРВМ

Ж : Т = 100 : 1; t = 24 °C; $[NH_3 \cdot H_2O] : [(NH_4)_2SO_4]$ = 4 моль/моль (pH = 9,55); $v_в$ = 95±2 л/ч

lower than that of ammonia; otherwise, the rate-limiting step becomes the chemical interaction between the Cu^+ ion and ammonia. Reaction (1) can only determine the overall process rate at a low concentration of Cu(II) in the solution, but as it increases, the oxidation of metallic copper also begins to proceed through reaction (3), where the main electron carriers in the system become $[Cu(NH_3)_4]^{2+}$ ions [21; 24; 57].

In [58], it was found that the autocatalytic dissolution of copper by reaction (3) limits its dissolution in ammonia, while reaction (2) proceeds fairly quickly. This may be due to the use of ammonia solution in the absence of ammonium salts, which promotes the formation of copper hydroxocomplexes and hydroxides on the particle surfaces, complicating the mechanism of oxidative dissolution of copper in ammonia [59]. A similar conclusion is presented by the authors of [22], who consider the rate-limiting step to be the removal of reaction (2) products due to the formation of copper hydroxide on

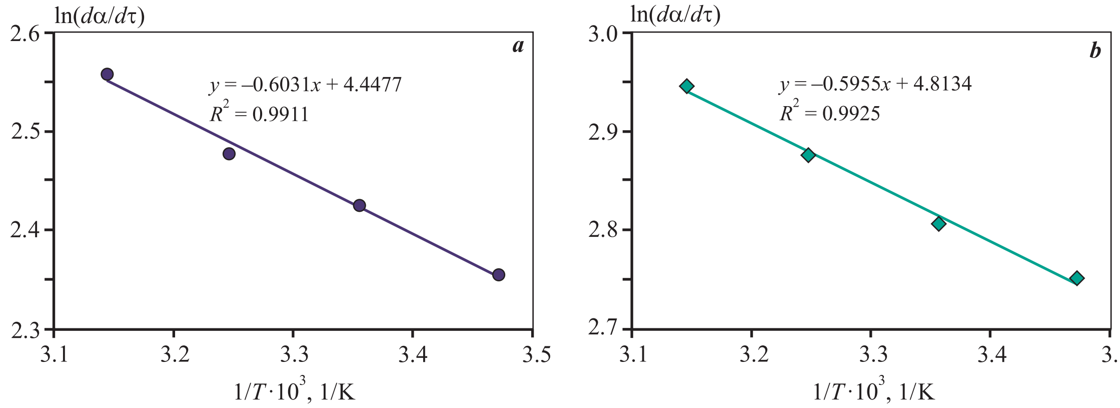

Fig. 10. Dependence of $\ln(d\alpha/d\tau)$ on $1/T$ for ammonia-ammonium leaching of copper from secondary copper electrolytic refining slime
L : S = 100 : 1; $[NH_3{\cdot}H_2O] : [(NH_4)_2SO_4]$ = 4 mol/mol; v_{air} = 95±2 L/h) and total concentration $C_{\Sigma[NH_3 \cdot H_2O] + [NH_4^+]}$ = 1 mol/L (***a***) and 2 (***b***)

Рис. 10. Зависимость $\ln(d\alpha/d\tau)$ от $1/T$ процесса аммиачно-аммонийного выщелачивания меди из шлама ЭРВМ
Ж : Т = 100 : 1; $[NH_3{\cdot}H_2O] : [(NH_4)_2SO_4]$ = 4 моль/моль; $v_в$ = 95±2 л/ч) и $C_{\Sigma[NH_3 \cdot H_2O] + [NH_4^+]}$ = 1 моль/л (***a***) и 2 моль/л (***b***)

the Cu particle surfaces because of ammonia deficiency in the reaction zone. The formation of $Cu(OH)_2$ also occurs when oxidized copper dissolves in ammonium salts without the addition of ammonia [60]. In [60], it was established that the activation energy for the dissolution of oxidized copper ore in an NH_4Cl solution is 71 kJ/mol.

The use of ammonia-ammonium solutions significantly reduces the activation energy of the copper dissolution process. For example, in [24], during copper leaching with a solution containing copper, free ammonia, and ammonium sulfate in amounts of 0.2, 2.4, and 0.5 mol/L, respectively, the E_a was 22.8 kJ/mol, and increasing the Cu^{2+} content in the solution increased the copper dissolution rate. The authors consider the rate-limiting step to be the removal of reaction (2) products. In [46; 61], E_a values of 23.3 and 22.5 kJ/mol were obtained for the leaching of copper from oxidized ore with a solution containing 0.5 mol/L $NH_3{\cdot}H_2O$ and 2 mol/L NH_4Cl, and the dissolution of copper from printed circuit boards in a solution composed of $4NH_3{\cdot}H_2O + 1(NH_4)_2SO_4 + 0.63Cu(II)$, finding that the processes are limited by the internal diffusion of the reagent through a layer of non-reactive impurities. The reduction in activation energy when using the ammonia-ammonium leaching system is confirmed in [62], where, during the dissolution of malachite ore in an AA-solution (0.74 mol/L $NH_3{\cdot}H_2O$), CO_3^{2-} ions are released into it, forming $(NH_4)_2CO_3$. In this case, the activation energy is 22.3 kJ/mol, and the reaction order for ammonia is 1, indicating that the process occurs in the diffusion domain. The activation energy for the dissolution of malachite ore in an AA-solution (5 mol/L $NH_3{\cdot}H_2O$ and 0.3 mol/L $(NH_4)_2CO_3$) decreases to 15 kJ/mol [63]. The minimum value of E_a = 3.8 kJ/mol was obtained during the leaching of CuO from pyrite cinder with a solution composed of: $7.2NH_3{\cdot}H_2O +$ $+ 3.8NH_4Cl$ mol/L [64].

From the above, it follows that the activation energy of the copper leaching process decreases as the proportion of oxidized copper in the initial raw material increases, as confirmed by the results of the kinetic studies conducted on copper leaching from SCER slimes. The dissolution of copper in the presence of oxidized forms Cu^+ and Cu^{2+} through reactions (2) and (3) may likely be complicated by the presence of various forms of copper ammine complexes and other compounds.

Based on the above, it can be assumed that AA-leaching of copper from SCER slime at a concentration of the ammonia-ammonium buffer system less than 1.5 mol/L proceeds via reactions

$$0.5Cu_2O_{(s)} + 2NH_3{\cdot}H_2O_{(aq)} = \\ = [Cu(NH_3)_2]^+_{(aq)} + OH^-_{(aq)} + 1.5H_2O, \quad (39)$$

$$[Cu(NH_3)_2]^+_{(aq)} + 0.25O_2 + OH^-_{(aq)} + 2.5H_2O = \\ = Cu(OH)_{2(s)} + 2NH_3{\cdot}H_2O_{(aq)}, \quad (40)$$

$$Cu(OH)_{2(s)} + 4NH_3{\cdot}H_2O_{(aq)} = \\ = [Cu(NH_3)_4]^{2+}_{(aq)} + 2OH^-_{(aq)} + 4H_2O, \quad (41)$$

$$[Cu(NH_3)_4]^{2+}_{(aq)} + Cu_{(s)} = 2[Cu(NH_3)_2]^+_{(aq)}, \quad (42)$$

and is accompanied by the formation of an intermediate phase—copper hydroxide, which forms an intradiffusion

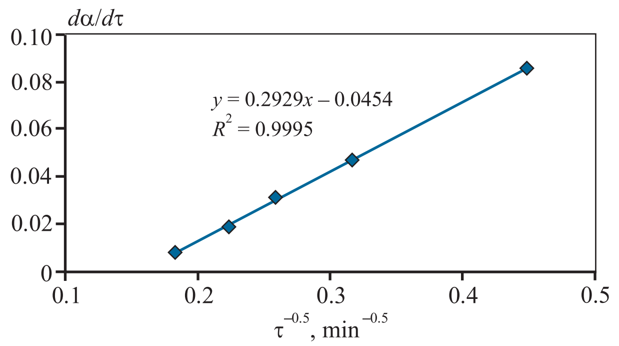

Fig. 11. Dependence of $d\alpha/d\tau$ on $\tau^{-0,5}$

$C_{\Sigma[NH_3 \cdot H_2O] + [NH_4^+]} = 1$ mol/L and $t = 25$ °C

Рис. 11. Зависимость $d\alpha/d\tau$ от $\tau^{-0,5}$

$C_{\Sigma[NH_3 \cdot H_2O] + [NH_4^+]} = 1$ моль/л, $t = 25$ °C

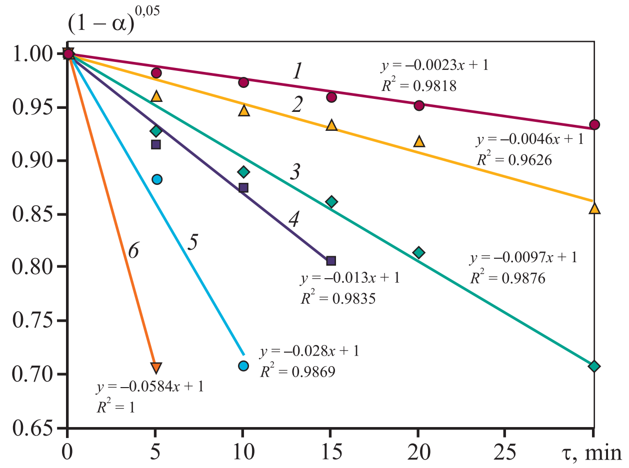

Fig. 12. Dependence of $(1 - \alpha)^{(1 - \beta)}$ on the duration copper leaching at $\beta = 0.95$ and $C_{\Sigma[NH_3 \cdot H_3O] + [NH_4^+]}$, mol/L: 0.5 (***1***), 1.0 (***2***), 1.5 (***3***), 2.0 (***4***), 3.0 (***5***) and 3.5 (***6***)

L : S = 100 : 1; $t = 24$ °C; $[NH_3 \cdot H_2O] : [(NH_4)_2SO_4] = 4$ mol/mol; $v_{air} = 95 \pm 2$ L/h

Рис. 12. Зависимость $(1 - \alpha)^{(1 - \beta)}$ от продолжительности выщелачивания меди при $\beta = 0{,}95$ и $C_{\Sigma[NH_3 \cdot H_3O] + [NH_4^+]}$, моль/л: 0,5 (***1***), 1,0 (***2***), 1,5 (***3***), 2,0 (***4***), 3,0 (***5***) и 3,5 (***6***)

Ж : Т = 100 : 1; $t = 24$ °C; $[NH_3 \cdot H_2O] : [(NH_4)_2SO_4] = 4$ моль/моль; $v_в = 95 \pm 2$ л/ч

layer according to reaction (40) and simultaneously disappears according to reaction (41), as evidenced by the linear nature of the dependence of $d\alpha/d\tau$ on $\tau^{-0.5}$ at a buffer solution concentration of 1 mol/L and a leaching process temperature of 25 °C (Fig. 11).

The leaching rate of copper from SCER slime is directly proportional to the surface area of the particles, which changes during the process. The dependence of the surface area on the degree of leaching can be described by a power function $S = S_0(1 - \alpha)^{\beta}$. By integrating equation (38) considering the consumption of the ammonia-ammonium buffer system for the formation of $[Cu(NH_3)_4]^{2+}$, the dependence of the degree of copper extraction from slime on the leaching duration was obtained (43):

$$(1-\alpha)^{1-\beta} = 1-(1-\beta)ke^{-E_a/(RT)} \times$$
$$\times S_0\left(C_{\Sigma[NH_3 \cdot H_2O]+[NH_4^+]} - vG_0\alpha\right)^{n_1}\tau, \qquad (43)$$

where S_0 is the initial specific surface area of the particles, dm^2/g; β is the reaction order with respect to the solid; n_1 is the reaction order for the $NH_3 \cdot H_2O$—$(NH_4)_2SO_4$, buffer system, equal to 0.24 and 0.91 for $C_{\Sigma[NH_3 \cdot H_2O]+[NH_4^+]} > 1.5$ mol/L and $C_{\Sigma[NH_3 \cdot H_2O]+[NH_4^+]} <$ < 1.5 mol/L, respectively; G_0 is the mass of copper in the slime, g; $\nu = 0.63$ mol/(L·g) is the change in reagent concentration corresponding to the transition of a unit mass of leached copper from the slime into solution.

The value of the parameter β depends on the nature of the leached material: for monodisperse material with particles of the same shape, they are equal to 2/3, 1/2, and 0 for isometric, columnar, and flat particles, respectively, while in the most common case of leaching polydisperse material with particles of different shapes, β approaches 1 [30]. Fig. 12 shows the results of the mathematical processing of the data from the study of the kinetics of copper leaching from SCER slime using equation (43) with a β value of 0.95, which ensures linear dependencies. It can be seen that the high level of linear approximation (>0.95) for the linear dependencies of $(1 - \alpha)^{(1-\beta)}$ on the process duration, achieved at $\beta = 0.95$, corresponds to a constant factor of 0.0096 ± ± 0.0002. Thus, the kinetics of copper leaching from SCER slime, depending on the process duration, with a ratio of $[NH_3 \cdot H_2O] : [(NH_4)_2SO_4] = 4$ mol/mol (pH = = 9.55) and an ammonia-ammonium buffer system concentration greater than 1.5 and less than 1.5 mol/L, can be described by the equations:

$$\frac{d\alpha}{d\tau} = 0.0096e^{-5000/(RT)} \times$$
$$\times \left(C_{\Sigma[NH_3 \cdot H_2O]+[NH_4^+]} - 0.63G_0\alpha\right)^{0.24} S_0(1-\alpha)^{0.95}, \qquad (44)$$

$$\frac{d\alpha}{d\tau} = 0.0096e^{-5000/(RT)} \times$$
$$\times \left(C_{\Sigma[NH_3 \cdot H_2O]+[NH_4^+]} - 0.63G_0\alpha\right)^{0.91} S_0(1-\alpha)^{0.95}, \qquad (45)$$

Conclusions

1. Comprehensive studies of secondary copper electrolytic refining slime revealed an elevated copper content of 55.12 %, underscoring the importance of finding an effective method for extracting copper from this slime. The presence of the $Cu_4(OH)_6SO_4$ phase, corresponding to brochantite, was detected, for which there is no existing data regarding its occurrence in slimes. The total silver content in SCER slime is 2.43 %, with 69.1 % of the silver in metallic form, and the remainder as chloride. The contents of associated components $PbSO_4$, $BaSO_4$, and SnO_2 are 13.52 %, 9.33 %, and 4.73 %, respectively.

2. Based on thermodynamic analysis, the potential for effective and selective copper extraction from SCER slime by a hydrometallurgical method in an ammoniaammonium system without heating was established. The composition of the initial reagent solutions, including ammonia hydrate $NH_3{\cdot}H_2O$ and ammonium sulfate $(NH_4)_2SO_4$, their consumption, as well as the characteristics of the leach pulp, were determined.

3. Technological studies confirmed the effectiveness of the recommended conditions for low-temperature ammonia-ammonium leaching (Θ = 4 mol/mol, χ = = 20 % of the SNQ for reaction (31)) and the process control criteria ([$[Cu(NH_3)_4]^{2+}$] = 0,72 ± 0,01 mol/L and pulp ORP +260 ± 10 mV relative to SHE (52 ± 10 mV relative to SCE), which ensure 99.4 % copper extraction and prevent silver from dissolving into the leach solution.

4. Kinetic studies of the copper leaching process from SCER slime determined the apparent activation energy to be 5 ± 0.25 kJ/mol within the temperature range of 15 to 45 °C, at total buffer system concentrations of $[NH_3{\cdot}H_2O] + [NH_4^+]$ of 1 and 2 mol/L. The reaction order at a temperature of 24 ± 1 °C was found to be 0.24 ± 0.02 and 0.91 ± 0.05 for $[NH_3{\cdot}H_2O] + [NH_4^+]$ greater than 1.5 mol/L and less than 1.5 mol/L, respectively. A transition in the leaching regime from external diffusion-controlled to kinetic-controlled, with the rate limited by reagent adsorption on the surface of solid particles, was observed as $[NH_3{\cdot}H_2O] + [NH_4^+]$ increased from 0.5—1.5 to 1.5—3.5 mol/L at a temperature of 24 ± 1 °C. The formal kinetics equation for the studied process was determined.

References

1. International Copper Study group (Monthly Press Release). Lisbon, 2024. URL: https://icsg.org/press-releases/# (accessed: 01.03.2024).
2. International Copper Study group (Yearbook Press Release). Lisbon, 2023. URL: https://icsg.org/press-releases/# (accessed: 01.03.2024).
3. International Copper Study group (The World Copper Factbook 2023). Lisbon, 2023. URL: https://icsg.org/copper-factbook/ (accessed: 01.03.2024).
4. Hunt A.J, Matharu A.S., King A.H., Clark J.H. The importance of elemental sustainability and critical element recovery. *Green Chemistry*. 2015;17:1949—1950. https://doi.org/10.1039/C5GC90019K
5. Copper Market Analysis: The pathway for copper to 2030. RFC Ambrian, 2022. 30 p.
6. Vanyukov A.V., Utkin N.I. Complex processing of copper and nickel raw materials. Chelyabinsk: Metallurgiya, Chelyabinskoe otdelenie, 1988. 432 p. (In Russ.).
Ванюков А.В., Уткин Н.И Комплексная переработка медного и никелевого сырья. Челябинск: Металлургия. Челябинское отд-ние, 1988. 432 с.
7. Mastyugin S.A., Nabojchenko S.S., Lastochkina M.A. Electrolytic copper refining slimes Ekaterinburg: UrFU, 2013. 258 p. (In Russ.).
Мастюгин С.А., Набойченко С.С., Ласточкина М.А. Шламы электролитического рафинирования меди. Екатеринбург: УрФУ, 2013. 258 с.
8. Schlesinger M.E., Sole K.C., Davenport W.G., Alvear Flores G.R.F. Extractive metallurgy of copper. Sixth edition. Amsterdam: Elsevier Ltd., 2022. 572 p.
9. Adams M.D. Advances in gold ore processing. Amsterdam: Elsevier Ltd., 2005. 1028 p.
10. Tesfaye F., Lindberg D., Hamuyuni J., Taskinen P., Hupa L. Improving urban mining practices for optimal recovery of resources from e-waste. *Minerals Engineering*. 2017;111:209—221.
https://doi.org/10.1016/j.mineng.2017.06.018
11. Cooper W.C. The treatment of copper refinery anode slimes. *JOM*. 1990;42:45—49.
https://doi.org/10.1007/BF03221054
12. Habashi F. Handbook of extractive metallurgy. Vol. II: Primary metals, secondary metals, light metals. Weinheim, 1997.
13. Petrov G.V., Belen'kiy A.M., Andreev Yu.V., Kovalev V.N. Current status and technological prospects for processing electrolytic copper refining slimes. *Trudy SPbGTU*. 2009;510:70—73. (In Russ.).
Петров Г.В., Беленький А.М., Андреев Ю.В., Ковалев В.Н. Современное состояние и технологические перспективы переработки медеэлектролитных шламов. *Труды СПбГТУ*. 2009;510:70—73.
14. Lyapishchev Yu.B. Current status of processing electrolytic copper refining slimes. *Zapiski Gornogo instituta*. 2006;2(167):245—247. (In Russ.).
Ляпищев Ю.Б. Современное состояние переработки электролитных шламов медного производства. *Записки Горного института*. 2006;2(167):245—247.
15. Information and technical guide to the best available technologies ITS 14-2020 "Production of precious

metals". Moscow: Buro NDT, 2020. 153 p. (In Russ.).
Информационно-технический справочник по наилучшим доступным технологиям ИТС 14-2020 «Производство драгоценных металлов». М.: Бюро НДТ, 2020. 153 с.

16. Chanturia V.A., Shadrunova I.V., Gorlova O.E. Innovative processes of deep and complex processing of technogenic raw materials in the context of new economic challenges. In: *Effective technologies for the production of non-ferrous, rare and precious metals:* Materials of Int. Scientific-Practical Conf. Almaty, 2018. P. 7–13. (In Russ.).
Чантурия В.А, Шадрунова И.В., Горлова О.Е. Инновационные процессы глубокой и комплексной переработки техногенного сырья в условиях новых экономических вызовов. В сб.: *Эффективные технологии производства цветных, редких и благородных металлов:* Матер. Междунар. научно-практ. конф. Алматы, 2018. С. 7—13.

17. Romanova O.A. Sirotin D.V. Digital support for the metallurgical complex of the Urals in the context of the development of industry 4.0. In: *Russian regions in the focus of change:* Collection of reports of the XIV Inter. Conf. (Yekaterinburg, November 14–16, 2019). Ekaterinburg: UMC UPI, 2020. P. 729–732. (In Russ.).
Романова О.А. Сиротин Д.В. Цифровое обеспечение металлургического комплекса Урала в условиях развития индустрии 4.0. В сб.: *Российские регионы в фокусе перемен:* Сб. докл. XIV Междунар. конф. (г. Екатеринбург, 14—16 нояб. 2019 г.). Екатеринбург: УМЦ УПИ, 2020. С. 729—732.

18. Lobanov V.G., Naumov K.D., Korolev A.A. Theory of copper-electrolyte slimes decoppering in the presence of hydrogen peroxide. *Materials Science Forum.* 2019;946:585—590.
https://doi.org/10.4028/www.scientific.net/MSF.946.585

19. Naboychenko S.S., Karelov S.V., Mamyachenkov S.V., Zauzolkov I.V. Processing of copper-containing scrap and waste with complex extraction of non-ferrous metals. Moscow: TsNIITsMEI, 1990. 27 p. (In Russ.).
Набойченко С.С., Карелов С.В., Мамяченков С.В., Заузолков И.В. Переработка медьсодержащих лома и отходов с комплексным извлечением цветных металлов. М.: ЦНИИЦМЭИ, 1990. 27 с.

20. Naboychenko S.S., Smirnov V.I. Hydrometallurgy of copper. Moscow: Metallurgiya, 1974. 272 p. (In Russ.).
Набойченко С.С., Смирнов В.И. Гидрометаллургия меди. М.: Металлургия, 1974. 272 с.

21. Lu Benjamin C.-Y., Graydon W.F. Rates of copper dissolution in aqueous ammonium hydroxide solutions. *Journal of the American Chemical Society.* 1955;77(23):6136—6139.
https://doi.org/10.1021/ja01628a012

22. Lane R.W., McDonald H.J. Kinetics of the reaction between copper and aqueous ammonia. *Journal of the American Chemical Society.* 1946;68(9):1609—1704.
https://doi.org/10.1021/ja01213a005

23. Halpern J. Kinetics of the dissolution of copper in aqueous ammonia. *Journal of The Electrochemical Society.* 1953;100(10):421—428.
https://doi.org/10.1149/1.2780873

24. Klein S.E., Karelov S.V., Chemezova T.A., Doroshkevich A.P. Kinetics of oxidation of metallic copper by cupriions in ammonia sulfate solutions. *Izvestiya. Non-Ferrous Metallurgy.* 1978;(1):27—31. (In Russ.).
Кляйн С.Э., Карелов С.В., Чемезова Т.А., Дорошкевич А.П. Кинетика окисления металлической меди куприионами в аммиачно-сульфатных растворах. *Известия вузов. Цветная металлургия.* 1978;(1):27—31.

25. Naboychenko S.S., Bogdashev V.F. Kinetics of dissolution of copper-zinc alloys in an ammonia environment at elevated temperatures at elevated temperatures and oxygen pressure. *Zhurnal prikladnoi khimii.* 1976;49(5):1028—1031. (In Russ.).
Набойченко С.С., Богдашев В.Ф. Кинетика растворения медно-цинковых сплавов в аммиачной среде при повышенных температурах при повышенных температурах и давлении кислорода. *Журнал прикладной химии.* 1976; 49(5):1028—1031.

26. Naboychenko S.S., Bogdashev V.F., Khudyakov I.F. Study of the kinetics of dissolution of Cu—Sn alloys in sulfuric acid and ammonia solutions at elevated temperatures and oxygen pressure. *Izvestiya. Non-Ferrous Metallurgy.* 1975;6:35—39. (In Russ.).
Набойченко С.С., Богдашев В.Ф, Худяков И.Ф. Исследование кинетики растворения сплавов Cu—Sn в сернокислых и аммиачных растворах при повышенных температурах и давлении кислорода. *Известия вузов. Цветная металлургия*. 1975;6:35—39.

27. Batsaikhan Sh., Naboychenko S.S. Indicators of ammonia autoclave leaching of copper polymetallic concentrate. *Izvestiya. Non-Ferrous Metallurgy.* 1992;(5/6):38—40. (In Russ.).
Батсайхан Ш., Набойченко С.С. Показатели аммиачного автоклавного выщелачивания медного полиметаллического концентрата. *Известия вузов. Цветная металлургия*. 1992;(5/6):38—40.

28. Zheleznova A.N., Ilyin A.A., Ilyin A.P., Smirnov N.N., Komarov Yu.M. Low-temperature oxidation of copper in the process of mechanochemical activation in a steam-ammonia-oxygen environment. *Izvestiya vuzov. Khimiya i khimicheskaya tekhnologiya*. 2013;56(4):43—47. (In Russ.).
Железнова А.Н., Ильин А.А., Ильин А.П., Смирнов Н.Н., Комаров Ю.М. Низкотемпературное окисление меди в процессе механохимической

активации в паро-аммиачно-кислородной среде. *Известия вузов. Химия и химическая технология.* 2013;56(4):43—47.
29. Meng X., Han K.N. The principles and applications of ammonia leaching of metals: A review. *Mineral Processing and Extractive Metallurgy Review.* 1996;16:23—61. https://doi.org/10.1080/08827509608914128
30. Voldman G.M., Zelikman A.N. Theory of hydrometallurgical processes: Textbook manual for universities. 4th ed., revised. and additional Moscow: Intermet Engineering, 2003. 464 p. (In Russ.).
Вольдман Г.М., Зеликман А.Н. Теория гидрометаллургических процессов: Учеб. пособие для вузов. 4-е изд., перераб. и доп. М.: Интермет Инжиниринг, 2003. 464 с.
31. Lidin R.A., Andreeva L.L., Molochko V.A. Constants of inorganic substances: reference book. Moscow: Drofa, 2008. 685 p. (In Russ.)
Лидин Р.А., Андреева Л.Л., Молочко В.А. Константы неорганических веществ: справочник. М.: Дрофа, 2008. 685 с.
32. Medvedev A.S., Bogatyreva E.V. Theory of hydrometallurgical processes: Theory and practice of hydrometallurgical processes underlying the production of nonferrous and rare metals: Textbook. allowance. Moscow: MISIS, 2009. 347 p. (In Russ.).
Медведев А.С., Богатырева Е.В. Теория гидрометаллургических процессов: Теория и практика гидрометаллургических процессов, лежащих в основе производства цветных и редких металлов: Учеб. пособие. М.: Изд. Дом МИСИС, 2009. 347 с.
33. Fainberg S.Yu. Analysis of non-ferrous metal ores. 2nd ed., corrected and additional Moscow: Metallurgizdat, 1953. 832 p. (In Russ.).
Файнберг С.Ю. Анализ руд цветных металлов. 2-е изд., исправ. и доп. М.: Металлургиздат, 1953. 832 с.
34. Piskareva S.K., Barashkov K.M., Olshanova K.M. Analytical chemistry: Textbook for secondary specialized educational institutions. Moscow: Vysshaya shkola, 1994. 384 p. (In Russ.).
Пискарева С.К., Барашков К.М., Ольшанова К.М. Аналитическая химия: Учеб. для сред. спец. учеб. заведений. 2-е изд., перераб. и доп. М.: Высшая школа, 1994. 384 с.
35. Lurie, Yu.Yu. Handbook of analytical chemistry. Ed. 4-th, rev. and additional. Moscow: Khimiya, 1971. 456 p. (In Russ.).
Лурье, Ю.Ю. Справочник по аналитической химии. Изд. 4-е, перераб. и доп. М.: Химия, 1971. 456 с.
36. Zittlau A.H., Shi Q., Boerio-Goates J., Woodfield B.F., Majzlan J. Thermodynamics of the basic copper sulfates antlerite, posnjakite, and brochantite. *Geochemistry.* 2013;73(1):39—50. https://doi.org/10.1016/j.chemer.2012.12.002
37. Glinka N.L. General chemistry: Textbook for universities. Leningrad: Khimiya, 1988. 704 p. (In Russ.).
Глинка Н.Л. Общая химия: Учеб. пос. для вузов. Л.: Химия, 1988. 704 с.
38. Raymond B. Chemical amendment of dairy cattle slurry for the control of phosphorus in runoff from grassland: Diss. of Doctor of Philosophy. Ireland: University of Galway, 2015.
39. Alekseev V.N. Quantitative analysis. Ed. 4-th. Moscow: Khimiya, 1972. 504 p. (In Russ.).
Алексеев В.Н. Количественный анализ. Изд. 4-е, перераб. М.: Химия, 1972. 504 с.
40. Naboychenko S.S., Ni L.P., Shneerson Ya.M., Chugaev L.V. Autoclave hydrometallurgy of non-ferrous metals. Ekaterinburg: USTU–UPI, 2002. 940 p. (In Russ.).
Набойченко С.С., Ни Л.П., Шнеерсон Я.М., Чугаев Л.В. Автоклавная гидрометаллургия цветных металлов. Екатеринбург: УГТУ—УПИ, 2002. 940 с.
41. Peretrutov A.A., Petrovsky A.M., Chubenko M.N., Kim P.P., Kalachev N.A., Litova T.V. Inherent properties of ammonia-ammonium aqueous solutions of copper ammonia. *Mezhdunarodnyi zhurnal prikladnykh i fundamental'nykh issledovanii.* 2018;12:219—224. (In Russ.).
Перетрутов А.А., Петровский А.М., Чубенко М.Н., Ким П.П., Калачев Н.А., Литова Т.В. Имманентные свойства аммиачно-аммонийных водных растворов аммиакатов меди. *Международный журнал прикладных и фундаментальных исследований*. 2018;12:219—224.
42. Groysman A.Sh., Khomutov N.E. Solubility of oxygen in electrolyte solutions. *Uspekhi Khimii AN SSSR.* 1980;59(8):1217—1250. (In Russ.).
Гройсман А.Ш., Хомутов Н.Е. Растворимость кислорода в растворах электролитов. *Успехи химии АН СССР.* 1980;59(8):1217—1250.
43. Narita E., Lawson F., Han K.N. Solubility of oxygen in aqueous electrolyte solutions. *Hydrometallurgy.* 1983;10:21—37. https://doi.org/10.1016/0304-386X(83)90074-9
44. Tromans D. Oxygen solubility modelling in ammoniacal leaching solutions: leaching of sulphide concentrates. *Minerals Engineering.* 2000;13(5):497—515. https://doi.org/10.1016/S0892-6875(00)00031-5
45. Tereshkin V., Fantgof Zh., Grigorieva L. Etching of printed circuit boards and regeneration of etching solutions. *Tekhnologii v elektronnoi promyshlennosti.* 2007;3:26—29. (In Russ.).

Терешкин В., Фантгоф Ж., Григорьева Л. Травление печатных плат и регенерация травильных растворов. *Технологии в электронной промышленности*. 2007;3:26—29.

46. Lin P., Werner J., Ali Z.A., Bertuccim L., Groppo J. Kinetics and modeling of counter-current leaching of waste random-access memory chips in a Cu—NH_3—SO_4 system utilizing Cu(II) as an oxidizer. *Materials*. 2023;16:6274. https://doi.org/10.3390/ma16186274
47. Habashi F. Fundamentals of applied metallurgy. Vol. 1: Theoretical foundations. Moscow: Metallurgiya, 1975. 231 p. (In Russ.).
Хабаши Ф. Основы прикладной металлургии. Т. 1: Теоретические основы. М.: Металлургия, 1975. 231 с.
48. Targanov I.E. Solodovnikov M.A., Troshkina I.D. Oxidative leaching of rhenium from grinding waste of rhenium-containing superalloys. *Izvestiya. Non-Ferrous Metallurgy*. 2023;29(5):25—33. (In Russ.).
https://doi.org/10.17073/0021-3438-2023-5-25-33
Тарганов И.Е. Солодовников М.А., Трошкина И.Д. Окислительное выщелачивание рения из шлифотходов ренийсодержащих суперсплавов. *Известия вузов. Цветная металлургия*. 2023;29(5):25—33.
https://doi.org/10.17073/0021-3438-2023-5-25-33
49. Targanov I.E., Troshkina I.D. Kinetics of sulfuric acid leaching of nickel from grinding waste of rhenium-containing superalloys. *Izvestiya. Non-Ferrous Metallurgy*. 2021;27(4):24—31. (In Russ.).
https://doi.org/10.17073/0021-3438-2021-4-24-31
Тарганов И.Е., Трошкина И.Д. Кинетика серно-кислотного выщелачивания никеля из шлифотходов ренийсодержащих суперсплавов. *Известия вузов. Цветная металлургия*. 2021;27(4):24—31.
https://doi.org/10.17073/0021-3438-2021-4-24-31
50. Kurniawan K. Lee J., Kim J., Kim R., Kim S. Leaching kinetics of selenium, tellurium and silver from copper anode slime by sulfuric acid leaching in the presence of manganese(IV) oxide and graphite. *Materials Proceedings*. 2021;3(1):16. https://doi.org/10.3390/IEC2M-09233
51. Schosseler J. Trentmann A., Frienrich B., Hahn K., Wotruba H. Kinetic investigation of silver recycling by leaching from mechanical pre-treated oxygen-depolarized cathodes containing PTFE and nickel. *Metals*. 2019;9(2):187. https://doi.org/10.3390/met9020187
52. Shu Q., Zhang J., Yan B., Liu J. Phase formation mechanism and kinetics in solid-state synthesis of undoped and calcium-doped lanthanum manganite. *Materials Research Bulletin*. 2009;44(3):649—653.
https://doi.org/10.1016/j.materresbull.2008.06.022
53. Free M.L. Hydrometallurgy: Fundamentals and applications. USA, NJ: John Wiley & Sons, 2013. 432 p.
54. Voldman G.M. On the use of the Erofeev-Kolmogorov equation to describe the kinetics of heterogeneous processes. *Izvestiya. Non-Ferrous Metallurgy*. 1973;6:91—96. (In Russ.).
Вольдман Г.М. Об использовании уравнения Ерофеева—Колмогорова для описания кинетики гетерогенных процессов. *Известия вузов. Цветная металлургия*. 1973;6:91—96.
55. Sun Z., Cao H., Venkatesan P., Jin W., Xiao Y., Sietsma J., Yang Y. Electrochemistry during efficient copper recovery from complex electronic waste using ammonia based solutions. *Frontiers of Chemical Science and Engineering*. 2016;11:308—316.
https://doi.org/10.1007/s11705-016-1587-x
56. Habashi F. Kinetics and mechanism of copper dissolution in aqueous ammonia. *Berichte der Bunsengesellschaft für physikalische Chemie*. 1963;67(4):402—406.
https://doi.org/10.1002/bbpc.19630670412
57. Kakovsky I.A., Naboychenko S.S. Thermodynamics and kinetics of hydrometallurgical processes. Alma-Ata: Nauka, 1986. 272 p. (In Russ.).
Каковский И.А., Набойченко С.С. Термодинамика и кинетика гидрометаллургических процессов. Алма-Ата: Наука, 1986. 272 с.
58. Zembura Z. Piotrowski A., Kolenda Z. A mass transfer model for the autocatalytic dissolution of a rotating copper disc in oxygen saturated ammonia solutions. *Journal of Applied Electrochemistry*. 1990;20: 365—369.
https://doi.org/10.1007/BF01076042
59. Larin V.I., Khobotova E.B., Dobriyan M.A., Datsenko V.V., Pshenichnaya S.V. The process of chemical dissolution of copper in ammonia solutions. *Vestnik Khar'kovskogo natsional'nogo universiteta*. 2006;731:230—237. (In Russ.).
Ларин В.И., Хоботова Э.Б., Добриян М.А., Даценко В.В., Пшеничная С.В. Процесс химического растворения меди в аммиачных растворах. *Вестник Харьковского национального университета*. 2006;731:230—237.
60. Ekmekyapar A., Oya R., Kunkul A. Dissolution kinetics of an oxidized copper ore in ammonium chloride solution. *Chemical and Biochemical Engineering Quarterly*. 2003;17(4):261—266.
https://doi.org/10.15255/CABEQ.2014.593
61. Wei L., Tang M., Tang C., He J., Yang S., Yang J. Dissolution kinetics of low grade complex copper ore in ammonia-ammonium chloride solution. *Transactions of Nonferrous Metals Society of China*. 2010;20:910—917.
https://doi.org/10.1016/S1003-6326(09)60235-1
62. Kunkul A., Muhtar Kocakerim M., Yapici S., Demirbag A. Leaching kinetics of malachite in ammonia solutions.

International Journal of Mineral Processing. 1993;41:167—182. https://doi.org/10.1016/0301-7516(94)90026-4

63. Bingol D., Canbazoglu M., Aydogan S. Dissolution kinetics of malachite in ammonia/ammonium carbonate leaching. *Hydrometallurgy*. 2005;76:55—62. https://doi.org/10.1016/j.hydromet.2004.09.006
64. Peretrutov A.A., Ksandrov N.V., Gagarina T.B., Chubenko M.N., Kim P.P. Thermodynamic and kinetic basis of ammonia-ammonium extraction of zinc and copper compounds from technogenic ones. *Trudy Nizhegorodskogo gosudarstvennogo tekhnicheskogo universiteta im. R.E. Alekseeva*. 2013;2:228—236. (In Russ.).
Перетрутов А.А., Ксандров Н.В., Гагарина Т.Б., Чубенко М.Н., Ким П.П. Термодинамические и кинетические основы аммиачно-аммонийного извлечения соединений цинка и меди из техногенных. *Труды Нижегородского государственного технического университета им. Р.Е. Алексеева*. 2013;2:228—236.

Information about the authors

Stepan O. Vydysh – Postgraduate Student of the Department of Non-Ferrous Metals and Gold, National University of Science and Technology «MISIS» (NUST MISIS).
https://orcid.org/0009-0007-4742-3966
E-mail: vydyshso@yandex.ru

Elena V. Bogatyreva – Dr. Sci. (Eng.), Professor of the Department of Non-Ferrous Metals and Gold, NUST MISIS.
https://orcid.org/0000-0003-2753-3424
E-mail: Helen_Bogatureva@mail.ru

Информация об авторах

Степан Олегович Выдыш – аспирант кафедры цветных металлов и золота, Национальный исследовательский технологический университет «МИСИС» (НИТУ МИСИС).
https://orcid.org/0009-0007-4742-3966
E-mail: vydyshso@yandex.ru

Елена Владимировна Богатырева – д.т.н., проф., доцент кафедры цветных металлов и золота, НИТУ «МИСИС».
https://orcid.org/0000-0003-2753-3424
E-mail: Helen_Bogatureva@mail.ru

Contribution of the authors

S.O. Vydysh – defined the purpose of the work, conducted experiments, wrote the article.

E.V. Bogatyreva – defined the purpose of the work, conducted experiments, wrote the article.

Вклад авторов

С.О. Выдыш – подготовка и проведение экспериментов, написание текста статьи.

Е.В. Богатырева – формирование основной концепции, определение цели работы, проведение экспериментов, корректировка текста и выводов.

The article was submitted 25.04.2024, revised 15.07.2024, accepted for publication 23.07.2024

Статья поступила в редакцию 25.04.2024 г., доработана 15.07.2024 г., подписана в печать 23.07.2024 г.

METALLURGY OF NON-FERROUS METALS / МЕТАЛЛУРГИЯ ЦВЕТНЫХ МЕТАЛЛОВ

UDC 546.74 : 66.081
https://doi.org/10.17073/0021-3438-2024-3-25-33

Research article
Научная статья

Hydrometallurgical recovery of nickel from oxidized ores

V.I. Dudarev, G.N. Dudareva, A.A. Yakovleva

Irkutsk National Research Technical University
83 Lermontova Str., Irkutsk 664074, Russia

✉ Vladimir I. Dudarev (vdudarev@mail.ru)

Abstract: A significant portion of the world's reserves of Ni-containing raw materials (40–66 %) is concentrated in oxidized nickel ores. One of the alternatives to the high-cost pyrometallurgical and ammonia-carbonate methods for processing such ores could be the chlorammonium recovery of nickel from relatively low-grade ores. The halide-ammonia decomposition and recovery technology of nickel from oxidized nickel ores, supplemented by a sorption process, is less stage-intensive and simpler in practical implementation. Nickel adsorption recovery is feasible using carbon sorbents that exhibit high chemical stability, withstand high-temperature exposure, and strong acidic treatment. Sorbents were obtained through steam-gas activation of extracted carbonizates from fossil coals. The sorption capacity for Ni(II) ions was studied, and the patterns and characteristic parameters of the process on carbon sorbents were identified using adsorption isotherms while varying experimental conditions. The experimental results were processed using the Freundlich and Langmuir equations. The sorbents have several distinctive features determined by their predominant microporous structure and multifunctional surface with active complex-forming atomic groups, characteristic of ampholytes with cation- and anion-exchange properties. The adsorption process is described by a pseudo-first-order equation with rate constants ranging from 0.204 to 0.287 s^{-1}. For the adsorption recovery of Ni(II), a scheme with two adsorbers and a pseudo-fluidized sorbent bed is proposed. Nickel desorption and sorbent regeneration were carried out with a 2.3 % sulfuric acid solution, desorbing 95 to 98 % of nickel. Standard chemical machinery and equipment are recommended for these processes.

Keywords: oxidized ores, carbon sorbents, nickel recovery.

For citation: Dudarev V.I., Dudareva G.N., Yakovleva A.A. Hydrometallurgical recovery of nickel from oxidized ores. *Izvestiya. Non-Ferrous Metallurgy*. 2024;30(3):25–33. https://doi.org/10.17073/0021-3438-2024-3-25-33

Гидрометаллургическое извлечение никеля из окисленных руд

В.И. Дударев, Г.Н. Дударева, А.А. Яковлева

Иркутский национальный исследовательский технический университет
664074, Россия, г. Иркутск, ул. Лермонтова, 83

✉ Владимир Иванович Дударев (vdudarev@mail.ru)

Аннотация: Большая часть мировых запасов Ni-содержащего сырья (40–66 %) сосредоточена в окисленных никелевых рудах. Одной из альтернативных высокозатратным пирометаллургическому и аммиачно-карбонатному методам переработки таких руд может быть хлораммонийное извлечение никеля из относительно бедных по содержанию металла руд. Технология галогенидно-аммиачного разложения и извлечения никеля из окисленных никелевых руд, дополненная сорбционным процессом, является менее длительной по стадийности и проще в практическом исполнении. Адсорбционное извлечение никеля возможно углеродными сорбентами, обладающими высокой химической устойчивостью, выдерживающими высокотемпературное воздействие и сильнокислотную обработку. Сорбенты получены путем парогазовой активации выделенных карбонизатов ископаемых углей. Изучена сорбционная способность ионов Ni(II), выявлены закономерности и характеристические параметры процесса на углеродных сорбентах с помощью изотерм адсорбции при варьировании условий проведения экспериментов. Обработку экспериментальных результатов выполняли с использованием уравнений Фрейндлиха и Ленгмюра. Сорбенты имеют ряд особенностей, определяемых преобладающей микропористой структурой и полифункциональной поверхностью с активными комплексообразующими группировками атомов, характерными для амфолитов с катионо- и анионообменными свойствами. Процесс адсорбции описан уравнением псевдопервого порядка с константами скорости от 0,204 до 0,287 $с^{-1}$. Для адсорбционного извлечения Ni(II) предложена схема с двумя адсорберами и псевдоожиженным слоем сорбента. Десорбция никеля и регенерация сорбента проведены 2,3 %-ным раствором серной кислоты. При этом десорбируется от 95 до 98 % никеля. В процессах рекомендуются стандартные химические машины и аппараты.

Ключевые слова: окисленные руды, углеродные сорбенты, извлечение никеля.

Для цитирования: Дударев В.И., Дударева Г.Н., Яковлева А.А. Гидрометаллургическое извлечение никеля из окисленных руд. *Известия вузов. Цветная металлургия*. 2024;30(3):25–33. https://doi.org/10.17073/0021-3438-2024-3-25-33

Introduction

In the global reserves of Ni-containing raw materials, a significant portion (from 40 to 66 %) is composed of oxidized nickel ores (ONO) [1—3], in which the average Ni content is only 0.7—1.2 %. Therefore, their targeted processing by pyrometallurgical methods is high-cost and, as a rule, unprofitable [2—4]. The combined scheme for processing ONO developed by scientists at the Ural Federal University named after the first President of Russia B.N. Yeltsin (Yekaterinburg) [5] (thermochemical treatment — aqueous leaching — hydroxide precipitation) allows obtaining a nickel concentrate, which enhances the economic feasibility of applying pyrometallurgical technology. However, the scheme involves thermochemical treatment of the entire ore mass, including barren rock, as well as requiring preliminary treatment of ONO with significant volumes of hydrochloric acid and roasting to obtain insoluble forms of interfering components. All this significantly complicates the process of nickel recovery.

Researchers at Tomsk Polytechnic University [6; 7] propose using a single reagent, ammonium chloride, for the initial processing of ONO. The main ore mass, including SiO_2 oxides (51 %) and Al_2O_3 (5 %), does not interact with the reagent, while oxides of other associated metals start interacting at a temperature of 473 K. Nickel oxide transitions to a water-soluble nickel chloride through an intermediate product $NiCl_2 \cdot nNH4Cl$ at T = 600 K. Subsequent aqueous leaching of the thermally treated ore and ammonia precipitation of hydroxides allow sequential separation of ONO into individual target components [6]. Incorporating a sorption process into such innovative technology can significantly enhance the efficiency of nickel recovery from ONO [8; 9].

The adsorption recovery of nickel is possible with sorbents from various raw materials, including carbon sorbents, which have a developed porous structure with a specific surface area of more than 500 m^2/g [10—21]. Carbon sorbents of the AD type, synthesized at INRTU, possess high chemical stability, withstand high-temperature exposure, and resist strong acid treatment [22; 23]. They have several features defined by their microporous structure and multifunctional surface with active complex-forming atomic groups, characteristic of ampholytes with cation- and anion-exchange properties [24].

Sorbents obtained through steam-gas activation of extracted carbonizates from fossil coals are dark granules of irregular shape with an average particle size of 1 to 2 mm, a specific surface area of 550 m^2/g, mechanical abrasion resistance of 82 %, a total pore volume (by water) of 0.61 cm^3/g, iodine adsorption activity of 84 %, and a bulk density of 560 g/dm^3 [23].

The aim of this work was to study the adsorption characteristics of the AD carbon sorbent and to develop recommendations for the hydrometallurgical recovery of nickel from oxidized ores.

Research methodology

The analysis of the sorption capacity for nickel ions, the identification of regularities, and characteristic parameters of the process were carried out using adsorption isotherms while varying the experimental conditions in both static and dynamic modes. The structure, porosity, and surface compound properties of the sorbents were studied using various physicochemical methods with modern instrumentation [24—26].

The AD sorbent possesses amphoteric ion-exchange properties. The ion-exchange capacity was determined by reverse titration methods using 0.1 N solutions of HCl and NaOH. The cation-exchange capacity for H^+ was 0.92 meq/g, and the anion-exchange capacity for OH^- was 7.52 meq/g. These data indicate that the sorbent surface contains functional groups with exchangeable H^+ and OH^- ions that can be replaced by metal ions. The optimization of nickel sorption recovery was carried out by varying the acidity and temperature of the solutions, as well as considering the nature of the adsorption on the porous material surface.

The effect of medium acidity on sorption capacity was evaluated under static conditions. A 0.5 g sample of the adsorbent was placed in 100 cm^3 of a solution prepared from reagent-grade nickel chloride. The reaction flask volume was 250 cm^3, and the initial metal concentration in the solution was 0.51 $mmol/dm^3$. The pH value in the range of 3 to 11 was adjusted using ammonia-acetate buffer solutions. A magnetic stirrer was used for mixing until adsorption equilibrium was established.

Quantitative analysis of nickel was performed by spectrophotometric methods using analytical reagents such as dimethylglyoxime or N-acyl-acetohydrazone [26]. Periodically, additional control of nickel ion concentration in solutions and the metal content in the sorbent after thermo-acid decomposition of the dried sorbent was carried out by atomic absorption analysis according to standard methodology [27]. The adsorption amount (A, mmol/g) was calculated using the formula

$$A = (C_0 - C_p)V/m, \qquad (1)$$

where C_0 and C_p are the initial and equilibrium concentrations of the adsorbate, respectively, $mmol/dm^3$; m is the mass of the adsorbent, g; V is the volume of the working solution, dm^3.

Studies at elevated temperatures were conducted in thermostated cells.

Results and discussion

The nature of the sorption interaction, observed at temperatures of 298, 318, and 338 K, is shown by the adsorption isotherms of Ni(II) ions on the carbon sorbent (Fig. 1).

The processing of experimental results in the low nickel concentration range in solutions was performed using the classical Freundlich equation:

$$A = K_F C_p^{1/n}. \qquad (2)$$

After performing arithmetic transformations and

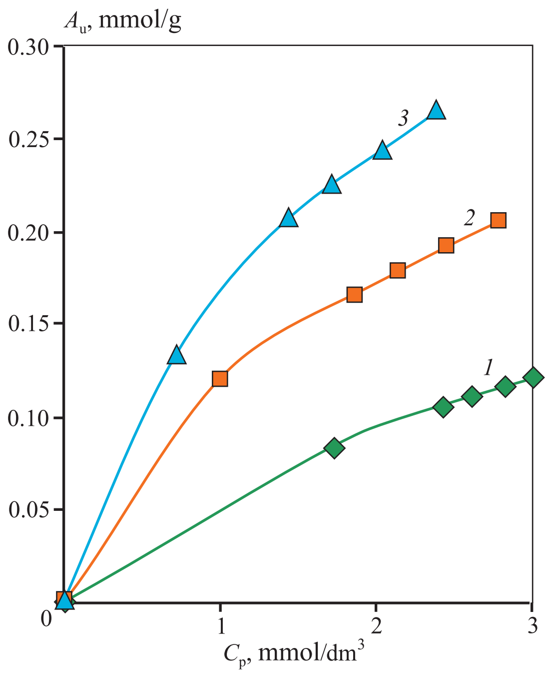

Fig. 1. Adsorption isotherms of Ni (II) ions at temperatures 298 K (*1*), 318 K (*2*), and 338 K (*3*)

A_u – concentration of metal on the sorbent

Рис. 1. Изотермы адсорбции ионов Ni(II) при температурах 298 K (*1*), 318 K (*2*) и 338 K (*3*)

A_u – концентрация металла на сорбенте

plotting the linear dependence of the logarithmic form of the equation:

$$\lg A = \lg K_F + 1/n \lg C_p \qquad (3)$$

both constant parameters K_F and n were determined graphically. The constant K_F represents the millimolar adsorption coefficient, as it corresponds to the adsorption value at an adsorbate concentration C = = 1 $mmol/dm^3$. The exponent $1/n$ is a proper fraction and generally characterizes the degree of the adsorption isotherm's approach to the abscissa axis. From the data presented in Table 1, it follows that with increasing temperature, both constants of the Freundlich equation (2)

Table 1. **Constants of the Freundlich equation (R^2 = 0.92)**

Таблица 1. Константы уравнения Фрейндлиха (R^2 = 0,92)

Constants	Temperature, K		
	298	318	338
K_F	0.19	0.25	0.29
n	1.73	1.84	1.94

increase. The value of the coefficient K_F suggests that the adsorption of Ni(II) ions in the initial period occurs with high efficiency.

To describe the process upon reaching the adsorption limit, the Langmuir equation was used. In its linear form, it is represented as a straight-line equation:

$$1/A = 1/A_\infty + 1/A_\infty K_p C, \qquad (4)$$

where C is the concentration of the metal in the solution, mmol/dm^3; A_∞ are the ultimate adsorption values, mmol/g; K_p is the adsorption equilibrium constant.

By plotting the dependence in the coordinates $1/A = f(1/C)$, the constants A_∞ and K_p in the Langmuir equation were determined graphically. The results are presented in Table 2.

It is evident that temperature affects both the ultimate adsorption value and the adsorption equilibrium constants, which also increase with temperature.

Analysis of the results shows that the process of nickel adsorption on the carbon sorbent is not purely physical adsorption. The standard thermodynamic parameter, Gibbs free energy (ΔG), was calculated using the classical chemical affinity equation:

$$\Delta G = -RT \ln K_p, \qquad (5)$$

where R = 8.314 J/mol·K is the universal gas constant; T is the process temperature in K.

From the data presented in Table 2, it is evident that with increasing temperature, the likelihood of the spontaneous adsorption process increases.

For the graphical determination of the adsorption enthalpy of Ni(II), the isobar equation in its differential form was used:

$$\ln K_p = \frac{\Delta H}{RT}. \qquad (6)$$

As a result, its value was –8.96 kJ/mol (see Table 2).

The evaluation of kinetic regularities was conducted using the classical method of selecting the axes of kinetic equations. The linear dependencies $\ln C = f(t)$ at all temperatures (Fig. 2) confirm that the adsorption process is described by a pseudo-first-order equation. The values of the rate constants (k_c) obtained in this way are presented in Table 2.

Contrary to the Van't Hoff rule for homogeneous chemical reactions, the adsorption rate constant grows significantly slower, indicating the complexity of the process mechanism. This is also confirmed by the activation energy (E_a), graphically determined by linearizing the Arrhenius equation:

$$\ln k = \ln k_0 \frac{E_a}{RT}. \qquad (7)$$

The experimentally determined activation energy for the adsorption process was 7.1 kJ/mol, indicating the process occurs in the diffusion region [28].

To address the question of the limiting stage of adsorption, experiments with process interruption in dynamic mode were conducted for a specified time. The results showed that in all cases, a 24-hour inter-

Table 2. **Thermodynamic sorption constants (R^2 = 0.96)**

Таблица 2. Термодинамические константы адсорбции (R^2 = 0,96)

Parameter	Temperature, K		
	298	318	338
A_∞, 10^{-4} mmol/g	1.01	1.53	1.66
K_p	394	416	524
k_c, s^{-1}	0.204	0.229	0.287
ΔG, kJ/mol	–20.5	–22.1	–24.7
ΔH, kJ/mol		–8.96	
E_a, kJ/mol		7.1	

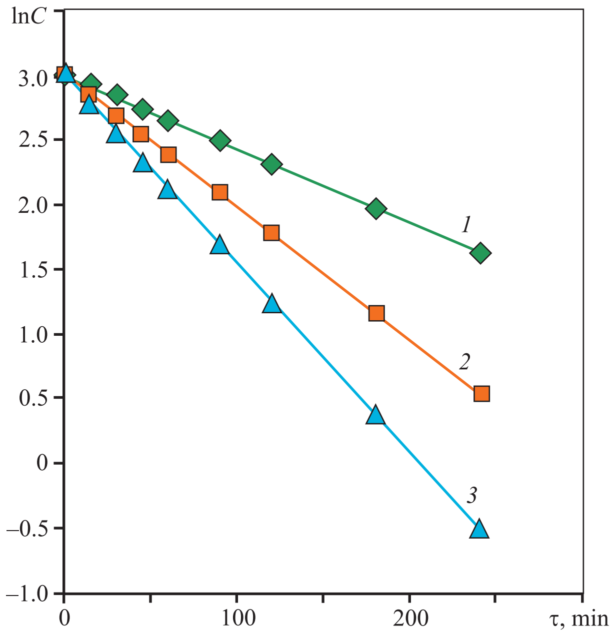

Fig. 2. Kinetic dependences of Ni(II) ion sorption at temperatures 298 K (*1*), 318 K (*2*), and 338 K (*3*)

Рис. 2. Кинетические зависимости сорбции ионов Ni(II) от температуры 298 K (*1*), 318 K (*2*) и 338 K (*3*) ruption of the adsorption flow resulted in a decreased concentration of the adsorbed metal in the solution exiting the column. The discontinuity in the adsorption exit curves suggests that the limiting stage of the adsorption kinetics of Ni(II) ions on the carbon adsorbent under the studied conditions is diffusion within the adsorbent granules, i.e., adsorption occurs under "gel" kinetics, and its rate is hindered by intradiffusion processes. The possible sorption mechanism can be considered as the diffusion process of complex Ni(II) ions, specifically the hydroxo-pentaammin cation $[Ni(NH_3)_5(OH)]^+$, into the granules and their interaction with functionally active groups on the sorbent surface through ion exchange.

Studies using IR spectroscopy methods showed that the observed results of metal ion sorption involve the participation of double bonds of compound fragments located on the carbon surface. Changes were observed in the overtones of $=CH_2$, $=C—NH_2$, and $=C—OH$ bonds, as well as in the conjugated fragments of $=C=C=C=$ and $R—C=O$, $R—OH$ bonds. This indicates the participation of π-electrons of these molecular fragments or their exchange parts in the reactions. They likely act as electron pair donors, with the free d-orbitals of the adsorbed metal serving as acceptors in the corresponding complexes. This conclusion confirms the nature of metal ion interaction with the adsorbent surface. The appearance of bands in its spectrum after metal ion sorption at $\nu = 574$, 604, and 836 cm^{-1}, corresponding to the characteristic deformation vibration bands of Me—O—C and Me—O—Me bonds, indicates the presence of such bonds in the investigated compounds.

The analysis of results also showed that during adsorption, with increasing temperature, the sorbent's capacity for nickel increases. The adsorption of Ni(II) ions in this case does not correspond to the classical behavior of metal ions: for many of them, adsorption results in an exothermic effect [29]. It is likely that the high stability of associated nickel compounds: amine complexes ($K_u = 5{,}3\cdot10^8$), aqua-amine complexes ($K_u = 4{,}2\cdot10^6$), and hydroxo-amine complexes ($K_u = 5{,}8\cdot10^6$) [26], predetermines the need for additional energy to break them down before sorption. This energy may be greater than the energy of the exothermic ion exchange reaction when Ni(II) is fixed on the sorbent surface, making the overall sorption process appear endothermic.

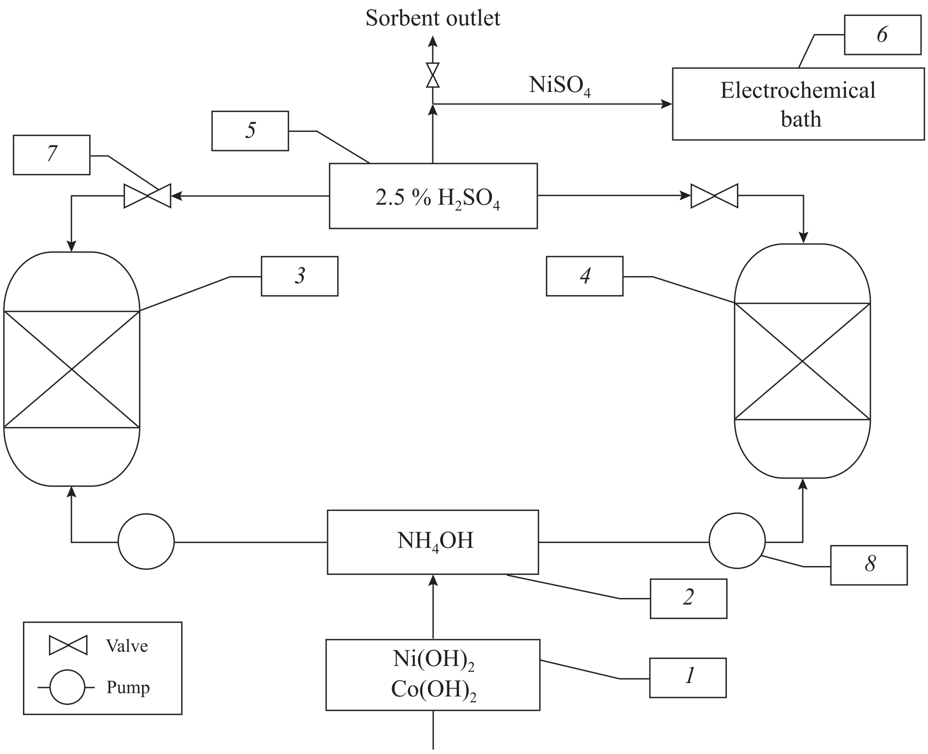

Fig. 3. Schematic diagram of the apparatus chain for nickel sorption extraction
1, ***2***, ***5***, ***6*** –solution tanks; ***3***, ***4*** – adsorbers; ***7*** – valves; ***8*** – pumps

Рис. 3. Схема цепи аппаратов для сорбционного извлечения никеля
1, ***2***, ***5***, ***6*** – емкости для растворов; ***3***, ***4*** – адсорберы; ***7*** – вентили; ***8*** – насосы

In the chlorammonium technology for nickel recovery from oxidized ores, the active reagent used for the technological transformation of metal oxides is regenerated and returned to the head of the process for the decomposition of a new batch of ONO [6]. The selectivity of ammonium chloride allows for the initial stage to free most of the ore. During ore opening, 75 % of nickel is extracted as hydroxide [7]. It seems reasonable to introduce a stage of adsorption recovery of nickel in the process of separating the technological solution, where precipitation and separation of nickel hydroxide will occur at pH = 8.0÷8.5 [8]. For the adsorption recovery of Ni(II), a scheme with two adsorbers with a pseudo-fluidized sorbent bed is proposed (Fig. 3).

During the adsorption studies, insights into the process mechanism were obtained, enabling the development of practical recommendations for implementing the proposed scheme. Before initiating the process, it is necessary to adjust the acidity of the technological solution to optimal values, which is achieved by adding an ammonium hydroxide solution. The solution is pumped from the bottom into the adsorber for the adsorption process. Compared to other designs, adsorbers with a pseudo-fluidized sorbent bed offer advantages such as an increased phase contact area with the same loading volume and a longer phase contact time.

For the adsorption recovery of metal, a cylindrical column design with a conical bottom and distribution grids inside the apparatus was chosen. To organize a continuous recovery process, two adsorbers are used: after the sorbent in the first unit becomes saturated, it switches to reloading while the second unit switches to adsorption. After reloading, the sorbent is directed to a desorber equipped with a stirrer, where a diluted (1 : 20, or 2.3 %) sulfuric acid solution is supplied. It was found that using H_2SO_4 at this concentration as the eluent desorbs 95 to 98 % of the nickel. The saturated Ni(II) solution after desorption is proposed for use in the electrolytic recovery of the metal.

When operating the sorption columns, it should be noted that the degree of nickel recovery from solutions decreases by 3—5 % after each cycle. The adsorbers should be switched before complete saturation of the load, as at times close to full saturation of the adsorbent, the concentration of metals in the solution approaches equilibrium, and the adsorption rate realistically decreases. The estimated total operating time of one adsorber before reloading the carbon is 648 hours. It is advisable to use only standard chemical machinery and apparatus in the processes.

Conclusion

The chlorammonium hydrometallurgical technology for nickel recovery from oxidized ores is based on the solid-phase chlorination of oxidized nickel ores with ammonium chloride at T = 473 K, followed by aqueous leaching of soluble nickel chlorides and other valuable components. It is advisable to include a nickel adsorption recovery process in the above-mentioned technological scheme at the stage of obtaining ammonia solutions (Ni^{2+}, Co^{2+}, Mn^{2+}, Mg^{2+}, Ca^{2+}). It is most likely that after precipitation, the metals are present in the technological solution as complex ammines.

The study showed that adsorption interaction in the “metal-containing solution — carbon sorbent” system proceeds quite intensively: the rate constants range from 0.204 до 0.287 s^{-1}. The activation energy value (E_a = = 7.1 kJ/mol) indicates that the adsorption process occurs in the diffusion region. The change in Gibbs free energy (ΔH = –8.96 kJ/mol) suggests that the likelihood of the spontaneous adsorption process increases with temperature.

For the adsorption recovery of Ni(II), a scheme with two adsorbers with a pseudo-fluidized sorbent bed and bottom supply of a weakly alkaline technological solution is proposed. Nickel desorption is carried out with a 2.3 % sulfuric acid solution, desorbing 95 to 98 % of the nickel.

References

1. Naftal M.N., Dyachenko V.T., Serova N.V., Bryukvin V.A., Lysykh M.P. Oxidized nickel ores are a promising source of mineral raw materials for increasing the production of nickel and cobalt in LLC MMK Norilsk Nickel. *Tsvetnye metally*. 2012;6:25—28. (In Russ.).
Нафталь М.Н., Дьяченко В.Т., Серова Н.В., Брюквин В.А., Лысых М.П. Окисленные никелевые руды — перспективный источник минерального сырья для повышения объемов производства никеля и кобальта в ОАО «ГМК «Норильский никель». *Цветные металлы*. 2012;6:25—28.
2. Reznik I.D. , Ermakov G. P., Shneerson Ya.M. Nickel. Vol. 2. Moscow: Nauka i Tekhnologiya, 2001. 468 p. (In Russ.).
Резник И.Д., Ермаков Г.П., Шнеерсон Я.М. Никель. Т. 2. М.: Наука и технология, 2001. 468 с.
3. Kalashnikova M.I. Development of scientific foundations for the creation of new and improvement of existing hydrometallurgical technologies for processing of ore raw materials and intermediate products of copper-nickel production: Abstract of the Dissertation of Dr. Sci. (Eng.). St. Petersburg: SPbSPU, 2007. (In Russ.).

Калашникова М.И. Разработка научных основ создания новых и совершенствования действующих гидрометаллургических технологий переработки рудного сырья и промежуточных продуктов медно-никелевого производства: Автореф. дисс. ... докт. техн. наук. Санкт-Петербург: СПбГПУ, 2007.

4. Chunarev A.A., Kolmachikhina O.B., Naboychenko S.S. Overview of methods for processing oxidized nickel ores and prospects for the development of nickel production in the Urals. In: *Ural industrialny. Bakunin's Readings: Industrial Modernization of the Urals in the XVIII–XXI Centuries:* Mater. XII Al-Russian Scientific Conf. (4—5.12.2014). Yekaterinburg, 2014. Vol. 2. P. 333—335. (In Russ.).
Чунарев А.А., Колмачихина О.Б., Набойченко С.С. Обзор методов переработки окисленных никелевых руд и перспективы развития на Урале никелевого производства. В сб.: *Урал индустриальный. Бакунинские чтения: Индустриальная модернизация Урала в XVIII–XXI вв.:* Материалы XII Всероссийской научной конференции (4—5 дек. 2014 г.). Екатеринбург, 2014. Т. 2. С. 333—335.

5. Kolmachikhina, O.B. Combined technology for processing oxidized nickel ores (on the example of the serovskoye deposit): Diss. ... Cand. Sci. (Eng.). Yekaterinburg, UrFU, 2018. (In Russ.).
Колмачихина О.Б. Комбинированная технология переработки окисленных никелевых руд (на примере Серовского месторождения): Дис. ...канд. техн. наук. Екатеринбург: УрФУ, 2018. 132 с.

6. Andreev A.A., Dyachenko A.N., Kraydenko R.I. Processing of oxidized nickel ores using ammonium chloride. *Khimicheskaya tekhnologiya*. 2010;11(2): 91—96. (In Russ.).
Андреев А.А., Дьяченко А.Н., Крайденко Р.И. Переработка окисленных никелевых руд с применением хлорида аммония. *Химическая технология*. 2010;11(2): 91—96.

7. Andreev A.A., Dyachenko A.N., Kraydenko R.I. Chlorammonium technology of processing oxidized nickel ores. *Tsvetnye metally*. 2011;1:18—21.
Андреев А.А., Дьяченко А.Н., Крайденко Р.И. Хлораммонийная технология переработки окисленных никелевых руд. *Цветные металлы*. 2011;1:18—21.

8. Dudareva G.N., Irinchinova N.V., Dudarev V.I. Adsorption extraction of nickel (II) from aqueous solutions of technogenic character. *Izvestiya vuzov. Prikladnaya khimiya i biotechnologiya*. 2020;1(32):133—139. (In Russ.).
https://doi.org/10.21285/2227-2925-2020-10-1-133-139
Дударева Г.Н., Иринчинова Н.В., Дударев В.И. Адсорбционное извлечение никеля (II) из водных растворов техногенного характера. *Известия вузов. Прикладная химия и биотехнология*. 2020;1(32):133—139.
https://doi.org/10.21285/2227-2925-2020-10-1-133-139

9. Kurdyumov V.R., Timofeev K.L., Maletsev G.I., Lebed A.B. Sorption extraction of nickel (II) and manganese (II) ions from aqueous solutions. *Zapiski Gornogo instituta*. 2020;242:209. (In Russ.).
https://doi.org/10.31897/pmi.2020.2.209
Курдюмов В.Р., Тимофеев К.Л., Мальцев Г.И., Лебедь А.Б. Сорбционное извлечение ионов никеля (II) и марганца (II) из водных растворов. *Записки Горного института*. 2020;242:209.
https://doi.org/10.31897/pmi.2020.2.209

10. Tamjidi S., Esmaeili H., Moghadas B.K. Application of magnetic adsorbents for removal of heavy metals from wastewater: a review study. *Materials Research Express*. 2019;6(10):862—873.
https://doi.org/10.1088/2053-1591/ab3ffb

11. Çelebi H., Gök G., Gök O. Adsorption capability of brewed tea waste in waters containing toxic lead (II), cadmium (II), nickel (II), and zinc (II) heavy metal ions. *Scientific Reports*. 2020;10(1):12.
https://doi.org/10.1038/s41598-020-74553-4

12. Nilgün Onursal, Yalçın Altunkaynak, Ayşe Baran, Mehmet Can Dal. Adsorption of nickel (II) ions from aqueous solutions using Malatya clay: Equilibrium, kinetic, and thermodynamic studies. *Environmental Progress & Sustainable Energy*.2017;42(5):14150.
https://doi.org/10.1002/ep.14150

13. Olufemi B., Eniodunmo O., Adsorption of nickel (II) ions from aqueous solution using banana peel and coconut shell. *International Journal of Technology*. 2018;9(3):434—445.
https://doi.org/10.14716/ijtech.v9i3.1936

14. Chang Y.S., Au P.I., Mubarak N.M., Khalid M., Jagadish P., Walvekar R., Abdullah E.C. Adsorption of Cu(II) and Ni(II) ions from wastewater onto bentonite and bentonite/GO composite. *Environmental Science and Pollution Research*. 2020;27:33270—33296.
https://doi.org/10.1007/s11356-020-09423-7

15. Khan M.I., Almesfer M.K., Danish M., Ali I.H., Shoukry H., Patel R., Gardy J., Nizami A.S., Rehan M. Potential of Saudi natural clay as an effective adsorbent in heavy metals removal from wastewater. *Desalination and Water Treatment*. 2019;158:140—151.
https://doi.org/10.5004/dwt.2019.24270

16. Gupta S., Sharma S.K., Kumar A. Biosorption of Ni(II) ions from aqueous solution using modified Aloe barbadensis Miller leaf powder. *Water Science and Engineering*. 2019;12:27—36.
https://doi.org/10.1016/j.wse.2019.04.003

17. Islam M.A., Awual M.R., Angove M.J. A review on nickel (II) adsorption in single and binary component sys-

tems and future path. *Journal of Environmental Chemical Engineering.* 2019;7(5):103305.
https://doi.org/10.1016/j.jece.2019.103305

18. Shahat A., Hassan M.A. H., El-Shahat M.F., Osama El-Shahawy, Md. Rabiul Awual. Visual nickel (II) ions treatment in petroleum samples using a mesoporous composite adsorbent. *Chemical Engineering Journal.* 2018;334:957—967.
https://doi.org/10.1016/j.cej.2017.10.105
19. Praveen P., Munilakshmi N., Sravani P. Removal of nickel (II) ion from an aqueous solution using red brick as an adsorbent. *Journal of Solid Waste Technology and Management.* 2023;49(2):175—184.
https://doi.org/10.5276/jswtm/iswmaw/492/2023.175
20. Mahmoud O. Abd El-Magied, Ali M.A. Hassan, Hamdi M.H. Gad T.M. Removal of nickel (II) ions from aqueous solutions using modified activated carbon: A kinetic and equilibrium study. *Journal of Dispersion Science and Technology.* 2018;39(6).
https://doi.org/10.1080/01932691.2017.1402337
21. Qasem N.A., Mohammed R.H., Lawal D.U. Removal of heavy metal ions from wastewater: A comprehensive and critical review. *npj Clean Water.* 2021;4(1):1—15.
https://doi.org/10.1038/s41545-021-00127-0
22. Leonov S.B., Domracheva V.A., Elshin V.V., Dudarev V.I., Oznobikhin L.M., Randin O.I. Carbon sorbents based on fossil coals. Irkutsk: Irkutsk State Technical University, 2000. 268 p. (In Russ.).
Леонов С.Б., Домрачева В.А., Елшин В.В., Дударев В.И., Ознобихин Л.М., Рандин О.И. Углеродные сорбенты на основе ископаемых углей. Иркутск: ИрГТУ, 2000. 268 с.
23. Leonov S.B., Elshin V.V., Dudarev V.I., Domracheva V.A. Method of Sorbent Production: Patent 2064335 (RF). 1996. (In Russ.).
Леонов С.Б., Елшин В.В., Дударев В.И., Домрачева В.А. Способ получения сорбента: Патент 2064335 (РФ). 1996.
24. Dudareva G.N., Randin O.I., Petukhova G.A., Vakul'skaya T.I. On the mechanism of sorption of nickel (II) ions by modified carbon sorbents. *Protection of Metals and Physical Chemistry of Surfaces.* 2015;51(6):939—943.
https://doi.org/10.1134/S2070205115060064
25. Dudareva G.N., Irinchinova N.V., Dudarev V.I., Petukhova G.A. Study of removal of nickel(II) from aqueous solutions by sorption. *Protection of Metals and Physical Chemistry of Surfaces.* 2019;55(5):841—848.
https://doi.org/10.1134/S2070205119050071
26. Dudareva G.N. Sorption concentration and analytical determination of nickel: Monograph. Irkutsk: IRNITU, 2015. 154 p. (In Russ.).
Дударева Г.Н. Сорбционное концентрирование и аналитическое определение никеля: Монография. Иркутск: ИРНИТУ, 2015. 154 с.
27. Marochkina V.V., Bueva E.I., Kulagina E.S. Comparative analysis of methods for determining chromium, vanadium, copper, nickel, manganese in steels and cast irons by the method of atomic absorption spectrometry with atomization in the flame. *Zavodskaya laboratoriya. Diagnostika materialov.* 2023; 89(2):57—63. (In Russ.).
https://doi.org/10.26896/1028-6861-2023-89-2-II-57-64
Марочкина В.В., Буева Е.И., Кулагина Е.С. Сравнительный анализ методик определения хрома, ванадия, меди, никеля, марганца в сталях и чугунах методом атомно-абсорбционной спектрометрии с атомизацией в пламени. *Заводская лаборатория. Диагностика материалов.* 2023;89(2):57—63.
https://doi.org/10.26896/1028-6861-2023-89-2-II-57-64
28. Frolov Yu.G. Course of the colloid chemistry. Surface phenomena and disperse systems. Moscow: Khimiya, 1989. 462 p. (In Russ.).
Фролов Ю.Г. Курс коллоидной химии. Поверхностные явления и дисперсные системы. М.: Химия, 1989. 462 с.
29. Tsivadze A.Yu., RusanovA.I., Fomkin A.A.,Voloshchuk A.M., Tovbin Y.K., Tolmachev A.M., Avramenko V.A. Physical chemistry of adsorption phenomena. Moscow: Granitsa, 2011. 302 p. (In Russ.).
Цивадзе А.Ю., Русанов А.И., Фомкин А.А., Волощук А.М., Товбин Ю.К., Толмачев А.М., Авраменко В.А. Физическая химия адсорбционных явлений. М.: Граница, 2011. 302 с.

Information about the authors

Vladimir I. Dudarev – Dr. Sci. (Eng.), Professor of the Department of Chemistry and Biotechnology named after Prof. V.V. Tuturina, Irkutsk National Research Technical University (INRTU).
https://orcid.org/0009-0001-6477-4422
E -mail: vdudarev@mail.ru

Galina N. Dudareva – Cand. Sci. (Chem.), Associate Professor of the Department of Chemistry and Biotechnology named after Prof. V.V. Tuturina, INRTU.
https://orcid.org/0009-0004-3234-0672
E-mail: gndudareva@mail.ru

Ariadna A. Yakovleva – Dr. Sci. (Eng.), Professor of the Department of Chemistry and Biotechnology named after Prof. V.V. Tuturina, INRTU.
https://orcid.org/0000-0002-5747-2864
E-mail: ayakovistu@mail.ru

Информация об авторах

Владимир Иванович Дударев – д.т.н., профессор кафедры химии и биотехнологии им. проф. В.В. Тутуриной, Иркутский национальный исследовательский технический университет (ИРНИТУ).
https://orcid.org/0009-0001-6477-4422
E -mail: vdudarev@mail.ru

Галина Николаевна Дударева – к.х.н., доцент кафедры химии и биотехнологии им. проф. В.В. Тутуриной, ИРНИТУ.
https://orcid.org/0009-0004-3234-0672
E -mail: gndudareva@mail.ru

Ариадна Алексеевна Яковлева – д.т.н., профессор кафедры химии и биотехнологии им. проф. В.В. Тутуриной, ИРНИТУ.
https://orcid.org/0000-0002-5747-2864
E -mail: ayakovistu@mail.ru

Contribution of the authors

V.I. Dudarev – developed of the main concept, set the goal and objectives of the study, prepared the text, and formulated the conclusions.

G.N. Dudareva – performed calculations, tested samples, and prepared the text of the article.

A.A. Yakovleva – provided scientific guidance, revised the text, and refined the conclusions.

Вклад авторов

В.И. Дударев – формирование основной концепции, постановка цели и задачи исследования, подготовка текста, формулировка выводов.

Г.Н. Дударева – осуществление расчетов, проведение испытаний образцов, подготовка текста статьи.

А.А. Яковлева – научное руководство, корректировка текста, корректировка выводов.

The article was submitted 05.01.2024, revised 14.03.2024, accepted for publication 18.03.2024

Статья поступила в редакцию 05.01.2024 г., доработана 14.03.2024 г., подписана в печать 18.03.2024 г.

METALLURGY OF NON-FERROUS METALS / МЕТАЛЛУРГИЯ ЦВЕТНЫХ МЕТАЛЛОВ

UDC 546.34 + 666.123.24 + 669.2/.8
https://doi.org/10.17073/0021-3438-2024-3-34-44

Research article
Научная статья

Obtaining lithium carbonate from the black mass of lithium-ion batteries

S.A. Aleynikov, N.V. Belousova

Siberian Federal University
79 Svobodny Prosp., Krasnoyarsk 660041, Russia

✉ Sergey A. Aleynikov (saaleynikov@yandex.ru)

Abstract: The article explores the possibility of obtaining lithium carbonate from the black mass – an intermediate product of lithium-ion batteries recycling. X-ray phase analysis and inductively coupled plasma atomic emission spectrometry of the black mass revealed that it contains 3 % lithium. It has been established that during water leaching, 40 % to 70 % of lithium can be selectively extracted from the black mass into the aqueous phase at L/S ratios ranging from 10 to 200. During water leaching, kinetic curves were recorded at temperatures of 25 °C and 80 °C. To remove Al ions from the leaching solution, we studied the sorption of aluminate ions on weaky basic (AN-31, CRB05) and strongly basic (A500) anion exchangers under static conditions using a model Li–Al solution. It was demonstrated that in an alkaline environment, strongly basic anion exchangers with quaternary amino groups are not able to adsorb Al ions, while AN-31 and CRB05 with hydroxyl clusters in their functional groups have a capacity of 2 to 3 g/dm^3 in terms of aluminum ions. The sorption of aluminum from the model Li–Al solution was conducted under dynamic conditions using the CRB05 anion exchanger (N-methylglucamine) at specific flow rates of 2 and 4 column volumes per hour. Elution sorption curves were plotted, and both the dynamic exchange capacity and the total dynamic exchange capacity were determined. Additionally, we showed that aluminum ions can be removed by sorption so that their residual concentration in the raffinate drops below 0.5 mg/dm^3. Sorption purification of the solution after water leaching of the black mass was performed using a weaky basic anion exchanger Diaion CRB05 and a chelate cation exchanger Purolite S950. After evaporation of the purified solution, we obtained lithium carbonate with a main substance content of 98.2 %.

Keywords: sorbent, lithium, ion exchange, extraction, purification, treatment.

For citation: Aleynikov S.A., Belousova N.V. Obtaining lithium carbonate from the black mass of lithium-ion batteries. *Izvestiya. Non-Ferrous Metallurgy*. 2024;30(3):34–44. https://doi.org/10.17073/0021-3438-2024-3-34-44

Получение карбоната лития из «черной массы» литий-ионных аккумуляторов

С.А. Алейников, Н.В. Белоусова

Сибирский федеральный университет
Россия, 660041, г. Красноярск, пр-т Свободный, 79

✉ Сергей Александрович Алейников (saaleynikov@yandex.ru)

Аннотация: Исследована возможность получения карбоната лития из «черной массы» – промежуточного продукта переработки литий-ионных аккумуляторов. Проведены рентгенофазовый анализ и атомно-эмиссионная спектроскопия с индуктивно связанной плазмой «черной массы», результаты которых показали, что содержание лития в ней составляет 3 %. Установлено, что при водном выщелачивании из «черной массы» в водную фазу можно селективно извлечь от 40 до 70 % лития при соотношении Ж : Т от 10 до 200. В процессе водного выщелачивания были сняты кинетические кривые при температурах 25 и 80 °С. Для удаления ионов Al из раствора выщелачивания исследовалась сорбция алюминат-иона на слабоосновных (АН-31, CRB05) и сильноосновных (A500) анионитах в статических условиях на модельном Li–Al-растворе. Показано, что в щелочной среде сильноосновные аниониты с четвертичными аминогруппами не способны поглощать ионы Al, в то время как АН-31 и CRB05, имеющие в составе функциональных групп гидроксильные группировки, обладают емкостью от 2 до 3 г/дм^3 по ионам Al. Проведена сорбция алюминия из модельного Li–Al-раствора в динамических условиях с использованием анионита CRB05 (N-метилглюкамин) при удельной скорости потока 2 и 4 колоночных объема в час, сняты выходные кривые сорбции, рассчитаны динамическая обменная и полная динамическая обменная емкости. Показано, что ионы Al могут быть удалены сорбцией до остаточной концентрации в рафинате менее 0,5 мг/дм^3. Также была проведена сорбционная очистка раствора водного выщелачивания «черной массы» с использованием слабоосновного анионита Diaion CRB05 и хелатного катионита Purolite S950. После упаривания очищенного раствора был получен карбонат лития с содержанием основного вещества 98,2 %.

Ключевые слова: сорбент, литий, ионный обмен, извлечение, очистка, переработка.

Для цитирования: Алейников С.А., Белоусова Н.В. Получение карбоната лития из «черной массы» литий-ионных аккумуляторов. *Известия вузов. Цветная металлургия.* 2024;30(3):34–44. https://doi.org/10.17073/0021-3438-2024-3-34-44

Introduction

The production of lithium-ion batteries (LIB) holds the largest share in global lithium consumption. In 2015, LIB manufacturing accounted for 35 % of global lithium production, and by 2019, this figure surged to 65 % . The service life of LIBs is limited by various factors contributing to the degradation of electrochemical energy storage systems. Consequently, the coming years are likely to see growth in the market for recycled lithium raw materials. Without control over the disposal of spent lithium-ion batteries, this could have serious environmental consequences.

The most popular lithium product is lithium carbonate, which is used for LIB production after being upgraded by purification from the technical (≥99.0 % Li_2CO_3) to battery (≥99.5 % Li_2CO_3) grade. Lithium in the active cathode and anode masses of lithium-ion batteries exists as mixed oxides (spinels): $LiCoO_2$ [2], $LiMnO_4$ [3], $Li_4Ti_5O_{12}$ [4]; phosphate $LiFePO_4$ [5], carbide LiC_6 [6], and other compounds. A mixture of cathode and anode masses of spent LIBs is an intermediate product of their processing and is referred to as "the black mass" in foreign scientific literature.

The following elements are used to transfer lithium, cobalt, and nickel from spent LIBs into solution: organic acids (oxalic, citric, ascorbic, etc.) [7; 8], including combinations with hydrogen peroxide [9—11], mixtures of organic acids (benzenesulfonic and formic) [12], inorganic acids (sulfuric, nitric, hydrochloric) [7; 13; 14], and ammonium [15; 16] and sodium [17] hydroxides.

Acid leaching presents a challenge for the further selective separation of lithium and non-ferrous metals since the resulting leaching solution contains many elements to be removed, such as Ni, Co, Mn, Al, and Fe.

Selective lithium extraction can be achieved by water leaching of the black mass, during which most lithium ions leave the mixed oxide structure and transfer into the solution as lithium hydroxide. The proposed mechanism for lithium transfer into the solution of mixed oxides is represented by the following reaction equations [18]:

$$2LiCoO_2 + H_2O = 2LiOH + Co_2O_3, \tag{1}$$

$$2LiMnO_2 + H_2O = 2LiOH + Mn_2O_3, \tag{2}$$

$$Li_4Ti_5O_{12} + 2H_2O = 4LiOH + 5TiO_2. \tag{3}$$

From the resulting lithium solution, lithium carbonate can be precipitated by passing carbon dioxide:

$$2Li^+ + 2OH^- + CO_2 = Li_2CO_3 + H_2O. \tag{4}$$

A problem arises due to aluminum contained in some cathode materials ($LiNi_xCo_yAl_{1-x-y}O_2$) and the presence of aluminum foil particles used in lithium-ion batteries as a cathode current lead. In the alkaline environment of a lithium hydroxide solution, aluminum oxide can partially dissolve, forming a complex ion $[Al(OH)_4]^-$:

$$2Li^+ + 2OH^- + Al_2O_3 + 3H_2O = \\ = 2Li^+ + 2[Al(OH)_4]^-. \tag{5}$$

When metallic aluminum reacts with a solution of lithium hydroxide, layered double aluminum-lithium hydroxide can form [19]:

$$Li^+ + OH^- + 2Al + 8H_2O = \\ = [LiAl_2(OH)_6]OH \cdot 2H_2O + 3H_2. \tag{6}$$

Therefore, before lithium carbonate precipitation, Al ions should be removed from the leaching solution. This can be facilitated by sorption on anion exchangers. A literature review showed that weak base anion exchangers with tertiary amino groups (AN-31) [20] or anion exchangers with N-methylglucamine active groups (D-403) [21] can be used for the sorption removal of Al ions.

The purpose of this study was to investigate the conditions for the direct extraction of lithium from the black mass of lithium-ion batteries to obtain lithium carbonate.

Materials and methods

The object of the study was the LIB black mass obtained by grinding spent lithium-ion batteries in a shredder and sifting the resulting material through a sieve with a mesh size of 0.63 mm.

To analyze the composition of the black mass, a subsample weighing 0.5 g was dissolved in 50 cm^3 of a mixture of sulfuric, perchloric, and hydrochloric acids at the ratio of 2 : 2 : 1. This mixture was heated to 200 °C for 4 hours to ensure complete dissolution of the subsample, including graphite. The resulting solution was then diluted with 6 M hydrochloric acid to bring the total volume to 100 cm^3. The solution was analyzed by inductively coupled plasma atomic emission spectrometry (ICP-AES). The results (wt.%) are presented below.

Ti 0.08
Mn 7.48
Cu 2.47
Fe.........................0.87
Ni.........................9.72
Al.........................3.39
P 0.68
Li 3.15
Co 14.97

The *X*-ray phase analysis of the black mass, performed on a Malvern Panalytical Empyrean powder diffractometer (PANalytical, Inc., the Netherlands), showed the presence of graphite, Co, Li_2CO_3, MnO, Cu, Cu_2O, and $Li(Fe_{0.16}Mn_{1.77})O_4$ in the sample (listed in order of decreasing content).

The experimental scheme is shown in Fig. 1. Water leaching of the black mass was performed at L/S ratios ranging from 10 to 200 to study the conditions for the most complete extraction of lithium into solution. Based on the ICP-AES analysis of the solution obtained during of the black mass leaching, a model Li-containing solution was prepared for use in experiments on static aluminum sorption. The main goal of these experiments was to select the sorbent with the highest capacity for aluminum ions. The selected sorbent was then used in experiments on the dynamic sorption of aluminum using a model Li-containing solution to select the optimal flow rate (FR) (specific loading) and calculate the sorbent dynamic exchange capacity (DEC) for Al ions. Based on the results obtained, we selected the volume of sorbent required for the sorption purification of the real black mass leaching solution from Al ions at the chosen specific loading.

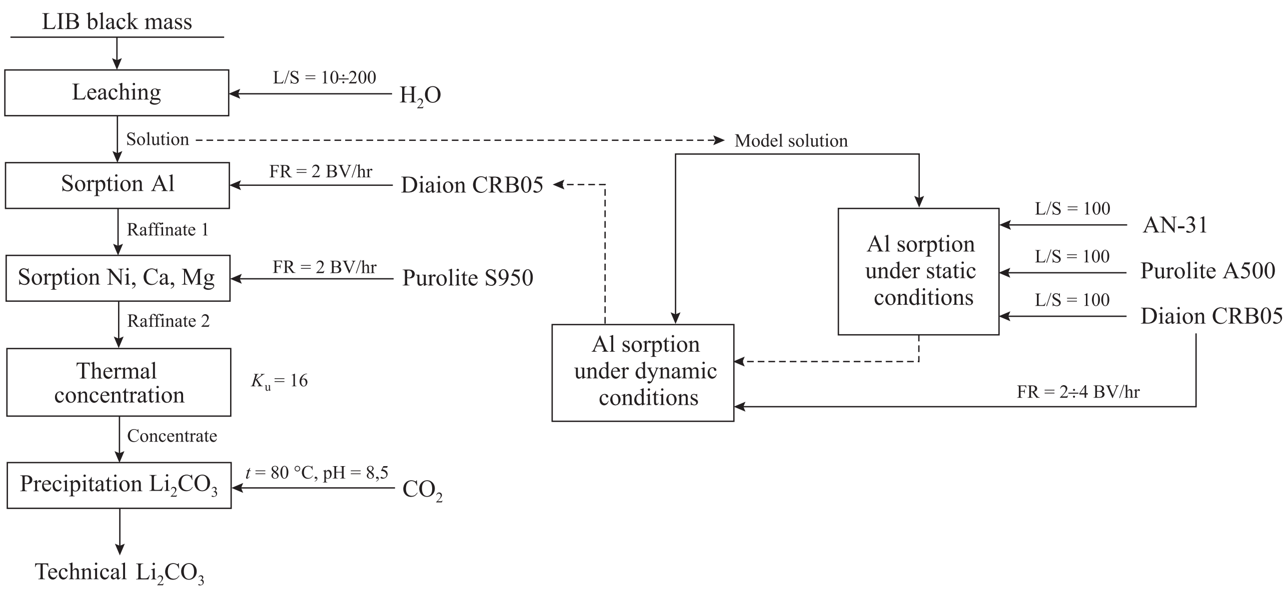

Fig. 1. Experiment scheme

Рис. 1. Схема проведения опытов

Alongside with the aluminum sorption, we performed sorption purification of the aluminum sorption raffinate from some impurity cations (Ni, Ca, Mg) using the Purolite S950 cation exchanger. After sorption purification, the Li-containing solution was concentrated by evaporation 16 times (K_u = 16) to achieve the Li concentration of 25 g/dm^3. After this, to precipitate lithium carbonate, carbon dioxide was passed through the concentrated Li solution heated to 80 °C until pH reached the value of 8.5.

Water leaching procedure

Water leaching of the black mass was performed in titanium crucibles with a volume of 100 ml at different L/S ratios (10, 50, 100, and 200) for 2 hours. The 5-position IKA RT5 stirrer (IKA-Werke GmbH & Co. KG, Germany) was used to create uniform conditions.

To record the kinetic curves of lithium leaching, water leaching of the black mass was performed in a titanium beaker with a volume of 600 ml at temperatures of 25 and 80 °C for 2 hours, with the solution being constantly stirred on an IKA C-MAG HS 7 magnetic stirrer at the ratio L/T = 10. This value was chosen as the most optimal for subsequent experiments on aluminum sorption. Samples were taken every 5 minutes, immediately filtered, and analyzed for lithium content using the ICP-AES method.

The solutions obtained during the recording of kinetic curves were combined. The data from ICP-AES analysis of the combined solution was used to prepare model systems containing Al and Li ions to study aluminum sorption under static and dynamic conditions.

Procedure for aluminum sorption under static conditions

Aluminum sorption under static conditions was performed to select a sorbent with the highest capacity for aluminum ions. We used the anion exchangers presented in Table 1. The model solution for aluminum sorption was prepared by dissolving 9 g of lithium hydroxide monohydrate $LiOH \cdot H_2O$ (TS 6-09-3763-85) and 1.4 g of aluminum chloride hexahydrate $AlCl_6 \cdot H_2O$ (GOST 3759-75) in 1 dm^3 of water. The resulting solution after filtration contained 154 mg/dm^3 of lithium and 1,465 mg/dm^3 of aluminum.

The model solution with a volume of 50 cm^3 was transferred into a flask with a volume of 100 cm^3 using a Research Plus automatic pipette (Eppendorf, Germany) and 1 cm^3 of sorbent sample was added. The solution was stirred for 24 hours on an S-3L.A20 orbital mixer (ELMI Ltd., Latvia). After the experiment was completed, the solutions were filtered and analyzed for the residual content of Al and Li ions.

Procedure for aluminum sorption under dynamic conditions

Sorption of aluminum under dynamic conditions was performed on a model solution to evaluate the dynamic and total dynamic exchange capacity (DEC) of the sorbent, as well as to determine the optimal flow rate (specific loading) that ensures maximum aluminum extraction. Diaion CRB05 (N-methylglucamine) sorbent was used in the experiment. An IOK VZOR 20/16/200 ion exchange column (VZOR LLC, Russia) was filled with 30 ml of CRB05 anion exchanger and the model solution. The model solution with a specific loading of 2 and 4 bed volumes per hour (BV/hr) (40 and 120 cm^3/hr, respectively) was passed through a column with a sorbent using a Masterflex L/S 7519-06 peristaltic pump (Cole-Parmer, USA) in an ascending flow. At the exit from the column, the raffinate was fractionated using a C660 fraction collector (BUCHI Labortechnik AG, Switzerland) at 4 BV/hr (120 cm^3).

The concentrations of Al and Li ions in the initial solution and raffinates were determined by ICP-AES. Based on the results of ICP-AES analysis of raffinate fractions, elution sorption curves were plotted, and the dynamic exchange capacity and the total dynamic exchange capacity of the sorbent were calculated.

Procedure for sorption purification of a solution after water leaching of the black mass

Fresh sorbent Diaion CRB05 was used for sorption purification of the solution (800 cm3), obtained by water leaching of the black mass at the ratio L/S = 10, from Al ions. Its volume was calculated based on the obtained DEC values for aluminum ions in the model experiment, which amounted to 2.47 g/dm^3 at the specific loading of 2 BV/hr. Taking into account the concentration of Al ions (C_0 = 112.7 mg/dm^3), the amount of CRB05 sorbent required to purify the solution obtained during water leaching of the black mass was calculated to be 37 ml.

Since the solution contains Ca, Mg, Fe and Ni ions, along with removing Al ions, the solution was additionally purified from these cations using 37 cm^3 of Purolite S950 chelate resin (aminophosphonic acid), which was previously converted into the Li-form by passing through a layer of 2M sorbent of lithium hydroxide solution at a flow rate of 111 cm^3/hr

Table 1. **Anion exchangers used for aluminum sorption under static conditions**

Таблица 1. Используемые аниониты для сорбции алюминия в статических условиях

Description	Active group	Active group structure	Working form
Purolite A500	Quaternary amine	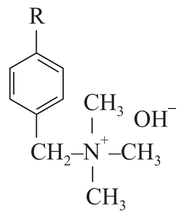	OH^-
AN-31	Tertiary amine, secondary amine	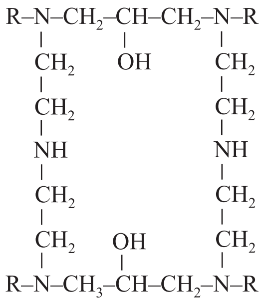	OH^-
Diaion CRB05	N-methylglucamine	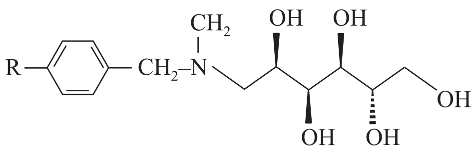	OH^-

(3 BV/hr) for 1 hour in an ascending flow, and then washed with water at a rate of 222 cm^3/hr (6 BV/hr) to displace the lithium hydroxide solution from the intergranular space.

The volume of Purolite S950 sorbent (37 cm^3) was selected based on the flow rate during purification amounting to 74 cm^3/hr (2 BV/hr), since the solution was simultaneously purified from anions and cations in the columns connected in sequence, with CRB05 and S950 sorbents. Before the sorption, they were dried and filled with the solution after water leaching of the black mass. The resulting purified solution (raffinate) was analyzed using the ICP-AES method.

Lithium carbonate precipitation technique and analysis

Since the concentration of Li (1.6 g/dm^3) in the solution purified by sorption makes the lithium carbonate precipitation impossible due to its relatively high solubility in water, the raffinate was concentrated by evaporation in a titanium beaker on a magnetic stirrer to 50 cm^3. During the process, the precipitate was formed, which is likely to be attributed to the interaction of lithium hydroxide with carbon dioxide contained in the air. After evaporation, carbon dioxide was passed through the solution heated to 80 °C until pH reached the value of 8.5 for more complete precipitation of lithium carbonate. The resulting precipitate was separated from the solution by vacuum filtration, washed with alcohol and dried for 1 hour at a temperature of 150 °C.

To analyze the impurity composition, the ICP-AES method was used. The mass fraction of the main substance (lithium carbonate) was estimated by acidometric titration by dissolving its subsample, adding hydrochloric acid, heating the solution to remove carbon dioxide, and titrating the excessive hydrochloric acid with a sodium hydroxide solution.

The mass fraction of water was determined using a MX-50 moisture analyzer (AND, Japan) at a temperature of 120 °C.

Results and discussion

Results of water leaching of lithium from the black mass

The water leaching results (Table 2) showed that lithium extraction is directly proportional to the L/S ratio (Fig. 2), the maximum degree of its extraction reaching 72.5 %.

We suppose that lithium recovery is incomplete due to a number of factors. Thus, as the Li concentration in the solution increases, so does the pH value (Table 2), which creates the conditions for the aluminum oxide dissolution, to be followed by the precipitation of aluminum hydroxide, which can absorb Li ions to form double layered aluminum-lithium hydroxide [22; 23].

Another possible reason is related to the black mass graphite component being hydrophobic. Most anode materials for Li-ion batteries are made of lithiated graphite [24], which can reversibly intercalate and deintercalate Li ions. During leaching, a graphite film emerged and remained on the solution surface throughout the experiment. The most obvious solution to this problem is to introduce surfactants, for example sodium laureth sulfate, into the pulp, but further concentration of the solution creates difficulties with foaming and precipitate filtration, therefore surfactants were not used at this stage of the research.

The third reason why the lithium extraction is incomplete may be associated with the sorption activity of some spinels: in particular, lithium manganates [25; 26] and lithium titanates [27; 28] are Li-selective sorbents, and when they are used, lithium desorption is realized in an acidic environment.

The analysis of kinetic curves (Fig. 3) shows that in the first 20 minutes of the leaching process, Li ions actively transfer into the solution and then the process slows down.

The ICP-AES analysis of the combined solution after the black mass leaching (Table 3) showed that the Al content in the solution exceeds 100 mg/dm^3. In addition, the solution contains other impurity elements (Ca, Mg, Fe, Ni) that can negatively affect the quality of the resulting lithium carbonate.

Numerous studies [29—31] are devoted to the sorption removal of Ca and Mg cations, as well as a number of other metals and choosing a sorbent is not an issue, since many chelate cation exchangers form more stable complexes with cations of bivalent metals than with Li ions. As noted above, the Al ions present in the solution in the form of [Al(OH)4]— pose a problem, so further investigation was aimed at finding a suitable anion exchanger.

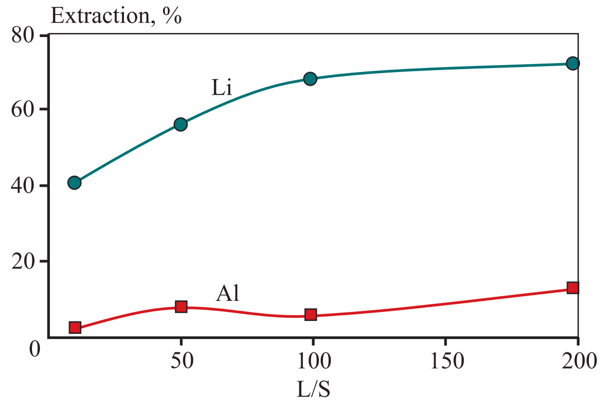

Fig. 2. Dependence of lithium and aluminum extraction on the L/S ratio during water leaching of the black mass

Рис. 2. Зависимость извлечения лития и алюминия от соотношения Ж : Т при водном выщелачивании «черной массы»

Results of aluminum sorption under static conditions

The results of sorption under static conditions show that strong base anion exchangers cannot remove hydroxoaluminate ions, while weak base anion exchangers AN-31 and CRB05 in an alkaline environment have a capacity from 2 to 3 g/dm^3 (Table 4). The mechanism of aluminum sorption on these sorbents is apparently based on the formation of a complex due to them having hydroxyl groups, and not due to ion exchange, since the amino groups are not protonated in an alkaline environment. This is evidenced by the results of aluminum sorption on the strong base anion exchanger Purolite A500, which cannot absorb aluminate ions due to the absence of hydroxyl groups.

Table 2. **Results of water leaching of lithium from the LIB black mass**

Таблица 2. Результаты водного выщелачивания лития из «черной массы» литий-ионных аккумуляторов

pH_{equil}	L/S	Content, mg/dm^3		Li/Al	Extraction, %		Li/Al
		Li	Al		Li	Al	
10.72	198	115.2	22.4	5.14	72.5	13.1	5.54
10.81	98	218.4	20.9	10.45	68.2	6.1	11.26
10.93	50	354.5	57.1	6.21	56.2	8.4	6.69
11.09	10	1301.0	96.6	13.47	41.2	2.8	14.51

Table 3. **The result of ICP-AES analysis of the solution for water leaching of the black mass before and after the sorption purification**

Таблица 3. Результаты ИСП-АЭС анализа раствора водного выщелачивания «черной массы» до и после сорбционной очистки

Element	Content, mg/dm^3	
	Before purification	After purification
Ti	<0.1	<0.1
Ca	13.8	0.5
Mn	<0.1	<0.1
Cu	<0.1	<0.1
Fe	2.6	0.75
Ni	4.0	1.95
Al	112.7	<0.5
Mg	3.0	0.6
Na	148.2	67.05
P	7.7	5.4
K	141.1	127.5
Li	1648.9	1661.4
Co	<0.1	<0.1

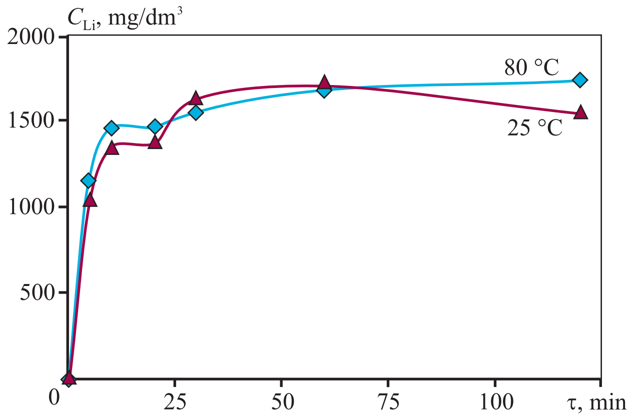

Fig. 3. Kinetic curves representing leaching of lithium ions from the black mass

Рис. 3. Кинетические кривые выщелачивания ионов лития из «черной массы»

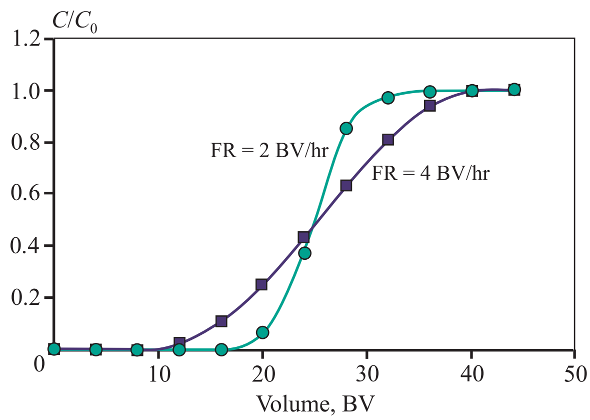

Fig. 4. Elution curves of aluminum sorption on CRB05 sorbent

Рис. 4. Выходные кривые сорбции алюминия на сорбенте CRB05

Since CRB05 has a higher capacity for aluminum ions (2.86 g/dm^3) than AN-31 (2.15 g/dm^3), it was chosen for further sorption experiments under dynamic conditions.

Results of aluminum sorption under dynamic conditions

In the model experiment on the aluminum dynamic sorption, our main task was to determine the dynamic and total dynamic exchange capacities, as well as to select the optimal flow rate for purifying the real solution after water leaching of the black mass from aluminum ions. Fig. 4 features the elution curves of aluminum sorption at the flow rates (FR) of 2 and 4 BV/hr. It can be observed that at the specific loading of 2 BV/hr, aluminum ion breakthrough occurs later, which enables to obtain a larger volume of raffinate purified from aluminum ions than at FR = 4 BV/hr with the same amount of sorbent.

Table 4. **Results of aluminum sorption under static conditions**

Таблица 4. Результаты сорбции алюминия в статических условиях

Sorbent	Solution volume, cm^3	Sorbent volume, cm^3	Sorbent mass, g	Concentration, mg/dm^3		SEC, g/dm^3	
				Al	Li	Al	Li
A500	50	1	0.3372	153.6	1469.6	0.04	0
AN-31	50	1	0,2713	111.4	1429.2	2.15	1.80
CRB05	50	1	0.3588	97.2	1475.6	2.86	0

The ICP-AES analysis of raffinates showed that the CRB05 dynamic exchange capacity at the specific loading of 2 BV/hr amounted to 2.47 g/dm^3, which is two times higher than at FR = 4 BV/hr (1.23 g/dm^3). Meanwhile, the total DEC for Al ions in both cases was about 3.5 g/dm^3. Their concentration in the raffinate before their breakthrough did not exceed 0.5 mg/dm^3 (below the ICP-AES detection limit).

Results of sorption purification of a solution after water leaching of the black mass

The sorption purification of the Li-containing solution after water leaching of the black mass at the specific loading of 2 BV/hr on Diaion CRB05 and Purolite S950 ion exchangers enabled to completely remove Al ions and partially remove Ca, Mg, Fe and Ni ions (Table 3).

The resulting purified solution was used to obtain lithium carbonate.

Results of lithium carbonate precipitation

The X-ray phase analysis of the white precipitate formed during thermal concentration (evaporation) of the water leaching solution purified from impurities showed that its main component is lithium carbonate and a phase with a cubic crystal system (space group $R\bar{3}m$) is present as an impurity (~2 %), its structure being similar to that of lithium cobaltite [32], however, its reliable identification proved impossible.

The proportion of the main substance amounted to 98.2 %. The resulting lithium carbonate in terms of the content of alkali and alkaline earth metals is comparable to technical lithium carbonate obtained from natural sources (Albemarle, USA, Rockwood Lithium, USA), but currently many manufacturers do not regulate the content of some elements, such as Ti, Co, Cu, Al and Ni, which are not typical for lithium carbonate obtained from natural hydro- and solid mineral sources.

Aluminum accounts for the largest share of impurities in lithium carbonate, although it was not detected in the solution after sorption removal due to the ICP-AES detection limit for Al ions — 0.5 mg/dm3. Apparently, the solution contained a certain amount of aluminum ions, which contaminated lithium carbonate in the course of the solution concentration during evaporation. In this regard, further research will be aimed at determining optimal sorption conditions and solving another problem — relatively low lithium extraction during water leaching (40—70 %).

Table 5. **Results of chemical analysis of the precipitate based on lithium carbonate**

Таблица 5. Результаты химического анализа осадка на основе карбоната лития

Element, compound	Content, wt.%	Method of analysis
Li_2CO_3	98.2	Acidometry
Ti	0.0170	ICP-AES
Ca	0.0204	ICP-AES
Mn	0.0006	ICP-AES
Cu	N/D	ICP-AES
Fe	0.0053	ICP-AES
Ni	N/D	ICP-AES
Al	0.0888	ICP-AES
Mg	0.0146	ICP-AES
Na	0.0111	ICP-AES
P	0.0304	ICP-AES
K	0.0105	ICP-AES
Co	N/D	ICP-AES
B	0.0052	ICP-AES
S	0.0006	ICP-AES
H_2O	0.2	Gravimetry

Conclusion

In the course of investigations aimed at obtaining lithium carbonate from the black mass of lithium-ion batteries, we explored the process of water leaching of lithium at various L/S ratios. During the study, we:

— derived the dependencies of lithium extraction on the L/S ratio and plotted kinetic leaching curves;

— explored the process of sorption removal of aluminum from the model alkaline Li—Al solution using some weak base anion exchangers (CRB05 and AN-31);

— determined the capacity of anion exchangers under static and dynamic conditions;

— plotted elution aluminum sorption curves for specific flow rates of 2 and 4 bed volume per hour;

— performed sorption purification of the solution after aqueous leaching of the black mass using a weak base anion exchanger Diaion CRB05 and a chelate cation exchanger Purolite S950.

After evaporation of the purified solution, we obtained lithium carbonate with a content of the main substance of 98.2 %.

References

1. Sarkarov R.A., Belan S.I., Guseinov N.M. Assessment of the current state and prospects for the production of lithium and its compounds in Russia. *Industrial'naya ehkonomika*. 2022;1(2):57—68. (In Russ.).
https://doi.org/10.47576/2712-7559_2022_2_1_57
Саркаров Р.А., Белан С.И., Гусейнов Н.М. Оценка современного состояния и перспективы добычи лития и его соединений в России. *Индустриальная экономика*. 2022;1(2):57—68.
https://doi.org/10.47576/2712-7559_2022_2_1_57
2. Mizushima K., Jones P.J., Wiseman J.B., Goodenough J.B. Li_xCoO_2 ($0 < x < -1$): A new cathode material for batteries of high energy density. *Materials Research Bulletin*. 1980;15:783—789.
https://doi.org/10.1016/0025-5408(80)90012-4
3. Thackeray M.M., Johnson P.J., De Picciotto L.A., Bruce P.G., Goodenough J.B. Electrochemical extraction of lithium from $LiMn_2O_4$. *Materials Research Bulletin*. 1984;19(2):179—187.
https://doi.org/10.1016/0025-5408(84)90088-6
4. Zaghib K., Simoneau, M., Armand M., Gauthier M. Electrochemical study of $Li_4Ti_5O_{12}$ as negative electrode for Li-ion polymer rechargeable batteries. *Journal of Power Sources*. 1999;81:300—305.
https://doi.org/10.1016/S0378-7753(99)00209-8
5. Padhi A.K., Nanjundaswamy K.S., Goodenough J.B. Phospho-olivines as positive-electrode materials for rechargeable lithium batteries. *Journal of the electrochemical society*. 1997;144(4):1188.
https://doi.org/10.1149/1.1837571
6. Shi P., Li T., Zhang R., Shen X., Cheng X. B., Xu R., Huang X. C. Liu H., Zhang Q. Lithiophilic LiC_6 layers on carbon hosts enabling stable Li metal anode in working batteries. Advanced Materials. 2019;31(8):1807131.
https://doi.org/10.1002/adma.201807131
7. Aaltonen M., Peng C., Wilson B.P., Lundström M. Leaching of metals from spent lithium-ion batteries. *Recycling*. 2017;2(4):20. https://doi.org/10.3390/recycling2040020
8. Lie J., Liu J.C. Closed-vessel microwave leaching of valuable metals from spent lithium-ion batteries (LIBs) using dual-function leaching agent: Ascorbic acid. *Separation and Purification Technology*. 2021;266:118458.
https://doi.org/10.1016/j.seppur.2021.118458
9. Golmohammadzadeh R., Faraji F., Rashchi F. Recovery of lithium and cobalt from spent lithium ion batteries (LIBs) using organic acids as leaching reagents: A review. *Resources, Conservation and Recycling*. 2018;136:418—435.
https://doi.org/10.1016/j.resconrec.2018.04.024
10. De Oliveira Demarco J., Cadore J. S., da Silveira de Oliveira F., Tanabe E. H., Bertuol D. A. Recovery of metals from spent lithium-ion batteries using organic acids. *Hydrometallurgy*. 2019;190:105169.
https://doi.org/10.1016/j.hydromet.2019.105169
11. Esmaeili M., Rastegar S.O., Beigzadeh R., Gu T. Ultrasound-assisted leaching of spent lithium ion batteries by natural organic acids and H_2O_2. *Chemosphere*. 2020;254:126670.
https://doi.org/10.1016/j.chemosphere.2020.126670
12. Fu Y., He Y., Chen H., Ye C., Lu Q., Li R., Xie W., Wang J. Effective leaching and extraction of valuable metals from electrode material of spent lithium-ion batteries using mixed organic acids leachant. *Journal of Industrial and Engineering Chemistry*. 2019;79:154—162.
https://doi.org/10.1016/j.jiec.2019.06.023
13. Gao W., Liu C., Cao H., Zheng X., Lin X., Wang H., Zhang Y., Sun Z. Comprehensive evaluation on effective leaching of critical metals from spent lithium-ion batteries. *Waste Management*. 2018;75:477—485.
https://doi.org/10.1016/j.wasman.2018.02.023
14. Urbańska W. Recovery of Co, Li, and Ni from spent Li-ion batteries by the inorganic and/or organic reducer assisted leaching method. *Minerals*. 2020;10(6):555.
https://doi.org/10.3390/min10060555
15. Nayl A.A., Elkhashab R.A., Badawy S.M., El-Khateeb M.A. Acid leaching of mixed spent Li-ion batteries. *Arabian Journal of Chemistry*. 2017;10:S3632—S3639.
https://doi.org/10.1016/j.arabjc.2014.04.001
16. Ku H., Jung Y., Jo M., Park S., Kim S., Yang D., Rhee K., An E.M. Sohn J., Kwon K. Recycling of spent lithium-ion battery cathode materials by ammoniacal leaching. *Journal of hazardous materials*. 2016;313:138—146.
https://doi.org/10.1016/j.jhazmat.2016.03.062
17. Gaye N., Gueye R.S., Ledauphin J., Balde M., Seck M., Wele A., Diaw M. Alkaline leaching of metals from cathodic materials of spent lithium-ion batteries. *Asian Journal of Applied Chemistry Research*. 2019: 3(2);1—7.
https://doi.org/10.9734/AJACR/2019/v3i230088
18. Kim D., Quang N. D., Hien T. T., Chinh N. D., Kim C., Kim D. 3D inverse-opal structured $Li_4Ti_5O_{12}$ Anode for fast Li-ion storage capabilities. *Electronic Materials Letters*. 2017:13(6):505—511.
https://doi.org/10.1007/s13391-017-7101-x
19. Wang S.L., Lin C.H., Yan, Y.Y., Wang M.K. Synthesis of Li/Al LDH using aluminum and LiOH. *Applied Clay Science*. 2013;72:191—195.
https://doi.org/10.1016/j.clay.2013.02.001
20. Chistyakov A.A., Chirkst D.E., Cheremisina O.V. Sorption of aluminate from alkaline solutions on D-403 anion exchanger. *Russian Journal of Physical Chemistry A*. 2011:85(11);1995—1999.
https://doi.org/10.1134/s0036024411110069

Чистяков А.А., Чиркст Д.Э., Черемисина О.В. Сорбция алюмината из щелочных растворов на анионите D-403. *Журнал физической химии*. 2011:85(11): 2137—2141.
21. Cheremisina O.V., Ponomareva M.A., Sagdiev V.N. Sorption extraction of gallium and aluminum from alkaline solutions on the AN-31 anion-exchange resin. *Izvestiya. Non-Ferrous Metallurgy*. 2017;(3):56—64. (In Russ.). https://doi.org/10.17073/0021-3438-2017-3-56-64
Черемисина О.В., Пономарева М.А., Сагдиев В.Н. Сорбционное извлечение галлия и алюминия из щелочных растворов на анионите АН-31. *Известия вузов. Цветная металлургия*. 2017:(3);56—64. https://doi.org/10.17073/0021-3438-2017-3-56-64
22. Ramazanov A.Sh., Sveshnikova D.A., Ataev D.R. Kinetics of lithium cation sorption with freshly precipitated aluminum hydroxide from natural brine. *Sorbtsionnye i khromatograficheskie protsessy*. 2021:21(2):225—234. (In Russ.). https://doi.org/10.17308/sorpchrom.2021.21/3356
Рамазанов А.Ш., Свешникова Д.А., Атаев Д.Р. Кинетика сорбции катиона лития свежеосажденным гидроксидом алюминия из природного рассола. *Сорбционные и хроматографические процессы*. 2021:21(2);225—234. https://doi.org/10.17308/sorpchrom.2021.21/3356
23. Jiang H., Yang Y., Sun S., Yu J. Adsorption of lithium ions on lithium-aluminum hydroxides: Equilibrium and kinetics. *The Canadian Journal of Chemical Engineering*. 2020:98(2);544—555. https://doi.org/10.1002/cjce.23640
24. Zhang H., Yang Y., Ren D., Wang L., He X. Graphite as anode materials: Fundamental mechanism, recent progress and advances. *Energy Storage Materials*. 2021;36:147—170. https://doi.org/10.1016/j.ensm.2020.12.027
25. Wajima T., Munakata K., Uda T. Adsorption behavior of lithium from seawater using manganese oxide adsorbent. *Plasma and Fusion Research*. 2012;7:2405021. https://doi.org/10.1585/pfr.7.2405021
26. Chitrakar R., Kanoh H., Miyai Y., Ooi K. Recovery of lithium from seawater using manganese oxide adsorbent ($H_{1.6}Mn_{1.6}O_4$) derived from $Li_{1.6}Mn_{1.6}O_4$. *Industrial & Engineering Chemistry Research*. 2001:40(9):2054—2058. https://doi.org/10.1021/ie000911h
27. Hossain S.M., Ibrahim I., Choo Y., Razmjou A., Naidu G., Tijing L., Kim J., Shon H.K. Preparation of effective lithium-ion sieve from sludge-generated TiO_2. *Desalination*. 2022;525:115491. https://doi.org/10.1016/j.desal.2021.115491
28. Li X., Chen L., Chao Y., Chen W., Luo J., Xiong J., Zhu F., Chu X., Li H., Zhu W. Amorphous TiO_2 — derived large — capacity lithium ion sieve for lithium recovery. *Chemical Engineering & Technology*. 2020:43(9); 1784—1791. https://doi.org/10.1002/ceat.201900374
29. Volkova T.S., Rudskikh V.V. Study of the possibility of purifying lithium chloride solution to remove impurities by sorption method. *Russian Journal of Applied Chemistry*. 2019;92(8):1113—1121. https://doi.org/10.1134/S1070427219080093
Волкова Т.С., Рудских В.В. Исследование возможности очистки раствора хлорида лития от примесей сорбционным методом. *Журнал прикладной химии*. 2019;92(8):1021—1029. https://doi.org/10.1134/S0044461819080097
30. Kiefer R., Höll W.H. Sorption of heavy metals onto selective ion-exchange resins with aminophosphonate functional groups. *Industrial & Engineering Chemistry Research*. 2001;40(21):4570—4576. https://doi.org/10.1021/ie010182l
31. Milyutin V.V., Nekrasova N.A., Rudskikh V.V., Volkova T.S. Preparation of high-purity lithium carbonate using complexing ion-exchange resins. *Russian Journal of Applied Chemistry*. 2020;93:549—553. https://doi.org/10.1134/S1070427220040096
Милютин В.В., Некрасова Н.А., Рудских В.В., Волкова Т.С. Получение высокочистого карбоната лития с использованием комплексообразующих ионитов. *Журнал прикладной химии*. 2020;93(4): 540—544. https://doi.org/10.31857/S0044461820040088
32. Hertz J.T., Huang Q., McQueen T., Klimczuk T., Bos J.W.G., Viciu L., Cava R.J. Magnetism and structure of Li_xCoO_2 and comparison to Na_xCoO_2. *Physical Review B*. 2008;77(7):075119. https://doi.org/10.1103/PhysRevB.77.075119

Information about the authors

Sergey A. Aleynikov – Postgraduate Student of the Department of non-ferrous metals, Siberian Federal University (SibFU).
https://orcid.org/0009-0001-7589-7049
E-mail: saaleynikov@yandex.ru

Natalya V. Belousova – Dr. Sci. (Chem.), Professor, Head of the Department of Non-Ferrous Metals, SibFU.
https://orcid.org/0000-0002-1355-7399
E-mail: netmamba@mail.ru

Информация об авторах

Сергей Александрович Алейников – аспирант кафедры цветных металлов, Сибирский федеральный университет (СФУ).
https://orcid.org/0009-0001-7589-7049
E-mail: saaleynikov@yandex.ru

Наталья Викторовна Белоусова – д.х.н., профессор, зав. кафедрой цветных металлов, СФУ.
https://orcid.org/0000-0002-1355-7399
E-mail: netmamba@mail.ru

Contribution of the authors

S.A. Aleynikov – determining the purpose of the work, conducting experiments, ICP-AES, and XRF analyses, writing the article.

N.V. Belousova – determining the purpose of the work and participating in the discussion of the results.

Вклад авторов

С.А. Алейников – определение цели работы, проведение экспериментов и ИСП-АЭС, РФА анализов, участие в обсуждении результатов, написание текста статьи.

Н.В. Белоусова – постановка цели работы, участие в обсуждении результатов.

The article was submitted 10.02.2024, revised 14.03.2024, accepted for publication 18.03.2024

Статья поступила в редакцию 10.02.2024 г., доработана 14.03.2024 г., подписана в печать 18.03.2024 г.

METALLURGY OF RARE AND PRECIOUS METALS / МЕТАЛЛУРГИЯ РЕДКИХ И БЛАГОРОДНЫХ МЕТАЛЛОВ

UDC 546.34 + 666.123.24 + 669.2/.8
https://doi.org/10.17073/0021-3438-2024-3-45-56
Research article
Научная статья

Development and solution of the kinetics equation and adsorption isotherm for gold adsorption from cyanide solutions onto activated carbon

V.V. Elshin, A.P. Mironov, A.A. Lisitsyna

Irkutsk National Research Technical University
83 Lermontov Str., Irkutsk 664074, Russia

✉ Anastasia A. Lisitsyna (Gerasimovan19@rambler.ru)

Abstract: This paper presents the results of theoretical and experimental studies on the process of gold adsorption from cyanide solutions onto activated carbon (AC). One of the objectives of the study was to identify the functional relationship between the mass loading of AC in the volume of the adsorption column solution and the kinetics of the process. To achieve this, a modified adsorption kinetics equation (considering the heterogeneity of the process) was proposed, which incorporates the solid phase of the carbon sorbent in the unit volume of solution as a third intermediate agent of adsorption interaction between the adsorbate ions and the free active sites of the AC. As a result, a modified third-order adsorption kinetics equation for gold adsorption on AC was derived, taking into account the solid phase loading of AC in the solution volume, along with its analytical solutions under conditions of constant gold content in the initial solution and the process conducted in a closed volume with varying gold concentrations in the solution according to the material balance equation. The relationship between the solutions of the kinetic equation and the adsorption isotherm equation was established. From the solutions of the kinetic equation, a modified Langmuir isotherm equation was derived, which allows determining the equilibrium concentrations of gold on the AC and in the solution a priori under the condition that the process is conducted in a closed volume, with known initial gold contents in the solution and on the AC, as well as with a known AC loading in the adsorber volume. The theoretical dependencies of the adsorption and desorption rate constants on temperature, convective, and diffusion parameters are discussed. The presented mathematical model of adsorption kinetics is valid under the conditions of gold adsorption on AC from gold cyanide solutions with an adsorption time of up to 2 days and a sorbent capacity utilization degree of 40–60%.

Keywords: gold, kinetics, adsorption, carbon adsorbent, adsorption isotherm, cyanide solution, reaction rate constant, mathematical modeling.

Acknowledgments: The authors express their gratitude to the staff of Laboratory No. 15 of "Irgiredmet" OJSC for providing experimental data on the kinetics of gold adsorption onto activated carbon and for assisting with the analyses.

For citation: Elshin V.V., Mironov A.P., Lisitsyna A.A. Development and solution of the kinetics equation and adsorption isotherm for gold adsorption from cyanide solutions onto activated carbon. *Izvestiya. Non-Ferrous Metallurgy.* 2024;30(3):45–56.
https://doi.org/10.17073/0021-3438-2024-3-45-56

Разработка и решение уравнения кинетики и изотермы адсорбции золота из цианистых растворов на активированный уголь

В.В. Ёлшин, А.П. Миронов, А.А. Лисицына

Иркутский национальный исследовательский технический университет
Россия, 664074, г. Иркутск, ул. Лермонтова, 83

✉ Анастасия Андреевна Лисицына (Gerasimovan19@rambler.ru)

Аннотация: Представлены результаты теоретических и экспериментальных исследований процесса адсорбции золота из цианистых растворов на активированный уголь (АУ). Одной из задач работы было выявление функциональной зависимости между загрузкой массы АУ в объеме раствора адсорбционной колонны и кинетикой процесса. Для ее решения предложено модифицированное уравнение кинетики адсорбции (с учетом гетерогенности процесса) в виде включения твердой фазы угольного сорбента в единице объема раствора в качестве третьего промежуточного агента адсорбционного взаимодействия между ионами адсорбата и свободными активными центрами АУ. В результате получены модифицированное уравнение кинетики адсорбции золота на АУ 3-го порядка с учетом твердой фазы загрузки АУ в объеме раствора и его аналитические решения при условиях постоянства содержания золота в исходном растворе и проведения процесса в замкнутом объеме с изменяющейся концентрацией золота в растворе согласно уравнению материального баланса. Установлена взаимосвязь между решениями кинетического уравнения и уравнением изотермы адсорбции. Из решений кинетического уравнения получено модифицированное уравнение изотермы Ленгмюра, позволяющее находить равновесные концентрации золота на АУ и в растворе доопытно при условии проведения процесса в замкнутом объеме и известных начальных значениях содержаний золота в растворе и на АУ, а также при известной загрузке АУ в объеме адсорбера. Обсуждены теоретические зависимости констант скоростей адсорбции и десорбции от температуры, конвективных и диффузионных параметров. Представленная математическая модель кинетики адсорбции справедлива для условий проведения процесса адсорбции золота на АУ из золотоцианистых растворов при времени адсорбции до 2 суток и степени заполнения полной предельной емкости сорбента 40–60 %.

Ключевые слова: золото, кинетика, адсорбция, угольный адсорбент, изотерма адсорбции, цианистый раствор, константа скорости реакции, математическое моделирование.

Благодарности: Авторы благодарят сотрудников лаборатории № 15 АО «Иргиредмет» (г. Иркутск) за предоставленные экспериментальные данные по кинетике адсорбции золота на активированный уголь и за содействие в проведении анализов.

Для цитирования: Ёлшин В.В., Миронов А.П., Лисицына А.А. Разработка и решение уравнения кинетики и изотермы адсорбции золота из цианистых растворов на активированный уголь. *Известия вузов. Цветная металлургия*. 2024;30(3):45–56.
https://doi.org/10.17073/0021-3438-2024-3-45-56

Introduction

A fundamental problem in the field of carbon-sorption technology for the extraction of gold from gold-cyanide solutions is the lack of a universally accepted, theoretically grounded kinetics equation that can adequately describe both the dynamics and statics of the sorption process, taking into account variable operating factors — such as the concentrations of metal and the mass of activated carbon (AC) in the solution volume. Of the currently existing equations, the most widely used in practice are two semi-empirical Fleming kinetics equations [1—3]. The first of these cannot, in principle, adequately represent the sorption process because it does not assume the existence of an isotherm, while the second is only valid for a sorption process with a linear isotherm, which in our case is unacceptable as it contradicts experimental data.

Therefore, it is necessary to select a theoretically grounded adsorption kinetics equation from the existing developments in this field and, if needed, refine it to qualitatively align with the currently established patterns of the adsorption process. One of the main conditions should be the possibility of analytically deriving an isotherm equation from the selected kinetics equation. For further refinement of the mathematical model to quantitatively correspond to the kinetic characteristics of the adsorption process, a series of standard experimental studies must be conducted to obtain kinetic curves under various initial conditions for the determining operating factors — such as the initial concentration of gold in the solution and the carbon loading in the adsorber volume. The experimental kinetic curves and the isotherm curve can be used to identify the predictive mathematical model, with the final result being the numerical values of the identification constants that correspond to the characteristic properties of the carbon sorbent.

Thus, the objective of this work was to attempt to solve a fundamental problem in the theory and practice of gold adsorption from gold-cyanide solutions onto activated carbon — the theoretical justification of the physical meaning of the proposed kinetics equation and the adsorption process isotherm equation to create a predictive mathematical model capable of adequately describing the dynamics of the adsorption process at a quantitative level, within the framework of developing industrial process schemes and optimizing their operation. This study precedes a subsequent series of articles dedicated to the problem of modeling noble metal sorption processes onto AC, addressing issues of intradiffusion kinetics, countercurrent sorption processes from solutions and pulps (CIL and CIP processes).

1. Research methodology

To construct the isotherm for gold adsorption onto activated carbon (NORIT-3515), a static method with constant AC mass of 1.5 g and varying gold concentrations from 3.2 to 39.8 mg/dm^3 in cyanide solutions with NaCN concentration = 176.0 mg/dm^3, pH = 10.8, was used. The solution temperature was maintained between 20—22 °C throughout the experiments.

The adsorber was a circular vessel made of organic glass with a flat bottom and an agitation device equipped with a stirrer speed regulator. The height-to-diameter ratio of the adsorber was 2.5 : 1.0, with a solution volume of 3 dm^3 for each experiment. The total time required to achieve one equilibrium isotherm value was 216 hours. Samples were taken at regular intervals from the start of the experiment to construct kinetic curves.

The gold concentration in the solutions was determined using an atomic absorption spectrophotometer ICE 3300 (Thermo Fisher Scientific, USA) at the certified analytical center of "Irgiredmet" OJSC (Certificate No. 222.0132/RA.RU.311866/2021 for measurement methodology accreditation). The standard deviation of reproducibility for gold concentrations in solutions ranging from 0.01—0.10 mg/dm^3 was between 0.003 to 0.007 with an error margin of ±0.006 to ±0.014 mg/dm^3 at a confidence level of P = 0.95. The error margins at P = 0.95 for the concentration ranges 0.2—1.0 mg/dm^3 were ±0.04 to ±0.08 mg/dm^3, for 3.0—10.0 mg/dm^3 were ±0.2 to ±0.5 mg/dm^3, and for 20.0—50.0 mg/dm^3 were ±1.0 to ±2.5 mg/dm^3. The experimental results were statistically processed, calculating the mean, standard deviation, and confidence intervals for reproducibility for each isotherm point and kinetic curve.

1.1. Theoretical foundations of gold adsorption kinetics from cyanide solutions onto activated carbon

1.1.1. Theoretical justification for choosing a third-order kinetics equation

Experimental modeling of the adsorption kinetics process can be conducted in two ways. In the first case, adsorption occurs under conditions of constant gold content in the solution, while in the second, it occurs in a closed volume with continuously changing gold concentration in the solution according to the material balance. Although the adsorption mechanism and the kinetics equation describing the process remain unchanged, the solutions to the kinetics equations differ in each case and have different practical applications. [4; 5] The solution obtained from the kinetics equation for adsorption in a closed volume, taking into account additional conditions related to the ionic composition of the solution and its continuous flow through the adsorbers, can be directly used in the calculations of a continuous countercurrent gold adsorption process onto activated carbon [6—10], carried out in a series of sequentially arranged adsorption apparatus.

The widely accepted gold adsorption kinetics equation from cyanide solutions onto AC, considering the reversibility of the adsorption process and the existence of a sorbent's maximum capacity, is as follows:

$$\frac{dC_{\text{y}}}{dt} = K_1(C_0 - C_{\text{y}})C_{\text{p}} - K_2C_{\text{y}}, \qquad (1)$$

where C_{y} is the gold content in the loaded carbon, mg/g; C_{p} is the gold concentration in the solution, mg/dm^3; C_0 is the maximum adsorption capacity of the sorbent, mg/g; K_1 is the adsorption rate constant, dm^3/(mg·h); K_2 is the desorption rate constant, h^{-1}; t is time, h.

This is the classical form of the equation for a reversible second-order homogeneous chemical reaction, and since it describes a heterogeneous adsorption process, it is assumed a priori that the mass of the solid-phase adsorbent in the adsorption process is constant and is automatically considered in the adsorption rate constant. For the practical application of the kinetics equation (1), whose behavior largely depends on the adsorbent loading, it is necessary to establish a functional relationship between the adsorption rate and the mass of AC in the solution. This issue can be addressed by considering that the heterogeneous physicochemical process of $AuCN_2^-$ adsorption onto AC has a third-order interaction, unlike the second-order homogeneous chemical reaction (1).

The difference between these two processes is that in a chemical reaction, two substances, evenly dissolved in a liquid, interact with equal probability at any point in the solution, whereas in the adsorption process, the ions dissolved in the liquid phase have different probabilities of reaching the adsorbent surface depending on their location to interact with the free active sites contained in the finely dispersed solid phase of the adsorbent distributed in the liquid phase of the solution.

Thus, the act of paired interaction between an adsorbate ion and the active sites of the adsorbent is divided into two sequential processes: the first is the transport of the adsorbate ion in the solution phase to the surface of the adsorbent's solid phase, and the second is the interaction of some ions that have reached the surface with the free active sites of the adsorbent, while another portion desorbs back into the solution phase.

The kinetics of the adsorption process is critically influenced by internal operational parameters such as the loading of a certain mass of AC per unit volume of solution and the gold concentration in the solution. Since adsorption is a mass-statistical process, it must obey the law of mass action. This means that the intensity of any paired interactions is always directly proportional to the product of the concentrations of the interacting agents. If the interaction of agents occurs indirectly through an intermediate stage that screens out some portion of one of the agents, the intensity of the final paired interaction of these agents will equal the product of the remaining concentration of the agent that passed through the intermediate stage and the concentration of the second agent.

According to the law of mass action, the product $C_p \cdot m/V$ characterizes the intensity of the first interaction of dissolved $AuCN_2^-$ with the surface of the solid phase of the adsorbent granules, where m/V (g/dm^3) represents the content, or loading, of the adsorbent mass (m, g) per unit volume of solution (V, dm^3). This parameter includes all the physicochemical characteristics of the adsorbent, including granule size, effective surface area, porosity, and its nature, which should be reflected in the rate constant K_1.

The intensity of the second paired interaction between the $AuCN_2^-$ ions that have reached the solid phase surface and the free active sites of the adsorbent will be proportional, according to the law of mass action, to the product $C_p \cdot m/V$ and the content of free active sites in the mass of the adsorbent's solid phase $C_0 - C_y$, i.e. $C_p \cdot m/V \cdot (C_0 - C_y)$.

Based on the above concepts of the $AuCN_2^-$ adsorption process onto AC, we record the third-order adsorption kinetics differential equation considering the heterogeneity and reversibility of the process:

$$\frac{dC_y}{dt} = K_1(C_0 - C_y)\left(C_p \frac{m}{V}\right) - K_2 C_y, \qquad (2)$$

where K_1 is the adsorption rate constant, (dm^3)^2/(g·mg·h).

This equation is valid only for the first two stages of adsorption: convective mass transfer and film-near-surface diffusion, i.e., approximately up to 40—60 % of the full capacity of the carbon [1—3]. This work is limited to considering only these two fastest stages of the adsorption process. It is assumed that in the initial period, up to about 2 days, the contribution of the third, slower and significantly longer intradiffusion stage is negligible.

1.1.2. Analytical solutions of the kinetics equation and derivation of the isotherm equation

The first analytical solution of the kinetics equation (2) is obtained under the condition that the gold concentration in the solution is constant and equal to C_{p0}. In practice, such conditions can be realized with a low AC loading in a large volume of solution (in the unlimited case).

The particular solution of equation (2), assuming C_p = const and for the initial conditions $C_p = C_{p0}$, $C_y = C_{y0}$, at $t = 0$, will have the form:

$$C_y = \frac{K_1 C_0 C_{p0}\, m/V}{K_1 C_{p0}\, m/V + K_2}\left(1 - e^{-(K_1 C_{p0} m/V + K_2)t}\right) + C_{y0}\, e^{-(K_1 C_{p0} m/V + K_2)t}, \qquad (3)$$

where C_{y0} is the initial gold content in the carbon, mg/g; C_{p0} is the initial constant gold concentration in the cyanide solution, mg/dm^3.

The solution (3) shows that at $t \to \infty$, $e^{-(K_1 C_{p0} m/V + K_2)t} \to 0$, and therefore, the value will tend towards its isothermal value determined by the expression:

$$C_y = \frac{C_0 C_{p0}\, m/V}{C_{p0}\, m/V + K_2/K_1}, \qquad (4)$$

which represents a modified form of the Langmuir isotherm considering the loading m/V of the adsorbent in the adsorber volume. Given that C_{p0} = const, the time required to reach the equilibrium value C_y, can be quite long, sometimes taking months.

To solve the kinetics equation (2) under adsorption conditions in a closed volume, it must be supplemented by the material balance equation:

$$(C_y - C_{y0})m = (C_{p0} - C_p)V, \qquad (5)$$

where m is the mass of the carbon, g; V is the solution volume, dm^3; C_{p0} is the initial gold concentration in the cyanide solution, mg/dm^3.

From equation (5), the expression for the current value C_p can be found as:

$$C_p = C_{p0} - \frac{m}{V}(C_y - C_{y0}), \qquad (6)$$

substituting this into (2), we obtain a nonlinear first-order differential equation with the right-hand side in the form of a quadratic trinomial relative to C_y with constant coefficients:

$$\frac{dC_y}{dt}=K_1\left(\frac{m}{V}\right)^2 C_y{}^2-$$
$$-\left[K_1C_0\left(\frac{m}{V}\right)^2+K_1C_{p0}\frac{m}{V}+K_1\left(\frac{m}{V}\right)^2C_{y0}+K_2\right]C_y+$$
$$+K_1C_0C_{p0}\frac{m}{V}+K_1\left(\frac{m}{V}\right)^2C_0C_{y0}. \qquad (7)$$

It is known that a quadratic trinomial can always be represented as the product of two linear binomials if its roots are known, which can be found by equating the right side of equation (7) to zero:

$$C_{y1}=0{,}5\left[C_0+\frac{V}{m}C_{p0}+C_{y0}+\frac{K_2}{K_1}\left(\frac{V}{m}\right)^2\right]+$$
$$+\sqrt{0{,}25\left[C_0+\frac{V}{m}C_{p0}+C_{y0}+\frac{K_2}{K_1}\left(\frac{V}{m}\right)^2\right]^2-\left[\frac{V}{m}C_0\left(C_{p0}+C_{y0}\frac{m}{V}\right)\right]}, \qquad (8)$$

$$C_{y2}=0{,}5\left[C_0+\frac{V}{m}C_{p0}+C_{y0}+\frac{K_2}{K_1}\left(\frac{V}{m}\right)^2\right]-$$
$$-\sqrt{0{,}25\left[C_0+\frac{V}{m}C_{p0}+C_{y0}+\frac{K_2}{K_1}\left(\frac{V}{m}\right)^2\right]^2-\left[\frac{V}{m}C_0\left(C_{p0}+C_{y0}\frac{m}{V}\right)\right]}. \qquad (9)$$

Knowing the roots C_{y1} and C_{y2}, equation (7) can be rewritten as:

$$\frac{dC_y}{dt}=K_1\left(\frac{m}{V}\right)^2(C_y-C_{y1})(C_y-C_{y2}). \qquad (10)$$

This expression represents the mass-action equation with a known solution [11]. In our case, it looks as follows:

$$C_y=\frac{c_1C_{y2}e^{K_1(m/V)^2(C_{y1}-C_{y2})t}-c_2K_1(m/V)^2C_{y1}}{c_1e^{K_1(m/V)^2(C_{y1}-C_{y2})t}-c_2K_1(m/V)^2}, \qquad (11)$$

where c_1 and c_2 are arbitrary constants.

Thus, (11) is effectively the solution of two equations: the differential kinetics equation and the material balance equation, so the particular solution for the initial conditions $t = 0$, $C_y = C_{y0}$ and $C_p = C_{p0}$ has the form

$$C_y=\frac{C_{y2}\left(\dfrac{C_{y0}-C_{y1}}{C_{y0}-C_{y2}}\right)\cdot e^{K_1(m/V)^2(C_{y1}-C_{y2})t}-C_{y1}}{\left(\dfrac{C_{y0}-C_{y1}}{C_{y0}-C_{y2}}\right)\cdot e^{K_1(m/V)^2(C_{y1}-C_{y2})t}-1}. \qquad (12)$$

Analysis of solution (12) shows that at $t \to \infty$ the value $C_y = C_{y2}$. Since C_y in each specific case, at different values of C_{p0}, C_{y0} and $t \to \infty$ will tend toward the isothermal value, equal to C_{y2}, meaning that C_{y2} should represent the isothermal point for the kinetics curve, and the collection of these points for different values of C_{p0} will form the isothermal curve. Therefore, the dependence of C_{y2} on the final equilibrium concentration of gold in the solution C_p, which can be obtained from the material balance equation, is the isotherm equation.

Returning to expression (9), it is evident that C_{y2} depends on many parameters, including the initial gold concentration in the solution C_{p0} its content in the regenerated carbon C_{y0}, as well as the mass loading of carbon m/V in the adsorber volume. Since the isotherm equation must link C_{y2} with the final equilibrium gold concentration in the solution C_p, from the material balance equation (5) for a given value of C_{y2} we find the value of C_p.

Expressing C_{p0} and C_{y0} through the equilibrium values C_{y2} and C_p and substituting them into expression (9), after a series of elementary transformations, we obtain an equation linking C_{y2} with C_p and m/V:

$$C_{y2}=\frac{C_0C_p\,m/V}{K_2/K_1+C_p\,m/V}, \qquad (13)$$

where C_{y2} is the equilibrium gold content, mg/g; C_0 is the maximum adsorption capacity of the sorbent, mg/g; C_p is the equilibrium gold concentration in the solution, mg/dm^3; m is the mass of carbon, g; V is the volume of solution, dm^3; K_1 is the adsorption rate constant, (dm^3)^2/(g·mg·h); K_2 is the desorption rate constant, h^{-1}.

Thus, the root C_{y2} is the equilibrium isothermal gold content on the carbon for a given equilibrium gold concentration in the solution C_p, and these quantities are linked by equation (13), which is a modified Langmuir isotherm equation adjusted for carbon loading. That is, the Langmuir isotherm, as expected, is valid for adsorption in a closed volume. Considering expression (9), which directly links C_{y2} with the initial parameters C_{p0}, m, V, and C_{y0}, note that there is a possibility of predictive determination of C_{y2} under given initial conditions, which, in turn, allows finding the equilibrium gold concentration in the solution:

$$C_p=\frac{\dfrac{C_{y2}K_2}{K_1}\dfrac{V}{m}}{C_0-C_{y2}}. \qquad (13.1)$$

2. Results and discussion

2.1. Identification of the adsorption mathematical model based on experimental data: calculated and experimental kinetics and isotherm curves

The identification of the model coefficients was conducted using the isotherm equation (9) obtained from experimental isothermal values. The first approximation of the coefficients K_{21} and C_0 was determined using the least squares method based on the linearized isotherm equation. The refinement or adjustment of the coefficients was performed iteratively based on the criterion of the sum of squares of deviations between the calculated and experimental isotherm values.

The identification of the isotherm (9), considering that $K_{21} = K_2/K_1$ is a constant value, allowed for the determination of the numerical values of the constants $K_{21} = 1.753$ g·mg/(dm^3)^2 и $C_0 = 56.996$ mg/g, which are valid over a wide range of varying internal operational parameters for adsorption kinetics: the initial gold concentration in the solution C_{p0} and the mass of AC (m) loaded in the adsorber volume V: $3.2 < C_{p0} <$ < 39.8 mg/dm^3 и $0.5 < m/V < 50$ г/dm^3.

These parameter ranges cover the full spectrum of practically encountered scenarios for gold concentrations in solutions and AC loadings in adsorbers. The values of K_{21} and C_0 for this specific type of AC are physical constants that do not need to be determined each time the technological parameters are changed. In contrast, the identification parameter K_1 depends on the internal operational conditions,

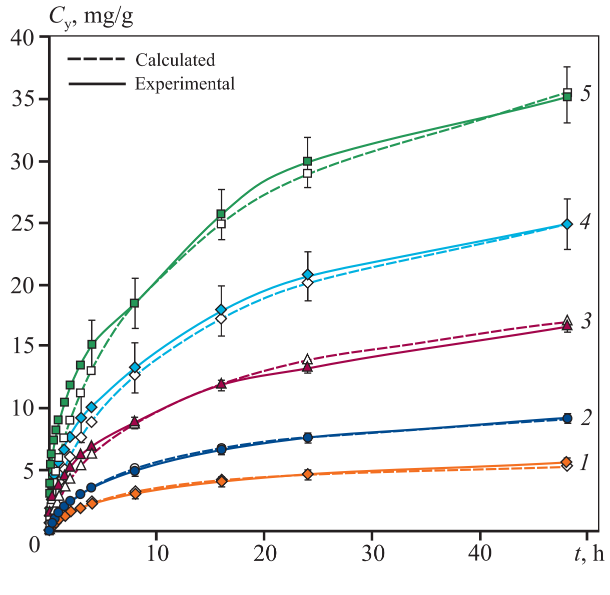

Fig. 1. Kinetic curves of $AuCN_2^-$ adsorption onto activated carbon at different initial gold concentrations in the solution and AC loading $m/V = 0.5$ g/dm^3 ($m = 1.5$ g, $V = 3$ dm^3)

1 – $C_{p0} = 3.2$, ***2*** – 5.9, ***3*** – 12.7, ***4*** – 21.6, ***5*** – 39.8 mg/ dm^3

Рис. 1. Кинетические кривые адсорбции $AuCN_2^-$ на активированном угле при различной начальной концентрации золота в растворе и загрузке АУ $m/V = 0{,}5$ г/дм^3 ($m = 1{,}5$ г, $V = 3$ дм^3)

1 – $C_{p0} = 3{,}2$, ***2*** – 5,9, ***3*** – 12,7, ***4*** – 21,6, ***5*** – 39,8 мг/дм^3

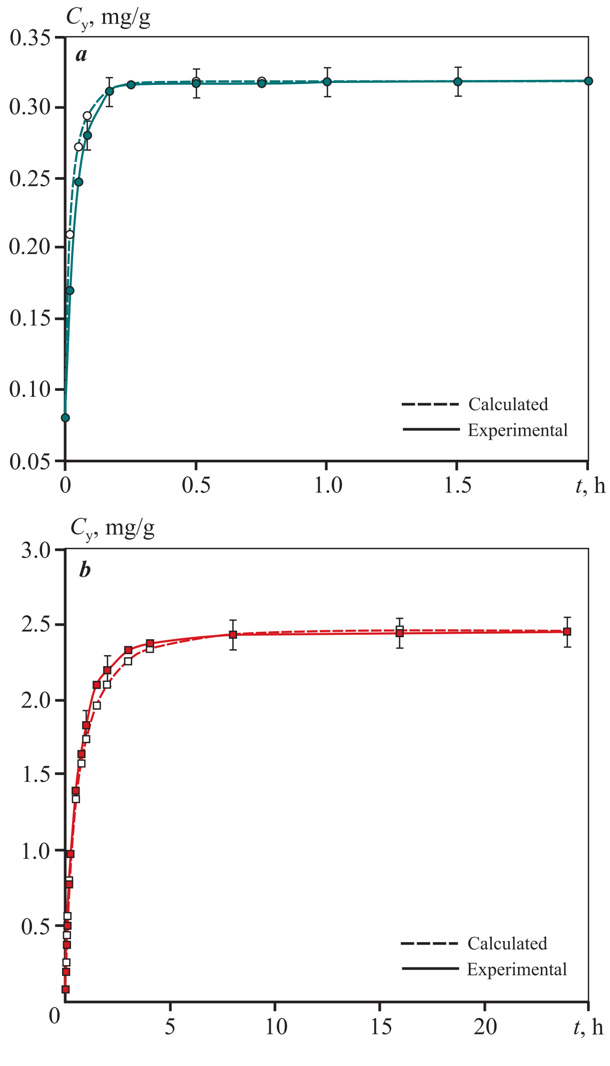

Fig. 2. Kinetic curves of $AuCN_2^-$ adsorption onto activated carbon at the initial gold concentration in solution $C_{p0} = 11.9$ mg/dm^3 and AC loading $m/V = 50$ g/dm^3 (***a***) and $m/V = 5$ g/dm^3 (***b***)

a – $m = 75$ g, $V = 1.5$ dm^3; ***b*** – $m = 7.5$ g, $V = 1.5$ dm^3

Рис. 2. Кинетические кривые адсорбции $AuCN_2^-$ на АУ при начальной концентрации золота в растворе $C_{p0} = 11{,}9$ мг/дм^3 и загрузке АУ $m/V = 50$ г/дм^3 (***a***) и 5 г/дм^3 (***b***)

a – $m = 75$ г, $V = 1{,}5$ дм^3; ***b*** – $m = 7{,}5$ г, $V = 1{,}5$ дм^3

and for solution (12) to be applicable in practical calculations, it is necessary to find the functional dependence of K_1 on C_{p0} and m/V. Only in this case does expression (12) become a mathematical model with predictive properties that can be practically applied for calculating and optimizing the technological process of gold sorption from gold-cyanide solutions onto AC (Fig. 1 and 2).

During the identification of (12) based on the set of experimental kinetic curves obtained under various C_{p0} and m/V, a functional dependence of K_1 on these parameters was found. Further computational studies showed that the constant K_1 depends not only on internal operational parameters but also on time: this dependence is inversely proportional to $\sqrt[3]{t}$. Considering this pattern, the final form of the functional dependence of K_1 on C_{p0}, m/V and t is as follows:

$$K_1 = \frac{K_{01}}{\sqrt[3]{C_{p0}\, m/V}\,\sqrt[3]{t}}, \tag{14}$$

where $K_{01} = 0.0098$ is the adsorption rate identification constant, independent of internal operational parameters and time.

The identification parameter K_1 in equation (14) is a functional dependence on operational factors and time. The coefficient K_1 is a part of K_{01} as an identification constant, obtained from the collective values of K_1, during the identification of kinetic curves at different values of C_{p0} and m/V. The time dependence is related not to time itself but to changes in the sorption conditions during the filling of the sorbent grains with the adsorbed metal.

2.2. Analysis of the modified isotherm equation under conditions of limiting transitions to Henry, Freundlich, and maximum adsorption isotherms

Analysis of equation (13) shows that at low values of C_p and small carbon loadings m/V, we obtain a linear isotherm because in this case $K_2 >> K_1C_p\, m/V$, and the terms $K_1C_p\, m/V$ in the denominator can be neglected, resulting in:

$$C_y = \frac{K_1}{K_2} C_0 C_p \frac{m}{V}. \tag{15}$$

Considering that the adsorption and desorption rate constants (K_1 and K_2) depend not only on internal but also on external operational parameters, such as temperature and stirring speed, their temperature dependence, according to the Arrhenius equation, can be represented as:

$$K_1 = K'_{10}\, e^{\frac{-E_1}{RT}}, \tag{16}$$

$$K_2 = K'_{20}\, e^{\frac{-E_2}{RT}}, \tag{17}$$

where K'_{10} and K'_{20} are the pre-exponential factors for the adsorption and desorption rate constants, depending on internal operational parameters and stirring speed; E_1 and E_2 are the activation energies for adsorption and desorption, kcal/mol; T is temperature, K; $R = 9872$ cal/(K·mol) is the universal molar gas constant.

Therefore,

$$\Gamma = \frac{K_{10}}{K_{20}}\, e^{\frac{-(E_1 - E_2)}{RT}}\, C_0. \tag{18}$$

Taking this expression into account, equation (15) becomes a modified form of the Henry linear isotherm, considering the carbon loading (m/V), per unit solution volume, and in its final form, it will appear as follows:

$$C_y = \Gamma C_p \frac{m}{V}. \tag{19}$$

At large values of C_p and m/V, when $K_1C_p\, m/V >> K_2$, the term K_2 can be neglected. In this case, C_y will approach the maximum equilibrium capacity of the adsorbent, i.e., $C_y \to C_0$. For moderate values of the product $C_p \cdot m/V$ within a relatively narrow range of varying gold concentrations in the solution and moderate carbon loading, the Langmuir isotherm can be approximated by the modified Freundlich isotherm [12]:

$$C_y = K\left(C_p \frac{m}{V}\right)^{\alpha}, \tag{20}$$

where α is the identification constant.

Thus, if at least one kinetic curve and an experimental adsorption isotherm are available, obtained over a sufficiently wide range of varying gold concentrations in the solution and AC loadings, then by identifying the isotherm (13) based on this data and solving the kinetics equation (3) or (12) using the constants K_1, K_2, and C_0 as identification coefficients, it is always possible to achieve the required accuracy in describing these curves by selecting appropriate values for K_1, K_2, C_0.

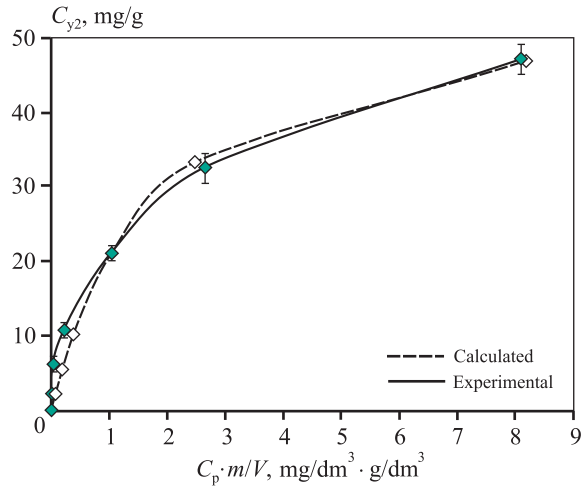

Fig. 3. Experimental and calculated adsorption isotherm according to formula (9)

Рис. 3. Экспериментальная и расчетная по формуле (9) изотермы адсорбции

When graphically representing the obtained modified isotherms (Fig. 3), the generalized parameter $C_{p0} \cdot m/V$ or $C_p \cdot m/V$ should be plotted along the x-axis. The found constants K_1, K_2, and C_0 can be used to calculate the equilibrium values of C_{y2} and C_p, as well as the concentrations C_y and C_p for various time points within the same range of initial conditions where the experimental curves used for identification were obtained.

The same result can be achieved by identifying the solution (12) based on the points of the experimental kinetics curves of the adsorption process using these parameters. The solution (12), obtained within the framework of the proposed adsorption process kinetics equation operating in a closed volume, and its analysis, including the derivation of the modified Langmuir isotherm equation, demonstrate the adequacy of the theoretical justification for selecting the kinetics equation to the real process of gold adsorption from cyanide solutions onto AC.

2.3. Theoretical justification of the functional dependencies of adsorption and desorption rate constants on external operational factors and diffusion coefficient

In practice, adsorption proceeds through a multistage mechanism with successive periods where different stages limit the process [13—17]. Initially, the process is limited by convective mass transfer in the solution, and the process speed is entirely determined by the stirring rate of the solution. As the surface layer of the adsorbent becomes saturated with the target component, the process gradually transitions to the next stage, which is subsequently limited by the film-surface diffusion rate. According to the authors of works [1—3; 18], when the adsorbent reaches 40—60 % saturation, the process shifts to the intradiffusion stage, which is not reflected in equation (2), meaning this equation and its solution are valid only for the adsorption process during the first two stages, which corresponds well with experimental data.

Identifying solution (12), which represents a theoretical kinetic curve derived from the points of experimental kinetic curves using three identification coefficients K_1, K_2, and C_0, provides calculated kinetic curves that nearly coincide with experimental ones within the accuracy limits of the experiments (see Fig. 1 and 2). The graphs of the kinetics indicate the confidence interval for the points of experimental values, calculated with a reliability of P = 0.95; the accuracy ranges for different gold concentrations in the solution are provided above in the “Research Methodology” section.

The identification coefficients have clear physical meaning and can be further experimentally studied to reveal their functional dependence not only on the internal operational parameters established by us but also on various external conditions and internal characteristics of the adsorbent, as they represent integral characteristics. The influence of stirring speed and temperature on the values of K_1, K_2 can be determined based on general theoretical concepts.

The adsorption and desorption rate constants (K_1, K_2) depend on external operational parameters — stirring speed ϑ and temperature T — as well as on the internal characteristic of the adsorbent—diffusion coefficient (D). The general functional structure of these constants, depending on external conditions considering the temperature dependence based on the Arrhenius equation [19] and the internal characteristic—diffusion coefficient, can be represented as follows:

$$K_1 = K_{10} f(\beta, D) e^{\frac{-E_1}{RT}}, \tag{21}$$

$$K_2 = K_{20} f(\beta, D) e^{\frac{-E_2}{RT}}, \tag{22}$$

where K_{10} and K_{20} are identification parameters that do not depend on external operational parameters and the diffusion coefficient but depend on the internal operational parameters C_{p0} and m/V; $f(\beta, D)$ is the generalized mass transfer coefficient in the adsorption process —

a function depending on β and D; β is the convective mass transfer coefficient, directly proportional to the stirring speed ϑ as $\beta = \alpha\vartheta$; D is the generalized coefficient of film-surface diffusion of gold in AC.

The unit act of mass transfer of the gold cyanide complex from the solution to AC consists of two sequentially occurring processes. The first is mass transfer within the solution volume from areas of current concentration ϑ to areas of depleted concentration, i.e., directly to the adsorption surface of the carbon granules. The rate of this process entirely depends on the solution stirring rate C_{p} and represents convective mass transfer. The second process is film and diffusion mass transfer in the near-surface thin layer of the carbon granules, i.e., in the macro- and micropores of the adsorbent. The overall result of the sequential micro-processes occurring within the solution volume and on the surface of the carbon adsorbent granules during mass transfer can be approximately represented as a mass exchange process depending on a certain generalized mass transfer coefficient (K), inverse to the total mass transfer resistance (r). This coefficient depends both on the stirring conditions of the solution and the physicochemical characteristics of the carbon adsorbent.

It is known that mass transfer resistance in sequential processes follows the law of additive resistances for mass exchange processes [20]. Considering this, we can write the expression for the total mass transfer resistance (r) in the adsorption process. We assume that the convective $r_{\text{к}}$ and diffusion $r_{\text{д}}$ resistances are expressed by formulas inversely dependent on the convective (β) and diffusion (D) mass transfer coefficients:

$$r_{\text{к}} = \frac{1}{\beta}, \tag{23}$$

$$r_{\text{д}} = \frac{1}{D}. \tag{24}$$

The total resistance for sequential mass transfer processes, according to the law of additive resistances, will be equal to:

$$r = r_{\text{к}} + r_{\text{д}} = \frac{1}{\beta} + \frac{1}{D}. \tag{25}$$

Therefore, the expression for the generalized mass transfer coefficient will have the form:

$$K = \frac{1}{r} = \frac{\beta D}{\beta + D}. \tag{26}$$

Since $\beta = \alpha\vartheta$, we can finally write:

$$K = \frac{\alpha\,\vartheta\,D}{\alpha\,\vartheta + D}. \tag{27}$$

The sought function $f(\beta, D)$ is the generalized mass transfer coefficient, i.e., $K = f(\beta, D)$. Considering the obtained relationships, the rate constants K_1 and K_2 are described by the following equations:

$$K_1 = K_{10}\frac{\alpha\vartheta D}{\alpha\vartheta + D}\,e^{\frac{-E_1}{RT}}, \tag{28}$$

$$K_2 = K_{20}\frac{\alpha\vartheta D}{\alpha\vartheta + D}\,e^{\frac{-E_2}{RT}}. \tag{29}$$

The presented expressions (28), (29) reflect one of the fundamental patterns of adsorption processes, namely the proportional, or linear, dependence of the adsorption process rate on the stirring speed. As it increases (at low values), the adsorption rate increases proportionally, with the kinetic curve rising linearly. At a moderate stirring speed, its increase leads to a nonlinear change in the adsorption process rate, expressed by a bending of the kinetic curve and its gradual flattening. At higher stirring speeds, the adsorption process rate stops increasing, characterized by the curve reaching a plateau.

This is partly related to the concept of limiting stages of the adsorption process — either the convective mass transfer stage, if the adsorption rate depends on the stirring speed, or the surface (film) mass transfer stage, or purely intradiffusion stage [20—22].

Another important factor that confirms the validity of the obtained expressions for the constants K_1 and K_2 is that the kinetic parameters β and D are incorporated into the constants K_1 and K_2 in such a way that in the isotherm equation (9), they mutually cancel out and do not affect the behavior of the isotherm curve, which is fully consistent with the theoretical concepts of isothermal equilibrium states.

Conclusion

Based on the theoretical concepts of the adsorption mechanism of $AuCN_2^-$ from cyanide solutions onto activated carbon, a third-order adsorption kinetics equation was proposed, taking into account the loading of activated carbon per unit volume of solution. This allowed for the derivation of adequate analytical solutions not only for the kinetics but also for the adsorption isotherm. The resulting isotherm equation is derived from the solution of the kinetics equation, enabling the calculation of equilibrium isothermal values C_{y} and C_{p} for various initial parameters $C_{\text{y}0}$, $C_{\text{p}0}$, m, and V. The developed mathematical model allows for the determination of standardized physical constants C_0 and K_{21} based on experimental adsorption isotherm data for different types of carbon under standard conditions.

The theoretical justification for the functional dependencies of the physical constants of adsorption and desorption rates on external operational parameters (such as temperature and stirring speed) and the internal physicochemical characteristics of the adsorbent (such as the diffusion coefficient) has been presented. The obtained results can be used for practical calculations in optimizing the technological process of gold adsorption from cyanide solutions, provided the contact time between the carbon adsorbent and the cyanide solution does not exceed 2 days.

References

1. Nicol M. J., Fleming C. A., Cromberge G. The absorption of gold cyanide onto activated carbon. I. The kinetics of absorption from pulps. *Journal of the Southern African Institute of Mining and Metallurgy*. 1984; 84 (2):50—54.
2. Nicol M. J., Fleming C. A., Cromberge G. The absorption of gold cyanide onto activated carbon. II. Application of the kinetic model to multistage absorption circuits. *Journal of the Southern African Institute of Mining and Metallurgy*. 1984; 84 (3):70—78.
3. Nicol M. J., Fleming C. A. The absorption of gold cyanide onto activated carbon. III. Factors influencing the rate of loading and the equilibrium. *Journal of the Southern African Institute of Mining and Metallurgy*. 1984;84(4):85—93.
4. Vegter N.M. The distribution of gold in activated carbon during adsorption from cyanide solutions. *Hydrometallurgy*. 1992; 30(1-3):229—242.
https://doi.org/10.1016/0304-386X(92)90086-F
5. Jinsong X., Rajashekhar M., Twinney J., Ghahreman A. A review on adsorption mechanism of gold cyanide complex onto activation carbon. *Journal of Industrial and Engineering Chemistry*. 2022;111:35—42.
https://doi.org/10.1016/j.jiec.2022.04.014
6. Buah W. K., Darmey J. and Osei F. Effects of maturity of coconut shells on gold adsorption efficiencies of derived activated carbons. *Ghana Mining Journal*. 2019;19(2): 50—54. https://doi.org/10.4314/gm.v19i2.7
7. Khosravi R., Azizi A., Ghaedrahmati R., Gupta V.K, Agarwal S. Adsorption of gold from cyanide leaching solution onto activated carbon originating from coconut shell — Optimization, kinetics and equilibrium studies. *Journal of Industrial and Engineering Chemistry*. 2017;54:464—471.
http://dx.doi.org/10.1016/j.jiec.2017.06.036
8. Efremova S.V., Kablanbekov A.A., Anarbekov K.K., Bunchuk L.V., Sukharnikov Y.I., Bogdanovich N.I., Terlikbaeva A.Z., Zharmenov A.A. Carbon sorbent based on special fine coke for the extraction of gold. *Solid Fuel Chemistry*. 2019; 53(4):18—25. (In Russ.).
https://doi.org/10.1134/S0023117719040066
Ефремова С.В., Каблaнбеков А.А., Анарбеков К.К., Бунчук Л.В., Сухарников Ю.И., Богданович Н.И., Терликбаева А.Ж., Жарменов А.А. Углеродный сорбент на основе мелочи спецкокса для извлечения золота для извлечения золота. *Химия твердого топлива*. 2019;53(4):18—25.
https://doi.org/10.1134/S0023117719040066
9. Larin A.V. Material balance equations and their solutions in linear adsorption dynamics. *Protection of Metals and Physical Chemistry of Surfaces*. 2022;58(1):3—7 (In Russ.).
https://doi.org/10.31857/S0044185622010132
Ларин А.В. Уравнения материального баланса и их решения в линейной динамике адсорбции. *Физикохимия поверхности и защита материалов*. 2022;58(1): 3—7.
https://doi.org/10.31857/S0044185622010132
10. Elshin V.V., Kolodin A.A., Ovsyukov A.E. Measurement of gold concentration in cyanide solutions. *Vestnik Irkutskogo gosudarstvennogo tekhnicheskogo universiteta*. 2010;5(45):187—194. (In Russ.).
https://www.elibrary.ru/item.asp?id=15255131
Ёлшин В.В., Колодин А.А., Овсюков А.Е. Измерение концентрации золота в цианистых растворах. *Вестник Иркутского государственного технического университета*. 2010;5(45):187—194.
https://www.elibrary.ru/item.asp?id=15255131
11. Kamke E. Differentialgleichungen. Leipzig: Akademische Veragsgesellschaft Geest & Portig K.-G., 1962. 336 p.
12. Adamson A. Physical chemistry of surfaces. New York: Wiley, 1976. 698 p.
13. Jianping J., Yuexin H., Hui L., Yangyang H., Yongjun P., Xiaotian G., Wei Y. Mineral phase and structure changes during roasting of fine-grained carbonaceous gold ores and their effects on gold leaching efficiency. *Chinese Journal of Chemical Engineering*. 2019;27(5):1184—1190.
https://doi.org/10.1016/j.cjche.2018.08.006
14. Lobanov V.G., Timofeev E.I.. Development and implementation of modern technology of cyanide leaching of gold from gravity concentrates. *Metallurg*. 2017;(6):75—79. (In Russ.).
https://doi.org/10.1007/s11015-017-0522-9
Лобанов В.Г., Тимофеев Е.И. Разработка и внедрение современной технологии цианистого выщелачивания золота из гравитационных концентратов. *Металлург*. 2017;(6):75—79.
https://doi.org/10.1007/s11015-017-0522-9
15. Schwaab M., Steffani E., Barbosa-Coutinho E., Severo Júnior J.B.. Critical analysis of adsorption/diffusion

modelling as a function of time square root. *Chemical Engineering Science*. 2017;173:179—186.
https://doi.org/10.1016/j.ces.2017.07.037

16. McLaughlin J., Agar G.E. Development and application of a first order rate equation for modelling the dissolution of gold in cyanide solution. *Minerals Engineering*. 1991;4(12):1305—1314.
https://doi.org/10.1016/0892-6875(91)90174-T
17. Voiloshnikov G.I., Murashova O.N., Byvaltsev A.V. Mathematical modeling and optimization of the countercurrent sorption process of gold extraction. *Vestnik Irkutskogo gosudarstvennogo tekhnicheskogo universiteta*. 2010;6(46):183—188. (In Russ.).
https://www.elibrary.ru/item.asp?id=15486093
Войлошников Г.И., Мурашова О.Н., Бывальцев А.В. Математическое моделирование и оптимизация противоточного сорбционного процесса извлечения золота. *Вестник Иркутского государственного технического университета*. 2010; 6(46):183—188.
https://www.elibrary.ru/item.asp?id=15486093
18. Chu K.H. Extracting surface diffusion coefficients from batch adsorption measurement data: application of the classic Langmuir kinetics model. *Environmental Technology*. 2017;40(5):543—552.
https://doi.org/10.1080/09593330.2017.1397767
19. Stiller W. Arrhenius equation and non-equilibrium kinetics: 100 years Arrhenius equation. Leipzig: BSB B.G. Teubner, 1989. 160 p.
20. Ibragimova R.I., Grebennikov S.F., Guryanov V.V., Fedyukevich V.A., Vorobyev-Desyatovsky N.V. Effect of the porous structure of activated carbon on the adsorption kinetics of gold (I) cyanide complex. *Russian Journal of Physical Chemistry A*. 2014;88(2):1052—1057.
https://doi.org/10.7868/S0044453714060168
Ибрагимова Р.И., Гребенников С.Ф., Гурьянов В.В., Федюкевич В.А., Воробъев-Десятовский Н.В. Влияние пористой структуры активированного угля на кинетику адсорбции цианидного комплекса золота (I). *Журнал Физической химии*. 2014;88(2): 1052—1057.
https://doi.org/10.7868/S0044453714060168
21. Inglezakis V.J., Fyrillas M.M., Park J. Variable diffusivity homogeneous surface diffusion model and analysis of merits and fallacies of simplified adsorption kinetics equations. *Journal of Hazardous Materials*. 2019;367: 224—245.
http://dx.doi.org/10.1016/j.jhazmat.2018.12.023
22. Tukmakov D.A. Mathematical model of non-stationary sorption in a two-phase medium taking into account the spatial unequality of the distribution of the micro-component concentration distribution in the sorbent phase. *Vestnik Tverskogo gosudarstvennogo universiteta. Seriya Khimiya*. 2019;38(4):26—35. (In Russ.).
https://doi.org/10.26456/vtchem2019.4.3
Тукмаков Д.А. Математическая модель нестационарной сорбции в двухфазной среде, учитывающая пространственную неравномерность распределения концентрации микрокомпонента в фазе сорбента. *Вестник ТвГУ. Серия Химия*. 2019;38(4):26—35.
https://doi.org/10.26456/vtchem2019.4.3

Information about the authors

Viktor V. Elshin – Dr. Sci. (Eng.), Professor of the Department “Automation and Control”, Irkutsk National Research Technical University (INRTU).
https://orcid.org/0000-0002-0447-4831
E-mail: dean_zvf@istu.edu

Alexander P. Mironov – Cand. Sci. (Eng.), Associate Professor of the Department “Automation and Control”, INRTU.
https://orcid.org/0009-0002-0530-8015
E-mail: mironoff.alexander@yandex.ru

Anastasia A. Lisitsyna – Assistant Lecturer of the Department “Automation and Control”, INRTU.
https://orcid.org/0009-0008-9781-1593
E-mail: Gerasimovan19@rambler.ru

Информация об авторах

Виктор Владимирович Ёлшин – д.т.н., профессор кафедры автоматизации и управления, Иркутский национальный исследовательский технический университет (ИРНИТУ).
https://orcid.org/0000-0002-0447-4831
E-mail: dean_zvf@istu.edu

Александр Петрович Миронов – к.т.н., доцент, науч. сотрудник кафедры автоматизации и управления, ИРНИТУ.
https://orcid.org/0009-0002-0530-8015
E-mail: mironoff.alexander@yandex.ru

Анастасия Андреевна Лисицына – ассистент кафедры автоматизации и управления, ИРНИТУ.
https://orcid.org/0009-0008-9781-1593
E-mail: Gerasimovan19@rambler.ru

Contribution of the authors

V.V. Elshin – conceptualized the study, formulated the research objectives, wrote the manuscript, and participated in the discussion of the results.

A.P. Mironov – processed the experimental data, contributed to manuscript writing, and participated in the discussion of the results.

A.A. Lisitsyna – performed mathematical processing of the experimental data, contributed to manuscript writing, and participated in the discussion of the results.

Вклад авторов

В.В. Ёлшин – определение концепции исследования, формулирование цели работы, корректировка текста статьи, участие в обсуждении результатов.

А.П. Миронов – обработка экспериментальных данных, написание текста статьи, участие в обсуждении результатов.

А.А. Лисицына – проведение математической обработки экспериментальных данных, оформление статьи, участие в обсуждении результатов.

The article was submitted 07.12.2023, revised 23.03.2024, accepted for publication 06.05.2024

Статья поступила в редакцию 07.12.2023 г., доработана 23.03.2024 г., подписана в печать 06.05.2024 г.

METALLURGY OF RARE AND PRECIOUS METALS / МЕТАЛЛУРГИЯ РЕДКИХ И БЛАГОРОДНЫХ МЕТАЛЛОВ

UDC 661.865
https://doi.org/10.17073/0021-3438-2024-3-57-72

Research article
Научная статья

Extraction of rare earth elements from phosphogypsum and uranium in situ leaching solutions

V.N. Rychkov, E.V. Kirillov, S.V. Kirillov, G.M. Bunkov, M.S. Botalov, D.V. Smyshlyaev

Ural Federal University named after the first President of Russia B.N. Yeltsin
19 Mira Str., Yekaterinburg 620002, Russia

✉ Maxim S. Botalov (ms.botalov@urfu.ru)

Abstract: The paper investigates the extraction of rare earth elements (REE) from technogenic sources – phosphogypsum and uranium *in situ* leaching (ISL) solutions. We found that mechanical activation significantly increases the degree of REE leaching from phosphogypsum. We also obtained data on sorption leaching of REEs from phosphogypsum. It has been shown that, depending on the ion exchanger used and its form, chemical activation can double the leaching degree of the target components. The paper presents the findings of the study on the sorption recovery of scandium from uranium *in situ* leaching solutions. We determined that Sc sorption from uranium ISL solutions on the Purolite S-957 cation exchanger is much more effective than on Lewatit TP-260, Purolite S-950, Tulsion CH-93 CH-93, and ECO-10 ampholites. However, it should be pointed out that none of the listed sorbents is highly selective towards scandium ions. The paper presents comparative data on Sc extraction from uranium ISL solutions using Lewatit VP OC-1026 and Axion 22 commercial solid extractants synthesized according to the method described in the paper. We determined the mechanism of scandium extraction from uranium ISL solutions using Axion-22 and proved that it shows high selectivity towards scandium ions. Studies on the desorption of scandium from the saturated solid extractant showed that the most effective desorption agent is an aqueous solution of hydrofluoric acid. Additionally, the paper investigates the sorption extraction of REEs from uranium ISL solutions on cation exchangers KU-2, KM-2P, and KF-11. We found that the best eluents for the desorption of REEs from the saturated cation exchanger are solutions of calcium chloride and ammonium nitrate. It has been shown that the concentration of REEs in the solution and the removal of major impurities (Fe and Al) are quite effective when REEs precipitate from the desorption solution by fractional hydrolysis. The paper describes the separation of La, Nd, and Sm by elution from the saturated impregnate containing phosphorylpodande and Di(2-ethylhexyl) phosphoric acid in its structure. It should also be noted that ionic liquids can be useful for the extraction of REEs from the solutions of various electrolytes. We presented one of the technological schemes illustrating REE extraction from phosphogypsum.

Keywords: technogenic deposits, rare-earth elements (REE), scandium, ion exchange, solid extractant, extraction, uranium in situ leaching (ISL) solutions.

For citation: Rychkov V.N., Kirillov E.V., Kirillov S.V., Bunkov G.M., Botalov M.S., Smyshlyaev D.V. Extraction of rare earth elements from phosphogypsum and uranium in situ leaching solutions. *Izvestiya. Non-Ferrous Metallurgy*. 2024;30(3):57–72.
https://doi.org/10.17073/0021-3438-2024-3-57-72

Извлечение редкоземельных металлов из фосфогипса и растворов подземного выщелачивания урана

В.Н. Рычков, Е.В. Кириллов, С.В. Кириллов, Г.М. Буньков, М.С. Боталов, Д.В. Смышляев

Уральский федеральный университет имени первого Президента России Б.Н. Ельцина
Россия, 620002, Свердловская обл., г. Екатеринбург, ул. Мира, 19

✉ Максим Сергеевич Боталов (ms.botalov@urfu.ru)

Аннотация: Проведены исследования по извлечению редкоземельных элементов (РЗЭ) из техногенных источников – фосфогипса и растворов подземного выщелачивания урана (ПВУ). Установлено, что механоактивация в значительной мере увеличивает степень выщелачивания РЗЭ из фосфогипса. Также получены данные по сорбционному выщелачиванию РЗЭ из фосфогипса. Показано, что химическая активация в зависимости от используемого ионита и его формы может в 2 раза увеличить степень выщелачивания по целевым компонентам. Представлены результаты исследования по сорбционному извлечению скандия из растворов подземного выщелачивания урана. Установлено, что сорбция Sc из растворов ПВУ на катионите Purolite S-957 происходит значительно лучше, чем на амфолитах Lewatit TP-260, Purolite S-950, Tulsion CH-93 и ЭКО-10. Однако необходимо отметить и тот факт, что все рассмотренные сорбенты не отличаются высокой селективностью по отношению к ионам Sc. Приведены сравнительные данные по извлечению Sc из растворов ПВУ коммерческим сорбентом ТВЭКС Lewatit VP OC-1026 и ТВЭКС Axion-22, синтезированными по приведенной в работе методике. Определен механизм экстракции скандия из растворов ПВУ с использованием Axion-22 и установлено, что он имеет довольно высокую селективность по отношению к ионам Sc. Представлены результаты исследования по десорбции скандия из насыщенного ТВЭКС. Показано, что наиболее эффективным десорбирующим агентом является водный раствор фтористо-водородной кислоты. Также в работе рассмотрено сорбционное извлечение РЗЭ из растворов ПВУ на катионитах КУ-2, КМ-2П, КФ-11. Выявлено, что что лучшими элюентами для десорбции РЗЭ из насыщенного катионита являются растворы хлорида кальция и нитрата аммония. Показано, что значительное концентрирование суммы РЗЭ и очистку от основных примесей (Fe и Al) достаточно эффективно можно осуществить на стадии осаждения РЗЭ из раствора десорбции посредством дробного гидролиза. Представлены данные по разделению La, Nd и Sm путем элюирования из насыщенного импрегната, содержащего в своей структуре фосфорилподанд и Д2ЭГФК. Также отмечено, что для экстракции РЗЭ из растворов различных электролитов значительный интерес представляют ионные жидкости. В качестве примера извлечения РЗЭ из фосфогипса представлена одна из разработанных технологических схем.

Ключевые слова: техногенные месторождения, редкоземельные элементы (РЗЭ), скандий, ионный обмен, твердый экстрагент, экстракция, растворы подземного выщелачивания урана (ПВУ).

Для цитирования: Рычков В.Н., Кириллов Е.В., Кириллов С.В., Буньков Г.М., Боталов М.С., Смышляев Д.В. Извлечение редкоземельных металлов из фосфогипса и растворов подземного выщелачивания урана. *Известия вузов. Цветная металлургия.* 2024;30(3):57–72. https://doi.org/10.17073/0021-3438-2024-3-57-72

Introduction

The past few decades saw an unprecedented breakthrough in the development of artificial intelligence, digital economy, green energy, etc., which would have been impossible without rare and scattered metals [1]. Solid and liquid production wastes can be valuable sources of rare earth elements (REE). Such wastes are often referred to as technogenic mineral formations (TMF). Some of them can now be safely reclassified into technogenic deposits (TD).

Depending on the stage of the technological process that generated the given TD, all anthropogenic wastes can be classified as follows:

— mineral processing tailings from mining operations;

— waste from metallurgical and chemical processing of raw materials;

— waste generated from the combustion of fossil fuels;

— radioactive waste of industrial, scientific and military enterprises.

As a rule, in initial ore materials, rare earth metals (REM) are included in the structure of other mineral formations. Thus, the research conducted at Ural Federal University revealed the following the scandium concentrates:

• in titanomagnetite ores — diopside $Ca(Mg,Al)(Si,Al)_2O_6$, hornblende $Ca_2(Mg,Fe,Al)_5(Al,Si)_8O_{22}(OH)_2$,

• in ilmenite ores — ilmenite $FeTiO_3$, pyroxene $(Me_xMe_yMe_z)Si_2O_6$,

• in bauxites — boehmite γ-AlO(OH), gibbsite α-$Al(OH)_3$,

• in uranium sandstones — metatyuyamunite $Ca(UO_2)_2(VO_4)_2{\cdot}3H_2O$,

and the following REM concentrates:

• in apatite ores — apatite $Ca_{10}(PO_4)_6(OH,F,Cl)_2$,

• in uranium sandstones — brunnerite $(U,Ca,Th,Y)(Ti,Fe)_2O_6$.

As the main component is separated, rare earth metals retain their original mineral forms (diopside in the tailings of wet magnetic separation (WMS) during the beneficiation of titanomagnetite ores), pass into uranium in-situ leaching (ISL) solutions, solutions of hydrolyzed sulfuric acid — waste of titanium dioxide pigment production from ilmenite ores) or are transformed into new mineral forms in the course of temperature and chemical treatments (phosphogypsum forms when apatite concentrates are processed into phosphate fertilizers and red mud is a by-product of bauxite processing into alumina) [2].

Solid products of feedstock processing pose the greatest difficulty for REE recovery during the target component extraction. Numerous researches [3—7] explored the issues of scandium extraction from wet magnetic separation wastes, and they are not addressed in this paper.

The aim of this work is to investigate the main techniques of enhancing the efficiency of REE extraction from solid technogenic waste on the example of their extraction from phosphogypsum.

Materials and methods

For our research, we used phosphogypsum generated as a waste product at the Balakovo mineral fertilizer plant of JSC Apatit (Russia). The raw material for its production is apatite concentrate from the Kola Peninsula processed according to the dihydrate scheme. For experiments on sorption extraction of REEs and Sc from uranium in-situ leaching solutions, we used the recovered solution (RS) of in-situ leaching of JSC Dalur (Russia).

Mechanical activation of phosphogypsum samples was carried out in a batch bead mill that includes a DISPERMAT LC75 laboratory dissolver equipped with an APS 500 grinding system (VMA-GETZMANN GMBH, Germany). We conducted wet activation of phosphogypsum in the 0.5 dm3 grinding chamber with the ZrO_2 inner coating. The beads used for milling were also of ZrO_2.

Sorption leaching was studied in 150 ml glass beakers. The mixture of acid and phosphogypsum prepared in advance in the required ratio was placed in a beaker and later ion exchange resin was added. During the sorption leaching, the solution was vigorously stirred by an overhead stirrer.

Tests on sorption extraction of REEs and Sc from uranium ISL solutions were carried out in 50-ml laboratory sorption columns filled with the investigated resin.

All water samples were analyzed on an ICP-MS NexION 350x mass spectrometer (Perkin Elmer, USA). Qualitative *X*-ray phase analysis of the samples was performed on a Xpert PRO MRD diffractometer (Malvern Panalytical B.V., the Netherlands) and their IR spectra were obtained on a Vertex-70 spectrometer (Bruker Corporation, USA).

Results and discussion

Phosphogypsum is formed when apatite concentrates are processed into phosphate fertilizers according to the following reaction:

$$Ca_5(PO_4)_3F + 5H_2SO_4 + mH_2O \rightarrow$$
$$\rightarrow 5CaSO_4{\cdot}mH_2O + 3H_3PO_4 + HF. \qquad (1)$$

Depending on the process conditions and impurities present in the phosphate raw material, calcium sulfate can be obtained in one of three forms: dihydrate $CaSO_4{\cdot}2H_2O$ (FDG), hemihydrate $CaSO_4{\cdot}0,5H_2O$ (FPG) or anhydrite $CaSO_4$ form [8]. In the dihydrate product, about 50 % of REEs from the solution crystallize in the solid phase. In the hemihydrate mode, the amount of co-crystallized REEs increases to 70—85 % [9; 10]. The average REE content of the resulting calcium sulfate generally ranges from 0.2 to 0.6 %.

Depending on reaction implementation method (1) REE can be present as an independent orthophosphate phase, enriching the celestine phase, or be a part of the crystalline phase of calcium sulfate, isomorphically replacing Ca [11; 12].

It is obviously difficult to extract REEs from phosphogypsum when they incorporate into the crystal structure of gypsum or celestine. To do so, the formed phosphogypsum phase should be fully dissolved or the minerals containing rare earth elements should be recrystallized. This process is very expensive and inefficient. The mechanical and chemical activation methods can help to significantly enhance the efficiency of REE extraction from such anthropogenic objects.

Mechanical activation increases the degree of REE extraction from minerals in which rare earth elements form part of the crystal lattice, which creates more defects and larger specific surface area. Therefore, this process underlies the technology for the extraction of scandium from wet magnetic separation (WMS) tailings [13] and REEs from red muds [14]. Figure 1 illustrates the impact of mechanical activation on the rates of REE recovery from phosphogypsum. It also significantly increases the degree of amorphization of phosphogypsum (Fig. 2), which is accompanied by the accumulation of residual stresses of III type: periodicity in the atoms arrangement in the crystal is disturbed. Meanwhile, gypsum retains its crystalline structure.

The scientific community shows great interest in sorption leaching as a type of chemical activation. In such a process, REE recovery increases due to the shift of the reaction equilibrium towards the products as the ion exchanger absorbs them according to the reactions

$$[M_y^x A_x^y]_{\text{тв}} \rightarrow yM^x + xA^y, \qquad (2)$$

$$yM^x + x[R_yY^y]_{\text{и-т}} \rightarrow y[R_xM^x]_{\text{и-т}} + xY^y, \qquad (3)$$

where M is a metal cation; A is an anion; x and y are valences of the cation and anion, respectively; R_yY^y is ion exchange resin.

For example, the use of cation exchanger in a hydrogen form triggers two processes:

1) equilibrium shift due to sorption:

$$yM^x + x[RH]_{\text{и-т}} \rightarrow [R_xM^x]_{\text{и-т}} + xH^+, \qquad (4)$$

where RH is the ion exchange resin in a hydrogen form;

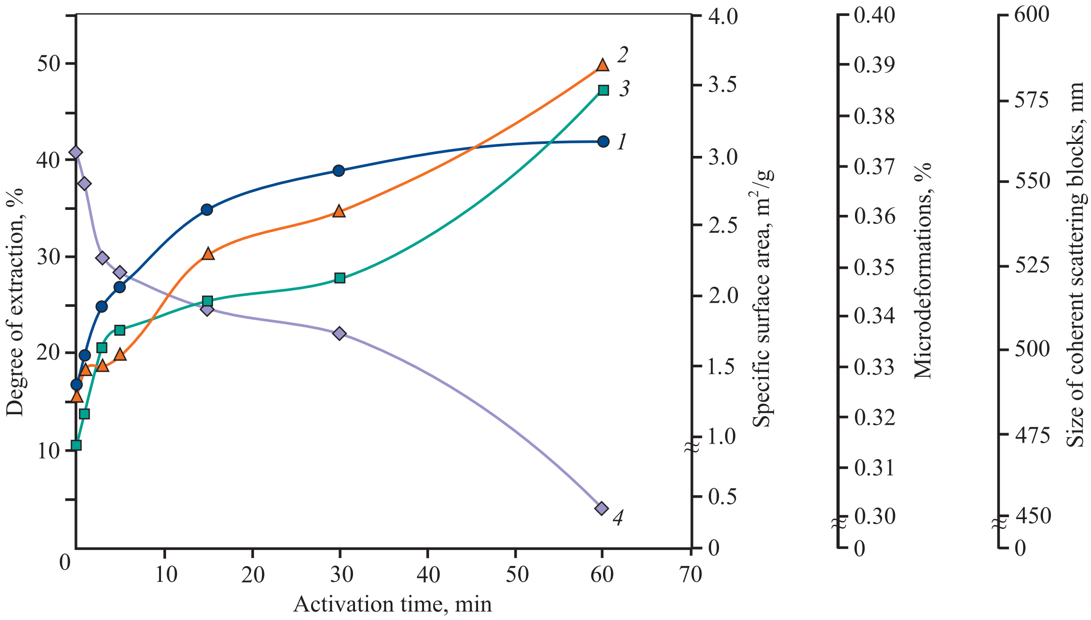

Fig. 1. Impact of mechanical activation on the degree of REE extraction from phosphogypsum with sul-furic acid with a concentration of 10 g/dm^3 (*1*), as well as on the specific surface area (*2*), micro-deformations (*3*) and the size of coherent scattering blocks (*4*)

Рис. 1. Влияние механоактивации на степень извлечения РЗЭ из фосфогипса серной кислотой с концентрацией 10 г/дм^3 (*1*), удельную поверхность (*2*), микродеформацию (*3*) и размер блоков когерентного рассеяния (*4*)

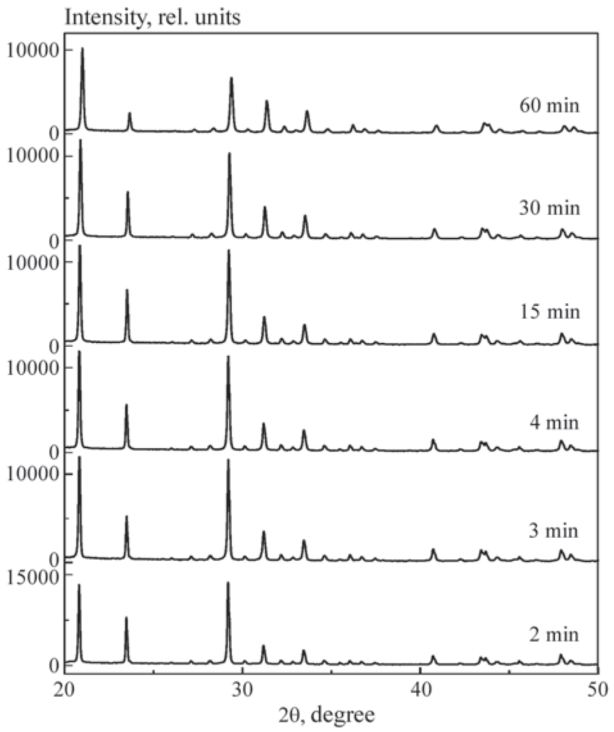

Fig. 2. Diffraction patterns of activated phosphogypsum at different times of mechanical activation

Рис. 2. Дифрактограммы активированного фосфогипса при различном времени механоактивации

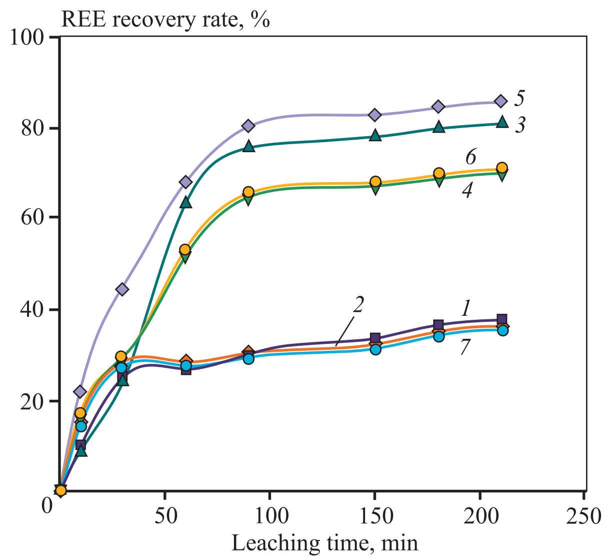

Fig. 3. Impact of chemical activation (sorption leaching) on the degree of REE extraction from phos-phogypsum

1 – without an ion exchanger, *2* – S-150 Na^+, *3* – SGC-650 Ca^{2+}, *4* – SGC-650 H^+, *5* – S-150 Ca^{2+}, *6* – S-150 H^+, *7* – SGC-650 Na^+

Рис. 3. Влияние химической активации (сорбционное выщелачивание) на степень извлечения РЗЭ из фосфогипса

1 – без ионита, *2* – S-150 Na^+, *3* – SGC-650 Ca^{2+}, *4* – SGC-650 H^+, *5* – S-150 Ca^{2+}, *6* – S-150 H^+, *7* – SGC-650 Na^+

2) formation of an equivalent amount of acid involved in the leaching reaction:

$$[M_y^x A_x^y]_{тв} + xH^+ \rightarrow yM^x + xHA^{(x+1)}. \quad (5)$$

The results confirming high efficiency of sorption leaching of REEs and Sc from red muds and phosphogypsum are presented in Fig. 3 and in research papers [14; 15]. Purolite C150 macroporous sulfocationite and Purolite SGC 650 gel sulfocationite were used in the studies. Figure 3 shows that the ion exchanger presence in the pulp, as well as its salt form, considerably affect the REE extraction from phosphogypsum.

Selective extraction of the target component and its subsequent concentration from solutions of complex composition is a challenging and important task to be considered when any technologies are developed. Solution of this task requires the use of ion-exchange materials of various compositions selective to any given element. As an example of such technology development, we present the data on sorption extraction of scandium from uranium in-situ leaching solutions of the following composition, mg/L:

Fe	1449	Mo	1.2
Na	1588	Y	5.3
Al	2218	Ti	2.3
Ca	444	Th	1.8
REM	33.4	U	0.5
Sc	0.81		

Fig. 4 features elution curves of scandium sorption from uranium ISL solutions on a number of commercial phosphorus-containing ion exchangers, the structure of which is presented in Table 1. The plotted dependences show that the sorption of scandium on S-957 cation exchanger is much more efficient than on the studied ampholites.

When ions are sorbed from such complex objects as uranium *in situ* leaching solutions, it is important to understand the behavior of all the components, not only the main one (in our case, scandium). Figure 5 and Table 2 show the data on sorption and desorption of element ions present in uranium ISL solutions, on one of the sorbents used in the research — Tulsion CH-93.

Recently, solvent impregnated resins (SIR) that combine the extraction capacity of any given organic compound with the technique of applying sorption processes have been actively used for extracting elements from complex solutions. Solvent impregnated

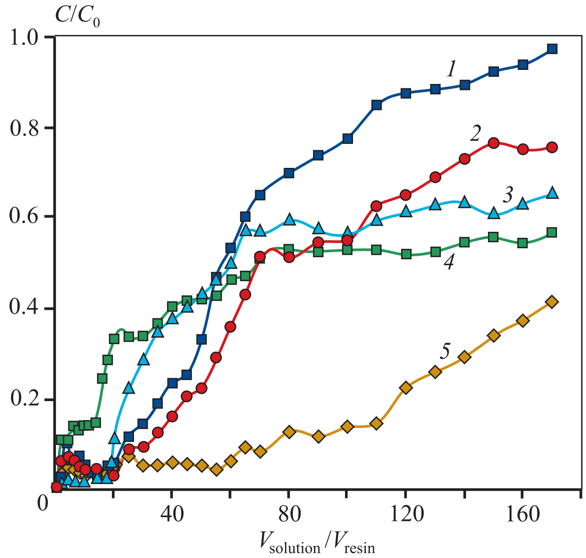

Fig. 4. Elution curves of scandium sorption from uranium ISL solutions on commercial ion exchang-ers

1 – TP-260, ***2*** – CH-93, ***3*** – S-950, ***4*** – ECO-10, ***5*** – S-957
C/C_0 – the ratio of the concentration at the column outlet to the initial concentration or sorbent saturation degree;
$V_{solution}/V_{resin}$ – the ratio of circulating solution volume to the sorbent volume or number of column specific volumes

Рис. 4. Выходные кривые сорбции скандия из раствора ПВУ на коммерческих ионитах

1 – TP-260, ***2*** – CH-93, ***3*** – S-950, ***4*** – ЭКО-10, ***5*** – S-957
C/C_0 – отношение концентрации на выходе из колонны к исходной, или степень насыщения сорбента;
$V_{р\text{-}ра}/V_{смолы}$ – отношение пропущенного объема раствора к объему сорбента, или количество удельных объемов колонны

resin — chelating sorbents — are most promising solvents for extracting scandium from solutions of various electrolytes [16].

Table 3 presents the sorption characteristics of some commercially available SIR obtained during the extraction of scandium from sulfuric uranium in-situ leaching solutions. According to the obtained data, Lewatit VP OC-1026, a solid extractant based on Di(2-ethylhexyl) phosphoric acid (DEHPA), has the highest capacity.

Fig. 6 shows the data on the behavior of scandium and ions of other elements in the solution and below are the values of the total exchange capacity (TEC), mg/g:

Sc	3.94	Ti	2.3
Na	0.6	Fe	17.4
Al	0.7	Th	0.05
Ca	0.22	U	0.3

We see that scandium is effectively sorbed when this SIR, VP OC-1026 grade, is used, and as the solution

Table 1. **Characteristics of ion exchangers used in the research**

Таблица 1. Характеристика использованных в работе ионитов

Ion exchanger grade	Functional group	Capacity, mg-eq/L
Purolite S-950	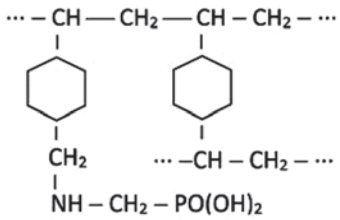	2.3
Lewatit TP-260		2
Tulsion CH-93		1.9
ECO-10		–
Purolite S-957	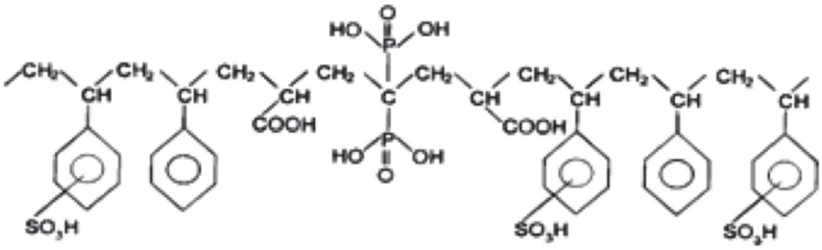	3.1

Table 2. **Total dynamic exchange capacity (TDEC) of the Tulsion CH-93 ion exchanger by elements and the degree of their desorption by Na_2CO_3 solution (180 g/dm^3) in the dynamic mode**

Таблица 2. Полная динамическая обменная емкость (ПДОЕ) ионита Tulsion CH-93 по элементам и степень их десорбции раствором Na_2CO_3 (180 г/дм^3) в динамическом режиме

Indicator	Sc	Al	Fe	Ti	Th	U
TDEC, mg/g of the ion exchanger	0.3	7.4	3.2	1.4	0.6	0.4
Desorption degree, %	94.15	21.25	28.1	18.7	98.85	64.1

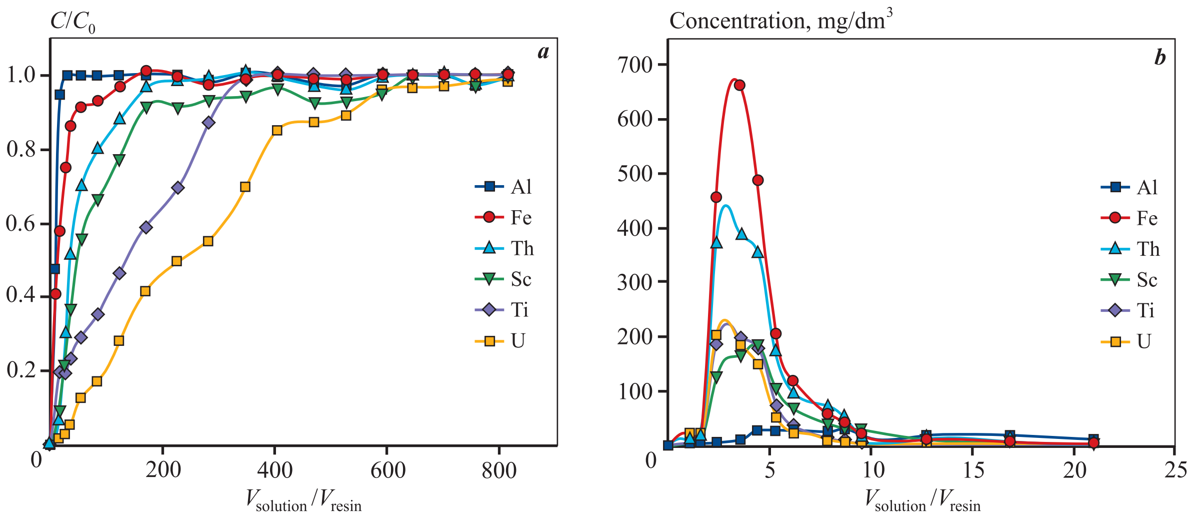

Fig. 5. Elution curves of sorption from uranium ISL solutions on Tulsion CH-93 ampholyte (***a***) and de-sorption of elements from the phase of the ion exchanger saturated with Na_2CO_3 solution with the concentration of 180 g/dm^3 (***b***)

Рис. 5. Выходные кривые сорбции из растворов ПВУ амфолитом Tulsion CH-93 (***a***) и десорбции элементов из фазы насыщенного ионита раствором Na_2CO_3 с концентрацией 180 г/дм^3 (***b***)

Table 3. **Static exchange capacity of solid extractants for scandium during its sorption from the uranium ISL solution**
Таблица 3. Статическая обменная емкость ТВЭКС по скандию при его сорбции из раствора ПВУ

SIR	Active ingredient (extractant)	Capacity, mg_{Sc}/g
TP-923	Mixture of trialkylphosphine oxides	2.94
VP OC-1026	DEHPA	4.05
TP-272	Bis(2,4,4-trimethylpentyl) phosphinic acid	2.44
TR-TBF	Tributyl phosphate	2.22

passes through the sorbent for a long time, thorium is displaced. In addition to scandium, iron is well sorbed, and so is titanium in appreciable amounts.

Despite all its good properties, VP OC-1026 sorbent has disadvantages as well. The main reasons are its small granule size and unsatisfactory scandium sorption kinetics. Therefore, a new SIR was synthesized for selective extraction of scandium from uranium ISL solutions. Its active functional component was composed of DEHPA, tributyl phosphate (TBP) and trioctylphosphine oxide (TOPO) [17]. Axion solid extractant was synthesized using reagents of the following composition, wt.%:

DEHPA.. 8.74—9.93
Tri-n-octylphosphinoxide ....1.10—2.18
Tributyl phosphate....................................0.22—0.44
Benzoyl peroxide ....0.22—0.25
Isododecane .... 4.41—5.46
0.7 % starch solution in water.................. 72.48—73.26
Styrene ....8.03—8.48
Divinylbenzene ....2.12—2.68

Figure 7 shows the results of sorption of REE from the uranium ISL solution by Axion solid extractant and Fig. 8 presents the comparative data on scandium extraction the uranium ISL solutions by the commercial solid extractant, VP OC-1026 grade, and synthesized extractants following the given technique. The sorption rate and dynamic exchange capacity of these solid extractants increase, as they are affected by the conditions of the synthesis, during which open macropores are formed due to the use of isododecane or kerosene, which are characterized by delamination properties for the monomer-polymer mixture. The polymerization results in emergence of a certain intrapore space, and tri-n-octylphosphinoxide and tributyl phosphate serve as intermediates

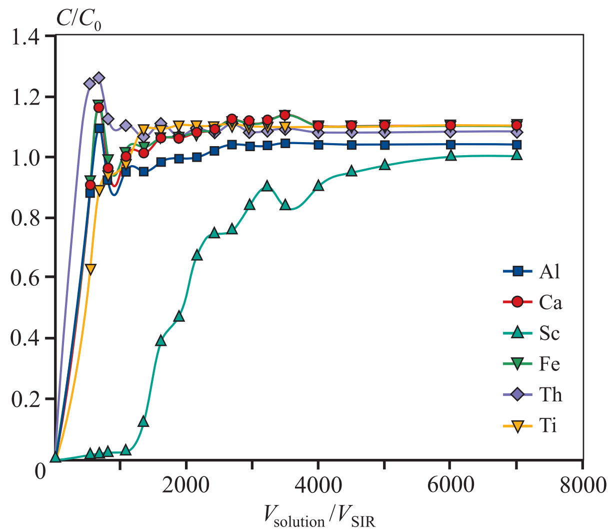

Fig. 6. Elution curves of sorption of element ions by the SIR, VP OC-1026 grade, from uranium ISL solutions

Рис. 6. Выходные кривые сорбции ионов элементов на ТВЭКС марки VP OC-1026 из растворов ПВУ

that increase the DEHPA and scandium interac tion rate.

Scandium extraction using Axion solid extractants proceeds by the following reaction:

$$Sc^{3+} + (HR)_2\,(o) + 2{\cdot}HR\,(o) + TBP\,(o) + TOFO\,(o) \leftrightarrow$$

$$\leftrightarrow Sc(HR_2){\cdot}2R{\cdot}TBP{\cdot}TOFO\,(o) + 3H^+. \quad (6)$$

Figure 9 shows that in the IR spectrum of Axion-22 solid extractants in the Sc^{3+} form, the band in the region $\nu = 1232\ cm^{-1}$, responsible for valence and strain vibrations of P=O groups, is narrowed, and absorption bands, about $\nu = 1200\ cm^{-1}$ [18], related to stretching vibrations of the P=O → Sc group, emerge. Such changes in the spectra suggest the formation of strong coordination bonds between scandium ions and functional groups of the SIR. In the region $\nu = 1150\ cm^{-1}$, the intensity of P—O—(H) valence vibrations subsides,

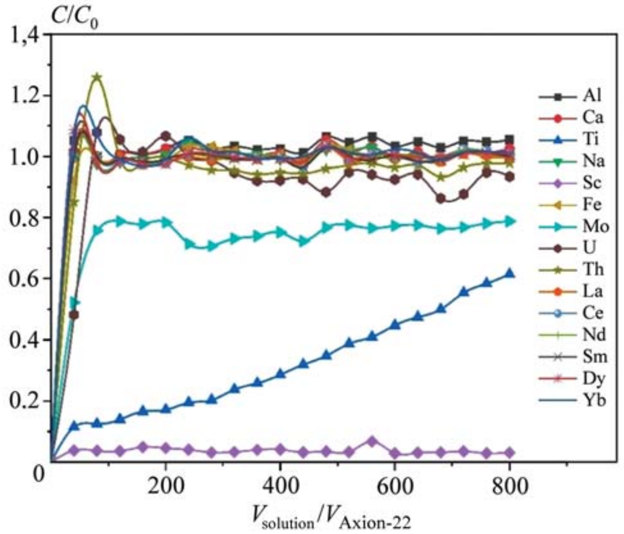

Fig. 7. Elution curves of Sc and related elements sorption from the uranium ISL solutions by Axion-22 solid extractants

Рис. 7. Выходные кривые сорбции Sc и сопутствующих элементов из растворов ПВУ на ТВЭКС Axion-22

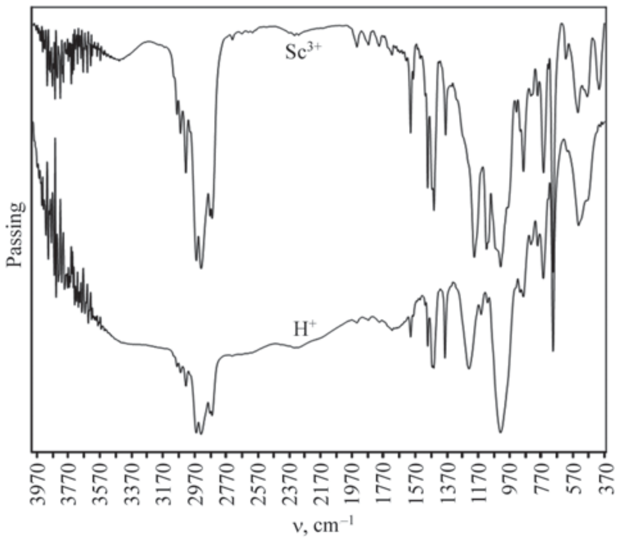

Fig. 9. IR-spectra of Axion-22 in H^+ and Sc^{3+} form

Рис. 9. ИК-спектры ТВЭКС Axion-22 в H^+-форме и Sc^{3+}-форме

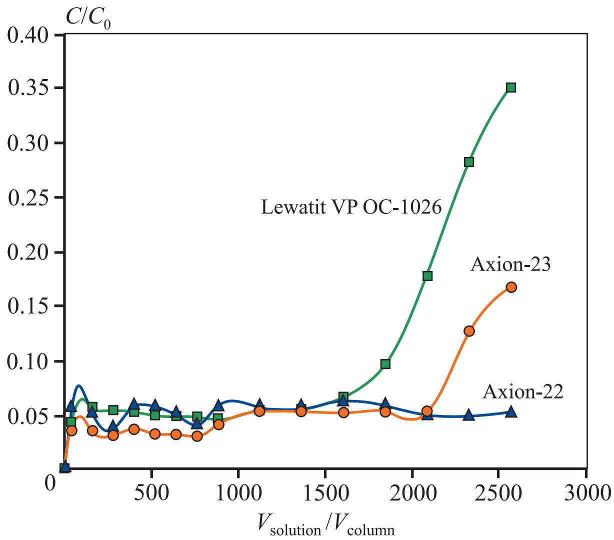

Fig. 8. Elution curves of scandium sorption from the uranium ISL solutions by Lewatit VP OC-1026, Axion-22 and Axion-23 SIR

Рис. 8. Выходные кривые сорбции скандия из растворов ПВУ на ТВЭКС Lewatit VP OC-1026, Axion-22 и Axion-23

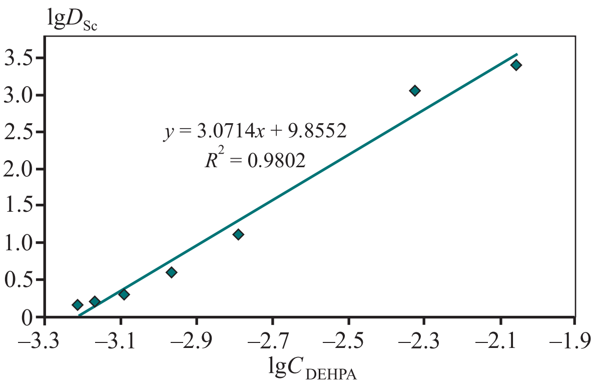

Fig. 10. Dependence of $\lg D_{Sc}$ on DEHPA concentration during scandium sorption with the use of Axion-22 solid extractants

Рис. 10. Зависимость $\lg D_{Sc}$ от концентрации Д2ЭГФК при сорбции скандия с использованием ТВЭКС Axion-22

indicating that cation-exchange groupings are involved in the sorption reaction. [19].

To determine the number of DEHPA molecules involved in the exchange reaction, the graph was plotted in logarithmic coordinates showing the experimental dependence of the scandium distribution coefficient on the DEHPA concentration (Fig. 10). The value of the slope angle of this linear dependence indicates the number of DEHPA molecules. The activity coefficients for the compounds involved in the extraction were assumed to be constant [20]. The evidence presented suggests that when scandium is extracted from sulfuric acid aqueous solutions by Axion-22 SIR, the slope angle is equal to 3.

The analysis of the IR spectrum and the dependence $\lg D_{Sc} = f(\lg_{CDEHPA})$ (see Fig. 9 and 10) gives grounds to conclude that the selectivity of scandium extraction is achieved through donor-acceptor bonds with the complex compound being formed in the solid extractant phase (Fig. 11).

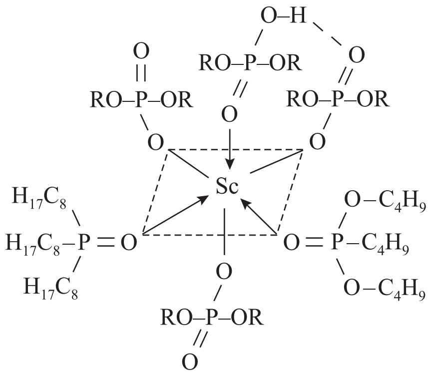

Fig. 11. Coordination scheme for the sorption of scandium ions by Axion-22 solid extractant

Рис. 11. Координационная схема сорбции ионов скандия на ТВЭКС Axion-22

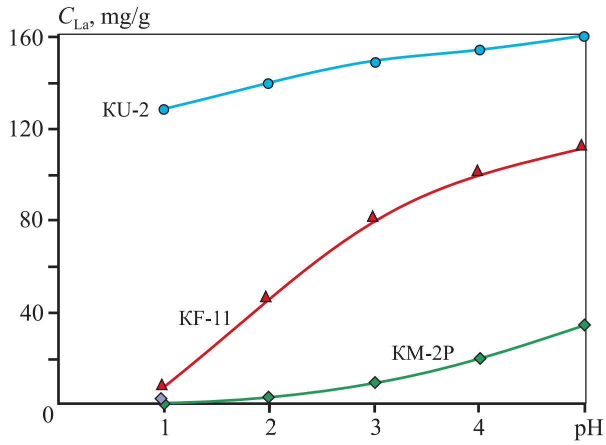

Fig. 12. Impact of the sulfate solution pH on the sorption of lanthanum (III) ions by cation exchangers

Рис. 12. Влияние величины pH сульфатного раствора на сорбируемость ионов лантана (III) катионитами

Along with scandium, uranium ISL solutions contain a significant amount of rare earth elements, the total content of which is comparable to the concentration of the main element to be extracted — uranium. The composition of the uranium ISL solutions used in the cited studies was as follows, mg/dm^3:

La	3.6	Tm	0.06
Ce	8.1	Yb	0.55
Pr	1.61	Lu	0.07
Nd	7.0	Y	5.65
Sm	1.55	Sc	0.75
Eu	0.38	Th	15.5
Gd	1.15	Fe	1150
Tb	0.29	Al	1453
Dy	1.08	Ca	425
Ho	0.31	Mg	370
Er	0.55	U	0.04

It should be noted that the content of the REE heavy group in the solution is abnormally high.

Ion exchangers of various classes and structures were used for the extraction and concentration of REE from the uranium ISL solutions: cation exchangers, aminocarboxylic and aminophosphoric acid ampholytes [21; 22]. This research analyzes the REE sorption from the uranium ISL solutions by cation exchangers. Fig. 12 shows the impact of solution acidity on the sorption of lanthanum (REE representative). Universal sulfocationite KU-2, carboxylic KM-2P, phosphoric acid KF-11 were used as cation exchangers (Table 4).

We selected cation exchanger KU-2 for further use although it is universal and is not characterized by high selectivity towards rare earth elements. We made this decision because uranium ISL solutions are acidic (pH = 1.0÷.5) and the REE sorption from them will be higher compared to other sorbents. Figure 13 shows the elution curves of element ions sorption from uranium ISL solutions after uranium is extracted from them. This information enables to draw the following conclusions:

— macroporous cation exchangers are characterized by a sufficiently high degree of selectivity towards rare earth metals;

— they are most selective towards light REEs;

— in the process of ion sorption in the dynamic mode, some cations, in particular calcium, are displaced from the cation exchanger by rare-earth metals.

It should be noted that the selectivity of macroporous cation exchangers is correlated with the radii of hydrated ions, the average values of which are given below, Å:

Sc^{3+}	8.4	Al^{3+}	7.6
K^{+}	2.7	Fe^{3+}	9.1
Na^{+}	3.2	Y^{3+}	4.8
Ca^{2+}	3.8	La^{3+}	4.6
Mg^{2+}	4.2		

consequently, it correlates with the dehydration energy of these ions as well. It can be argued that the ion selectivity is significantly affected by the sieve effect.

Table 4. **Comparative characteristics of used cation exchangers**

Таблица 4. Сравнительная характеристика использованных катионитов

Cation exchanger	Functional group	SEC, mg-eq/cm^3
KU-2	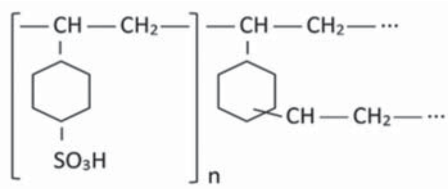	2.0
KM-2P	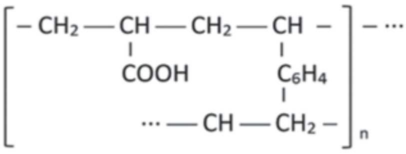	3.5
KF-11	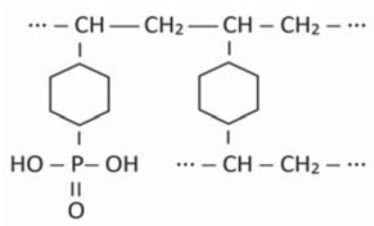	3.6

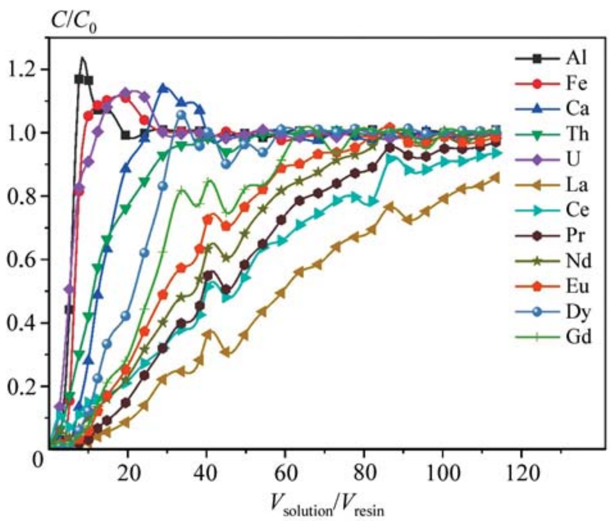

Fig. 13. Elution curves of ion sorption from uranium ISL solutions by macroporous cation exchanger Purolite C-100

Рис. 13. Выходные кривые сорбции ионов из растворов ПВУ макропористым катионитом Purolite C-100

REE concentration and decontamination can be implemented at the desorption stage. The hydrochloric and nitric acid solutions of alkali and alkaline earth metals are often used for desorption of rare earth metals from strongly acidic cation exchangers. Figure 14 shows dependences of REE desorption from sulfocationite on the concentration of ammonium, calcium and sodium salts. It can be observed that calcium chloride and ammonium nitrate solutions are the best eluents for REEs.

When SIR are used for extracting scandium from uranium ISL solutions, the process selectivity is attributed to the formation of high-strength coordination compounds. It complicates the desorption of scandium from these sorbents by many mineral acids and their salts. The complex compound can be destroyed by forming stronger ones. Alkali metal carbonates or hydrofluoric acid can be chosen as such eluents. The use of carbonate solutions leads to the extractant stripping from the resin phase, which ultimately causes a significant decrease in the amount of scandium that can be extracted. Therefore, the results of scandium desorption from Axion SIR by hydrofluoric acid solutions are presented below. Figure 15 shows that HF solutions are effective eluents for scandium during its desorption from the SIR.

At the stage of REE precipitation from solutions, they can be separated from a number of impurities, not only transferred from the solution to the precipitate with subsequent concentration. This can be clearly seen in Fig. 16, which features the curves showing hydrolysis of REEs and impurities in the solution. Table 5 presents the composition of the objects obtained during fractional hydrolysis.

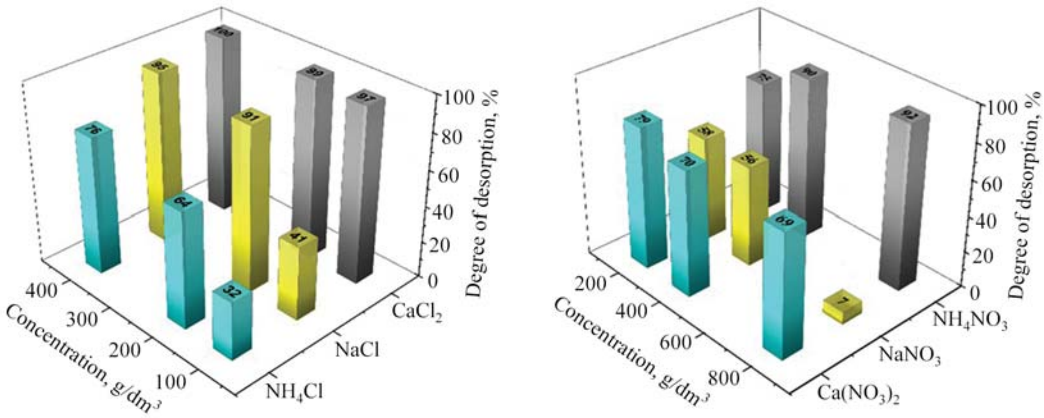

Fig. 14. Dependence of the degree of REE desorption from the cation exchanger phase by solutions of different desorbates

Рис. 14. Зависимость степени десорбции РЗЭ из фазы катионита растворами различных десорбатов

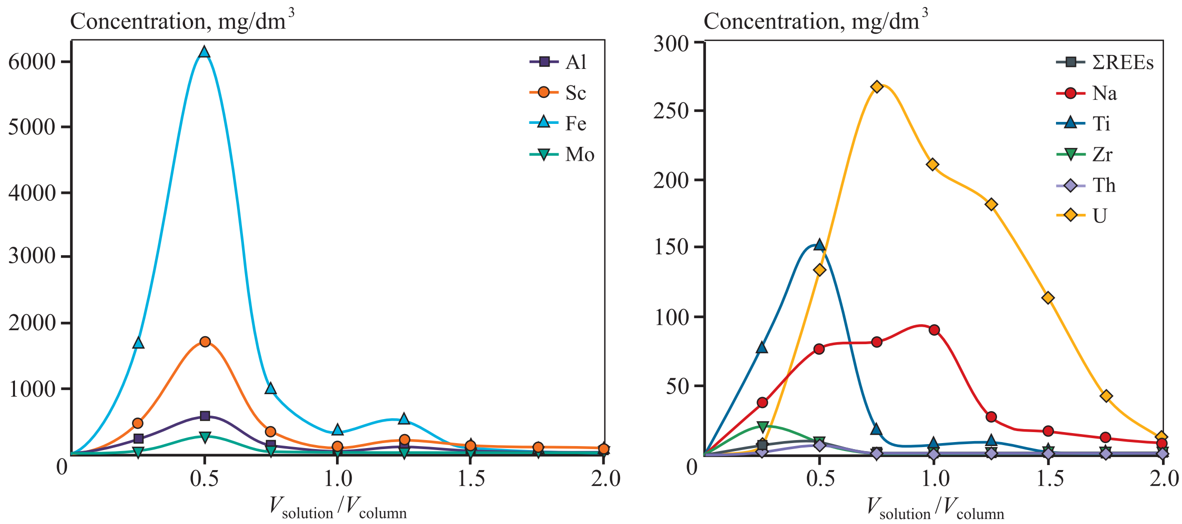

Fig. 15. Elution curves of desorption from saturated Axion-22 SIR by the HF solution with the concen-tration of 150 g/dm^3

Рис. 15. Выходные кривые десорбции из насыщенного ТВЭКС Axion-22 раствором HF с концентрацией 150 г/дм^3

The final stage of the REE extraction from anthropogenic wastes is secondary cleaning from impurities to obtain a high-purity product. As a rule, liquid extraction is used for this purpose.

At JSC Dalur JSC (Kurgan Region, Russia), the research team of the Ural Federal University developed and implemented the technique for producing scandium oxide of a purity exceeding 99.9 %. It includes the following operations:

— scandium extraction by SIR from recovered solutions of uranium in-situ leaching solutions;

— solid-phase re-extraction using fluoride-containing solutions;

— conversion of scandium fluoride to hydroxide;

— dissolution of the obtained scandium hydroxide in nitric acid;

— scandium oxalate precipitation;

— calcination to obtain scandium oxide.

Currently, the use of impregnates for the separation of collective REE concentrate into individual compounds seems to be a promising option [23]. The modern technologies usually use liquid extraction for this purpose. Figure 17 gives an example of some rare earth elements separation from the saturated impregnate at the elution stage. Control points, including peaks of the separated elements, were analyzed by mass spectrometry. The impregnates used contained phosphorylpodand XXa and DEHPA as active organic matter.

Table 5. **Composition of concentrates and semi-products of REE concentrate secondary cleaning**

Таблица 5. Состав концентратов и полупродуктов перечистки концентрата РЗЭ

Element	Precipitation mother solution, mg/dm^3		Concentrate, %	
	Fe–Al	REEs	Fe–Al	REEs
Al	34	7.8	31.1	0.13
Ca	545.7	520.1	6.2	0.7
Fe	3.41	2.8	1.6	0.03
Th	0.02	0.003	0.09	0.002
U	0.05	0.002	0.04	0.003
∑ REEs	695	3.1	2.3	51.9

Figure 17 shows quantitative separation of lanthanum, neodymium and samarium by the impregnate containing 33 % phosphorylpodand. However, the impregnate containing DEHPA only proved ineffective for REE separation.

The use of ionic liquids as extractants for REE extraction is a scientific challenge of great importance [24; 25]. Thus, when bis[(trifluoromethyl)sulfonyl]-imide 1-butyl-3-methylimidazolium (C_4mimTf_2N) ionic liquid is added to 2-phosphoryl-phenoacetic acid amide (compound I), the REE recovery rate surges dramatically (Fig. 18).

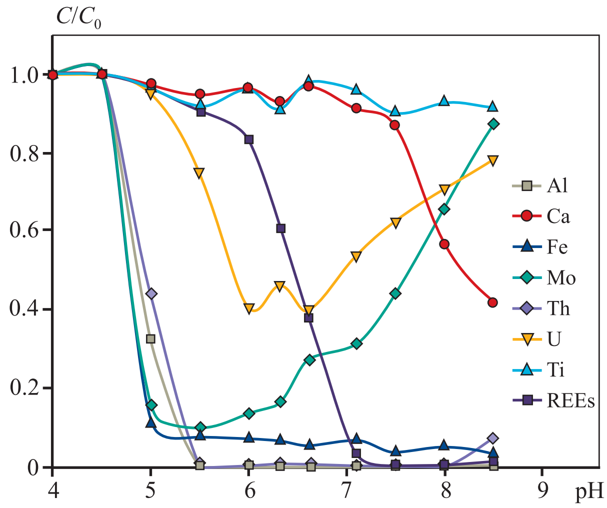

Fig. 16. Co-hydrolysis of ions of REE eluate elements

Рис. 16. Совместный гидролиз ионов элементов элюата РЗЭ

Figure 19 gives an example of one of the developed technological schemes for REE extraction from phosphogypsum. The obtained concentrate has the following composition, %:

∑LREE	49	Sr	0.03
∑HREE	2.5	Na	0.15
Ca	0.9	K	0.16
Fe	0.8	Th	0.004
Al	0.1		

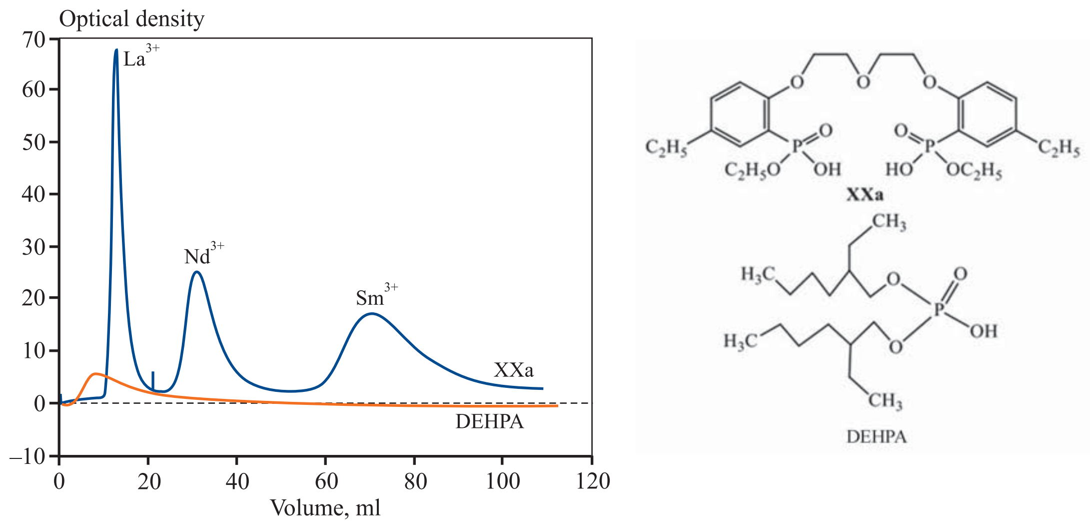

Fig. 17. Separation of La^{3+}, Nd^{3+} and Sm^{3+} at elution with 0.08 M HNO_3 by impregnates containing 33 % DEHPA and 33 % phosphorylpodand (XXa)

Sorbent carrier is LPS-500

Рис. 17. Разделение La^{3+}, Nd^{3+} и Sm^{3+} при элюировании 0,08 М HNO_3 на импрегнатах, содержащих 33 % Д2ЭГФК и 33 % фосфорилподанда (XXa)

Сорбент носитель – LPS-500

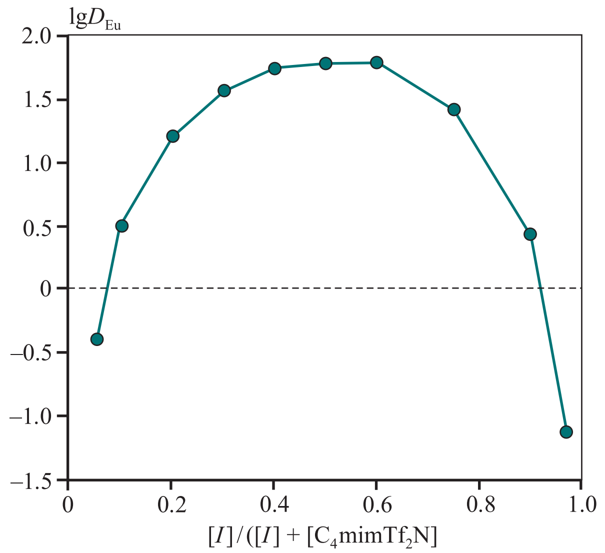

Fig. 18. Extraction of Eu^{3+} from 0.1 M HNO_3 solutions with isomolar mixtures of compound *I* and C_4mimTf_2N in dichloroethane depending on their initial molar ratio in the organic phase
$[I] + [C_4mimTf_2N] = 0.1$ M

Рис. 18. Экстракция Eu^{3+} из 0,1 М растворов HNO_3 изомолярными смесями соединения *I* и C_4mimTf_2N в дихлорэтане в зависимости от их исходного мольного соотношения в органической фазе
$[I] + [C_4mimTf_2N] = 0,1$ М

The presented data conclusively prove that in addition to obtaining REE-rich concentrate, the developed method enables to solve the issues related to complex processing of phosphogypsum.

Conclusion

The experimental and estimated data on the extraction of rare-earth metals from phosphogypsum and uranium in-situ leaching solutions, both of which are production wastes (technogenic deposits), presented in this paper prove that these objects can serve as potential sources of REEs.

The technologies for extracting rare earth elements using modern sorption extraction materials and ionic liquids developed and tested at the enterprises demonstrate that the prospects of their practical application are quite encouraging.

References

1. David S.A. The elements of power: Gadgets, guns, and the struggle for a sustainable future in the rare metal age. New Haven: Yale University Press., 2017. 336 p.

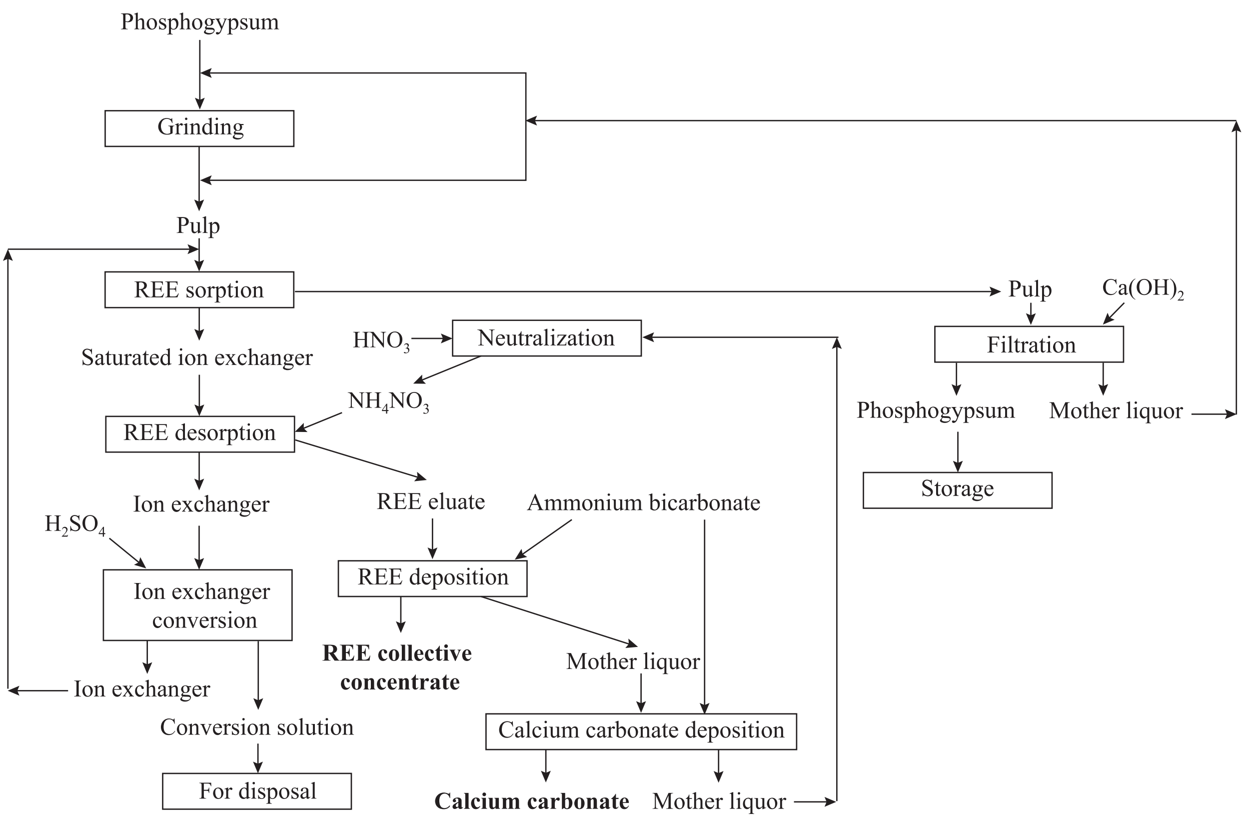

Fig. 19. Technological scheme for extracting rare earth elements from phosphogypsum

Рис. 19. Технологическая схема извлечения РЗЭ из фосфогипса

2. Wang W., Pranolo Y., Cheng C.Y. Metallurgical processes for scandium recovery from various resources: A review. *Hydrometallurgy*. 2011;108:100—108. https://doi.org/10.1016/j.hydromet.2011.03.001
3. Bykhovskii L.Z., Arkhangel'skaya V.V., Tigunov L.P., Anufrieva S.I. Prospects for the development of the mineral resource base and the development of scandium production in Russia and other CIS countries. *Mineral'nye resursy Rossii. Ekonomika i upravlenie*. 2007;5:27—32. (In Russ.).
Быховский Л.З., Архангельская В.В., Тигунов Л.П., Ануфриева С.И. Перспективы освоения минерально-сырьевой базы и развития производства скандия в России и других странах СНГ. *Минеральные ресурсы России. Экономика и управление*. 2007;5:27—32.
4. Kantemirov V.D., Titov R.S., Yakovlev A.M. Feasibility of complex processing of mineral resources of the Ural region. *Izvestiya Ural'skogo gosudarstvennogo gornogo universiteta*. 2023;3(71):64—76. (In Russ.). https://doi.org/10.21440/2307-2091-2023-3-64-76
Кантемиров В.Д., Титов Р.С., Яковлев А.М. К вопросу целесообразности комплексного освоения минеральных ресурсов Уральского региона. *Известия Уральского государственного горного университета*. 2023;3(71):64—76. https://doi.org/10.21440/2307-2091-2023-3-64-76
5. Stepanov S.I., Boyarintsev A.V., Khtet I.A., Chekmarev A.M. Scandium extraction from red slimes and wastes of wet magnetic separation of titanium-iron-vanadium ores. *Razvedka i okhrana nedr*. 2020;10:40—45. (In Russ.).
Степанов С.И., Бояринцев А.В., Хтет Й.А., Чекмарев А.М. Извлечение скандия из красных шламов и отходов мокрой магнитной сепарации титано-железо-ванадиевых руд. *Разведка и охрана недр*. 2020;10:40—45.
6. Botelho Junior B., Espinosa D.C.R., Tenório J.A.S., Vaughan J. Recovery of scandium from various sources: A critical review of the state of the art and future prospects. *Minerals Engineering*. 2021;172:107148. https://doi.org/10.1016/j.mineng.2021.107148
7. Stepanov S.I., P'ei K., Boyarintsev A.V., Giganov V.G., Aung M.M., Chekmarev A.M. Scandium extraction from sulfuric acid solutions by mixtures of D2EHPA and MTAA sulfate in toluene. *Theoretical Foundations of Chemical Engineering*. 2017;51:846—849. https://doi.org/10.1134/S0040579517050219
8. Mikheenkov M.A. Structure formation, properties and application of pressed phosphogypsum. Saarbrücken: LAP, 2011. 284 p. (In Russ.).
Михеенков М.А. Структурообразование, свойства и применение прессованного фосфогипса: Монография. Саарбрюккен: LAP, 2011. 284 с.
9. Binnemans K., Jones P.T., Blanpain B. Towards zero-waste valorisation of rare-earth-containing industrial process residues: A critical review. *Journal of Cleaner Production*. 2015;99:17—38. https://doi.org/10.1016/j.jclepro.2015.02.089
10. Mukaba J-L., Eze C.P., Pereao O., Petrik L.F. Rare earths' recovery from phosphogypsum: An overview on direct and indirect leaching techniques. *Minerals*. 2021;11(10):1051. https://doi.org/10.3390/min11101051
11. Lokshin E.P., Tareeva O.A., Elizarova I.R. Study of sulfuric acid leaching of rare earth metals, phosphorus and alkali metals from phosphodihydrate. *Zhurnal prikladnoi khimii*. 2010;83(6):906—912. (In Russ.).
Локшин Э.П., Тареева О.А., Елизарова И.Р. Исследование сернокислотного выщелачивания РЗМ, фосфора и щелочных металлов из фосфодигидрата. *Журнал прикладной химии*. 2010;83(6):906—912.
12. Lokshin E.P., Kalinnikov V.T. Physico-chemical justification and development of an economically feasible technology for extracting lanthanides from phos-phohemihydrate. In: *Formation of the foundations of a modern strategy for en-vironmental management in the Euro-Arctic region*. Apatity: Kol'skii nauchnyi tsentr RAN, 2005. P. 250–269. (In Russ.).
Локшин Э.П., Калинников В.Т. Физико-химическое обоснование и разработка экономически целесообразной технологии извлечения лантаноидов из фосфополугидрата. В кн.: *Формирование основ современной стратегии природопользования в Евро-Арктическом регионе*. Апатиты: Изд-во Кольского научного центра РАН, 2005. 250—269 с.
13. Stepanov S., P'ei Kh, Boyarintsev A., Giganov V., Chekmarev A., Aung M. Use of machining to increase the recovery of scandium from refractory silicate raw material. *Theoretical Foundations of Chemical Engineering*. 2018;52:898—902. https://doi.org/10.1134/S0040579518050275
14. Rychkov V., Botalov M., Kirillov E., Kirillov S., Semenishchev V., Bunkov G., Smyshlyaev D. Intensification of carbonate scandium leaching from red mud (bauxite residue). *Hydrometallurgy*. 2021;199:105524. https://doi.org/10.1016/j.hydromet.2020.105524
15. Rychkov V.N., Kirillov E.V., Smirnov A.L. Yazev V.A., Ivan'ko V.A. Method of extracting rare earth elements from phosphogypsum: Patent 2473708 (RF). 2013. (In Russ.).
Рычков В.Н., Кириллов Е.В., Смирнов А.Л., Язев В.А., Иванько В.А. Способ извлечения редкоземельных элементов из фосфогипса: Патент 2473708 (РФ). 2013.
16. Korovin V.Yu., Randarevich S.B. Synthesis, properties and use of solid extractants (Review). *Khimicheskaya tekhnologiya*. 1991;5:3—13. (In Russ.).

Коровин В.Ю., Рандаревич С.Б. Синтез, свойства и применение твердых экстрагентов (Обзор). *Химическая технология*. 1991;5:3—13.

17. Kondrutskii D.A., Kirillov E.V., Rychkov V.N., Kirillov S.V., Bun'kov G.M., Vostrov E.S., Tret'yakov V.A., Gadzhiev G.R., Poponin N.A., Smyshlyaev D.V. Solid extragen twith high dynamic exchange capacity for scandium ex-traction and the method of its preparation: Patent 265041 (RF). 2018. (In Russ.).
Кондруцкий Д.А., Кириллов Е.В., Рычков В.Н., Кириллов С.В., Буньков Г.М., Востров Е.С., Третьяков В.А., Гаджиев Г.Р., Попонин Н.А., Смышляев Д.В. Твердый экстрагент с высокой динамической емкостью для извлечения скандия и способ его получения: Патент 265041 (РФ). 2018.
18. Qi D. Extractants used in solvent extraction-separation of rare earths: Extraction mechanism, properties, and features. In: *Hydrometallurgy of rare earths*. Elsevier, 2018. P. 187—389.
https://doi.org/ 10.1016/B978-0-12-813920-2.00002-7
19. Noskova M.P. Radionov B.K., Kazantsev E.I. Study of the interaction of trivalent metal ions with phosphoric acid cation exchangers using vibrational spectroscopy. *Zhurnal fizicheskoi khimii*. 1981;55(8):2007—2012. (In Russ.).
Носкова М.П. Радионов Б.К., Казанцев Е.И. Изучение взаимодействия ионов трехвалентных металлов с фосфорнокислыми катионитами методом колебательной спектроскопии. *Журнал физической химии*. 1981;55(8):2007—2012.
20. Smirnov V.F. Nikonov V.I., Moiseeva E.I. Study of the interaction of scandium with di-2-ethylhexylphosphoric acid during extraction. *Zhurnal neorganicheskoi khimii*. 1969;14:3068—3071. (In Russ.).
Смирнов В.Ф. Никонов В.И., Моисеева Е.И. Изучение взаимодействия скандия с ди-2-этилгексилфосфорной кислотой при экстракции. *Журнал неорганической химии*. 1969;14:3068—3071.
21. Hermassi M., Granados M., Valderrama C., Skoglund N., Ayora C., Cortina J.L. Impact of functional group types in ion exchange resins on rare earth element recovery from treated acid mine waters. *Journal of Cleaner Production*. 2022;379(2):134742.
https://doi.org/10.1016/j.jclepro.2022.134742
22. Rychkov V.N., Kirillov E.V., Smirnov A.L., Dement'ev A.A., Poponin N.A. Method of extracting rare-earth metals from technological and productive solu-tions and pulps: Patent 2484162 (RF). 2012. (In Russ.).
Рычков В.Н., Кириллов Е.В., Смирнов А.Л., Дементьев А.А., Попонин Н.А. Способ извлечения суммы редкоземельных элементов из технологических и продуктивных растворов и пульп: Патент 2484162 (РФ). 2012.
23. Mory Traore, Aijun Gong, Yiwen Wang, Lina Qiu, Yuzhen Bai, Weiyu Zhao, Yang Liu, Yi Chen, Ying Liu, Huilin Wu, Shuli Li, Yueyi You. Research progress of rare earth separation methods and technologies. *Journal of Rare Earths*. 2023;41(2):182—189.
https://doi.org/10.1016/j.jre.2022.04.009
24. Quijada-Maldonado E., Romero J. Solvent extraction of rare-earth elements with ionic liquids: Toward a selective and sustainable extraction of these valuable elements. *Current Opinion in Green and Sustainable Chemistry*. 2021;27:100428.
https://doi.org/10.1016/j.cogsc.2020.100428
25. Rychkov V., Baulin V., Kirillov E., Kirillov S., Bunkov G., Smyshlyaev D., Botalov M., Semenishchev V., Malyshev A., Taukin A., Yuldashbaeva A., Gaidashov E. Recovery of rare earth elements from uranium leach liquors by adsorption with diglycolamic acid ligands and ionic liquids. *Hydrometallurgy*. 2021;204:105720.
https://doi.org/10.1016/j.hydromet.2021.105720

Information about the authors

Vladimir N. Rychkov – Dr. Sci. (Chem.), Professor of the Department of Rare Metals and Nanomaterials (RM&N), Ural Federal University named after the first President of Russia B.N.Yeltsin» (UrFU).
https://orcid.org/0009-0009-4776-5506
E-mail: v.n.rychkov@urfu.ru

Evgenii V. Kirillov – Cand. Sci. (Eng.), Docent of the Department of RM&N, UrFU.
https://orcid.org/0000-0002-0024-3120
E-mail: e.kirillov.umn@gmail.com

Sergei V. Kirillov – Cand. Sci. (Eng.), Docent of the Department of RM&N, UrFU.
https://orcid.org/0000-0001-9949-9881
E-mail: S.V.Kirillov@urfu.ru

Grigorii M. Bunkov – Cand. Sci. (Eng.), Docent of the Department of RM&N, UrFU.
https://orcid.org/0000-0002-8063-4390
E-mail: g.m.bunkov@urfu.ru

Maxim S. Botalov – Assistant, Leading Engineer of the Department of RM&N, UrFU.
https://orcid.org/0000-0001-5870-472X
E-mail: ms.botalov@urfu.ru

Denis V. Smyshlyaev – Assistant, Leading Engineer of the Department of RM&N, UrFU.
https://orcid.org/0009-0007-4580-6090
E-mail: Denis.smyshliaev@urfu.ru

Информация об авторах

Владимир Николаевич Рычков – д.х.н., профессор кафедры редких металлов и наноматериалов (РМиН), Уральский федеральный университет имени первого Президента России Б.Н. Ельцина (УрФУ).
https://orcid.org/0009-0009-4776-5506
E-mail: v.n.rychkov@urfu.ru

Евгений Владимирович Кириллов – к.т.н., доцент кафедры РМиН, УрФУ.
https://orcid.org/0000-0002-0024-3120
E-mail: e.kirillov.umn@gmail.com

Сергей Владимирович Кириллов – к.т.н., доцент кафедры РМиН, УрФУ.
https://orcid.org/0000-0001-9949-9881
E-mail: S.V.Kirillov@urfu.ru

Григорий Михайлович Буньков – к.т.н., доцент кафедры РМиН, УрФУ.
https://orcid.org/0000-0002-8063-4390
E-mail: g.m.bunkov@urfu.ru

Максим Сергеевич Боталов – ассистент, вед. инженер кафедры РМиН, УрФУ.
https://orcid.org/0000-0001-5870-472X
E-mail: ms.botalov@urfu.ru

Денис Валерьевич Смышляев – ассистент, вед. инженер кафедры РМиН, УрФУ.
https://orcid.org/0009-0007-4580-6090
E-mail: Denis.smyshliaev@urfu.ru

Contribution of the authors

V.N. Rychkov – scientific supervision, correcting the text and conclusions.

E.V. Kirillov – providing the resources, preparing and conducting the experiments, formulating the main concept, setting the purpose and objectives of the study; writing the text.

S.V. Kirillov – providing the resources, preparing and conducting the experiments, formulating the main concept, setting the purpose and objectives of the study; formulating the conclusions.

G.M. Bunkov – making the calculations, testing the samples, writing the text.

M.S. Botalov – formulating the main concept, setting the purpose and objectives of the study; writing the text, formulating the conclusions.

D.V. Smyshlyaev – making the calculations, analyzing the research results.

Вклад авторов

В.Н. Рычков – научное руководство, корректировка текста, корректировка выводов.

Е.В. Кириллов – обеспечение ресурсами, подготовка и проведение экспериментов, формирование основной концепции, постановка цели и задачи исследования, подготовка текста.

С.В. Кириллов – обеспечение ресурсами, подготовка и проведение экспериментов, формирование основной концепции, постановка цели и задачи исследования, формулировка выводов.

Г.М. Буньков – осуществление расчетов, проведение испытаний образцов, подготовка текста статьи.

М.С. Боталов – формирование основной концепции, постановка цели и задачи исследования, подготовка текста, формулировка выводов.

Д.В. Смышляев – проведение расчетов, анализ результатов исследований.

The article was submitted 15.12.2023, revised 20.03.2024, accepted for publication 17.04.2024

Статья поступила в редакцию 15.12.2023, доработана 20.03.2024, подписана в печать 17.04.2024

PRESSURE TREATMENT OF METALS / ОБРАБОТКА МЕТАЛЛОВ ДАВЛЕНИЕМ

UDC 621.77.014
https://doi.org/10.17073/0021-3438-2024-3-73-86

Research article
Научная статья

Finite element simulation of hot cladding parameters for thin-sheet rolled products made of experimental Al–2%Cu–2%Mn alloy

A.N. Koshmin[1,2], **A.V. Zinoviev**[2], **S.O. Cherkasov**[2], **K.A. Tsydenov**[2]

[1] **Moscow Polytechnic University**
38 Bolshaya Semyonovskaya Str., Moscow 107023, Russia

[2] **National University of Science and Technology "MISIS"**
4 Bld. 1 Leninskiy Prosp., Moscow 119049, Russia

✉ Aleksander N. Koshmin (koshmin.an@misis.ru)

Abstract: An analysis was performed on the temperature, rate and force parameters of the hot cladding process for the experimental Al–2%Cu–2%Mn alloy with technically pure aluminum grade 1050A, as well as on the stress-strain state of the metal in the deformation zone at reductions of 30, 40, and 50 %. Plastometric tests were conducted within the temperature range of 350–450 °C, strain rates of 0.1–20 s^{-1}, and true strain of 0.1–0.9, and coefficients for calculating the flow stress of the experimental alloy were determined. The thermal conductivity of the Al–2%Cu–2%Mn alloy under hot deformation conditions at temperatures of 350, 400, and 450 °C was theoretically calculated to be 161, 159, and 151 W/(m·K), respectively. The study of the cladding process on a two-high rolling mill was carried out using the QForm finite element simulation software. It was found that when the metal of the cladding layer comes into contact with the roll, its temperature decreases by approximately 100 °C, with the temperature across the height of the composite equalizing within 20–30 ms after exiting the deformation zone. The rolling force is evenly distributed between the two rolls in all cases considered, while the rolling torque on the roll on the cladding layer side is half that on the roll contacting the base layer, which is characteristic of asymmetric rolling. Points characterized by optimal bonding conditions of the rolled layers were identified, located at 10 % and 70 % of the deformation zone length along the rolling axis, where normal stresses significantly prevail over shear stresses. It was determined that the formation of these areas is due to the nature of plastic flow, including the presence of a non-deforming hard layer and a sticking zone.

Keywords: finite element simulation, hot rolling, cladding, aluminum alloy, rheology, plastic deformation, deformation zone (DZ).

Acknowledgments: The study was carried out with the financial support of the Russian Science Foundation grant Project No. 23-79-01172, https://rscf.ru/project/23-79-01172/

For citation: Koshmin A.N., Zinoviev A.V., Cherkasov S.O., Tsydenov K.A. Finite element simulation of hot cladding parameters for thin-sheet rolled products made of experimental Al–2%Cu–2%Mn alloy. *Izvestiya. Non-Ferrous Metallurgy*. 2024;30(3):73–86.
https://doi.org/10.17073/0021-3438-2024-3-73-86

Конечно-элементное моделирование параметров горячего плакирования тонколистового проката из экспериментального сплава Al–2%Cu–2%Mn

А.Н. Кошмин[1,2]**, А.В. Зиновьев**[2]**, С.О. Черкасов**[2]**, К.А. Цыденов**[2]

[1] **Московский политехнический университет**
Россия, 107023, г. Москва, ул. Большая Семеновская, 38

[2] **Национальный исследовательский технологический университет «МИСИС»**
Россия, 119049, г. Москва, Ленинский пр-т, 4, стр. 1

✉ Александр Николаевич Кошмин (koshmin.an@misis.ru)

Аннотация: Выполнен анализ температурных, скоростных и силовых параметров процесса горячего плакирования экспериментального сплава Al–2%Cu–2%Mn технически чистым алюминием марки 1050А, а также напряженно-деформированного состояния металла в очаге деформации при относительной деформации 30, 40 и 50 %. В интервалах температур 350–450 °С, скоростей деформации 0,1–20 с$^{-1}$ и истинной деформации 0,1–0,9, проведены пластометрические испытания и определены коэффициенты для расчета сопротивления деформации экспериментального сплава. Расчетно-теоретически определена теплопроводность сплава Al–2%Cu–2%Mn для условий горячего деформирования при температурах 350, 400 и 450 °С, которая составила 161, 159 и 151 Вт/(м·К) соответственно. Изучение особенностей процесса плакирования на двухвалковом стане выполнено в комплексе конечно-элементного моделирования QForm. Установлено, что при контакте металла плакирующего слоя с валком происходит его охлаждение на ~100 °С, а выравнивание температуры по высоте композита – в течение 20–30 мс после его выхода из очага деформации. Усилие прокатки равномерно распределено между двумя валками во всех рассматриваемых случаях, а момент прокатки на валке со стороны плакирующего слоя в 2 раза ниже, чем на контактирующем с основным, что характерно для асимметричной прокатки. Определены точки, характеризуемые оптимальными условиями соединения слоев проката, расположенные на расстоянии 10 % и 70 % по длине очага деформации вдоль оси прокатки, в которых нормальные напряжения существенно превалируют над касательными. Установлено, что возникновение данных областей обусловлено характером пластического течения, в том числе наличием зоны отсутствия деформации твердого слоя и зоны прилипания.

Ключевые слова: конечно-элементное моделирование, горячая прокатка, плакирование, алюминиевый сплав, реология, пластическая деформация, очаг деформации (ОД).

Благодарности: Исследование выполнено за счет гранта Российского научного фонда № 23-79-01172, https://rscf.ru/project/23-79-01172/

Для цитирования: Кошмин А.Н., Зиновьев А.В., Черкасов С.О., Цыденов К.А. Конечно-элементное моделирование параметров горячего плакирования тонколистового проката из экспериментального сплава Al–2%Cu–2%Mn. *Известия вузов. Цветная металлургия*. 2024;30(3):73–86. https://doi.org/10.17073/0021-3438-2024-3-73-86

Introduction

Aluminum-based alloys have found widespread use in various industries due to the advantageous combination of their operational characteristics and relatively low cost [1]. The most common group consists of heat-treatable alloys in the Al—Cu system (1201, D16, D20, etc.). However, a common drawback of materials in this group is the necessity of thermal processing — such as homogenization of ingots before deformation, quenching, and prolonged artificial aging of deformed semi-finished products (18—36 hours) — to achieve the maximum possible strength, which significantly complicates the manufacturing process of these semi-finished products.

In [2], a new deformable and non-heat-treatable Al—2%Cu—2%Mn alloy, economically alloyed with Zr and Sc, was studied. It was found to exhibit better manufacturability compared to its Al—Cu system counterparts. The research [3] indicates that even without additional alloying, the base experimental alloy demonstrates a good level of functional properties at room temperature and retains them when the temperature increases during operation.

It is known that aluminum alloys alloyed with copper are susceptible to stress corrosion cracking and exfoliation corrosion [4]. Therefore, various surface modification techniques are used to protect products made from these alloys [5]. Among them, cladding aluminum alloys with technical aluminum by roll bonding is the most straightforward to implement and, unlike other methods, provides reliable protection of the base layer under conditions of intense thermal and mechanical stresses [6].

Despite the rather long history of practical use of the hot cladding process for high-strength aluminum alloys and the large number of research works conducted, including those using finite element (FE) analysis [7; 8], the mechanisms of bonding dissimilar metals have not been fully established. Several theories explain the creation of a strong adhesive bond between metals as a result of pressure processing: the "film" theory, diffusion theory, and complex theory [9]. However, it is indisputable that the primary process determining metal bonding is joint plastic deformation. This process is characterized by the duration of exposure, the magnitude of the generated stresses, the value and rate of deformation, and the temperature conditions of the process [10; 11]. However, to date, there are no studies examining this problem in terms of the influence of the geometric parameters of the deformation zone (DZ), the force, and the speed conditions of deformation of layered flat rolled products on the bonding process.

The objectives of this study were to investigate the plastic characteristics of the Al—2%Cu—2%Mn alloy, develop and construct a finite element model for its cladding with technically pure aluminum under various deformation parameters, and analyze the results obtained.

Characteristics of research materials

The materials used for the workpieces were technically pure aluminum grade 1050A (EN 573-3:2007) and an experimental Al—2%Cu—2%Mn alloy (hereafter referred to as 2Cu2Mn). Their chemical composition is presented in Table 1. To obtain the physical and mechanical properties necessary for simulation, a billet of the 2Cu2Mn alloy measuring 20×120×135 mm was cast and then rolled at a temperature of 400 °C on a two-high rolling mill DUO210X300 at a roll circumferential speed of 30 rpm to a thickness of 15 mm to produce a deformed structure. Cylindrical samples with a diameter of 5 mm and a length of 10 mm were taken from the rolled sheet along the deformation direction. The rheology of these samples was studied using a quenching-deformation dilatometer DIL805A/D (TA Instruments, USA). The temperature and strain rate parameters of the dilatometer tests were selected based on the conditions characteristic of hot deformation for this material and included tests at temperatures (t) of 350, 400, 450 °C and strain rates ($\bar{\varepsilon}$) of 0.1, 1.0, 10, and 20 s^{-1}. The samples were tested by compression until a true strain value of $\varepsilon_t = 0.9$. As a result, deformation curves of the experimental alloy were obtained, from which, after adjusting for friction and temperature, the coefficients for the equation calculating the flow stress (σ) considering thermal softening were determined [12]:

$$\sigma = e^{A}\,\bar{\varepsilon}^{\,m}\varepsilon_t^{n_1}e^{\varepsilon_t n_2}e^{tl},$$

where A, m, n_1, n_2, l are coefficients characterizing the material properties.

The calculated values of the coefficients for the experimental and standard [13] alloys are given in Table 2. The table also presents the calculated correlation coefficient (R^2) and the Fisher criterion (F), confirming the adequacy of the alloy strengthening models.

A necessary parameter for the modeling of the experimental alloy is its thermal conductivity, which was calculated based on the Wiedemann—Franz law:

$$k/\gamma = LT,$$

where k is the thermal conductivity in W/(m·K); γ is the electrical conductivity in S/m; L is the Lorentz number, equal to $2.23\cdot10^{-8}$ W·Ω·K^{-2} for aluminum alloys [13]; T is the temperature in K.

Table 1. **Chemical composition of the alloys under investigation**

Таблица 1. Химический состав исследуемых сплавов

Alloy	Composition, wt.%				
	Al	Cu	Mn	Si	Fe
2Cu2Mn	Base	1.93 ± 0.05	1.94 ± 0.04	0.05 ± 0.04	≤ 0.01
1050A	99.79	–	–	0.18 ± 0.03	0.03 ± 0.02

Table 2. **Coefficients for flow stress calculation in hot rolling processes**

Таблица 2. Коэффициенты для расчета сопротивления деформации при горячей прокатке

Alloy	A	m	n_1	n_2	l	R^2	F
2Cu2Mn	6.2121	0.0756	–0.0382	–0.0046	–0.0616	0.9678	0.0170
1050A	4.9577	0.1475	0.1607	–0.0035	–0.0174	0.9744	0.0165

The specific electrical conductivity of a sample of the 2Cu2Mn alloy, taken from the hot-deformed sheet, was measured at room temperature using an eddy current structural analyzer VE-26NP (Russia) and was found to be $15{,}3\cdot10^6$ S/m. The value of γ for the experimental alloy at elevated temperatures was obtained by extrapolating known data [14] to the measured value. Thus, the calculated thermal conductivity of the alloy at temperatures of 350, 400, and 450 °C was 161, 159, and 151 W/(m·K), respectively. The thermal conductivity and specific heat capacity values for the cladding layer material were taken from the standard material library of the modeling software for the 1050A alloy and were 226 W/(m·K) and 930 J/(kg·K), respectively [15].

Finite element simulation methodology

Geometric parameters of the model and initial data

The hot rolling — cladding process was simulated in a plane strain mode using the QForm 10.3 software package [16]. The geometry of the tool, along with parameters and characteristics similar to those of the DUO210X300 rolling mill (Russia), was imported into the modeling program (Fig. 1, *a*). The workpieces used were two plates made from the studied alloys with different initial thicknesses h_b and h_c. The layered workpiece was then deformed with a reduction ε of 30 %, 40 %, and 50 %, so that the values of h_b and h_c in each case were 5.85 and 0.65 mm, 6.3 and 0.7 mm, and 6.75 and

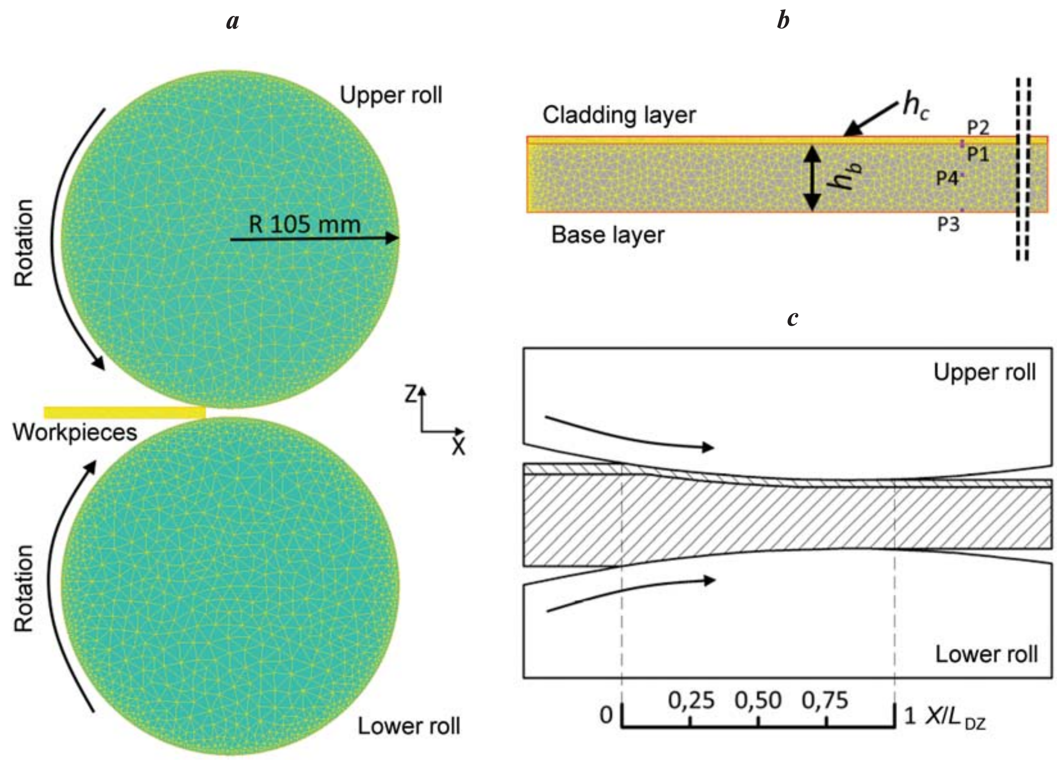

Fig. 1. The geometry of the roll unit (***a***), workpieces (***b***), and deformation center (***c***)

Рис. 1. Геометрия валкового узла (***a***), заготовок (***b***) и очага деформации (***c***)

0.75 mm, respectively. As a result, the final total thickness of the clad sheet was 5 mm. The initial length and the non-represented width in the plane strain model were each 100 mm.

Traced points, located through the thickness of the workpiece at key and particularly indicative sections, were used to study the contact stresses and flow velocities. According to Fig. 1, *b*, these points are located as follows:

— at the contact between the base layer (P1) and the cladding layer (P2);

— at the point of contact between the base layer and the lower roll (P3);

— in the middle of the total thickness of the rolled product (P4).

The primary work of consolidating the layers occurs directly due to the stresses within the deformation zone. Fig. 1, *c* shows a view of the deformation zone, where the length of the contact arc between the metal and the roll relative to the *X*-axis (X/L_{DZ}) is schematically indicated. The analysis of the modeling data and the construction of graphs were performed concerning this section.

The model used triangular-shaped finite elements (FE), which are well-suited for simulating plane strain rolling processes. To increase the calculation accuracy, an adaptive mesh refinement was chosen, with a mesh adaptation coefficient of 3 in the workpieces. This means that the ratio of the maximum size of the modeled object to the size of any finite element in the mesh will be maintained within a specified range, which is beneficial when using workpieces of different initial thicknesses and when they are thinned during rolling. The main initial parameters of the model are presented below:

Material of the rolls 41Cr4

Roll temperature, °C.. 25

Workpiece temperature, °C................................. 400

Ambient temperature, °C...................................... 25

FE number in the tool, thousand units 2.5

FE number in the workpiece
at the beginning/end of modeling,
thousand units..10/15

Time step, ms 2.5

Deformation and thermal models

The coordinate system was chosen so that the axis of the least deformation coincided with the missing axis

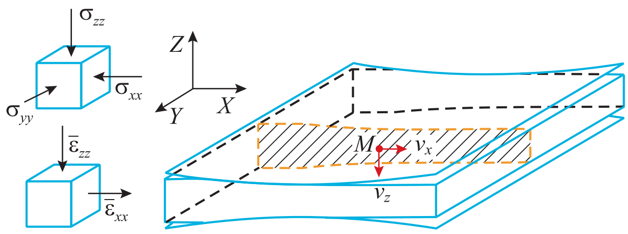

Fig. 2. Plane strain state in the case of thin sheet rolling

Рис. 2. Плоское деформированное состояние в случае прокатки тонкого листа

in the coordinate system. In the case of flat rolling, this direction can be considered the *Y*-axis (Fig. 2), as it is in this direction that only the widening of the metal occurs, which is significantly less than the reduction and elongation. In this case, the mesh elements move only in the directions of v_x and v_z, here are no shear stresses on the planes perpendicular to the *Y*-axis, and the normal stress in the *Y*-axis direction depends on the normal stresses along the other axes and during plastic deformation is equal to:

$$\sigma_{yy} = \frac{1}{2(\sigma_{xx} + \sigma_{zz})}.$$

Stress tensors (T_σ) and final strains (T_E) in the case under consideration are as follows:

$$T_\sigma = \begin{pmatrix} \sigma_{xx} & 0 & \sigma_{xz} \\ 0 & \sigma_{yy} & 0 \\ \sigma_{zx} & 0 & \sigma_{zz} \end{pmatrix}, \quad T_E = \begin{pmatrix} E_{xx} & 0 & E_{xz} \\ 0 & 0 & 0 \\ E_{zx} & 0 & E_{zz} \end{pmatrix}.$$

The equivalent (plastic) strain (ε_{eq}) was calculated using the equivalent plastic strain rate ($\bar{\varepsilon}_{eq}$) by integrating the sum of the increments along the particle's trajectory:

$$\varepsilon_{eq} = \int_t \bar{\varepsilon}_{eq} dt,$$

$$\bar{\varepsilon}_{eq} = \sqrt{\frac{4}{9}\left\{\frac{1}{2}[(\bar{\varepsilon}_{xx} - \bar{\varepsilon}_{zz})^2 + \bar{\varepsilon}_{xx}^2 + \bar{\varepsilon}_{zz}^2] + \frac{3}{4}\bar{\gamma}_{xz}^2\right\}}.$$

A "simple" heat exchange mode was applied for calculating the heat transfer between the pairs of workpiece—workpiece and workpiece—tool, which limited the movement of heat flow from one object to another by a near-surface layer with a thickness of 5 linear mesh elements. This mode was chosen due to the high speed of the rolling process and, consequently, the short contact time between the workpieces and the tool, measured in milliseconds. The propagation of the heat flow (q_n) in this case is normal in nature. Its magnitude is calculated by the equation:

$$q_n = b\alpha(t_1 - t_2),$$

where t_1 and t_2 are the temperatures of the model objects, °C; α is the heat transfer coefficient; $b = 0.05$ is a pause coefficient that accounts for the distance between the objects. The heat transfer coefficient values between the tool and the workpieces, as well as between the layers of the workpiece, were assumed to be 100 000 and 120 000 W/(m^2·K), respectively [17].

Contact model

The contact model of objects in the simulation of the cladding process is a crucial factor that influences the overall adequacy of the model. The Siebel law was used to describe the contact interaction between the workpiece—workpiece and workpiece—tool pairs, which defines the shear stress (τ) on the surface of the workpiece as the product of the friction factor (k_f) and the flow stress in the layers of the workpieces that are in contact with the tool and with each other (σ):

$$\tau = k_f \frac{\sigma}{\sqrt{3}}.$$

The friction factor was determined experimentally by measuring the duration of the rolling process for standard samples with a length of 200 mm made from alloys similar to those being studied and comparing this time with the modeled one. The friction factor for the workpiece—tool pairs, including at the roll—cladding layer and roll—base layer boundaries, was assumed to be 2.5, and for the workpiece—workpiece pair, it was 4. A higher friction factor between the workpieces was chosen based on the preparation of their surfaces in contact with each other by degreasing and mechanical processing (increasing roughness).

In QForm, a special contact element is used for the numerical implementation of the joint deformation of two modeled objects (workpieces) since the nodes of the finite element mesh in the contacting bodies do not generally coincide. Figure 3 schematically shows the principle of this interaction. For clarity, the contacting elements are separated along the normal by a distance comparable to the size of the element. The direction of the normal is indicated by the vector $\vec{n}$. The nodal velocities (v_p) are used as the nodal unknowns. In this case, the normal force function P_n, which ensures the minimization of penetration along

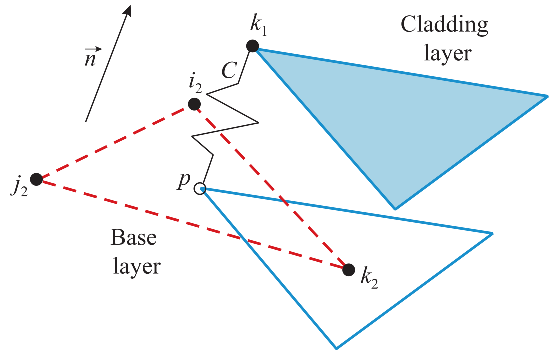

Fig. 3. Schematic of contacting finite elements of two workpieces [17]

Рис. 3. Схема контактирующих конечных элементов двух заготовок [17]

the normal to the contact surfaces of the workpieces, is as follows:

$$P_n = C(v_n^{k_1} - v_n^p).$$

where C is a penalty coefficient determined as a value that exceeds the largest of the diagonal coefficients of the stiffness matrices of the two contacting bodies. Thus, using shape functions, the forces at the nodes of the contact element are determined by the formula:

$$P_n = P_n^{k_1} - P_n^{i_2} - P_n^{j_2} - P_n^{k_2}.$$

Results and discussion

Temperature and force parameters of the cladding process

Regardless of the degree of deformation ε, the formation of temperature fields in the workpiece follows a similar pattern (Fig. 4). At the entry into the deformation zone (DZ), there is an almost instantaneous drop in the metal temperature at the contact with the tool — on average by 100 °C. As the workpieces move along the rolling axis, their surface temperatures gradually equalize, tending toward the temperature of the internal non-contact area. This is facilitated by the deformation heating of the base layer, which not only does not decrease but even increases its temperature by 10 °C from the initial value.

The cooling of the cladding layer deserves special attention. The drop in its temperature upon contact with the roll occurs throughout its thickness but does not spread to the base layer, whose temperature remains high. This fact is due to the peculiarities of the software calculation of heat transfer, which is conducted sepa-

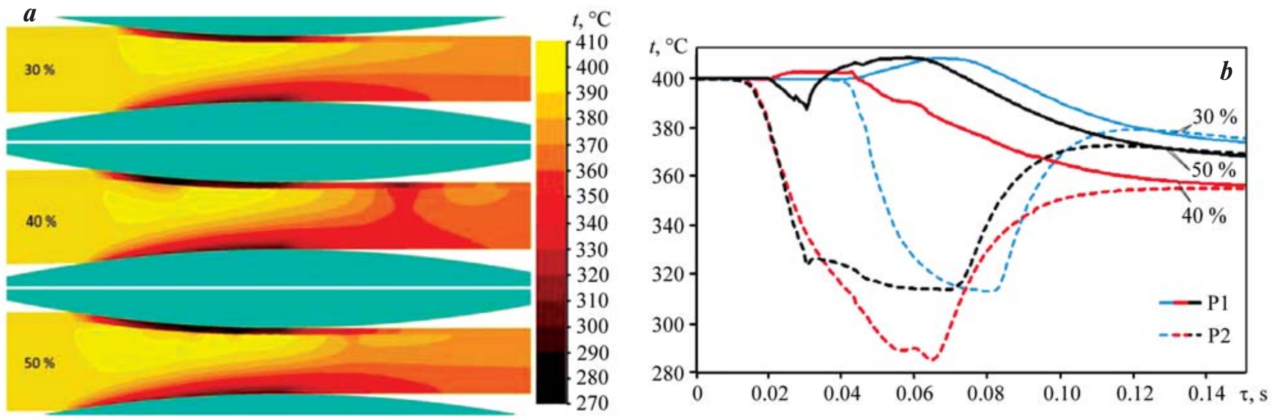

Fig. 4. Temperature fields in the deformation zone (***a***) and temperature as a function of deformation zone transit time in the base (P1) and cladding (P2) layers during rolling (***b***)

Numbers at the curves are values of the strain ratio

Рис. 4. Температурные поля в очаге деформации (***a***) и температура в зависимости от времени прохождения очага деформации в основном (P1) и плакирующем (P2) слоях в процессе прокатки (***b***)

Цифры у кривых – значения степени относительной деформации

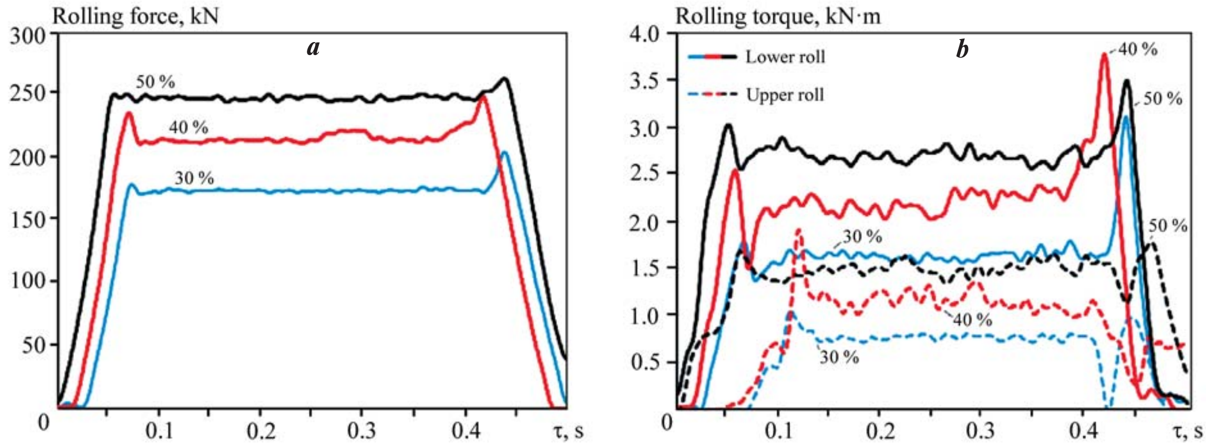

Fig. 5. Change in force (***a***) and torque (***b***) during the rolling process

Numbers at the curves are values of the strain ratio

Рис. 5. Изменение усилия (***a***) и момента (***b***) в ходе прокатки

Цифры у кривых – значения степени относительной деформации

rately for each workpiece without the possibility to exclude the consideration of the pause coefficient *b* after passing through the deformation zone. In other words, this temperature model does not account for the formation of a welded joint (adhesion) between the layers. Nevertheless, the results of the temperature changes in the layered rolled product appear adequate. The temperature of each layer in the contact areas tends to equalize within 20—30 ms after the composite exits the deformation zone.

The change in the force parameters of the cladding process follows a fairly traditional pattern. The rolling force change curves (Fig. 5) clearly show all the main stages of the process: the capture of the workpieces by the rolls, the steady stage, and the exit of the metal from the rolls. The force value at the steady stage is 175, 215, and 250 kN for reductions ε of 30 %, 40 %, and 50 %, respectively. Here, there is a trend of increasing rolling force by 20 % with a 10 % increase in reduction. The rolling torque varies less predictably over time. Peaks corresponding to the capture and exit of the metal from the rolls are also observed here, but the steady stage is characterized by numerous oscillations. This may be due to the presence of two objects in the deformation zone, whose interfacial friction is uneven along the DZ.

Another feature is the difference in the rolling torque acting on the upper and lower rolls. The torque on the lower roll, which is in contact with the metal of the base layer, is on average twice as high as that on the upper roll in all cases considered. This is due to the difference in the flow stress of the investigated alloys, which directly affects the conditions of contact friction. However, when comparing the rolling forces acting on the lower and upper rolls in each simulation case, such a high discrepancy was not observed, with a maximum difference of 10 %.

Stress-strain state of the rolled product in the deformation zone

The nature of the formation of equivalent strain (ε_{eq}) and the distribution of the equivalent plastic strain rate ($\bar{\varepsilon}_{eq}$) along the deformation zone (DZ) is shown in Fig. 6. As can be seen, the degree of relative reduction significantly influences these characteristics. As the reduction increases, the extent of the deformation zone noticeably expands, and consequently, the contact time of the joined surfaces under pressure also increases. The work hardening of the base layer occurs less intensively with increasing ε compared to the cladding layer. This is due to both the temperature conditions (significant cooling throughout the thickness of the cladding layer) and the different patterns of equivalent strain rate distribution, which in the contact zone of the cladding layer was 0.9, 1.25, and 1.6 for relative reductions of 30 %, 40 %, and 50 %, respectively. The values of the equivalent strain rate are roughly the same in all cases: up to 80 s^{-1} at the entry to the DZ (in the zone of maximum compression) and an average of 15 s^{-1} in the middle of the thickness of the rolled product (and on average throughout the entire DZ).

The distribution fields $\bar{\varepsilon}_{eq}$ also allow for some observations. Deformation is most intense at the entry and exit from the deformation zone in the areas where the workpieces contact the tool. The extent of these zones differs in each case, but their volumetric share relative to the entire geometric DZ is the same. The occurrence of such distinct X-shaped patterns in the distribution $\bar{\varepsilon}_{eq}$ is associated with the nature of metal flow and the accompanying development of shear deformations in these areas.

Several studies [18; 19] assert the existence of a pattern of adhesion in layered rolled products with significantly different strengths (hardness). They suggest that a high difference in the strength of the contact surfaces of the joined sheets promotes uneven metal flow of the workpieces within the deformation zone relative to each other. This creates additional shear stresses between the layers, reducing the effect of normal stresses and, as a result, hindering the formation of a strong welded joint in the DZ. Also, considering the “film” theory of metal bonding, it can be assumed that the high strength of the surfaces of the joined sheets will contribute to more effective oxide film destruction during deformation and the bonding of the formed juvenile areas.

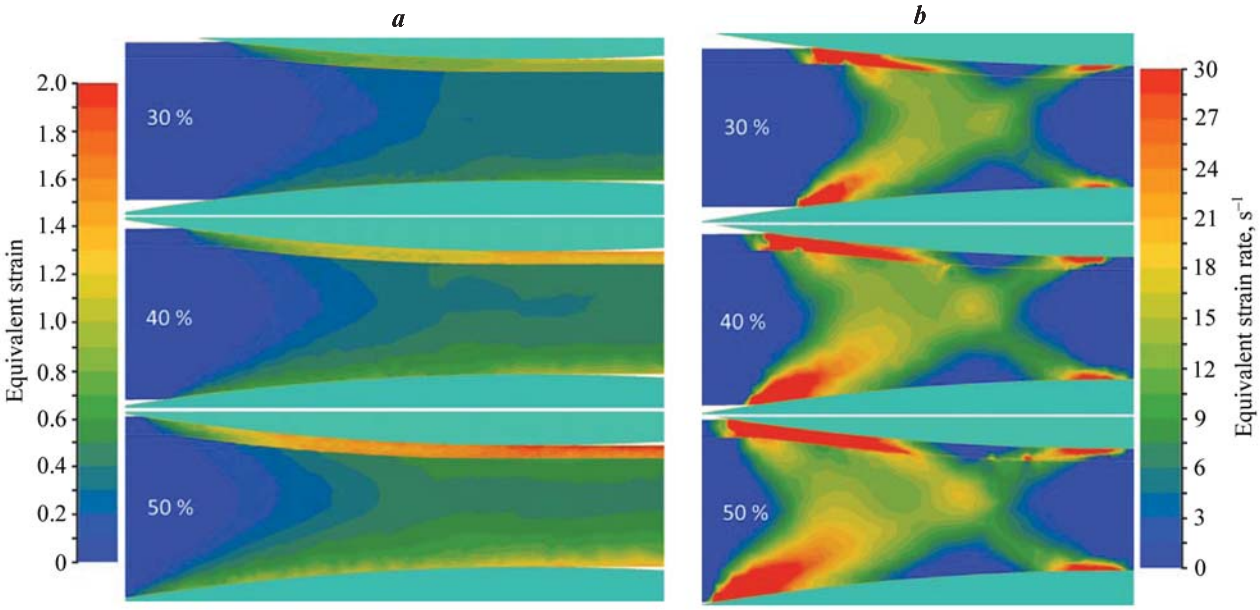

Fig. 6. Distribution fields of equivalent strain (***a***) and strain rate (***b***) in the deformation zone at different values of strain

Рис. 6. Поля распределения эквивалентной деформации (***a***) и скорости деформации (***b***) в ОД при разных значениях относительного обжатия

Figure 7 shows the change in flow stress (σ) of the base (P1) and cladding (P2) layers along the deformation zone. Flow stress in QForm is calculated as the distribution of σ (flow stress) values, set in the material properties, depending on the equivalent strain, strain rate, and temperature. It should be noted that the length of the DZ relative to the X-axis is standardized for all cases considered, but its actual geometric length, as well as the contact time under rolling force, increases by ~15 % with each 10 % increase in reduction. The graphs show that the flow stress of the base layer changes little with varying reduction and averages 100 MPa, while for the cladding layer, it is more affected by reduction: ~70 MPa at ε = 30 and ~80 MPa at ε = 40 and 50 %.

The increase in σ is due to the regular growth of ε_{eq} with increasing reduction, and the equal σ values at ε = 40 and 50 % can be explained by the greater cooling of the cladding layer at ε = 40, as clearly shown in Fig. 4. In all cases considered, at the length of the defor-

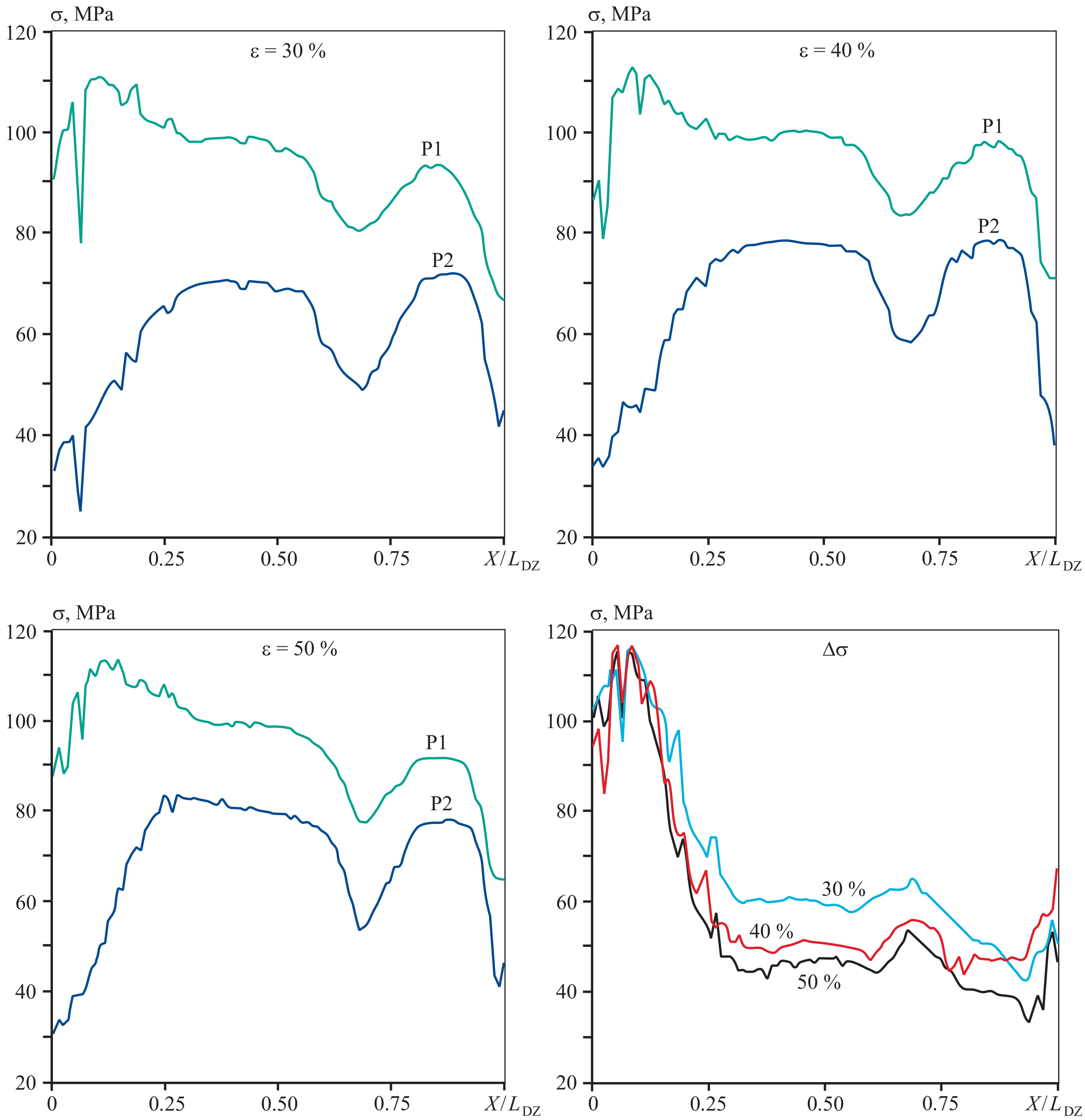

Fig. 7. Change in the flow stress of the base (P1) and cladding (P2) layers and the difference in their flow stresses (Δσ) along the length of the deformation zone

Рис. 7. Изменение сопротивления деформации основного (P1) и плакирующего (P2) слоев и разность их сопротивления деформации (Δσ) вдоль длины очага деформации mation zone of 0.65—0.70, a decrease in σ values of approximately 25 % can be observed, followed by their recovery to the previous level, which is maintained until the metal exits the rolls. This fact is explained by the passage of the traced points through an area with relatively low equivalent plastic strain rate (blue areas in Fig. 6, *b*), as well as a general reduction in the normal and shear stresses (σ_{xx} and σ_{zz}, respectively) acting in this section. Comparing the difference in flow stress values for each layer's surface (Δσ), a systematic decrease with increasing relative strain is noted, which is evident: the smallest Δσ value is achieved at a 50 % reduction. These graphs also indicate that the achievement of surface layer strength uniformity is ensured by the strengthening of the cladding layer on one side and the softening of the base layer due to heating on the other.

The combination of rolling process parameters that occur during the joint deformation of two workpieces, characterized by inhomogeneity along the length and height of the deformation zone (DZ), such as temperature, flow velocity, strain rate, surface strength of the layers, and others, leads to an increase in the shear stresses acting at the layer interfaces. To assess their influence on the formation of the composite bond, standard QForm subroutines — "Pressure" and "Friction" — were used to calculate the values of normal contact pressure (σ_p) and shear friction stress (τ_f).

Figure 8, *a* shows the change in shear stress along the deformation center. It is evident that the value of τ_f at each point of the DZ and in each case considered may differ from the presented one due to being subject to many poorly controlled factors of contact interaction between the two workpieces during joint deformation. Nonetheless, the nature of the obtained stress distribution patterns along the DZ remains consistent with rolling at different ε values. For example, it can be noted that τ_f remains almost unchanged from the moment the metal enters the deformation center until it reaches 0.1 of the DZ length, which is associated with the absence of plastic deformation in the base layer in this section. Then, as it progresses along the DZ, the inhomogeneity of strain rates and plastic flow in the layers increases, leading to a rise in τ_f. Approaching the neutral section of the DZ, the stress level gradually decreases toward zero, only to rise again afterward.

The nature of the normal stress variation along the deformation zone is more uniform. It fluctuates from 150 MPa at the entry to the DZ to 225 MPa at the exit. This is also reflected in the graph of the σ_p/τ_f (Fig. 8, *b*). As seen from the curves, this ratio is 5 for more than 70 % of the DZ length, indicating generally favorable conditions for the formation of an interlayer bond. In each case considered, two characteristic peaks can be noted on the curves — at 0.1 and 0.7 of the DZ length. The first peak symbolizes the onset of the welded bond formation between the layers, associated with the beginning of plastic deformation in the base layer, while the second is linked to improved contact interaction conditions in this section, specifically the drop in strain rate and the accompanying reduction of τ_f to zero. It can be assumed that in this point, the most significant bonding work between the layers occurs under the influence of normal stresses.

Discussion of modeling results

Figure 9 shows the change in the velocity of traced points located at the roll contact, at the interlayer

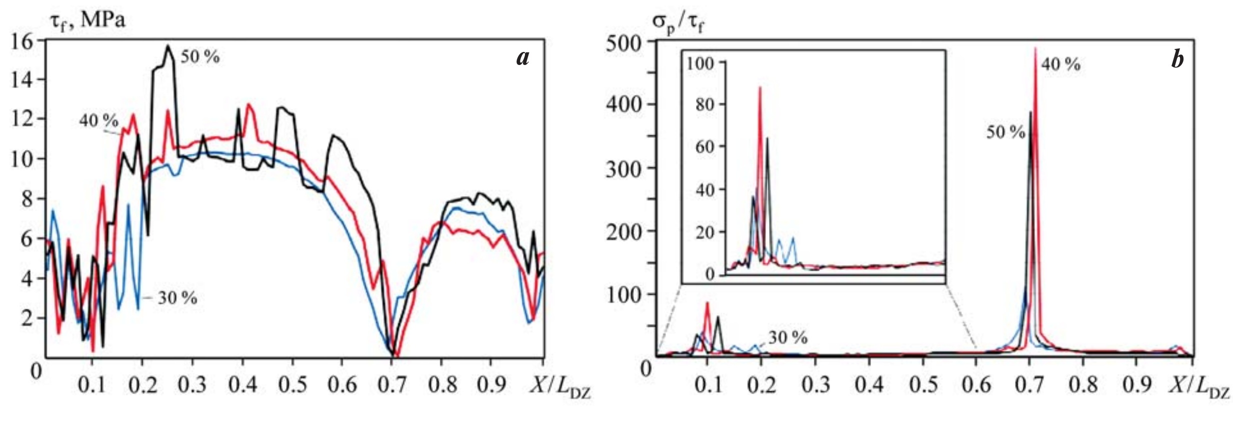

Fig. 8. Variation along the deformation zone of tangential stresses between rolled layers (***a***) and the ratio of normal stress to tangential stress (***b***)

Рис. 8. Изменение вдоль очага деформации касательных напряжений между слоями проката (***а***) и отношения нормального напряжения к касательному (***b***)

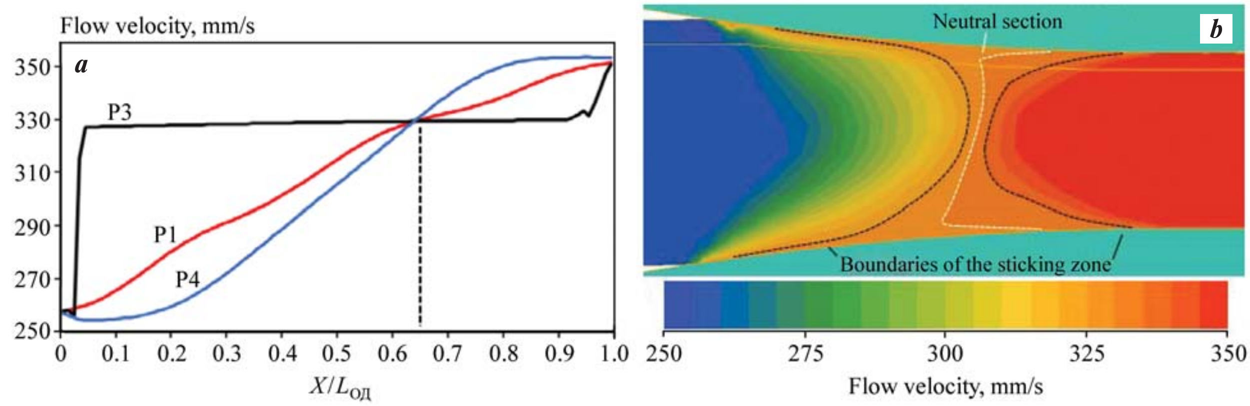

Fig. 9. Velocity of traced points along the *X*-axis (***a***) and flow velocity fields in the deformation zone (***b***)

Рис. 9. Скорость движения трассируемых точек вдоль оси *X* (***a***) и поля скорости течения в очаге деформации (***b***)

boundary, and at half the thickness of the composite during rolling with ε = 40 %. The curves represent a typical pattern for the longitudinal rolling process, allowing for the delineation of lagging and leading zones, positioned at 0.65 of the deformation zone length. At the same time, the sharp changes in values observed in Figs. 7 and 8 manifest themselves at a deformation zone length of 0.70. This is explained by the significant inhomogeneity in the distribution of metal flow velocity along the height of the deformation zone, as seen in the fields of the workpiece in Fig. 9. It can be noted that the sticking zone has an *I*-shaped form, and its center (neutral section) is slightly tilted, which is due to the rolling of dissimilar metals and, consequently, different torque values on the upper and lower rolls.

Thus, the nature of the plastic flow of metal in the deformation zone had the most significant influence on the results presented in the previous section. Under its influence, zones with low strain rate values were formed, which contributed to the reduction of flow stress in both layers. In this same area, the shear stresses are equal to zero.

The results obtained from the cladding modeling at different degrees of reduction are ambiguous. On one hand, increasing the degree of deformation has strengthened the cladding layer, thereby significantly reducing the ratio of the flow stress of the base layer to the cladding layer (σ_{p1}/σ_{p2}) from 3 to 1.5. On the other hand, the influence of the degree of deformation had little effect on the friction stresses acting along the rolling axis. This suggests that the influence of contact and interlayer friction under thin sheet rolling conditions is insignificant, and the success of metal layer bonding in this case is ensured by the action of normal stresses, which are enhanced by increasing the degree of deformation.

Overall, the comparison of the results obtained in this study with elements of the classical theory of longitudinal rolling [20—23] and modern computational and experimental results [24—29] allows us to conclude the adequacy of the developed model and the effectiveness of the applied computational methods and software package.

Conclusion

1. Using the QForm finite element simulation software, the cladding process of the experimental Al—2%Cu—2%Mn alloy with technically pure aluminum was simulated at reduction ratio of 30 %, 40 %, and 50 %. The temperature-rate and deformation parameters of the process, as well as the metal stresses in the layers along the deformation zone, were studied.

2. It was found that the strengthening of the cladding (softer) layer occurs more intensively with increasing deformation degree. The equivalent strain in the contact zone of the cladding layer with the base layer at relative reductions of 30 %, 40 %, and 50 % was 0.9, 1.25, and 1.6, respectively. This fact contributed to the reduction of the difference in flow stress between the contact surfaces of the rolled layers.

3. When studying the features of contact interaction between the surfaces of the layered rolled product, characteristic areas were identified along the length of the deformation zone at 0.1 and 0.7 relative to the *X*-axis, which are characterized by the dominance of normal stresses over shear stresses. The formation of these areas was facilitated by uneven metal flow in the deformation zone, caused by the difference in the deformation characteristics of the base and cladding layer materials.

4. The calculated values of normal and shear stresses between the layers of the workpieces along the deformation zone suggest that bonding will occur along the entire length of the rolled product in all cases considered, although the bonding strength will vary in each case.

References

1. Zakharov A.M. Industrial alloys of non-ferrous metals. Phase composition and structural components. Moscow: Metallurgiya, 1980. 255 p. (In Russ.).
   Захаров А.М. Промышленные сплавы цветных металлов. Фазовый состав и структурные составляющие. М.: Металлургия, 1980. 255 с.
2. Belov N.A., Alabin A.N., Matveeva I.A. Optimization of phase composition of Al—Cu—Mn—Zr—Sc alloys for rolled products without requirement for solution treatment and quenching. *Journal of Alloys and Compounds*. 2014;583:206—213.
   https://doi.org/10.1016/j.jallcom.2013.08.202
3. Belov N.A., Akopyan T.K., Shurkin P.K., Korotkova N.O. Comparative analysis of structure evolution and thermal stability of commercial AA2219 and model Al—2 wt.%Mn—2 wt.%Cu cold rolled alloys. *Journal of Alloys and Compounds*. 2021;864:158823.
   https://doi.org/10.1016/j.jallcom.2021.158823
4. Ghali E. Corrosion resistance of aluminum and magnesium alloys: Understanding, performance, and testing. Hoboken: John Wiley & Sons, Inc., 2010. 752 p.
5. Zarapin Yu.L., Chichenev N.A., Chernilevskaya N.G. Production of composite materials by forming. Recent achievements. Moscow: Metallurgiya, 1991. 351 p. (In Russ.).
   Зарапин Ю.Л., Чиченев Н.А., Чернилевская Н.Г. Производство композиционных материалов обработкой давлением. Последние достижения. М.: Металлургия, 1991. 351 с.
6. Zinoviev A.V., Kolpashnikov A.I., Polukhin P.I., Glebov Yu.P., Piryazev D.I., Gorokhov V.S., Galkin A.M. Technology of forming of non-ferrous metals and alloys: Textbook for universities. Moscow: Metallurgiya, 1992. 512 p. (In Russ.).
   Зиновьев А.В., Колпашников А.И., Полухин П.И., Глебов Ю.П., Пирязев Д.И., Горохов В.С., Галкин А.М. Технология обработки давлением цветных металлов и сплавов: Учебник для вузов. М.: Металлургия, 1992. 512 с.
7. Khan H.A., Asim K., Akram F., Hameed A., Khan A., Mansoor B. Roll bonding processes: State-of-the-Art and future perspectives. *Metals*. 2021;11:1344.
   https://doi.org/10.3390/met11091344
8. Li Z., Rezaei S., Wang T., Han J., Shu X., Pater Z., Huang Q. Recent advances and trends in roll bonding process and bonding model: A review. *Chinese Journal of Aeronautics*. 2023;36(4):36—74. https://doi.org/10.1016/j.cja.2022.07.004
9. Kobelev A.G., Lysak V.I., Chernyshev V.N., Kuznetsov E.V. Materials Science and Technology of Composite Materials. Moscow: Intermet Engineering, 2006. 368 p. (In Russ.).
   Кобелев А.Г., Лысак В.И., Чернышев В.Н., Кузнецов Е.В. Материаловедение и технология композиционных материалов: Учебник для вузов. М.: Интермет Инжениринг, 2006. 368 с.
10. Shatalov R.L., Kulikov M.A. Influence of outer parts of a strip on the deformation and force parameters of thin-sheet rolling. *Metallurgist*. 2020;64:687—698.
    https://doi.org/10.1007/s11015-020-01045-1
11. Shatalov R.L., Maksimov E.A. Development and application of the theory of rigid ends in thin-sheet rolling. *Metallurgist*. 2021;64:1035—1042.
    https://doi.org/10.1007/s11015-021-01084-2
12. Rao K.P., Doraivelu S.M., Gopinathan V. Flow curves and deformation of materials at different temperatures and strain rates. *Journal of Mechanical Working Technology*. 1982;6(1):63—88.
    https://doi.org/10.1016/0378-3804(82)90020-1
13. Polukhin P.I., Gun G.Y., Galkin A.M. Resistance to plastic deformation of metals and alloys. Handbook. Moscow: Metallurgiya, 1983. 352 p. (In Russ.).
    Полухин П.И., Гун Г.Я., Галкин А.М. Сопротивление пластической деформации металлов и сплавов: Справочник. М.: Металлургия, 1983. 352 с.
14. Aksöz S., Ocak Y., Maraşlı N., Çadirli E., Kaya H., Böyük U. Dependency of the thermal and electrical conductivity on the temperature and composition of Cu in the Al based Al—Cu alloys. *Experimental Thermal and Fluid Science*. 2010;34(8):1507—1516.
    https://doi.org/10.1016/j.expthermflusci.2010.07.015
15. Zinoviev V.E. Thermophysical properties of metals at high temperatures: Handbook. Moscow: Metallurgiya, 1989. 384 p. (In Russ.).
    Зиновьев В.Е. Теплофизические свойства металлов при высоких температурах: Справочник. М.: Металлургия, 1989. 384 с.
16. QForm. Version 10.3. Windows. Moscow: LLC “Kvantoform”, 2023.
    QForm. Версия 10.3. Windows. М.: ООО «Квантор-форм», 2023.
17. Vlasov A.V., Stebunov S.A., Evsyukov S.A., Biba N.V., Shitikov A.A. Finite-element modeling of technological processes of forging and stamping: textbook. Moscow: Bauman Moscow State Technical University, 2019. 383 p. (In Russ.).

Власов А.В., Стебунов С.А., Евсюков С.А., Биба Н.В., Шитиков А.А. Конечно-элементное моделирование технологических процессов ковки и объемной штамповки: Учеб. пособие. М.: Изд-во МГТУ им. Н.Э. Баумана, 2019. 383 с.
18. Qin Q., Zhang D., Zang Y., Guan B. A simulation study on the multi-pass rolling bond of 316L/Q345R stainless clad plate. *Advances in Mechanical Engineering.* 2015;7(7). https://doi.org/10.1177/1687814015594313
19. He Z., Chu Z., Shuang Y., Gou Y. The Bonding mechanism and experimental verification of pilger hot rolling clad tube. *Advances in Materials Science and Engineering.* 2020;2020:2689370.
https://doi.org/10.1155/2020/2689370
20. Kolpashnikov A.I. Rolling of light alloy sheets. Moscow: Metallurgiya, 1970. 232 p. (In Russ.).
Колпашников А.И. Прокатка листов из легких сплавов. М.: Металлургия, 1970. 232 с.
21. Tselikov A.I., Nikitin G.S., Rokotyan S.E. Theory of flat rolling. Textbook for students of machine-building and metallurgical universities. Moscow: Metallurgiya, 1980. 320 p. (In Russ.).
Целиков А.И., Никитин Г.С., Рокотян С.Е. Теория продольной прокатки: Учебник для студентов машиностроительных и металлургических вузов. М.: Металлургия, 1980. 320 с.
22. Polukhin P.I., Zinoviev A.V., Polukhin V.P., Burov A.V., Shevelkin S.D. Improving the quality of strips from nonferrous metals and alloys. Alma-Ata: Nauka, 1982. 288 p. (In Russ.).
Полухин П.И., Зиновьев А.В., Полухин В.П., Буров А.В., Шевелкин С.Д. Повышение качества полос из цветных металлов и сплавов. Алма-Ата: Наука, 1982. 288 с.
23. Kovalev S.I., Koryagin N.I., Shirkov I.V. Stresses and strains in flat rolling. Moscow: Metallurgiya, 1982. 256 p. (In Russ.).
Ковалев С.И., Корягин Н.И., Ширков И.В. Напряжения и деформации при плоской прокатке. М.: Металлургия, 1982. 256 с.
24. Kebriaei R., Vladimirov I.N., Reese S. Joining of the alloys AA1050 and AA5754 — Experimental characterization and multiscale modeling based on a cohesive zone element technique. *Journal of Materials Processing Technology.* 2014;214(10):2146—2155.
https://doi.org/10.1016/j.jmatprotec.2014.03.014
25. Bambach M., Pietryga M., Mikloweit A., Hirt G. A finite element framework for the evolution of bond strength in joining-by-forming processes. *Journal of Materials Processing Technology.* 2014;214(10):2156—2168.
https://doi.org/10.1016/j.jmatprotec.2014.03.015
26. Frolov Y., Nosko M., Samsonenko A., Bobukh O., Remez O. Roll bonding of Al-based composite reinforced with C10 steel expanded mesh inlay. *Metals.* 2021;11:1044.
https://doi.org/10.3390/met11071044
27. Frolov Y., Bobukh O., Samsonenko A., Nürnberger F. Patterning of surfaces for subsequent roll bonding in a low-oxygen environment using deformable mesh inlays. *Journal of Manufacturing and Materials Processing.* 2023;7:158.
https://doi.org/10.3390/jmmp7050158
28. Salikhyanov D.R. Investigation of the stress-strain state at the boundary between materials during rolling of a layered composite. *Chernye Metally.* 2023;9:34—39.
Салихянов Д.Р. Исследование напряженно-деформированного состояния на границе между материалами при прокатке слоистого композита. *Черные металлы.* 2023;9:34—39.
https://doi.org/10.17580/chm.2023.09.06
29. Salikhyanov D., Michurov N. Joining of dissimilar aluminum alloys AA5154 and AA2024 by cold roll bonding. *The International Journal of Advanced Manufacturing Technology.* 2023;129:255—277.
https://doi.org/10.1007/s00170-023-12292-2

Information about the authors

Aleksander N. Koshmin – Cand. Sci. (Eng.), Associate Professor of Scientific Activity Sector of Moscow Polytechnic University; Associate Professor of Metal Forming Department of National University of Science and Technology "MISIS" (NUST MISIS).
https://orcid.org/0000-0002-4095-1658
E-mail: koshmin.an@misis.ru

Aleksander V. Zinoviev – Dr. Sci. (Eng.), Professor, Senior Expert of Metal Forming Department, NUST MISIS.
https://orcid.org/0009-0004-6776-7414
E-mail: zinovyew@gmail.com

Stanislav O. Cherkasov – Engineer of Metal Forming Department, NUST MISIS.
https://orcid.org/0000-0001-5248-501X
E-mail: cherkasov.so@misis.ru

Kirill A. Tsydenov – Engineer of Metal Forming Department, NUST MISIS.
https://orcid.org/0000-0002-9290-4925
E-mail: kirillcydenov@yandex.ru

Информация об авторах

Александр Николаевич Кошмин – к.т.н., доцент сектора научной деятельности Московского политехнического университета; доцент кафедры обработки металлов давлением Национального исследовательского технологического университета «МИСИС» (НИТУ МИСИС).
https://orcid.org/0000-0002-4095-1658
E-mail: koshmin.an@misis.ru

Александр Васильевич Зиновьев – д.т.н., проф., вед. эксперт научного проекта кафедры обработки металлов давлением, НИТУ МИСИС.
https://orcid.org/0009-0004-6776-7414
E-mail: zinovyew@gmail.com

Станислав Олегович Черкасов – инженер научного проекта кафедры обработки металлов давлением, НИТУ МИСИС.
https://orcid.org/0000-0001-5248-501X
E-mail: cherkasov.so@misis.ru

Кирилл Андреевич Цыденов – инженер научного проекта кафедры обработки металлов давлением, НИТУ МИСИС.
https://orcid.org/0000-0002-9290-4925
E-mail: kirillcydenov@yandex.ru

Contribution of the authors

A.N. Koshmin – manuscript writing, methodology.

A.V. Zinoviev – conceptualization, manuscript review.

S.O. Cherkasov – simulation, results processing.

K.A. Tsydenov – experiment, results discussion.

Вклад авторов

А.Н. Кошмин – написание статьи, методология.

А.В. Зиновьев – концептуализация, рецензирование статьи.

С.О. Черкасов – моделирование, обработка результатов.

К.А. Цыденов – эксперимент, обсуждение результатов.

The article was submitted 12.02.2024, revised 18.04.2024, accepted for publication 25.04.2024

Статья поступила в редакцию 12.02.2024, доработана 18.04.2024, подписана в печать 25.04.2024

CORROSION AND PROTECTION OF METALS / КОРРОЗИЯ И ЗАЩИТА МЕТАЛЛОВ

UDC 620.193.2, 621.793
https://doi.org/10.17073/0021-3438-2024-3-87-96

Research article
Научная статья

High-entropy Fe–Co–Cr–Ni–(Cu) coatings with enhanced corrosion and tribocorrosion resistance obtained by vacuum electrospark deposition

M.N. Fatykhova, K.A. Kuptsov, A.N. Sheveyko, A.R. Gizatullina, P.A. Loginov, D.V. Shtansky

National University of Science and Technology "MISIS"
4 Bld. 1 Leninskiy Prosp., Moscow 119049, Russia

✉ Mariya N. Fatykhova (mariya.antonyuck@ya.ru)

Abstract: High-entropy coatings are highly promising for protecting steel parts in coastal and marine infrastructure from corrosion and tribocorrosion. This study examines the properties of medium- and high-entropy Fe–Co–Cr–Ni–(Cu) coatings produced by vacuum electrospark deposition. The coatings, with thicknesses of up to 30 μm and varying copper content, exhibit a single-phase solid solution structure with an FCC lattice and a dense, homogeneous morphology. The addition of 14 at.% Cu was found to enhance corrosion resistance, shifting the corrosion potential to 100 mV. In friction conditions within artificial seawater, the inclusion of copper also improved tribocorrosion properties, raising the corrosion potential during friction to –165 mV. This improvement is attributed to the galvanic deposition of dissolved copper on the worn areas of the coating, which also reduces the friction coefficient from 0.37 to 0.26. The Fe–Co–Cr–Ni–(Cu) coatings demonstrate high wear resistance, ranging from 5.6 to $9.6 \cdot 10^{-6}$ mm^3/(N·m). The findings confirm the potential of these coatings for applications in environments subject to both friction and corrosion.

Keywords: electrospark deposition, coatings, seawater, electrochemistry, wear resistance, corrosion resistance, tribocorrosion.

Acknowledgments: The research was supported by the Russian Science Foundation, grant No. 20-79-10104-П

For citation: Fatykhova M.N., Kuptsov K.A., Sheveyko A.N., Gizatullina A.R., Loginov P.A., Shtansky D.V. High-entropy Fe–Co–Cr–Ni–(Cu) coatings with enhanced corrosion and tribocorrosion resistance obtained by vacuum electrospark deposition. *Izvestiya. Non-Ferrous Metallurgy.* 2024;30(3):87–96. https://doi.org/10.17073/0021-3438-2024-3-87-96

Высокоэнтропийные покрытия Fe–Co–Cr–Ni–(Cu) с повышенной коррозионной и трибокоррозионной стойкостью, полученные электроискровым легированием в вакууме

М.Н. Фатыхова, К.А. Купцов, А.Н. Шевейко, А.Р. Гизатуллина, П.А. Логинов, Д.В. Штанский

Национальный исследовательский технологический университет «МИСИС»
Россия, 119049, г. Москва, Ленинский пр-т, 4, стр. 1

✉ Мария Николаевна Фатыхова (mariya.antonyuck@ya.ru)

Аннотация: Высокоэнтропийные покрытия представляют большой интерес для защиты стальных изделий, используемых в прибрежной и морской инфраструктуре, от коррозионного и трибокоррозионного воздействия. В данной работе исследованы свойства средне- и высокоэнтропийных покрытий Fe–Co–Cr–Ni–(Cu), полученных методом электроискрового легирования в вакууме. Показано, что покрытия толщиной до 30 мкм с различным содержанием меди характеризуются структурой однофазного твердого раствора с ГЦК-решеткой и плотной, однородной морфологией. Выявлено, что введение 14 ат.% Cu положительно влияет на коррозионную стойкость, смещая потенциал коррозии до 100 мВ. В условиях трения в искусственной морской воде добавление меди также улучшает трибокоррозионные свойства, повышая потенциал коррозии во время трения до –165 мВ. Это обусловлено гальваническим осаждением растворенной меди на изношенные части покрытия, что также положительно сказывается на коэффициенте трения, снижая его с 0,37 до 0,26. Полученные покрытия Fe–Co–Cr–Ni–(Cu) обладают высокой износостойкостью на уровне $(5,6\div9,6)\cdot10^{-6}$ мм^3/(Н·м). Результаты исследования подтверждают перспективность их использования в условиях трения и коррозии.

Ключевые слова: электроискровое легирование, покрытия, морская вода, электрохимия, износостойкость, коррозионная стойкость, трибокоррозия.

Благодарности: Исследование выполнено за счет гранта Российского научного фонда № 20-79-10104-П.

Для цитирования: Фатыхова М.Н., Купцов К.А., Шевейко А.Н., Гизатуллина А.Р., Логинов П.А., Штанский Д.В. Высокоэнтропийные покрытия Fe–Co–Cr–Ni–(Cu) с повышенной коррозионной и трибокоррозионной стойкостью, полученные электроискровым легированием в вакууме. *Известия вузов. Цветная металлургия*. 2024;30(3):87–96.
https://doi.org/10.17073/0021-3438-2024-3-87-96

Introduction

Due to the active use of marine resources, issues related to the quality and longevity of engineering equipment have become increasingly relevant [1; 2]. Sea water, being an aggressive medium, promotes the development of corrosion in metal parts during their operation [3; 4]. Most moving components of marine and coastal equipment, including pumps, bearings, valves, propellers, gears, etc., are subjected to the synergistic effects of wear and corrosion in sea water — a process known as tribocorrosion. This inevitably accelerates the damage and degradation of mechanical friction units, shortening their service life [5—8]. Additionally, parts that are in a prolonged contact with sea water are prone to biofouling — the growth of microorganisms on the surface, which leads to microbiologically influenced corrosion (MIC) [9]. As a result, the service life is reduced, and energy consumption of engineering equipment increases [10].

Stainless steels with high chromium content (up to 18 %) are widely used for marine equipment components due to the formation of a surface oxide film consisting of Cr_2O_3, which helps reduce corrosion on the surface. Recently, a new type of material, high-entropy alloys (HEAs), has been discovered. These alloys contain passivating elements such as Cr, Ni, Mo, and others, and exhibit superior corrosion and tribocorrosion properties in aggressive environments (sea water, acids) compared to conventional alloys [11; 12]. It is known that copper significantly affects MIC and biofouling by inhibiting the growth and reproduction of microorganisms involved in these processes [13; 14]. However, the introduction of Cu into multi-component Fe—Co—Cr—Ni-based coatings may lead to structural heterogeneity, such as the formation of a two-phase structure (FCC/BCC) or Cu segregation, resulting in the formation of Cu-rich and Cu-deficient zones, and consequently, more intense localized corrosion [15].

A promising application of corrosion-resistant high-entropy alloys is their use as coatings [16]. Economically, the cost of bulk HEAs produced by arc melting or casting is relatively high, considering the addition of expensive alloying elements. However, the deposiiton of coatings helps mitigate this issue. Currently, HEA-based coatings are produced using methods such as laser cladding [17; 18], electrospark deposition [12; 19], magnetron sputtering [20], etc.

Vacuum electrospark deposition (ESD) is a promising method for producing wear- and corrosion-resistant coatings on various steels [21], allowing the formation of "thick" coatings (up to 200 μm) with high adhesion strength due to the micro-welding process between the electrode material and the substrate during deposition. Additional advantages of ESD include its simplicity, the possibility of localized treatment of large parts, and easy automation of the process.

To improve the surface quality and efficiency of electrospark deposition, the process is carried out in a vacuum, which enhances the wettability of the surface by the melt [22]. This effect is associated with the simultaneous occurrence of two parallel processes — pulsed cathodic arc evaporation of the electrode initiated by spark breakdown and classical mass transfer of the electrode material onto the substrate.

The aim of this work is to develop Fe—Co—Cr—Ni—Cu protective coatings with varying copper content using vacuum electrospark deposition to protect steel parts from corrosion and tribocorrosion during operation in sea water.

Materials and methods

Fe—Co—Cr—Ni—Cux coatings with varying copper content were deposited by vacuum electrospark deposition [12]. Discs with a diameter of 30 mm made of 30X13 steel were used as substrates. Electrodes with different compositions (at.%): Fe_{25}—Co_{25}—Cr_{25}—Ni_{25}, Fe_{20}—Co_{20}—Cr_{20}—Ni_{20}—Cu_{20} и $Fe_{17.5}$—$Co_{17.5}$—$Cr_{17.5}$—$Ni_{17.5}$—Cu_{30}, were produced by powder metallurgy methods from elemental metal powders using the DSP-515 SA hot-pressing press ("Dr. Fritsch", Germany) at a temperature of 950 °C, a pressure of 35 MPa, and an isobaric hold time of 3 minutes [20].

During the coating deposition process, the pressure in the vacuum chamber was maintained at 20 Pa, the electrode rotation speed was 1000 rpm, and the scanning step and speed were 0.5 mm and 500 mm/min, respectively. To ensure high coating continuity, the scanning direction was changed to perpendicular after each treatment cycle.

The Fe—Co—Cr—Ni—Cux coatings were deposited using the Alier 303 metal electrospark power source (Moldova) with the following technological parameters: pulse current amplitude of 120 (± 20 %) A, pulse frequency of 1600 (± 20 %) Hz, and pulse duration of 40 (± 20 %) μs. The deposition time for each coating was 15 minutes.

The morphology, elemental, and phase composition of the coatings were investigated using scanning electron microscopy (SEM) on an S-3400N microscope ("Hitachi", Japan) equipped with an energy dispersive spectrometer NORAN ("Thermo Scientific", USA), as well as *X*-ray diffraction analysis using a D8 Advance diffractometer ("Bruker", Germany).

The electrochemical properties of the coatings were studied in a three-electrode cell using an IPC Pro MF potentiostat (Russia). A platinum electrode was used as the auxiliary electrode, and an Ag/AgCl electrode, widely used for its simplicity, reliability, and reproducibility of results, was used as the reference electrode. Before the experiments, the coating surfaces were covered with a non-conductive compound to exclude the influence of the substrate material on the electrochemical parameters. The working surface area was 1 cm^2.

The tribocorrosion resistance of the coatings was evaluated using a Tribometer ("CSM Instruments", Switzerland) equipped with a special three-electrode cell that allows the registration of electrochemical corrosion potential during tribological tests in a ball-on-disk configuration. The tests were conducted in artificial seawater at a load of 5 N, a sliding distance of 500 m, and a sliding speed of 10 cm/s. An aluminum oxide (Al_2O_3) ball with a diameter of 6 mm and a roughness of 0.8 μm was used as the counterbody. The wear tracks on the coatings were studied using optical profilometry on a WYKO NT1100 profilometer ("Veeco", USA) [21]. The wear volume of the coatings was calculated according to the method described in [22].

The hardness of the coatings was measured by microindentation on their surface using an automatic microhardness tester DuraScan 70 ("EMCO-TEST Prüfmaschinen GmbH", Austria) by calculating the average value from 10 measurements. The indentation load was 0.01 HV.

Results and discussion

Figure 1 presents SEM images and corresponding element distribution maps of the surface of coatings obtained using Fe—Co—Cr—Ni—Cu_x electrodes (x = 0, 20, 30 at.%) with samples designated as Cu0V, Cu2V, and Cu3V, respectively. All coatings exhibit uniform morphology without visible cracks or chips. According to the element distribution maps, the primary elements (Fe, Cr, and Cu) are evenly distributed (Fig. 1, *b*). The elemental composition of the coatings is provided in Table 1. It can be observed that the iron content is approximately the same, ranging from 39 to 43 at.%. The Cu2V and Cu3V samples contain 14 and 19 at.% copper, respectively, and with increasing copper concentration, the content of Cr, Ni, and Co decreases from 18—21 at.% to 12—16 at.%.

Figure 2 shows SEM images of cross-sections of high-entropy Fe—Co—Cr—Ni—Cu_x coatings. All coatings have dense and a defect-free structure (no cracks or pores). The distribution of Cu across the coating thickness is uniform with a slight decrease from the surface to the substrate (Fig. 2, *b*). As the copper content increases from 0 to 19 at.%, the coating thickness decreases from 30 to 21 μm.

Figure 3 shows the XRD patterns of Fe—Co—Cr—Ni—Cu_x coatings. All samples have a single-phase structure with an FCC lattice based on a solid solution of all metallic elements. Additionally, the structure of the coatings is characterized by a strong texture in the (200) direction, associated with directional crystallization during the solidification of the melt. As the Cu content in the coatings increases, the FCC peaks shift towards lower angles, which is associated with an increase in the lattice parameter from 3.570 to 3.582 Å due to the incorporation of more copper into the cubic phase (see inset in Fig. 3).

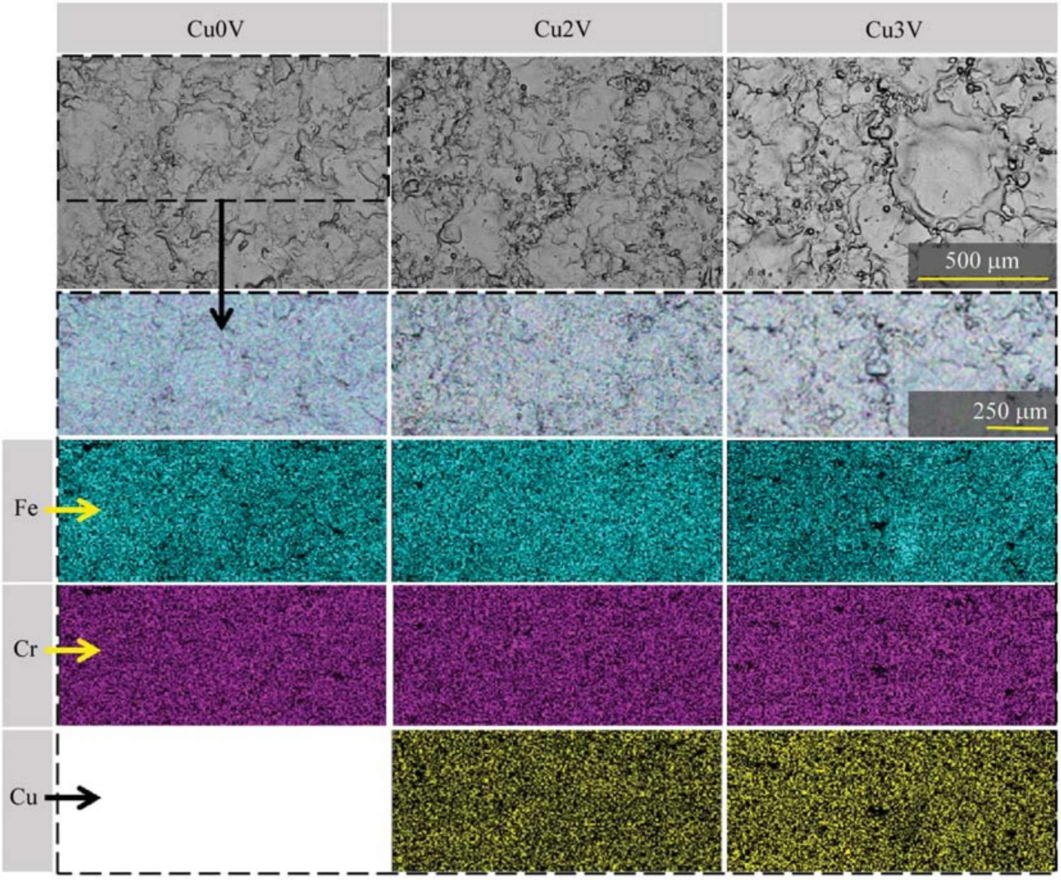

Fig. 1. SEM images of the surface and element distribution maps on the surface of Cu0V, Cu2V, and Cu3V coatings

Рис. 1. СЭМ-изображения поверхности и карты распределения элементов на поверхности образцов покрытий Cu0V, Cu2V и Cu3V

No separate copper-based phases were detected, indicating that all the copper dissolved in the main FCC phase. The crystallite size, estimated using the Debye-Scherrer method, showed minimal influence of copper on this parameter. The introduction of 19 at.% Cu led to a slight decrease in crystallite size from 36 nm (Cu0V) to 34 nm (Cu3V).

To evaluate the corrosion resistance of the coatings, electrochemical tests were conducted in artificial seawater, and the results are shown in Fig. 4. The corrosion potential of the Fe—Co—Cr—Ni coating (sample Cu0V) was +20 mV. The introduction of 14 at.% Cu shifted the corrosion potential in the positive direction to +100 mV, but further increasing the copper concentration to 19 at.% caused a sharp decrease in this value to –150 mV. Interestingly, despite the significant influence of copper on the corrosion potential, the corrosion current density (CCD) of the coatings remained almost unchanged, ranging from 1 to 2 μA/cm^2.

Table 1. **Elemental composition of coatings**

Таблица 1. Элементный состав покрытий

Coating sample	Content, at.%				
	Fe	Co	Cr	Ni	Cu
Cu0V	43	18	21	18	–
Cu2V	43	11	19	13	14
Cu3V	39	12	16	14	19

It is likely that when a certain copper concentration is exceeded, copper accumulates on the surface as iron and other components dissolve. This leads to the formation of individual copper particles, which act as cathodes relative to the surrounding surface. In this case, galvanic pairs form on the surface, leading to partial activation of the metal substrate near the cathodes, which is accompanied by a shift in the zero current potential towards negative values. The influence of these particles on the corrosion current density has two effects. On the one hand, the substrate near the particles dissolves more intensively; on the other hand,

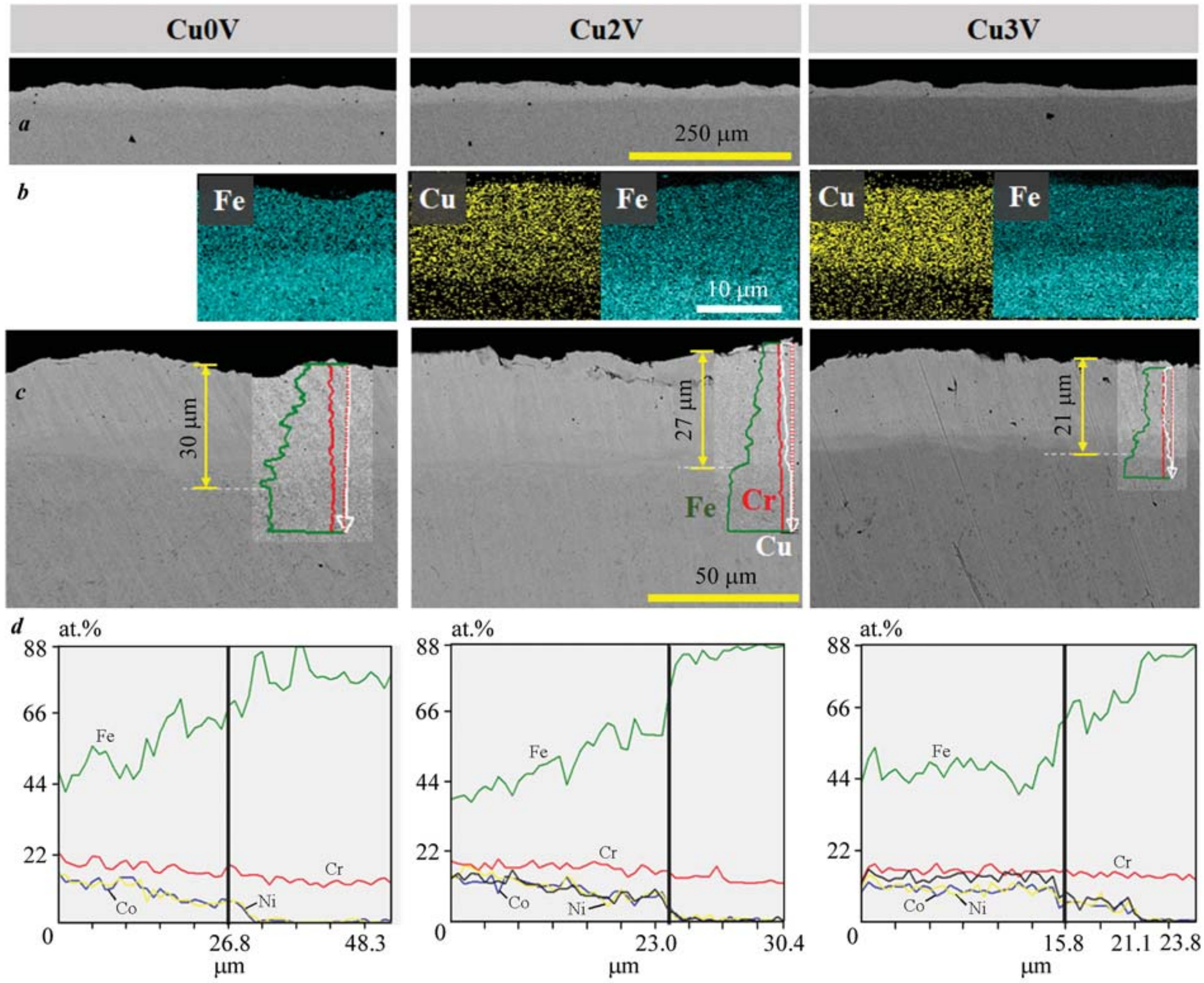

Fig. 2. SEM images of cross-sections of Cu0V, Cu2V, and Cu3V coatings (***a***, ***c***), Cu and Fe distribution maps (***b***), and element distribution profiles (***d***) across the coating thickness

Рис. 2. СЭМ-изображения шлифов покрытий Cu0V, Cu2V и Cu3V (***a***, ***c***), карты распределения Cu и Fe (***b***) и профили распределения элементов (***d***) по толщине покрытия

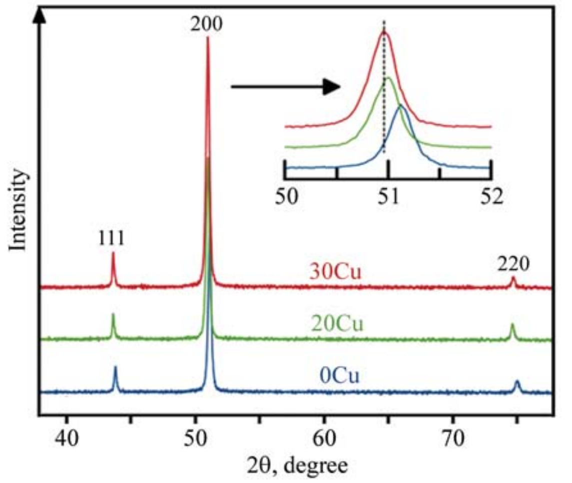

Fig. 3. XRD patterns of Cu0V (*1*), Cu2V (*2*), and Cu3V (*3*) coatings and the (200) peak at higher resolution

Рис. 3. Рентгенограммы покрытий Cu0V (*1*), Cu2V (*2*), Cu3V (*3*) и отдельно пика (200)

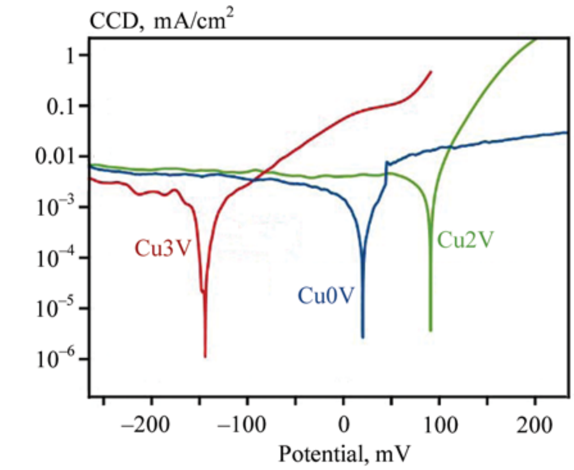

Fig. 4. Corrosion current density versus applied potential for coatings with different copper content

Рис. 4. Кривые зависимости плотности тока коррозии от приложенного потенциала для образцов покрытий с различным содержанием меди the presence of cathodes promotes better passivation of the matrix in more distant areas. The overlap of these effects leads to the retention of the average CCD at the previous level, although the likelihood of localized corrosion cannot be ruled out.

The synergistic effect caused by the simultaneous impact of wear and corrosion was evaluated through tribocorrosion tests in artificial seawater, during which the electrochemical potential was recorded under both stationary conditions (without friction) and during friction. The experimental results are shown in Fig. 5.

The friction coefficient of the base Cu0V sample monotonically increased from 0.3 to 0.37. The introduction of copper into the coating at 14 at.% (Cu2V) and 19 at.% (Cu3V) led to the stabilization and reduction of the friction coefficient to 0.29 and 0.26, respectively.

When friction started, all coatings experienced a sharp drop in corrosion potential to negative values

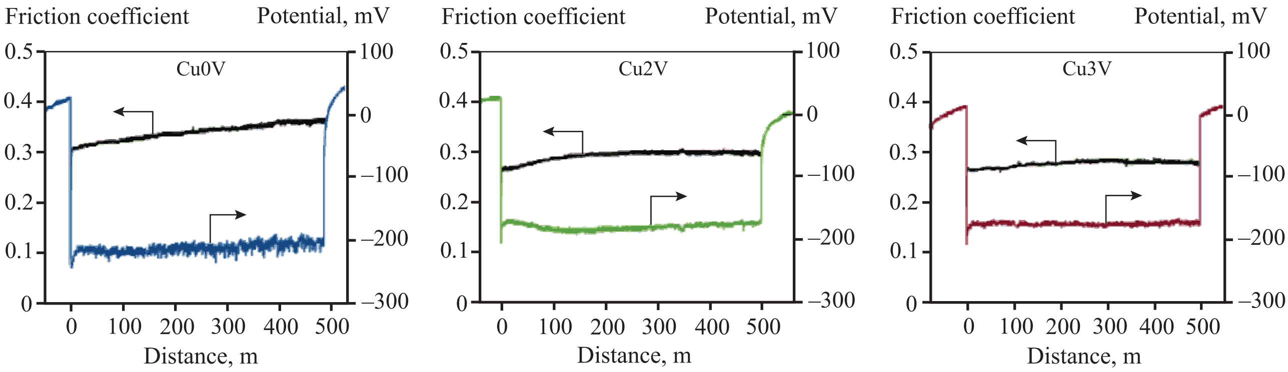

Fig. 5. Tribocorrosion test results of coatings in artificial seawater

Рис. 5. Результаты трибокоррозионных исследований покрытий в искусственной морской воде

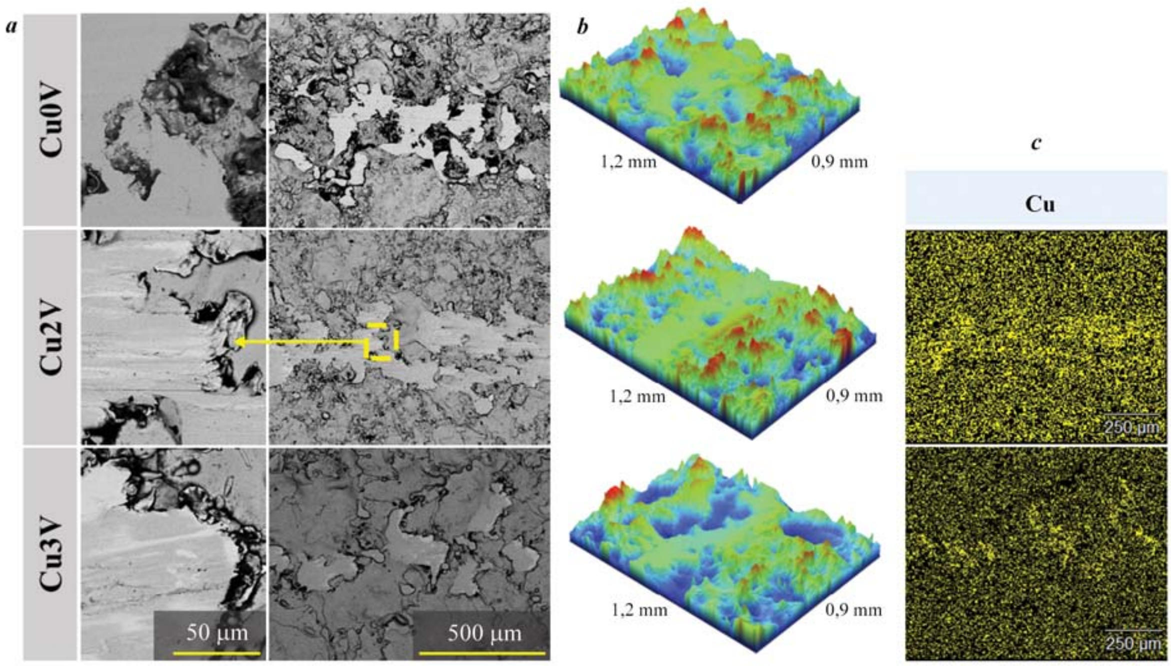

Fig. 6. Wear tracks of Cu0V, Cu2V, and Cu3V coatings

a – SEM images of wear tracks at different magnifications; ***b*** – wear track 3D profiles after tribocorrosion tests; ***c*** – Cu distribution maps in the area of wear tracks

Рис. 6. Дорожки износа образцов покрытий Cu0V, Cu2V и Cu3V

а – СЭМ-изображения дорожек износа при различных увеличениях; ***b*** – 3D-профили дорожек износа после трибокоррозионных исследований; ***c*** – карта распределения меди в области дорожек износа due to the removal of the protective passive film from their surface. The potential for the Cu0V sample was –200 mV, while for Cu2V and Cu3V coatings, it did not change during friction and remained at –165 mV, indicating more stable tribocorrosion behavior of these samples.

Figure 6 presents SEM images, 3D profiles of wear tracks, and EDS data of Fe—Co—Cr—Ni—Cu_x coatings. The wear tracks of all coatings have similar morphology: partial wear of the surface roughness is observed (Fig. 6, *a*). The areas between the worn regions are filled with wear and corrosion products, mainly consisting of Fe and Cr oxides, as well as residual components of artificial seawater (Table 2).

A unique feature of the tribology of Cu-containing coatings is the accumulation of copper in the wear tracks (Fig. 6, *c* and Table 3). Copper concentrates on the smooth worn areas of the coating due to its galvanic deposition. During corrosion and wear, some copper dissolves into the solution. During friction in the wear track, the surface potential drops significantly below the equilibrium potential for copper dissolution—deposition in this medium. Friction on areas with a worn passive film results in the negative potential, leading to copper deposition in these areas. The accumulation of copper in

Table 2. **Elemental composition of wear debris in wear tracks**

Таблица 2. Элементный состав продуктов износа в дорожке износа

Coating sample	Content, at.%									
	O	C	Mg	Si	Ca	Cr	Fe	Co	Ni	Cu
Cu0V	45	25	1	1	1	7	15	3	2	–
Cu2V	45	30	1	1	2	3	12	1	2	5
Cu3V	44	27	1	1	1	5	14	3	2	2

Table 3. **Composition of coating and worn surface of the wear track**

Таблица 3. Состав покрытия и изношенной поверхности дорожки

Area	Content, at.%						
	Cr	Fe	Co	Ni	Cu	O	C
Cu0V	17	40	10	11	–	6	16
Wear track	17	41	11	12	–	6	13
Cu2V	14	32	8	9	9	6	22
Wear track	13	28	10	11	18	5	15
Cu3V	14	33	10	12	15	3	13
Wear track	11	26	9	11	24	5	14

Table 4. **Results of tribological tests**

Таблица 4. Результаты трибологических испытаний

Coating sample	Specific wear rate, 10^{-6} mm^3/(N·m)	Hardness, GPa
Cu0V	5.6	2.8
Cu2V	6.3	2.4
Cu3V	9.6	2.3

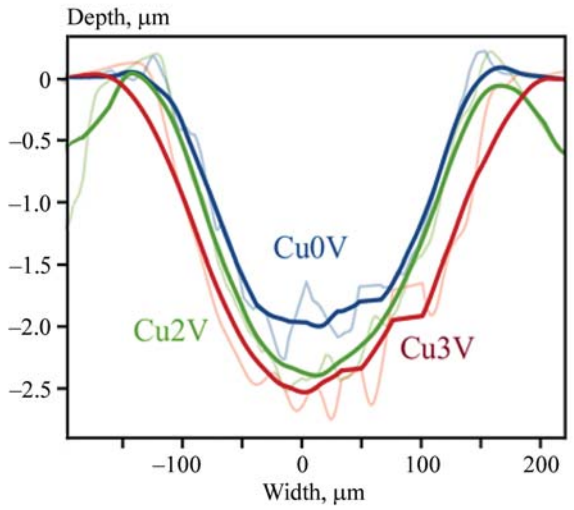

Fig. 7. Profiles of coating wear tracks

Рис. 7. Профили дорожек износа покрытий

the wear track results in a reduction of the friction coefficient.

To determine the wear rate of the coatings and to exclude the influence of the roughness of the ESD coatings, additional tribological tests were conducted on samples with a polished surface. The results obtained are shown in Fig. 7. It was found that all coatings exhibit high wear resistance; however, with an increase in copper content, the wear resistance slightly decreased from $5.6 \cdot 10^{-6}$ (Cu0V) to $9.6 \cdot 10^{-6}$ (Cu3V) mm^3/(N·m), wich correlates with the hardness that decreased from 2.8 (Cu0V) to 2.3 (Cu3V) GPa (Table 4).

Conclusions

1. Medium- and high-entropy Fe—Co—Cr—Ni—Cu coatings with a thickness of up to 30 μm and varying copper content were obtained by vacuum electrospark deposition. These coatings have a single-phase solid solution structure with an FCC lattice and are characterized by a dense, homogeneous morphology.

2. Under stationary conditions, the introduction of 14 at.% Cu positively affected corrosion resistance, significantly shifting the corrosion potential from +20 to +100 mV. However, further increasing the copper content to 19 at.% negatively affected the corrosion potential, shifting it to —150 mV. The corrosion current density values of all coatings differed slightly, remaining in the range of 1—2 μA/cm^2.

3. During friction in artificial seawater, the addition of copper also positively influenced tribocorrosion properties, allowing the corrosion potential during friction to increase from –200 to –165 mV due to the galvanic deposition of dissolved copper on the worn parts of the coating. The redeposition of copper also positively affected the friction coefficient, reducing it from 0.37 (Cu0V) to 0.26 (Cu3V). Additionally, the Fe—Co—Cr—Ni—(Cu) coatings exhibited high wear resistance in the range of (5.6÷9.6)·10—6 mm^3/(N·m).

References

1. Lu Z., Mao Y., Ren S., Pu J., Fu Z., Fan X., Gao S., Fan J. A novel design of VAlTiCrCu/WC alternate multilayer structure to enhance the mechanical and tribo-corrosion properties of the high-entropy alloy coating. *Materials Characterization*. 2021;176:111115. https://doi.org/10.1016/J.MATCHAR.2021.111115
2. Kuruvila R., Kumaran S.T., Khan M.A., Uthayakumar M. A brief review on the erosion-corrosion behavior of engineering materials. *Corrosion Reviews*. 2018;36:435—447. https://doi.org/10.1515/CORRREV-2018-0022/HTML
3. Feng Z., Huang J., Guo H., Zhang X., Li Y., Fang B., Li Y., Song G.L., Liu J. A magnetic "Band-Aid" incorporated with Fe_3O_4 NPs modified epoxy binder for in-situ repair of organic coating under seawater. *Colloids and Surfaces A: Physicochemical and Engineering Aspects*. 2023;676:132317. https://doi.org/10.1016/J.COLSURFA.2023.132317
4. Liu Z.X., Li Y., Xie X.H., Qin J., Wang Y. The tribo-corrosion behavior of monolayer VN and multilayer VN/C hard coatings under simulated seawater. *Ceramics International*. 2021;47:25655—25663. https://doi.org/10.1016/J.CERAMINT.2021.05.291
5. Usta O., Korkut E. Prediction of cavitation development and cavitation erosion on hydrofoils and propellers by Detached Eddy Simulation. *Ocean Engineering*. 2019;191:106512. https://doi.org/10.1016/J.OCEANENG.2019.106512
6. Shao T., Ge F., Dong Y., Li K., Li P., Sun D., Huang F. Microstructural effect on the tribo-corrosion behaviors of magnetron sputtered CrSiN coatings. *Wear*. 2018; (416-417):44—53. https://doi.org/10.1016/J.WEAR.2018.10.001
7. Niu D., Zhang X., Sui X., Shi Z., Lu X., Wang C., Wang Y., Hao J., Tailoring the tribo-corrosion response of (CrNbTiAlV)C_xN_y coatings by controlling carbon content. *Tribology International*. 2023;179:108179. https://doi.org/10.1016/J.TRIBOINT.2022.108179
8. Ma Y., Li Y., Wang F. The atmospheric corrosion kinetics of low carbon steel in a tropical marine environment. *Corrosion Science*. 2010; 52: 1796—1800. https://doi.org/10.1016/j.corsci.2010.01.022
9. Wang D., Luo H., Zhao S., Tan J., Liang X., Yang J., Zhou S. Seawater-triggered self-renewable amphiphilic coatings with low water swelling and excellent biofilm prevention properties. *Progress in Organic Coatings*. 2013;175:107351. https://doi.org/10.1016/J.PORGCOAT.2022.107351
10. Zhang X., Yu Y., Li T., Wang L., Qiao Z., Liu Z., Liu W. Effect of the distribution of Cu on the tribo-corrosion mechanisms of $CoCrFeNiCu_{0.3}$ high-entropy alloys. *Tribology International*. 2024;193:109401. https://doi.org/10.1016/J.TRIBOINT.2024.109401
11. Wu P., Gan K., Yan D., Fu Z., Li Z. A non-equiatomic FeNiCoCr high-entropy alloy with excellent anti-corrosion performance and strength-ductility synergy. *Corrosion Science*. 2021;183:109341. https://doi.org/10.1016/J.CORSCI.2021.109341
12. Kuptsov K.A., Antonyuk M.N., Sheveyko A.N., Bondarev A. V., Ignatov S.G., Slukin P. V., Dwivedi P., Fraile A., Polcar T., Shtansky D. V. High-entropy Fe—Cr—Ni—Co—(Cu) coatings produced by vacuum electro-spark deposition for marine and coastal applications. *Surface and Coatings Technology*. 2023;453:129136. https://doi.org/10.1016/J.SURFCOAT.2022.129136
13. Liu Z., Cui T., Chen Y., Dong Z. Effect of Cu addition to AISI 8630 steel on the resistance to microbial corrosion. *Bioelectrochemistry*. 2023;152:108412. https://doi.org/10.1016/j.bioelechem.2023.108412
14. Zeng Y., Yan W., Shi X., Yan M., Shan Y., Yang K. Enhanced bio-corrosion resistance by Cu alloying in a micro-alloyed pipeline steel. *Acta Metall Sin Engl Lett*. 2022;35(10):1731—1743. https://doi.org/10.1007/s40195-022-01392-9
15. Shi Y., Yang B., Liaw P. Corrosion-resistant high-entropy alloys: A review. *Metals*. 2017;7(2):43. https://doi.org/10.3390/met7020043
16. Zhang C., Lu X., Zhou H., Wang Y., Sui X., Shi Z.Q., Hao J. Construction of a compact nanocrystal structure for (CrNbTiAlV)N_x high-entropy nitride films to improve the tribo-corrosion performance. *Surface and Coatings Technology*. 2022;429:127921. https://doi.org/10.1016/J.SURFCOAT.2021.127921

17. Shon Y., Joshi S.S., Katakam S., Shanker Rajamure R., Dahotre N.B. Laser additive synthesis of high entropy alloy coating on aluminum: Corrosion behavior. *Materials Letters*. 2015;142:122—125.
https://doi.org/10.1016/J.MATLET.2014.11.161
18. Jin G., Cai Z., Guan Y., Cui X., Liu Z., Li Y., Dong M., Zhang D. High temperature wear performance of laser-cladded FeNiCoAlCu high-entropy alloy coating. *Applied Surface Science*. 2018;445:113—122.
https://doi.org/10.1016/J.APSUSC.2018.03.135
19. Li Q.H., Yue T.M., Guo Z.N., Lin X. Microstructure and corrosion properties of alcocrfeni high entropy alloy coatings deposited on AISI 1045 steel by the electrospark process. *Metallurgical and Materials Transactions A: Physical Metallurgy and Materials Science*. 2013;44: 1767—1778.
https://doi.org/10.1007/S11661-012-1535-4/FIGURES/15
20. An Z., Jia H., Wu Y., Rack P.D., Patchen A.D., Liu Y., Ren Y., Li N., Liaw P.K. Solid-solution CrCoCuFeNi high-entropy alloy thin films synthesized by sputter deposition. *Materials Research Letters*. 2015;3:203—209.
https://doi.org/10.1080/21663831.2015.1048904
21. Sheveyko A.N., Kuptsov K.A., Kiryukhantsev-Korneev P.V., Levashov E.A., Shtansky D.V. Hybrid technology combining electrospark alloying, cathodic arc evaporation and magnetron sputtering for hard wear-resistant coating deposition. *Powder Metallurgy and Functional Coatings*. 2018;4:92—103. (In Russ.).
https://doi.org/10.17073/1997-308X-2018-4-92-103
Шевейко А.Н., Купцов К.А., Кирюханцев-Корнеев Ф.В., Левашов А.Е., Штанский Д.В. Гибридная технология осаждения твердых износостойких покрытий, сочетающая процессы электроискрового легирования, катодно-дугового испарения и магнетронного напыления. *Известия вузов. Порошковая металлургия и функциональные покрытия*. 2018;(4):92—103.
https://doi.org/10.17073/1997-308X-2018-4-92-103
22. Sheveyko A.N., Kuptsov K.A., Antonyuk M.N., Bazlov A.I., Shtansky D.V. Electro-spark deposition of amorphous Fe-based coatings in vacuum and in argon controlled by surface wettability. *Materials Letters*. 2022;318:132195.
https://doi.org/10.1016/J.MATLET.2022.132195

Information about the authors

Mariya N. Fatykhova – Cand. Sci. (Eng.), Junior Researcher of the Scientific-Educational Center of SHS (SHS-Center) of MISIS–ISMAN, National University of Science and Technology "MISIS" (NUST "MISIS").
https://orcid.org/0000-0001-6817-5999
E-mail: mariya.antonyuck@ya.ru

Konstantin A. Kuptsov – Cand. Sci. (Eng.), Senior Researcher of SHS-Center of MISIS–ISMAN.
https://orcid.org/0000-0003-2585-0733
E-mail: kuptsov.k@gmail.com

Aleksanr N. Sheveyko – Researcher of SHS-Center of MISIS–ISMAN.
https://orcid.org/0000-0003-3704-515X
E-mail: sheveyko@mail.ru

Alfina R. Gizatullina – Research Assistant of SHS-Center of MISIS–ISMAN.
E-mail: alfina.gizatullina@yandex.ru

Pavel A. Loginov – Cand. Sci. (Eng.), Senior Lecturer of the Department of Powder Metallurgy and Functional Coatings of NUST MISIS; Senior Research Scientist of the Laboratory "In situ Diagnostics of Structural Transformations" of SHS-Center of MISIS–ISMAN.
https://orcid.org/0000-0003-2505-2918
E-mail: pavel.loginov.misis@list.ru

Dmitriy V. Shtansky – Dr. Sci. (Phys.-Math.), Head of the Research Center "Inorganic Nanomaterials" of NUST MISIS; Chief Researcher of SHS-Center of MISIS–ISMAN.
https://orcid.org/0000-0001-7304-2461
E-mail: shtansky@shs.misis.ru

Информация об авторах

Мария Николаевна Фатыхова – к.т.н., мл. науч. сотрудник Научно-учебного центра (НУЦ) СВС МИСИС–ИСМАН, Национальный исследовательский технологический университет «МИСИС» (НИТУ МИСИС).
https://orcid.org/0000-0001-6817-5999
E-mail: mariya.antonyuck@ya.ru

Константин Александрович Купцов – к.т.н., ст. науч. сотрудник НУЦ СВС МИСИС–ИСМАН.
https://orcid.org/0000-0003-2585-0733
E-mail: kuptsov.k@gmail.com

Александр Николаевич Шевейко – науч. сотрудник НУЦ СВС МИСИС–ИСМАН.
https://orcid.org/0000-0003-3704-515X
E-mail: sheveyko@mail.ru

Альфина Рустемовна Гизатуллина – лаборант-исследователь НУЦ СВС МИСИС–ИСМАН.
E-mail: alfina.gizatullina@yandex.ru

Павел Александрович Логинов – к.т.н, ст. преподаватель кафедры «Порошковая металлургии и функциональные покрытия» НИТУ МИСИС; ст. науч. сотрудник лаборатории «In situ диагностика структурных превращений» НУЦ СВС МИСИС–ИСМАН.
https://orcid.org/0000-0003-2505-2918
E-mail: pavel.loginov.misis@list.ru

Дмитрий Владимирович Штанский – д.ф.-м.н., зав. научно-исследовательским центром «Неорганические наноматериалы» НИТУ МИСИС; гл. науч. сотрудник НУЦ СВС МИСИС–ИСМАН.
https://orcid.org/0000-0001-7304-2461
E-mail: shtansky@shs.misis.ru

Contribution of the authors

M.N. Fatykhova – defined the research purpose and concept, wrote the article, prepared graphic materials, conducted microstructural studies, mechanical and tribocorrosion tests, and discussed and described the results.

K.A. Kuptsov – defined the research purpose and concept, contributed to writing the article, prepared graphic materials, conducted X-ray phase structural analysis, and participated in discussing and describing the results.

A.N. Sheveiko – conducted and described the electrochemical results.

A.R. Gizatullina – contributed to the discussion of research results, prepared graphic materials, and described the results of mechanical tests.

P.A. Loginov – produced the electrodes and contributed to the discussion of research results.

D.V. Shtansky – defined the research purpose and concept.

Вклад авторов

М.Н. Фатыхова – определение цели работы и концепции исследований, написание текста статьи, подготовка графического материала, проведение микроструктурных исследований, механических и трибокоррозионных испытаний, обсуждение и описание результатов.

К.А. Купцов – определение цели работы и концепции исследований, написание текста статьи, подготовка графического материала, проведение рентгенофазового структурного анализа, обсуждение и описание результатов.

А.Н. Шевейко – проведение и описание электрохимических результатов.

А.Р. Гизатуллина – обсуждение результатов исследований, подготовка графического материала, описание результатов механических испытаний.

П.А. Логинов – изготовление электродов, обсуждение результатов исследований.

Д. В. Штанский – определение цели работы и концепции исследований.

The article was submitted 15.04.2024, revised 24.04.2024, accepted for publication 29.04.2024

Статья поступила в редакцию 15.04.2024, доработана 24.04.2024, подписана в печать 29.04.2024